DISSERTATION

PALEOZOIC FACIES ARCHITECTURE IN LOW-INCLINED MIXED CARBONATE-SILICICLASTIC SEDIMENTARY SYSTEMS: DEPOSITIONAL AND TECTONIC SIGNATURES

Submitted by

Aleksandra Novak

Department of Geosciences

In partial fulfillment of the requirements

For the Degree of Doctor of Philosophy

Colorado State University

Fort Collins, Colorado

Fall 2019

Doctoral Committee:

Advisor: Sven Egenhoff

Lisa Stright
Derek Schutt
Joe von Fischer

ABSTRACT

PALEOZOIC FACIES ARCHITECTURE IN LOW-INCLINED MIXED CARBONATE-SILICICLASTIC SEDIMENTARY SYSTEMS: DEPOSITIONAL AND TECTONIC SIGNATURES

Low-inclined sedimentary systems occur in a variety of settings and throughout Earth history. They have not only been described from tectonically relatively quiet basin types, such as passive margins and intracratonic troughs, but also make up the low-inclined flanks of back-arc (Schwarz et al., 2018) and foreland basins (Van Wagoner, 1995), just to name a few. Low-inclined basin margins occur in Cambrian (Labaj and Pratt 2016) to Holocene (Purdy and Gischler 2003) strata, and have also been described from Precambrian settings (Sakurai et al., 2005). Despite their abundance throughout the rock record and their ubiquity worldwide many aspects of low-inclined margins are still not well understood. This thesis addresses three of them: (1) Sedimentation of mudstones in a distal open shelf setting using the Ordovician Tøyen Shale Formation, Norway and Sweden, as an example; (2) Shallow-marine sedimentation on an intracratonic basin margin and the varying expression of the middle member of the Devonian-Mississippian Bakken Formation, North Dakota, USA; and (3) Synsedimentary deformation of intracratonic basin deposits, Devonian-Mississippian Bakken Formation, North Dakota, USA.

The first chapter of this dissertation addresses the sedimentology and facies architecture of the Ordovician Tøyen Shale Formation in southern Scandinavia. The sedimentary record of the Tøyen Shale Formation provides an insight into open marine shelf deposition of fine-grained siliciclastic and carbonate rocks, preservation of organic matter, and expression of global eustatic sea-level fluctuations. This section shows that the transition between carbonate and siliciclastic mudstones in open shelf settings is likely controlled by a process that deposited fine-grained carbonates – either suspension settling or bed-load transport affected by the Coriolis force, sea-level changes during deposition and/or proximity to the

source of the siliciclastic sediment. Sedimentary structures preserved in the Tøyen Shale Formation point to deposition by current- or possibly wave-induced bed-load processes during high-energy events in distal realms, suggesting that other marine open shelf mudstones could have also been affected by storm-waves and, therefore, were likely deposited above storm wave base. Storm-induced fluxes of sediment probably contributed to the preservation of organic matter, while intensified in the Ordovician ecospace utilization by burrowing organisms determined the destruction of most of the organics. The regressive and transgressive 3rd-order cycles defined within the Tøyen Shale Formation correspond to global eustatic sea-level changes and could reflect previously undocumented glacio-eustatic, tectonically- or, alternatively, aquifer volume-driven variations of sea-level.

The second chapter provides a detailed overview of the sedimentary facies architecture of the mixed carbonate-siliciclastic Late Devonian – Early Carboniferous middle member of the Bakken Formation in the Williston basin, ND, USA, and discusses the mechanisms and controls of carbonate and siliciclastic mixing in low-inclined shelf settings. Intracratonic basins are geographically widespread and rich in mineral resources, e.g. the Williston and Michigan basins in the US (Gerhard et al., 1990;Catacosinos et al., 1990), Western Siberian basin in Russia (Khain, 1994), Paris basin in France (Brigaud et al., 2014), Cooper basin in Australia (Jadoon et al., 2017), Parana and Chapada Diamantina basins in Brazil (Bergamaschi et al., 2016; Magalhaes et al., 2015), and the Reggane, Ahnet, Mouydir and Illizi basins in North Africa (Perron et al., 2018). Successful mineral exploration requires careful delineation of potential reservoir units; this study presents a comprehensive depositional model based on detailed sedimentary facies descriptions, interpretations and mapping. Combined with fine-scale sequence stratigraphic framework, the model produced in this study explains the distribution of facies and mixing of carbonate and siliciclastic material during regressive and transgressive episodes of the middle Bakken depositional history. The mixing of carbonate and siliciclastic material in the middle Bakken member occurs via three distincs mechanisms: 1) basin-wide deposition of carbonates during sea-level highstands and a switch to siliciclastic deposition during the lowstands (reciprocal model); 2) coeaval deposition of carbonates and siliciclastics reflected in the close mixing on a grain scale; and 3) lateral variation in carbonate-siliciclastic proportion which resulted in the development of a carbonate factory towards the southwest of the study area and mixing of carbonate grains with predominantly siliciclastic facies in the center and the northeast of the study area. The model created for the middle Bakken member is an excellent illustration of a siliciclastic-dominated mixed system developed in an intracratonic basin that provides a valuable insight on carbonate-siliciclastic mixing mechanisms in similar basin settings, relatively stable roundish depressions situated on continental crust (e.g. Heine et al., 2008).

Models for the tectonic evolution of low-inclined cratonic margins and interiors suggest slow and stable subsidence (Heine et al., 2008; Vibe et al., 2018; Armitage and Allen, 2010), though intermittently interrupted by recurrent seismic activity due to the reactivation of pre-existing basement structures (Onasch and Kahle, 1991; El Taki and Pratt, 2012; Novak and Egenhoff, 2019). Nevertheless, the influence of basement heterogeneity on intracratonic basin facies architecture and its spatial and temporal distribution throughout a basin is rarely described in detail (but see Perron et al., 2018 and references therein). The third chapter of this dissertation describes various soft-sediment deformation structures (SSDS) that reflect brittle and ductile deformation and loss of sediment shear in compressional and extensional settings (Obermeier, 1996). In this study, SSDS are interpreted to have formed due to seismically-induced folding, liquefaction and fluidization of unconsolidated sediment, as well as microfaulting and brecciation of consolidated sediment, and reflect synsedimentary tectonic movements, e.g. along faults that were active during deposition. The distribution of SSDS follows the orientation of the major structural elements rooted in the basement of the Williston Basin. The stratigraphic and spatial distribution of SSDS suggests variable tectonic activity: cores near the most active fault systems have the highest net thickness of units with SSDS, whereas those farther from the most active faults exhibit only a few deformed units. The predominance of SSDS in the upper portion of the middle member suggests that there was a change from relative tectonic quiescence to a more active regime which in turn led to modifications of basin geometry and new accommodation patterns. Synsedimentary deformation might have had a positive effect on reservoir quality in deformed units by increasing porosity and permeability as a result of cohesion loss and rearrangement of grains. Additionally, multiple injection structures and complexes of small-scale normal and reverse faults could contribute to better connectivity of reservoir units.

REFERENCES

Bergamaschi, S., Oliveira, R. M. A. G., Campos, G. F., Souza, V. M. J. S., Pinto, G. P., Pessano, P. C., Ade, M. V. B., Pinheiro, A. E. P. P., and Martins, M. V. A., 2016, Paleoenvironmental evolution of the Itararé group (Paraná Basin) in the regions of Salto and Itu, east of São Paulo state, Brazil. Journal of Sedimentary Environment, v. 1, p. 145-158. 10.12957/jse.2016.21956

Brigaud, B., Vincent, B., Carpentier, C., Robin, C., Guillocheau, F., Yven, B., Huret, E., 2014, Growth and demise of the Jurassic carbonate platform in the intracratonic Paris Basin (France): Interplay of climate change, eustasy and tectonics. Marine and Petroleum Geology, v. 53, v. 3-29. 10.1016/j.marpetgeo.2013.09.008.

Catacosinos, P. A., Daniels Jr., P. A., Harrison III, W. B., 1990, Structure, Stratigraphy, and Petroleum Geology of the Michigan Basin: Chapter 30: Part II. Selected Analog Interior Cratonic Basins: Analog Basin, in: M. W. Leighton, D. R. Kolata, D. F. Oltz., and J. J. Eidel (eds.), Interior Cratonic Basins, American Association of Petroleum Geologists Memoir 51, p. 561-601.

Jadoon, Q.K., Roberts, E., Blenkinsop, T., Wust, R., 2017, Organic petrography and thermal maturity of the Permian Roseneath and Murteree shales in the Cooper basin, Australia. International Journal of Coal Geology, v. 154-155, p. 240-256.

Khain, V. E., 1994, Geology of Northern Eurasia (Ex USSR). Phanerozoic Fold Belts and Young Platforms, vol. 2, Bornträger, Berlin, 404 pp.

Łabaj, M., and Pratt, B., 2016, Depositional Dynamics In A Mixed Carbonate–Siliciclastic System: Middle–Upper Cambrian Abrigo Formation, Southeastern Arizona, U.S.A.. Journal of Sedimentary Research. V. 86, p. 11-37. 10.2110/jsr.2015.96.

Magalhães, A. J. C., Raja Gabaglia, G. P., Scherer, C. M. S., Bállico, M. B., Guadagnin F., Bento Freire, E., Silva Born, L.R., and Catuneanu, O., 2015. Sequence hierarchy in a Mesoproterozoic interior sag basin: from basin fill to reservoir scale, the Tombador Formation, Chapada Diamantina Basin, Brazil. Basin Research, v. 28, p. 393-432.

Perron, P., Guiraud, M., Vennin, E., Moretti, I., Portier, É., Le Pourhiet, L. and Konaté, M., 2018, Influence of basement heterogeneity on the architecture of low subsidence rate Paleozoic intracratonic basins (Reggane, Ahnet, Mouydir and Illizi basins, Hoggar Massif). Solid Earth, v. 9, p. 1239-1275.

Purdy, E. G., and Gishler, E., 2003, The Belize margin revisited: 1. Holocene marine facies. International Journal of Earth Sciences, v. 92, no. 4, p. 532-551.

Sakurai, R., Ito, M., Ueno, Y., Kitajima, K., and Maruyama, S., 2005, Facies architecture and sequence-stratigraphic features of the Tumbiana Formation in the Pilbara Craton, northwestern Australia: Implications for depositional environments of oxygenic stromatolites during the Late Archean. Precambrian Research, v. 138, p. 255-273. 10.1016/j.precamres.2005.05.008.

Van Wagoner, J. C., 1995. Sequence Stratigraphy and Marine to Nonmarine Facies Architecture of Foreland Basin Strata, Book Cliffs, Utah, U.S.A., in: J.C. Van Wagoner and G.T. Bertram (eds.), Sequence Stratigraphy of Foreland Basin Deposits, American Association of Petroleum Geologists Memoir 62.

ACKNOWLEDGEMENTS

I would first like to thank my advisor, Dr. Sven Egenhoff, for his guidance, encouragement and patience during the entire time I was his PhD student. I am very grateful to my family and my husband, Jake Childress, for being so understanding and supportive of any of my entrepreneurships.

I would like to thank American Association of Petroleum Geologists Foundation and the donors of the Fred Tietz Named Grant for supporting the Tøyen Shale Formation research project. I am thankful to Dr. Per Ahlberg and Frans Lundberg at the Department of Geology at the University of Lund, Sweden, for access to the cores and assistance with core handling, and Heather Lowers at the USGS Microbeam Lab for assistance with SEM sampling. I would like to thank Timothy O. Nesheim for providing data on the Williston basin structural elements. The North Dakota Geological Survey's Core Library in Grand Forks, North Dakota, and the US Geological Survey's Core Research Center in Denver, Colorado, are thanked for their assistance in core handling and sampling. Reviews by Brian Pratt and an anonymous reviewer significantly improved the quality of the manuscript. I would like to thank my research team mates Joel Spansel and Jimmy van Hook for their assistance in the field, and for creating a fun and productive work environment.

I would like to acknowledge Hess Corporation for sponsoring a part of of PhD by financing one of the projects, which is, however, not a part of this manuscript.

I am thankful to my committee memebrs Derek Schutt, Lisa Stright, Andrew Bliss and Joe von Fischer for their effort towards my development as a researcher and their time for improving this dissertation.

TABLE OF CONTENTS

PART I: DEVELOPING A MODEL FOR OPEN SHELF SHALE DEPOSITION: SEDIMENTOLOGY AND ARCHITECTURE OF THE ORDOVICIAN TØYEN SHALE FORMATION

INTRODUCTION

Technological advancement and success in unconventional plays exploration spurred significant production of hydrocarbons from organic-rich fine-grained rocks, commonly referred to as "black shales". Due to its economic importance, the research on mud-dominated systems has been revitalized in the past few decades providing some groundbreaking insights on sediment transport mechanisms, shale deposition and preservation of organic matter (e.g. Bohacs et al. 2005; Macquaker and Bohacs 2007; Macquaker et al. 2010a; Schieber et al. 2007; Schieber 2013). However, most recent studies focus exclusively on understanding organic-rich mudstones and their depositional settings as they represent a highly prolific source of hydrocarbons. Mudstone successions that do not contain large amounts of organic matter but were deposited in similar open shelf settings as many of the well-studied petroliferous examples, e.g. the Woodford shale (Cardott 2012), the Barnett (Loucks and Ruppel 2007), Bossier and Haynesville shales (Hammes and Frebourg 2012) have received nearly no attention as they have been regarded economically non-viable. However, these rocks are characterized by some of the same sedimentary structures and were deposited largely through the same processes as their organic-rich counterparts (Egenhoff and Maletz 2012; Egenhoff et al. 2019). Studying the depositional processes in those systems will, therefore, help to understand the specifics of open marine shelf deposition and shale facies architecture, and, ultimately, point to the crucial conditions that are required for the development of productive source rocks in open-shelf settings.

This study examines the Lower to Middle Ordovician Tøyen Shale Formation in several outcrop locations and drill cores across Scandinavia, from the Oslo region to southern Sweden, and uses it to build a comprehensive open-shelf shale depositional model. Silt-rich and gray- to dark gray-colored in outcrop and finer-grained and mostly black in core, the Tøyen Shale Formation contains low to moderate amounts of detrital graptolite or disseminated graptolitic organic material. Common for many other open marine shales depositional settings, accessibility of surficial exposures and detailed knowledge of local biostratigraphy make the Tøyen Shale Formation an ideal example for this study. Thorough investigation of proximal to distal facies relationships in a sequence stratigraphic framework built the foundation for the resulting depositional model. This model, although constructed based on an Early Paleozoic example, will aid a wider understanding of the sedimentary processes that influenced open shelf successions facies architecture in many similar unconventional systems worldwide**.**

GEOLOGICAL SETTING

The deposition of the Tøyen Shale Formation took place on the western margin of the Baltica plate during Early to Middle Ordovician time (cf. Cocks and Torsvik 2002). The microcontinent of Baltica formed after separating from Gondwana during the Early Cambrian (Calner et al. 2013). This rifting and subsequent drifting is associated with the deposition of coarse-grained siliciclastics, mostly sandstones, along the margins of Baltica and in several rift and trough systems (Nielsen and Schovsbo 2011). From the Middle Cambrian until the Middle Ordovician, Baltica moved northwards across the southern hemisphere, thereby rotating by approximately 120 degrees (Cocks and Torsvik 2005). Middle and Upper Cambrian strata are black shales with minor carbonates (e.g. Dworatzek 1987), likely deposited on a deep shelf under dysoxic conditions (Egenhoff et al. 2015). Ordovician strata show a differentiation of mostly shelf carbonates in the east, e.g. in Kinnekulle and Billingen (Jaanusson 1982), and intercalated carbonates and shales in the western part of Scandinavia, e.g. in the Hunneberg area (Egenhoff and Maletz 2012) and in the Oslo region (Egenhoff et al. 2010) (Fig. 1). During the Late Ordovician, Baltica climate turned warmer, culminating in tropical conditions, as reflected in, for instance, ooid deposition in southern to central Sweden (Stridsberg 1980). The Tøyen Shale Formation shows an average thickness of about 20 meters in the Oslo region (Owen et al. 1990). It is widely distributed throughout Sweden and Norway, and extends from Jämtland in central Sweden through the Oslo region of Norway to Västergötland and Scania in southern Sweden.

The unit is rich in graptolites (Maletz and Ahlberg 2011), and contains abundant trilobites and conodonts locally (see Maletz et al. 1996). Lithologically, the Tøyen Shale Formation is dominated by black to gray siliciclastic mudstones with some limestone intercalations (Erdtmann 1965; Egenhoff and Maletz 2007). The unit was originally subdivided into two members by Erdtmann (1965) based on data from an underground tunnel in the Oslo region. According to Erdtmann (1965) and Owen et al. (1990), the lower Hagastrand member, consists of grey siliciclastic mudstones with subordinate limestone beds, and the overlying Galgeberg member is comprised exclusively of black siliciclastic mudstones.

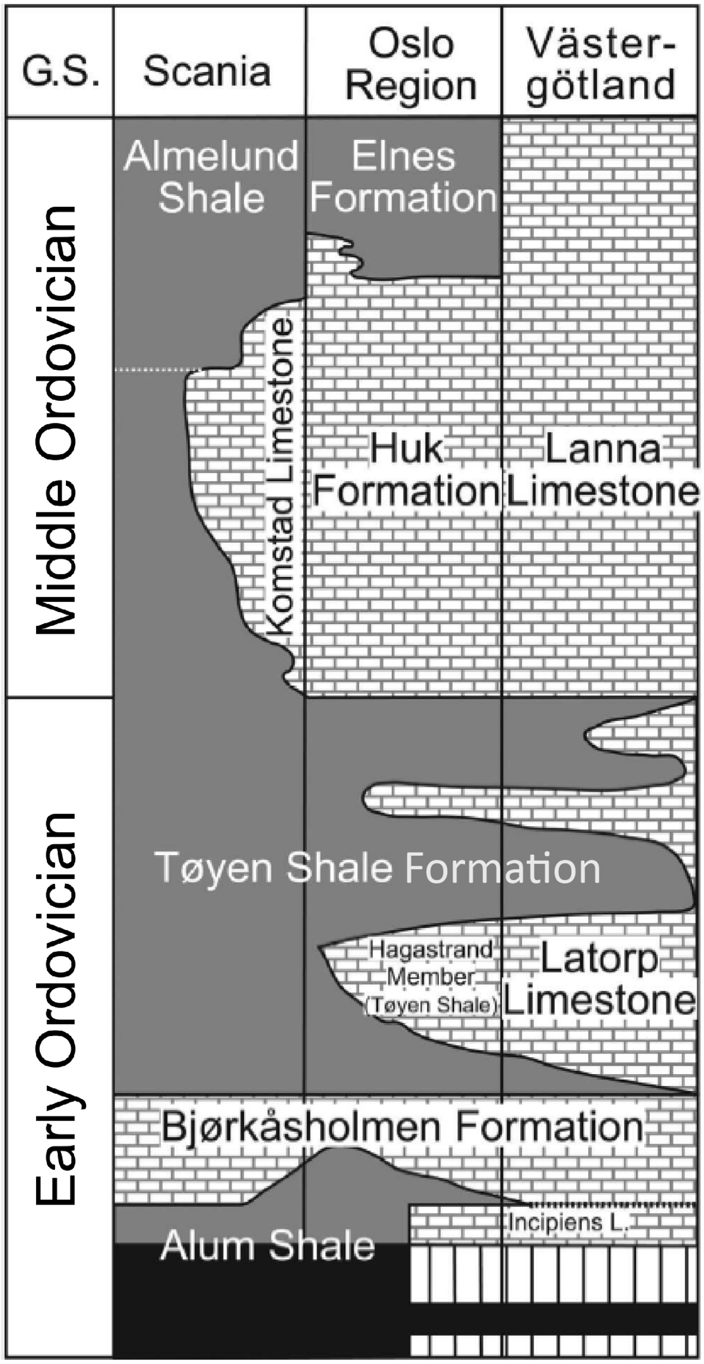

Figure 1: Stratigraphy of the Early to Middle Ordovician strata in Scandinavia. Modified after Egenhoff et al. (2018).

In the Oslo region, the Hagastrand member is between 7.3 and 10 meters-thick (Owen et al. 1990). The onset of the Hagastrand member shows an abrupt change from the limestones of the underlying Bjørkåsholmen Formation (Egenhoff et al. 2010) to intercalated gray siliciclastic mudstones and limestone beds. The basal 2.3 meters of the Hagastrand member consist of thick beds of gray mudstones with approximately 15 centimeters thick beds of limestone (Owen et al. 1990). Strings of pyrite nodules and concretions occur in the basal 50 centimeters of this unit. Pseudomorphs of calcite after barite, as suggested by Bjorlykke (1974), or gypsum, according to Erdtman (1965), are moderately abundant in the succeeding 1.55 meters. The uppermost 2.2 meters of the Hagastrand member consist of grey mudstones intercalated with 20 centimeters thick isolated limestone nodules. According to the compilation in Owen et al. (1990), this member contains both graptolites and trilobites. However, fossils are not abundant in the Hagastrand member. In contrast, the overlying Galgeberg member is richly fossiliferous (Monsen 1938; Spjeldnaes 1953; Erdtmann 1965; Maletz and Ahlberg 2011) and consists of interbedded pyrite-bearing dark gray organic-rich and light gray organic-lean siliciclastic mudstones. The Tøyen succession is not as well studied in southern Sweden as in the Oslo region. The Tøyen Shale Formation in Scania is biostratigraphically well-constrained using graptolite biozones and is described as highly faulted and in places brecciated greenish to clay- and organic-matter-rich black shale with phosphate- and silt-rich intervals (Egenhoff et al. 2018; Maletz and Ahlberg 2018).

METHODS

Detailed sedimentological descriptions were carried out on eight outcrop sections and two cores (Fig. 2). Six of the eight outcrops are located in the Oslo region near the town of Slemmestad, Norway, and are exposed in several road cuts and along the coast (Fig. 2, inset A). The remaining two stratigraphic sections were measured in southern Sweden at Mt. Hunneberg (Fig. 2, inset B). The core Fågelsångdalen was recovered at a drill site near the town of Sodra Sanby, 25 kilometers northeast from Malmö, and the Lerhamn core was recovered at a drill site near the town of Lerhamn, 80 kilometers northwest of Malmö, Sweden (Fig. 2). The cores are now stored at the Department of Geology at the University of Lund in Sweden. Thirty seven standard size polished thin sections were prepared by TPS Enterprises, Bellaire, TX, from the outcrop and core samples for microscopic analysis. Thin and ultra-thin sections were cut perpendicular to bedding, 20µm-thick for mudstones and 30µm-thick for carbonates. Scanning Electron Microscopy (SEM) was implemented on select thin section samples using an FEI Quanta scanning electron microscope at the Electron Microbeam Lab at the United States Geological Survey (USGS) in Denver, CO in order to determine the compositional and textural variations in the matrix. Total Organic Carbon (TOC) values were measured in 10 outcrop samples using a Leco carbon analyzer at Weatherford Labs in Golden, CO. The same samples were subjected to Rock-Eval pyrolysis executed by Weatherford Labs as well. Leco TOC and Rock-Eval data include measured TOC values (TOC, wt %), free volatile hydrocarbons (S1), remaining generative hydrocarbons (S2), carbon dioxide content (S3), temperature required for maximum release of hydrocarbons from kerogen cracking during pyrolysis (T_{max}, C^o), hydrogen (HI) and oxygen (OI) indices and are presented in Table 2.

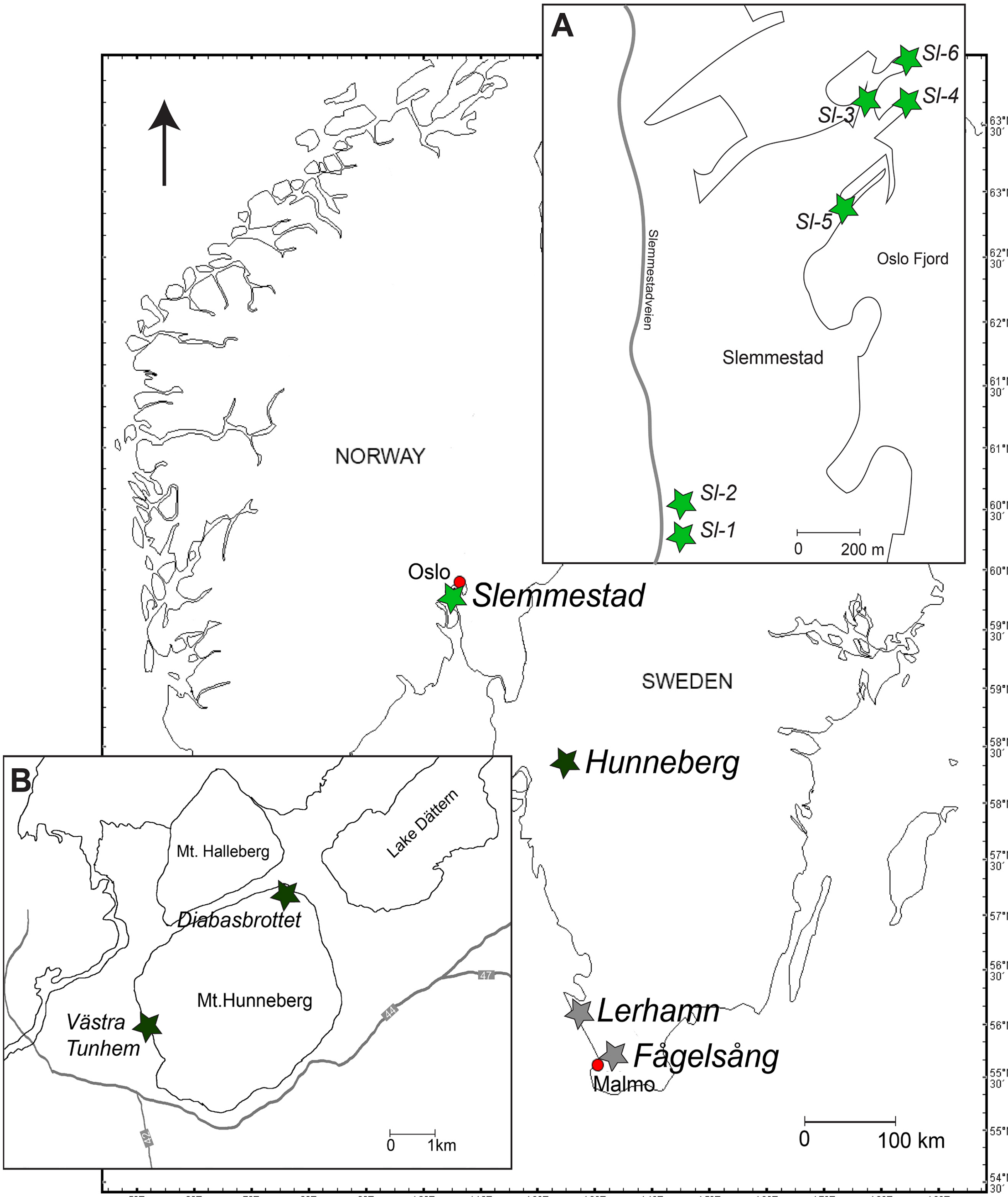

Figure 2: Study area and locations of outcrops and cores. Inset A - Slemmestad locality, Oslo region; Inset B - Mt. Hunneberg locality, Sweden.

DESCRIPTION

Sedimentary Facies

Seven sedimentary facies were identified within the Tøyen Shale Formation based on the detailed visual examination of outcrops and core samples, thin section, SEM, TOC analyses and Rock-Eval pyrolysis. Sedimentological attributes of the Tøyen Shale Formation facies are summarized in Table 1.

Table 1. Sedimentology and composition of facies identified within the Tøyen Shale Formation.

	Facies 1 – Organic-rich Siliciclastic Mudstone with Clay Clasts	**FA**
Description and Sedimentary Structures	Dark-gray to black in hand sample, medium-grey to medium-brown in thin section siliciclastic mudstone. Arranged in continuous horizontal sub-mm to mm-thick laminae with diffuse lower and sharp upper contacts. Laminae consists of sub-angular to sub-rounded light-color clay clasts and flakes of OM. The clay-clasts are made up of clay-rich siliciclastic mudstone with rare fine to medium silt-size fraction, are 0.03-0.05 millimeter-thick and up to 0.5 millimeter-long, and arranged parallel to sub-parallel to bedding. The OM flakes are tens of microns-thick and hundreds of microns-long. Contains millimeter to centimeter-size barite concretions/pseudomorphs, euhedral hexagonal barite crystals, abundant pyrite (framboids, concretions and individual euhedral, anhedral and needle-like crystals), and horizontal calcite-filled fractures with cone-in-cone structures at select intervals. Interbedded with facies 2 and 7.	1
Composition	<5% of bioclastic grains (agglutinated foraminifera, graptolites, conodonts), 5-7% sub-angular to sub-rounded silt-size quartz, carbonate and rare phosphate grains, 87-90% clay (illite and chlorite) dominated organic-matter-rich matrix (Fig. 3 A).	

Bioturbation	*Planolites* in places, *Phycosipon incertum*, BI~2-3 (Droser and Bottjer 1986)	
TOC	~1.92% or higher (visual estimation)	
Interpretation	Clay-clasts formed by up-dip erosion of water-rich mud by currents and re-deposition by bed-load processes (Schieber et al. 2010). Intermixed silt-size grains are also likely deposited by bed-load. Clay-clasts laminae may reflect individual events (e.g. storms). Incorporated organic flakes have likely been buried with and by the clay-clasts. Evidence of burrowing and benthic fauna indicate at least intermittently dysoxic conditions at the seafloor (Schieber 2009; Egenhoff and Fishman 2013).	
	Facies 2 – Siliciclastic Mudstone with Flakes of Organic Matter	**FA**
Description and Sedimentary Structures	Gray to dark gray in hand sample, light brown in thin section. Arranged in continuous to discontinuous massive horizontal 0.2-15 millimeters-thick lamina with diffuse contacts. Consists of clay- and silt-size material and contains elongate flakes of organic material (tens of microns-thick and tens to hundreds of microns-long) and randomly distributed silt-size quartz and carbonate grains. The organic flakes are often arranged in distinct laminae. Low-angle ripple cross-lamination occurs in places. Contains scattered euhedral to anhedral and needle-like pyrite crystals and framboidal pyrite aggregates and several millimeters to centimeters in diameter barite concretions/pseudomorphs in places overgrown by pyrite.	2, 3
Composition	Up to 10% of silt-size carbonate and quartz grains, <5% of bioclasts (graptolites and acritarchs), 85-90% clay- (illite and chlorite) rich matrix with flakes of organic matter (Fig. 3 B).	

Bioturbation	*Planolites* in places, *Phycosipon incertum*, BI~3-4 (Droser and Bottjer 1986)	
TOC	0.25-1.92%	
Interpretation	Cross-lamination preferentially consisting of organic matter and clay formed by lateral accretion and migration of clay-rich floccule ripples by bed-load processes (Schieber et al. 2007) with relatively quiet conditions between ripple migrations indicated by the accumulation of organic matter-rich laminae. Massive appearance of laminae is due to intense bioturbation. Bioturbation complicates direct interpretation of sedimantary processes and indicates dysoxic to oxic conditions.	
	Facies 3 - Carbonate-Rich Massive Siliciclastic Mudstone	**FA**
Description and Sedimentary Structures	Light-gray in hand sample structureless to faintly planar bedded. Laminae are silt-rich, 0.1-0.5 millimeters in thickness and laterally irregular. Abundant several millimeters to centimeters in diameter barite concretions/pseudomorphs in places overgrown by pyrite.	
Composition	Up to 20% of silt-size carbonate, quartz and rare feldspar grains, <5% of bioclasts (graptolites and acritarchs), ~75% clay-rich carbonate matrix (Fig. 3 C).	3, 4
Bioturbation	*Planolites*, *Chondrites, Phycosipon incertum*, BI~4-5 (Droser and Bottjer 1986)	
TOC	0.16-0.39%	
Interpretation	Silt-rich laminae most likely represent accreted ripples produced by bed-load transport processes (Li and Schieber 2018). Clay-rich mudstone laminae likely indicate suspension settling of fine-grained material from the	

	water column. Bioturbation obscures direct evidence of specific depositional processes. BI ~4-5 indicates well-oxygenated environment.	
	Facies 4 - Massive Carbonate Mudstone	**FA**
Description and Sedimentary Structures	Grayish-tan to orange in outcrop massive carbonate mudstone. Strongly recrystallized into sub-millimeter-scale euhedral calcite crystals. Contains recrystallized burrows, stylolites and carbonate concretions up to 2 centimeter in diameter in places. Millimeter to several centimeter-size barite concretions/pseudomorphs are common.	
Composition	Up to 10% of bioclasts (brachiopod shells, trilobites, graptolites, acritarchs)	
Bioturbation	*Phycosiphon incertum* ubiquitous, remnants of *Planolites(?),* BI~5 (Droser and Bottjer 1986)	4
Interpretation	Depositional processes are unclear due to complete reworking by burrowing. Presence of dominantly carbonate mud indicates suspension settling of carbonate particles, or deposition by bed-load transport (Schieber et al. 2013). The abundance of fecal strings and burrows suggests well-oxygenated conditions at the sea-floor during deposition.	
	Facies 5 - Phosphate-Rich Bioclastic Wacke- to Packstone	**FA**
Description and Sedimentary Structures	Structureless sub-millimeter up to 1 millimeter-thick laminae of dominantly phosphate clasts and carbonate bioclasts in carbonate matrix with diffuse lower and upper contacts. Clasts can be matrix-, grain-supported, or a combination of both. Phosphate clasts are patchy brownish in color, up to 0.5 millimeters in diameter, angular to rounded and roundish to elongate in shape. Carbonate clasts are sub-angular to sub-rounded. Most shell fragments are elongate and broken, some may be intact. All elongate bioclasts are oriented roughly parallel to bedding.	1, 2

Composition	Up to 40% of bioclasts (graptolites, acritarchs, shells), ~20% of phosphate clasts, 5-7% of silt-size quartz grains, clay-bearing carbonate matrix with some mica.	
Interpretation	The size of the grains and the amount of broken shells reflect up-dip erosion and re-deposition of debris by intermittent high-energy events, for example, storm-induced tempestites. Differing transport distances are likely due to the varying sizes and abrasion of lithologically equivalent grain types.	
	Facies 6 - Glauconite- and Phosphate-Rich Bioclastic Packstone	**FA**
Description and Sedimentary Structures	Structureless laminae up to 7 millimeters-thick comprised of sand-sized angular to sub-rounded carbonate and partially replaced with calcite/clay glauconite, angular to very well-rounded phosphate and intact or broken bioclastic grains oriented parallel to sub-parallel to bedding. The laminae have sharp lower and sharp to gradational upper contacts.	
Composition	8-10% of carbonate matrix, 40% diagenetically overprinted glauconite grains, 20% of bioclasts (graptolites, conodonts and acritarchs), 20% phosphate clasts and up to 2% silt-size quartz grains.	1
Interpretation	Lag deposits that concentrated sand-size grains and bioclasts during high-energy events while winnowing out the fine-grained material, hence the formation of sharp basal surfaces and breakage and abrasion of grains. The remaining muddy matrix was either captured between grains during the deposition or infiltrated afterwards during the waning of the high-energy event.	
	Facies 7 - Massive Siliciclastic Siltstone laminae	**FA**
Description	Up to four grain diameters-thick discontinuous laminae or lenses consisting	

and Sedimentary Structures	of sub-angular to sub-rounded medium- to coarse-grained quartz silt grains. The laminae are in places lenticular with local scours into underlying beds and diffuse upper contacts.	
Composition	Quartz silt grains with <10% of clays and mica.	
Bioturbation	*Phycosiphon incertum*, BI~1-2 (Droser and Bottjer 1986)	
Interpretation	Silt transport and deposition by high-energy events, most likely bed-load processes. Silt grains likely represent compacted ripple trains (Schieber 2011). Scour bases likely produced by the currents depositing the ripples on top of underlying mudstones. The diffuse upper contacts likely represent the waning of the flow, or is a function of burrowing. Depositional environment is likely dysoxic to oxic, as indicated by the cross-cutting *Phycosiphon incertum*.	1, 2

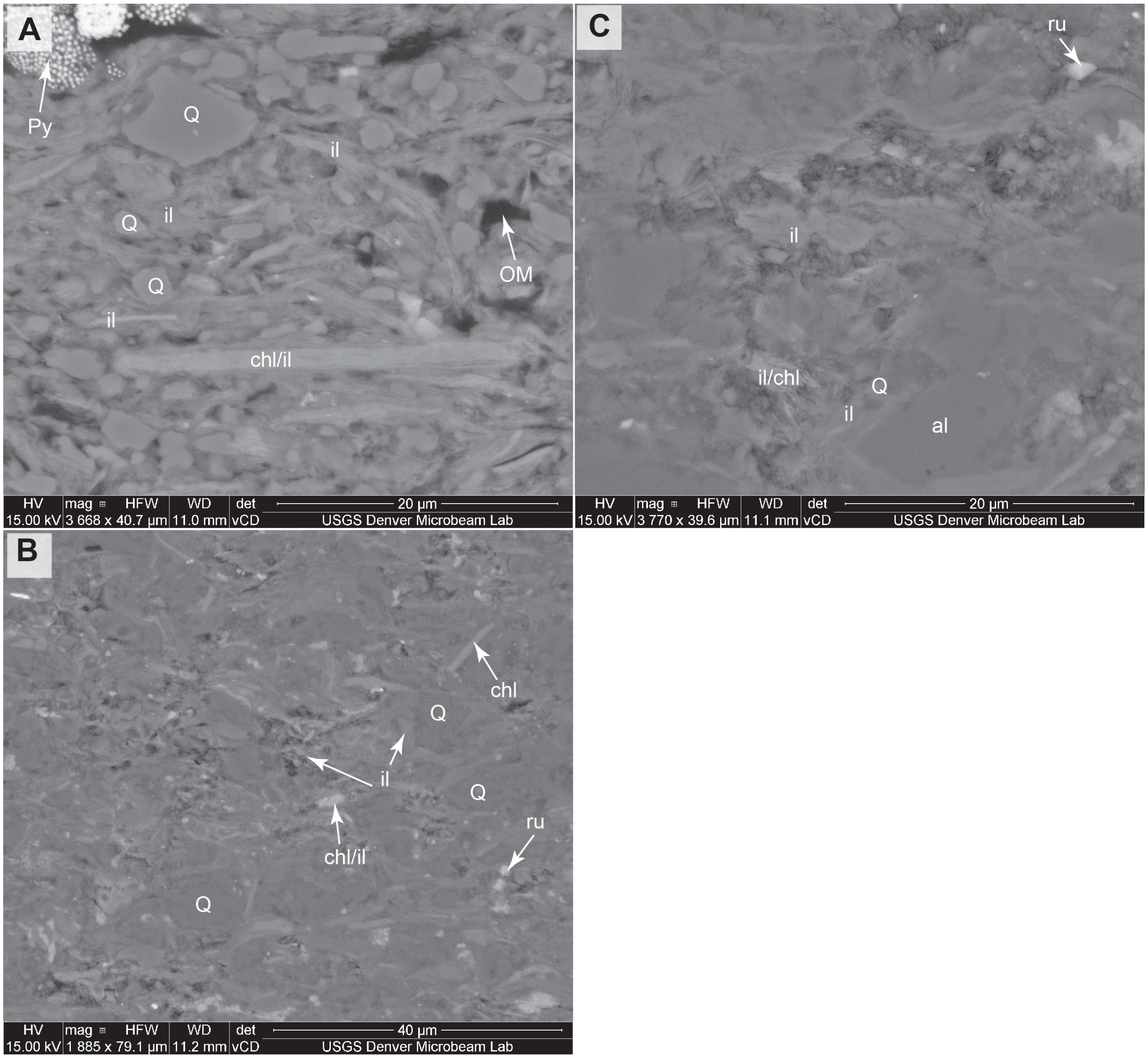

Figure 3: Scanning Electron Microscope back-scatter electron images of the Tøyen Shale Formation facies showcasing the mineralogical make-up of A) facies 1, Py – pyrite framboids, Q – quartz grains, il – illite clay particle, chl/il – mixed chlorite and illite clays, OM – organic matter; B) facies 2, chl – chlorite clay particle, ru – rutile/titanium oxide mineral; C) facies 3, al – albte, il/chl – mixed illite and chlorite clay.

Facies Associations

Sedimentary facies that were recognized in the Tøyen Shale Formation were grouped into 3 facies associations based on their stratigraphic distribution, and are described below.

FA 1 - Organic Matter-enriched Laminated Siliciclastic Mudstones

The rocks in FA 1 consist primarily of dark gray siliciclastic mudstone with flakes of organic matter (facies 2) interbedded on a millimeter-scale with black siliciclastic mudstones with clay clast- and organic matter-enriched laminae of facies 1 (Fig. 4 A; 6 A). Discontinuous sub-millimeter laminae and lenses of massive quartz siltstone of facies 7 are common in this facies association (Fig. 4 B). The matrix of this FA is clay-rich and contains 5-10% of silt-size quartz and carbonate grains. Clay-clasts are common in beds of facies 1 (Fig. 4 C); the clay-clasts are lighter in color than matrix (see Schieber et al. 2010), lens-shaped and typically 100-500 μm or less long. In general, the facies comprising FA 1 lack any sedimentary structures, however normally graded bed sets comprised of facies 7, 2 and 1 (from bottom to top) (Table 1) commonly with scour surface at the bases of each set and low-angle ripple cross-lamination were observed in several samples (Fig. 4 A, D). Millimeter-thick beds of phosphate-rich bioclastic wacke- to packstone (facies 5, Table 1) and glauconite- and phosphate-rich bioclastic packstone (facies 6; Table 1) occur in places (Fig. 5 A, B; Fig. 6). The phosphate-rich bioclastic wacke- to packstone beds are commonly interbedded with mudstones on a millimeter scale and show diffuse upper and lower contacts. The beds of glauconite- and phosphate-rich bioclastic packstone are typically up to several millimeters thick, and show a sharp scouring basal contact and a gradational upper transition into the overlying facies. Collapsed agglutinated benthic foraminifera tests occur locally within the organic-rich intervals (Fig. 4 E) exclusively in the Fågelsångdalen drill core succession. Other bioclasts identified in this facies association include organic-walled acritarch microfossils and fragments of graptolites. FA 1 is bioturbated (BI~2-3, see Droser and Bottjer 1986), and contains *Planolites* and *Phycosiphon incertum* burrows (Fig. 4 F). This facies association contains abundant millimeter to centimeter-size barite concretions/pseudomorphs and horizontal calcite-filled fractures with cone-in-cone structures occuring at select intervals. Organic matter is arranged in wispy parallel to bedding streaks and is commonly limited to the clay-clast-rich sub-

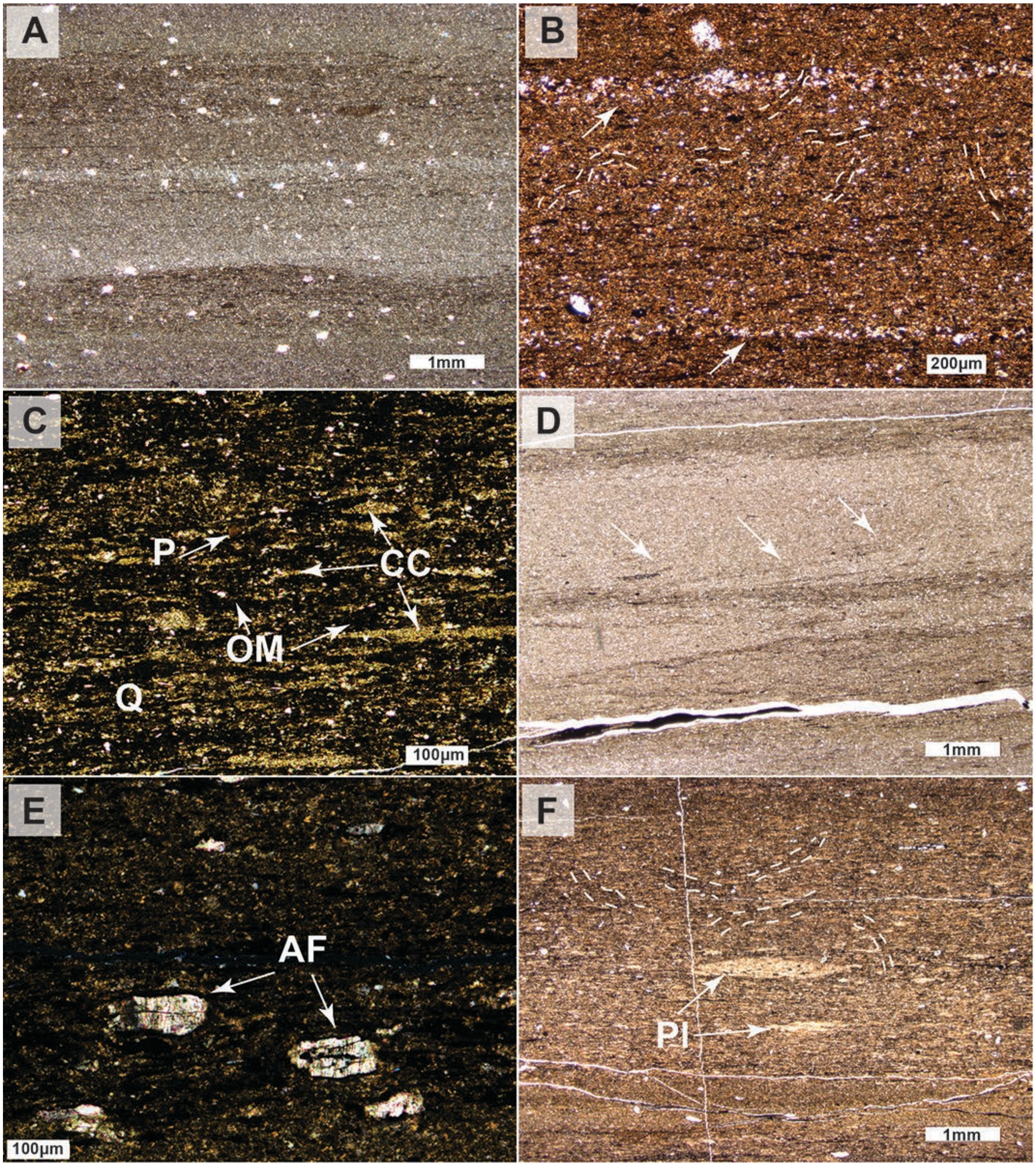

Figure 4: Sedimentological features of facies association 1. A) Normally graded lamina of FA 1 consisting of facies 7, 2 and 1 with a scour surface at the base of facies 7; B) Siliciclastic siltstone laminae of facies 7 in FA 1 with *Phycosiphon incertum* fecal traces outlined in dashes; C) Organic-rich siliciclastic mudstone of facies 1 with clay clasts (CC), phosphate (P) and quartz (Q) grains; D) Low angle ripple cross-lamination in facies 2; E) Agglutinated foraminifera (AF) in facies 1; F) Horizontal *Planolites* (PL) burrows (pointed by arrows) and *Phycosiphon incertum* fecal traces (outlined in dashes).

millimeter to millimeter thick beds. Total organic content ranges between 0.25-1.92% in the siliciclastic mudstone with flakes of organic material (facies 2), and is likely higher than 1.92% in organic-rich siliciclastic mudstone with clay-clasts (facies 1) based on visual estimation.

FA 2 – Quartz and Carbonate Silt-rich Faintly Bedded to Massive Siliciclastic Mudstones

The quartz and carbonate silt-rich faintly bedded to massive siliciclastic mudstones facies association comprises interbedded on several centimeter- to decimeter-scale siliciclastic mudstones with flakes of organic matter (facies 2) and carbonate-rich massive siliciclastic mudstones (facies 3) (Fig. 5 C, D). Light gray carbonate-rich mudstones of facies 3 comprise the bulk of FA 2 making up up to 70% of the succession (visual outcrop-based estimation), while dark gray siliciclastic mudstones of facies 2 make up roughly 30% of the total rock volume (Fig. 6 B). Discontinuous sub-millimeter-thick laminae of massive siliciclastic siltstone of facies 7 occur in places. Sedimentary structures are nearly absent in this facies association, however, rare remnants of planar bedding can be seen in places due to the contrast in organic matter content and the difference in grain size. The ichnofauna includes up to 3 millimeters-wide and 1 millimeter-tall compressed *Planolites* burrows with a lighter and more fine-grained fill than matrix, and sub-millimeter-size *Phycosiphon incertum* fecal strings occur and are oriented primarily sub-vertically (Egenhoff and Fishman 2013). This facies association contains abundant pyrite concretions and pyritized burrows as well as scattered euhedral, anhedral and needle-like pyrite crystals. Barite concretions/pseudomorphs ranging in size from several millimeters to centimeters in diameter are also common. Visible in thin section, organic matter is arranged in parallel to bedding flakes. This FA is characterized by the range of TOC from 0.16 to 1.92%.

FA 3 - Mixed Carbonate-Siliciclastic Massive Mudstones

The mixed carbonate-siliciclastic massive mudstones facies association is represented by interbedded in outcrop light gray carbonate-rich massive siliciclastic mudstone (facies 3; Fig. 5 D) and tan to orange massive carbonate mudstone (facies 4; Fig. 5 E, F). Both of these facies comprise roughly equal portions of FA 3 by volume (Fig. 6 C). The beds of each facies have gradational lower and upper contacts and typically range in thickness from several centimeters to decimeters. The mudstones in this FA appear

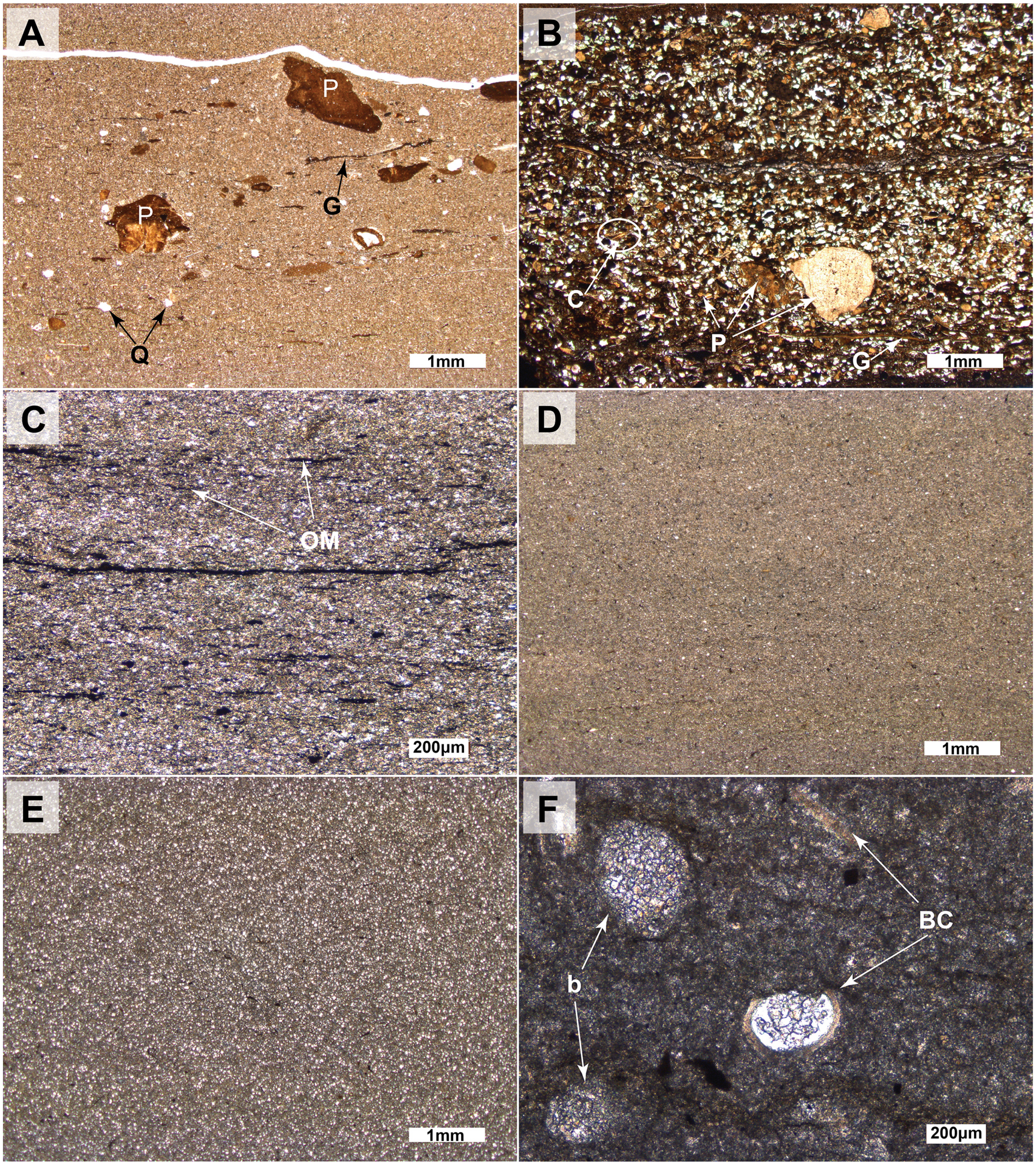

Figure 5: Sedimentological features of the Tøyen Shale Formation facies. A) Phosphate-rich bioclastic wacke- to packstone of facies 5, P – phosphatic grains, Q – quartz grains, G – graptolite fragments; B) Glauconite- and phosphate-rich bioclastic packstone, where slightly greenish white grains are glauconite grains overgrown by calcite, C – conodont fragments, P – phosphatic grains, G – graptolite fragments; C) Facies 2 - siliciclastic mudstone with flakes of organic matter (OM); D) Carbonate-rich massive siliciclastic mudstone of facies 3; E) Massive bioturbated carbonate mudstone of facies 4; F) Carbonate mudstone of facies 4 with recrystallized burrows (b) and bioclasts (BC).

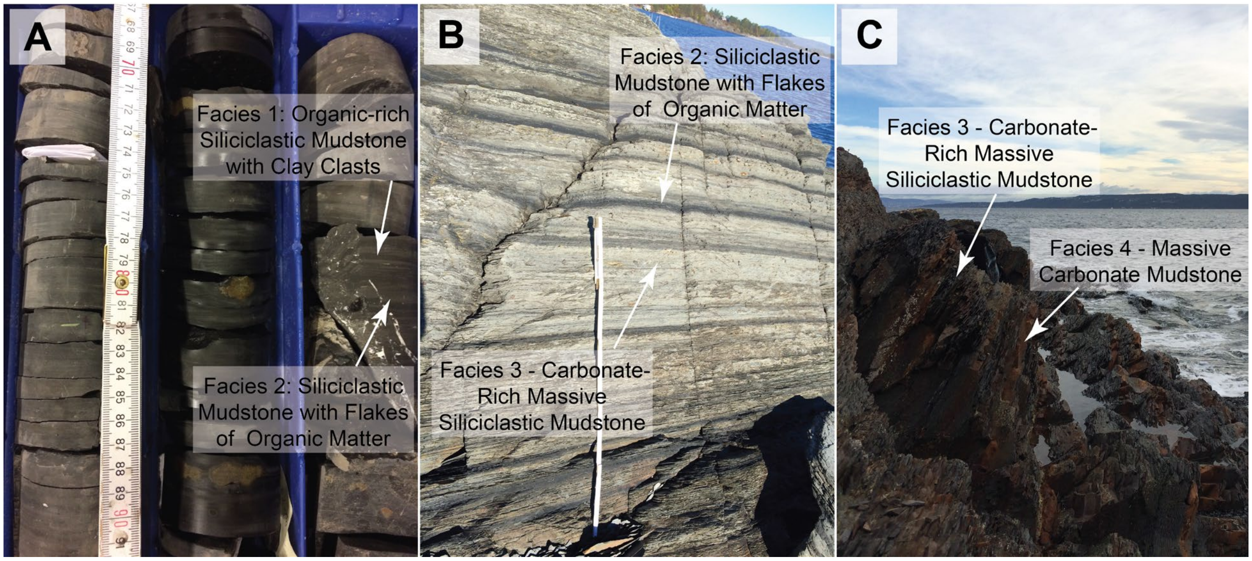

Figure 6. Facies associations defined within the Tøyen Shale Formation. A) Facies association 1 in the Lerhamn core; B) Facies association 2 in the Sl-6 outcrop section; C) Facies association 3 in the Sl-4 outcrop.

entirely structureless and lack any distinct ichnofaunal signatures; however, rare round recrystallized burrows (Fig. 5 F) were found in the carbonate mudstone facies. This FA is rich in quartz and carbonate silt, and contains abundant 1-3 centimeters in diameter barite concretions/pseudomorphs throughout the entire section. Typical bioclasts include 0.1-0.3 millimeters in diameter acritarchs, brachiopods and graptolites (Fig. 5 F). Bioclasts are rare in this facies association and are commonly recrystallized. Stylolitization of carbonate units has developed locally. Total organic content of this FA is 0.16-0.39% or less (based on the measurements from facies 3).

Stacking Patterns, Facies Architecture and Distribution

Stacking Patterns

Distinct stacking patterns are recognized within the Tøyen Shale Formation on two different scales, here referred to as “small-” and “large”-scale. Arranged in a repeating vertical order, the small-scale stacking pattern is reflected within individual facies associations and typically shows a 1-25 centimeter-thick shallowing- upward motif (Fig. 10 A, B). The large-scale stacking pattern generally manifests itself in shallowing- or rarely deepening-upward, 0.2-6 meter-thick cycles that span over several sets of small-scale stacking patterns. Shallowing-upward motifs contain a high amount of distal facies in the lower part, and more proximal facies towards the top of the succession. Likewise, a deepening-upward motif shows the reverse facies order. The large-scale cycles are correlatable across the study area over distances of up to several hundreds of kilometers (Fig. 7).

Facies Architecture and Distribution

Facies associations within the Tøyen Shale Formation show a distinct spatial and stratigraphic distribution (Fig. 7). FA 1, for example, only occurs in the Fågelsångdalen and Lerhamn drill cores in southern Sweden, and is absent in the Oslo Region and Mt. Hunneberg localities. FA 2 and FA 3 occur in all studied sections throughout the study area. Based on the stratigraphic distribution of facies associations and the stratal stacking patterns in the Oslo Region, the Tøyen Shale Formation can be subdivided into two distinct stratigraphic intervals – the lower and the upper. The lower interval is 8.5 to 11 meters-thick and is dominated by FA 3 in the basal 4-5 meters and top 1-2 meters, with FA 2 typically present in the middle segment. The lower interval consists of likely 3 large-scale stacking patterns. The upper interval can be distinguished from the underlying interval by the near complete absence of FA 3 throughout the section except for the topmost 1-2 meters, where FA 3 is present below the sharp contact with the overlying Huk Formation. Besides that, the upper interval is comprised entirely of FA 2 and

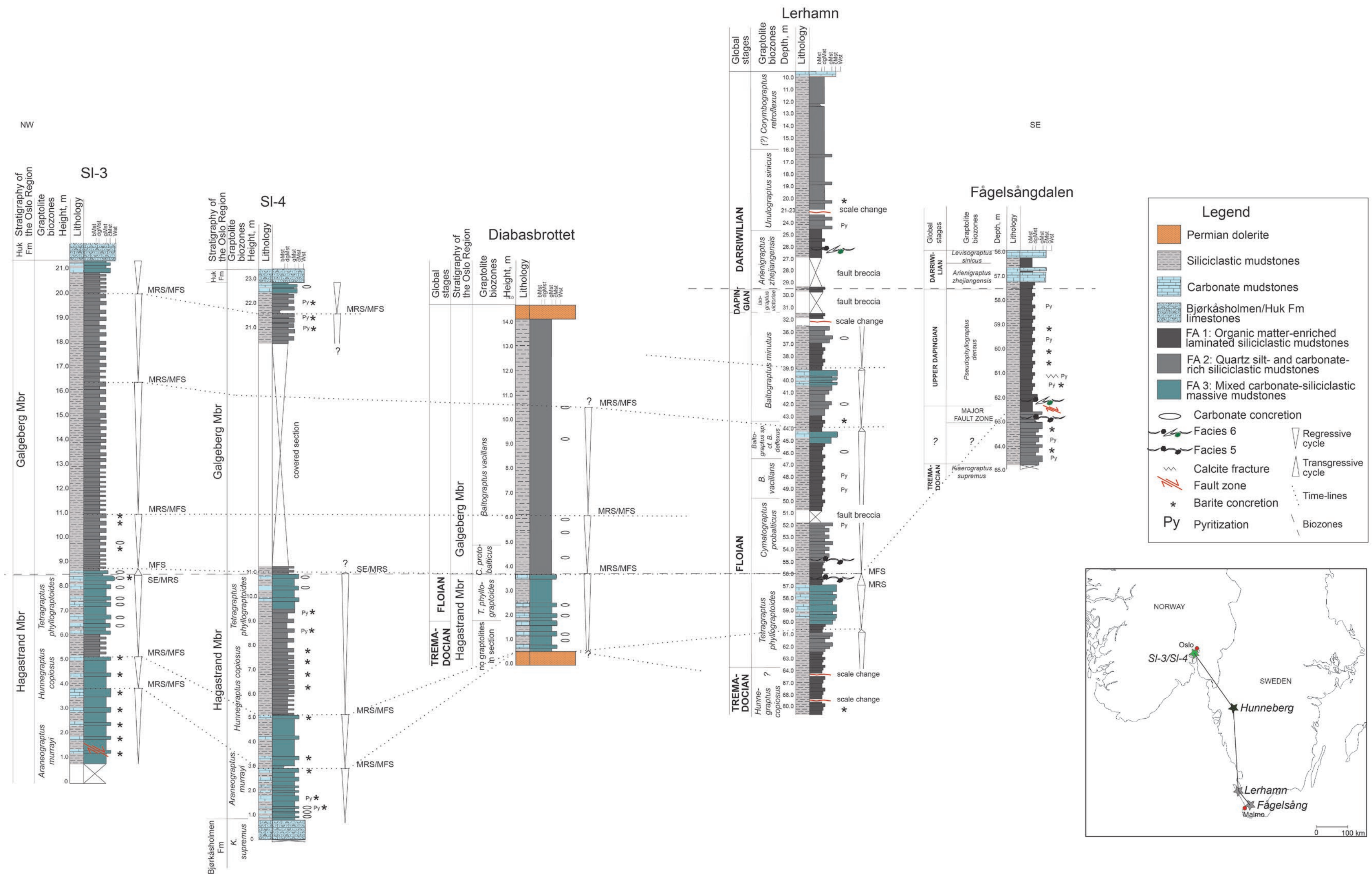

Figure 7: Regional stratigraphic correlation of sections from northwest to southeast across the study area; MRS – maximum regressive surface, MFS – maximum flooding surface, SE – subaerial exposure.

contains 4 or more large-scale stacking patterns. Total measured thickness of the upper interval ranges from 12 to 15 meters.

The same stratigraphic subdivision is present at the two Mt. Hunneberg localities, however, the upper interval at the Diabasbrottet outcrop exhibits concretionary growth associated with the carbonate-rich mudstone beds (facies 3), while none to very few concretions were observed in the same stratigraphic interval in the Slemmestad outcrops (Fig. 7).

The boundary between the lower and the upper stratigraphic intervals within the Tøyen Shale Formation in the Oslo Region and at Mt. Hunneberg corresponds to the top of the *Tetragraptus phyllograptoides* biozone (Egenhoff and Maletz 2012; Calner et al. 2013). This surface is marked by an irregular "wavy" top of a massive carbonate mudstone bed of facies 4 (Fig. 8).

The top of *T. phyllograptoides* biozone can be traced across the study area to the Lerhamn core in Scania, southern Sweden; however, the distribution of facies associations observed in the Oslo Region and Mt. Hunneberg no longer exists in Scania. In contrast to its northwestern counterparts, the Lerhamn succession is composed of roughly 55 meters of mainly FA 1 interbedded with 1 to 3 meter-thick units of FA 2 and FA 3. The top of the Lerhamn core section comprises 13 meters of FA 2 capped by 20 centimeters of recrystallized carbonate mudstone of the Komstad Limestone Formation. Seven large-scale stacking patterns were recognized in the Lerhamn succession in the interval from 26 to 64 meters; however, this number has to be treated with caution due to faulting in this area causing potential discrepancies between the measured and true section thicknesses.

The Fågelsångdalen succession shows a two-part distribution of facies associations where FA 2 occupies the basal 1.80 meters, and FA 1 straddles the top 5.5 meters sharply overlain by the Komstad Limestone Formation. Although the small-scale stacking patterns have the same expression in the Fågelsångdalen core as in every other studied section, the large-scale stacking patterns are not as well defined here. Similarly to the Lerhamn core, Fågelsångdalen is also highly faulted and brecciated, therefore, it is possible that some intervals within the middle portion of this sections could be faulted out, as also indicated by several missing graptolite biozones and an abnormally short Tøyen Shale Formation section.

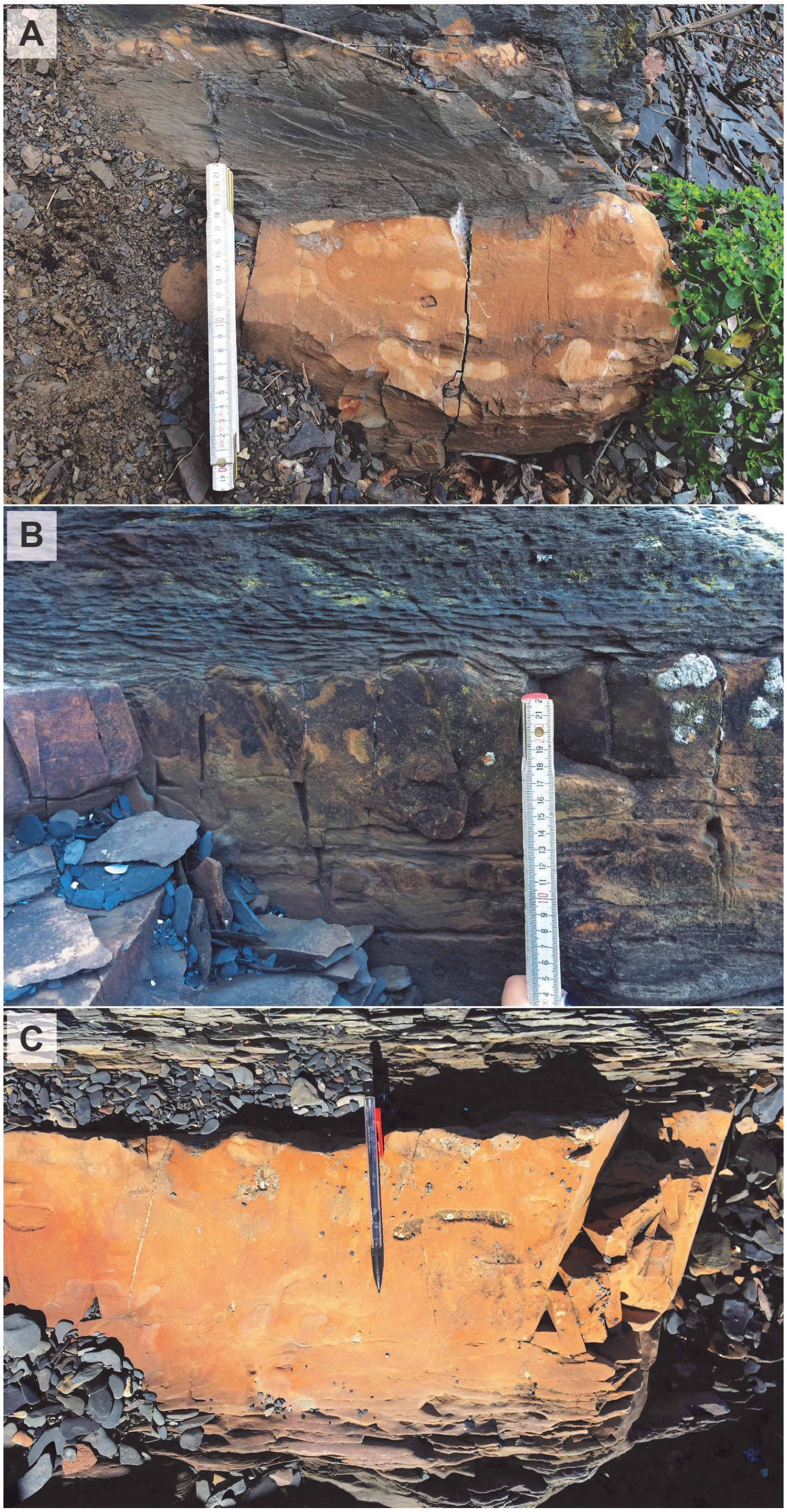

Figure 8: Karst in Slemmestad outcrops Sl-3 (A), Sl-6 (B) and Sl-4 (C). Note the irregular wavy top surface of the orange-color limestone bed and onlapping gray mudstone on top of it.

Total Organic Carbon and Rock-Eval Analysis

Ten samples from the Sl-4 and Sl-6 outcrops in Slemmestad locality near Oslo were chosen for TOC analysis and Rock-Eval pyrolysis to obtain TOC values and an array of other geochemical parameters (Table 2). Geochemical analysis was performed in order to determine the hydrocarbon potential and aid sedimentological differentiation of mudstone facies. Cross-plotted oxygen and hydrogen indices obtained from the pyrolysis of the 10 samples indicate kerogen type IV (Fig. 9). T_{max} values measure in the range of 306-319°C. Resulting TOC values range from 0.16% to 0.39% in facies 3 and from 0.25% to 1.92% in facies 2. A clear trend between TOC values and sample position within the small-scale stacking pattern can be observed: TOC values decrease towards the top (Fig. 10 B). On a formation scale, TOC values increase upward from 0.32% at 5.90 meters to 1.92% at 21.50 meters in the Sl-4 section, and then decrease from that point upwards (measurements of different facies compared separately).

Table 2. Results of TOC and Rock-Eval analyses. S1 – volatile hydrocarbon (HC) content, mg HC/g rock; S2 – remaining HC generative potential, mg HC/g rock; S3 – carbon dioxide content, mc CO_2/g rock; T_{max} – temperature at which the maximum rate of hydrocarbon generation occurs in a kerogen sample during pyrolysis; HI – hydrogen index (S2x100/TOC), mg HC/g TOC; OI – oxygen index (S3x100/TOC), mg CO_2/g TOC.

Sample #	Sample id	Facies	LECO TOC	S_1	S_2	S_3	T_{max} (°C)	HI	OI
1	Sl-4-4b	3	0.16	0.30	0.09	0.12	318.70	55.56	74.07
2	Sl-4-5b	2	0.32	0.35	0.07	0.04	315.40	21.81	12.46
3	Sl-4-7	2	0.25	0.45	0.07	0.12	-	27.78	47.62
4	Sl-4-9	3	0.39	0.62	0.06	0.17	307.50	15.50	43.93
5	Sl-4-10	2	1.92	0.74	0.06	0.26	319.00	3.13	13.54
6	Sl-4-11	3	0.16	0.37	0.03	0.28	306.40	18.29	170.73
7	Sl-6-1	2	1.06	0.43	0.04	0.21	-	3.77	19.81
8	Sl-6-2	3	0.24	0.32	0.05	0.14	316.80	21.19	59.32
9	Sl-6-5	2	0.32	0.34	0.04	0.06	310.70	12.42	18.63
10	Sl-6-6	3	0.19	0.33	0.04	0.20	317.80	21.16	105.82

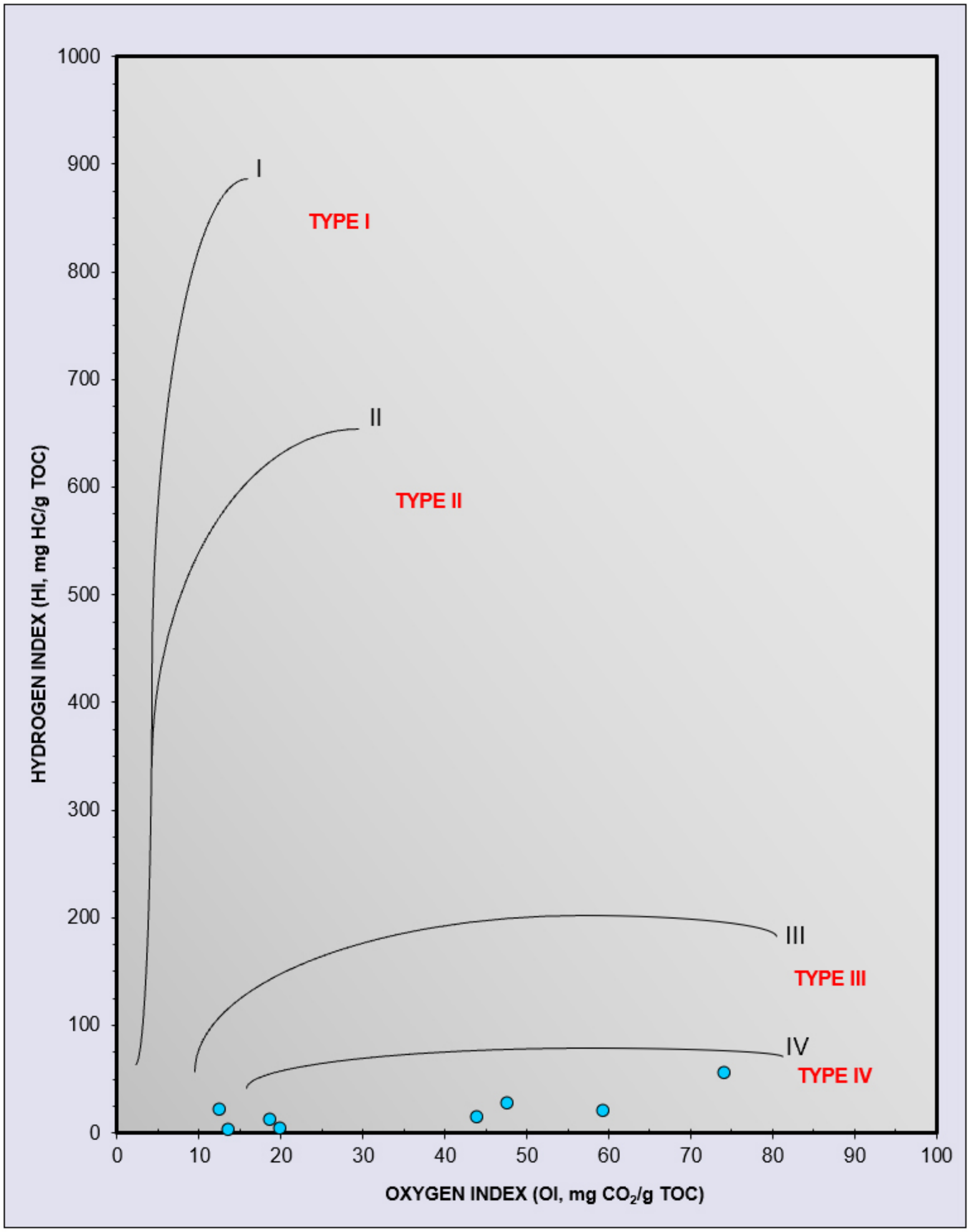

Figure 9: Van Krevelen diagram with cross-plotted oxygen (OI) and hydrogen (HI) indices values indicating kerogen type IV (inert kerogen) in the Tøyen Shale Formation samples.

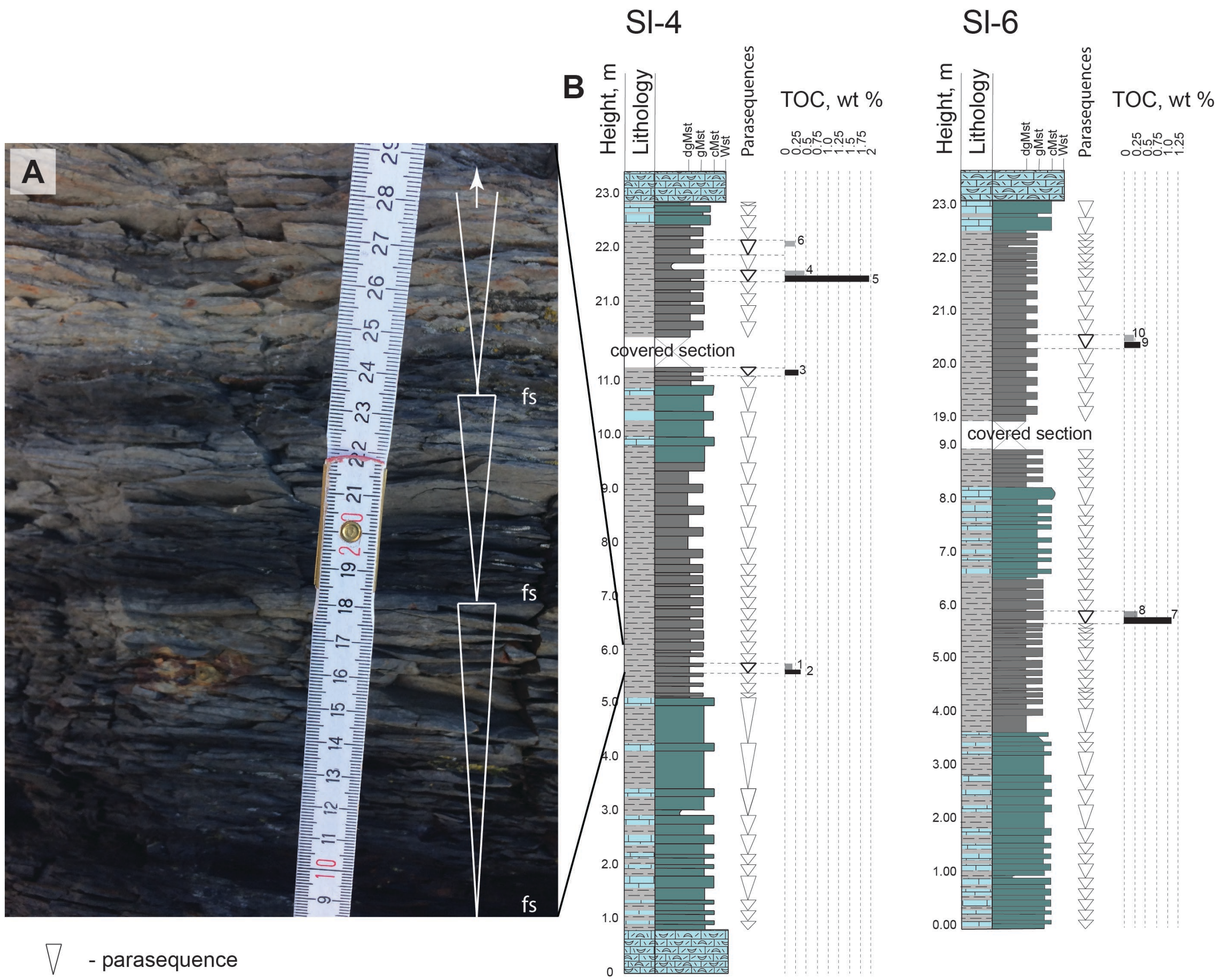

Figure 10: Small-scale stacking pattern/parasequences defined within the Tøyen Shale Formation. A) Small-scale stacking pattern/parasequence expression in outcrop; B) TOC distribution on a parasequence scale; black bars represent facies 2 samples, and gray bars represent facies 3 samples; numbers 1 to 10 next to the TOC bars correspond to the sample numbers in Table 2.

INTERPRETATION

Facies Associations and Depositional Model

The detailed analysis of sedimentary facies, their associations, stacking and distribution provided the basis for the understanding of the Tøyen Shale Formation depositional settings. The overall fine-grained nature of the sediment indicates deposition in an offshore environment, most likely in a medial to distal shelf position. This portion of the shelf is herein interpreted to be composed of 3 depositional zones each characterized by distinct facies associations. The organic-rich FA 1 occupies the most distal part of the depositional system, FA 2 straddles the intermediate zone, and the more silt- and carbonate-rich FA 3 takes up the relatively proximal position on the shelf transect and represents the zone of siliciclastic and carbonate mixing (Fig. 11).

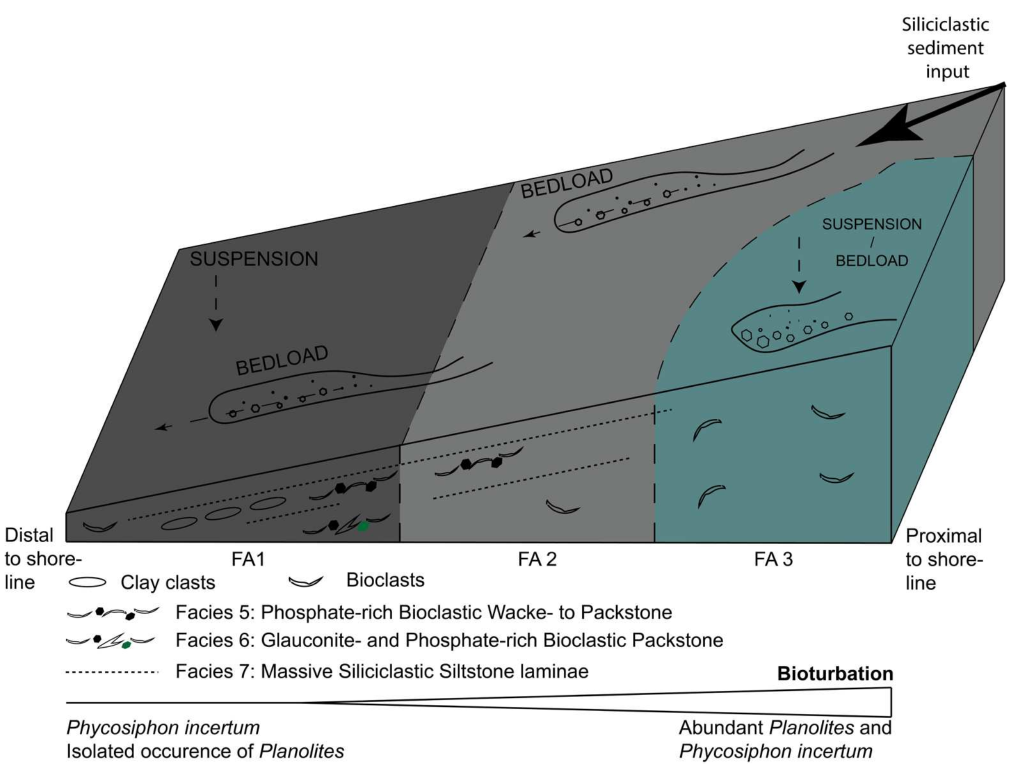

Figure 11: Proximal to distal transect displaying depositional zones and processes of the Tøyen Shale Formation. The low-inclined depositional profile is subdivided into 3 depositional zones, each one characterized by one specific facies associations.

FA 1 is interpreted to reflect the deposition on the most distal part of the system as it is composed of the most fine-grained deposits within the entire Tøyen succession. It is likely that only minor amounts of coarse-grained sediment were transported to this part of the shelf, leaving clay, mud and some silt grains the primary constituents in such a distal setting. Comprised of normally graded packages of intercalated facies 7, 2 and 1, FA 1 most likely represents storm-induced sediment transport and deposition by bed-load processes as indicated by common scouring surfaces, ripple structures, grading of beds and irregular in thickness and lateral continuity siltstone laminae and lag deposits of facies 5 and 6. Moreover, the presence of clay-clasts indicates up-dip rip-up of partially consolidated water-rich mud by currents (Schieber 2009) and subsequent transport and re-deposition by bed-load processes in an overall sediment-starved environment. Sporadic coarse-grained lamina of phosphate- and glauconite-rich bioclastic wacke- to packstones of facies 5 and 6 likely represent deposition by a high-energy event, for example, a storm, and are interpreted as lag deposits. The muddy matrix within these lamina was either captured during the deposition or infiltrated after the waning of the flow. Extensive bioturbation reflected in *Phycosiphon incertum* fecal strings and *Planolites* burrows in places as well as presence of agglutinated benthic foraminifers' tests point to relatively well-oxygenated bottom water conditions even in the deep portion of the shelf (but see Leiter and Altenbach, 2010).

FA 2 occupies the intermediate zone on the depositional profile and most likely represents slightly higher energy and shallower water conditions than FA 1 as indicated by higher quartz and carbonate silt content and the bioturbation index of 3 to 5. Although distinct sedimentary structures are rarely preserved in this facies association, the presence of low-angle ripple cross-lamination composed of silt- and organic-matter-rich laminae indicates migration of ripples during bed-load transport (Schieber et al. 2007; Schieber and Southard 2009) that were most likely deposited during intermittent pulses of sediment influx through high-energy events. Times of relatively quiet conditions that occurred in-between the high-energy events, allowed for settling of fine-grained clay particles and the organics, or deposition by weak low-density currents. Siltstone lamina as well as phosphate-rich bioclastic wacke- to packstone laminae were recorded in FA 2 and similarly to the ones observed in FA 1 interpreted as storm-derived lag deposits. This laminae, however, tend to have diffuse contacts rather than scouring, which is attributed to a higher degree of bioturbation compared to FA 1. Intense burrowing therewith likely indicates well-oxygenated conditions at the sea-floor which is also reflected in the diversity of burrows and fecal strings. The most proximal depositional zone is characterized by carbonate-dominated deposits of FA 3. Identification of the depositional processes is complicated because of complete reworking of the sediment by bioturbation; however, the dominance of carbonate mud in this facies association can be explained by suspension settling or by bed-load transport of carbonate mud (Schieber et al. 2013), likely from more proximal areas of the shelf. It is most likely that the change in depositional lithologies from the carbonates to the siliciclastics within FA 3 reflects the position of the shelf where offshore transport of carbonate largely stops, and mostly siliciclastic deposition prevails further offshore. The rocks comprising FA 3 are thoroughly bioturbated, which indicates that conditions on the sea-floor during deposition were likely well-oxygenated.

Sequence Stratigraphy

The sequence stratigraphic interpretation of the Tøyen Shale Formation is based on the character of vertical repetition of small- and large-scale stacking patterns primarily in the Oslo region (Fig. 7). Sequence stratigraphic subdivision of the Fågelsångdalen and Lerhamn core sections was performed with lesser precision and on select intervals because of abundant faulted sections. The small-scale shallowing-upward stacking pattern likely represents the highest-order cyclicity within the Tøyen Shale Formation. This stacking pattern shows a clear progradational nature which is reflected in the upward facies change from distal to proximal. Each of these high-frequency cycles is bounded by a surface across which an abrupt increase of paleo water-depth is observed, herein interpreted as a marine flooding surface, and represents one parasequence (Van Wagoner et al. 1988) (Fig. 10). The internal lateral and vertical variability within each parasequence and their thicknesses most likely represent a function of sediment supply, local erosion or non-deposition. Unlike classical coarse-grained sedimentary systems where typical parasequences can reach up to 100 feet (~33 meters) (Mitchum and Van Wagoner 1990), in fine grained sediment-starved systems like the Tøyen Shale Formation parasequences are expressed in much thinner packages (Bohacs 1998; Borcovsky et al. 2017).

The large-scale stacking pattern consisting of vertically stacked parasequences is interpreted to reflect a lower-order cyclicity. Shallowing-upward large-scale stacking patterns consist of either aggradational, e.g. interval from 3.8 to 5 meters in the Sl-3 section (Fig. 7), or progradational, see interval from 8.7 to 20 meters in the Sl-3 section (Fig. 7), parasequence sets and define regressive deposits (e.g. Embry 2002). The rarely preserved deepening-upward pattern, for example the interval from 8.5 to 8.7 meters in Sl-3 section (Fig. 7), represents transgressive deposits.

The base of the Tøyen Shale Formation has been interpreted as a transgressive surface (Egenhoff et al. 2010), marking the top of the lowstand systems tract represented by the lower two thirds of the Bjørkåsholmen Formation. From there on upwards, the lower 2 large-scale stacking patterns in the Hagastrand Member of the Tøyen Shale Formation represent the regressive cycles that are bounded by the maximum flooding surface amalgamated with the maximum regressive surface (Catuneanu et al. 2002). The overlapping of these two surfaces can be explained by the poor preservation or complete missing of the transgressive cycles. The lower 2 regressive cycles of the Hagastrand member are not well exposed in the Diabasbrottet succession at Mt. Hunneberg in part due to the cross-cutting and removal of the section by Permian dolerite intrusions.

Likewise, the Lerhamn and Fågelsångdalen sections do not show any distinct evidence of the lower 2 regressive cycles in the Hagastrand member; while it could have not been recovered in the Fågelsångdalen core as the basal contact of the Tøyen Shale Formation was not penetrated with the drill core, in the Lerhamn core it could have been faulted out as indicated by several missing graptolite biozones and presence of faults and brecciated intervals. The third large-scale shoaling-upward stacking pattern is interpreted as a third regressive cycle with a subaerial unconformity in the Oslo Region, and a maximum regressive surface at Mt. Hunneberg and in Scania at the top. The third maximum regressive surface is likely to represent the lowest position of relative sea-level recorded in the rocks of the Tøyen Shale Formation, as indicated by a very irregular, wavy karstified surface at the top of this cycle in the Slemmestad sections (Fig. 8), and a prominent carbonate-dominated top of the regressive cycle in the

Diabasbrottet and Lerhamn successions. Although the subaerial unconformity most likely coincides with the maximum regressive surface as it appears in the Slemmestad outcrops, these two surfaces are likely not time-equivalent, because subaerial erosion forms first during a sea-level fall, continues to prograde basinward as the sea-level continues to fall, and reaches its maximum at the end of the sea-level fall and the beginning of a sea-level rise, which is what forms the maximum regressive surface (Embry 2002). It is, however, unclear how much time is missing between the initial subaerial exposure and the onset of the transgression in the Oslo region.

A switch from carbonate- to siliciclastic-dominated sedimentation in the Galgeberg member is associated with an overall deepening of the depositional system, indicated by the predominance of siliciclastic facies. This part of the succession is interpreted to consist of 4 regressive cycles that are, similarly to the lower portion of the Tøyen Shale Formation, bounded by amalgamated maximum flooding and regressive surfaces in the Oslo region. Interpretation of small-scale parasequences and large-scale cycles and sequences in the Hunneberg succession is complicated by the partial contact metamorphism of the upper portion of the exposed section and scarcity of biostratigraphic information due to the difficulty to recover biostratigraphically relevant graptolites from this portion of the succession (Egenhoff and Maletz 2012). Nevertheless, at least two regressive cycles can be defined based on the development of carbonates and associated concretionary growths (Fig. 7), the concretions having been suggested to indicate breaks in sediment accumulation associated with the formation of transgressive surfaces (Macquaker and Jones 2002). Such surfaces, therefore, can be used to define the large-scale upward-shoaling regressive cycles. In the Lerhamn core section, 3 incomplete and 1 complete sequences comprised of regressive and transgressive cycles were interpreted based on the shallowing- and deepening trends reflected in the large-scale stacking patterns. The bounding surfaces of these sequences can be correlated with the Diabasbrottet and Slemmestad sections; however, it is unclear how these sequences relate to the Fågelsångdalen core section which does not show any apparent sedimentological or large-scale stacking trends. The Fågelsångdalen succession does, however, show the high-frequency cyclicity reflected in shoaling-upward parasequences, repeatedly stacked on top of one another. Similarly to other studied sections, the

Fågelsångdalen is interpreted to reflect the two-part subdivision into the lower Hagastrand and upper Galgeberg members of the Tøyen Shale Formation. The exact position of the lower to upper member transition in the Fågelsångdalen core cannot be identified precisely due to faulting and brecciation of the prospective transition zone, but it is most likely to be situated on top of the FA 2 at 62.50 meters, based on the lithology and biostratigraphy of this section. Laterally varying amount of carbonates from being absent in the Slemmestad sections to occurring at 0.5-1 meter-thick intervals in the Fågelsångdalen core can be related to the presence of a potential source of siliciclastic sediment near the present Oslo region that shut down the production of carbonate material (Wilson 1975). Being farther from the clastic sediment source, distal parts of the shelf were more prone to depositing carbonates.

Overall, the Oslo region part of the system is interpreted to have been deposited in a proximal setting relative to Mt. Hunneberg and the southern Sweden part. This is evident from 1) the absence of the most distal deposits (organic-matter- and clay-clast-rich facies 1 of FA 1) in the Oslo region, pointing to a higher-energy and better oxygenation of the depositional environment than at Mt. Hunneberg and in Scania; 2) the absence of carbonate facies in the Galgeberg member in the Oslo sections, which implies that a source of siliciclastic sediment was present nearby, thus preventing the development of a carbonate factory, and 3) the presence of a surface of subaerial exposure in some of the Slemmestad sections, confirming that this area must have been situated further up-dip than Mt. Hunneberg and Scania in order to be exposed during a relative sea-level fall.

Accumulation and destruction of organic matter

The results of the geochemical analysis support the relative visual estimation of TOC based on color of rocks: the darker the hand sample is, the higher the TOC content. It is therefore assumed that the dark-gray to black color of siliciclastic mudstones of facies 1 contain higher than 1.92% of total organic carbon, while the carbonate mudstones of facies 4 would most likely yield less than 0.16% TOC content. Cross-plotted on the Van Krevelen diagram hydrogen and oxygen indices yielded Kerogen type IV (inert) (Fig. 9) which indicates that the organic matter in the Oslo region samples is thermally immature and was likely extensively oxidized during deposition (Peters et al. 2012). Nevertheless, the organic matter enrichment trend towards the bases of small-scale stacking patterns likely represents the link between the depositional environment and processes and accumulation of TOC within parasequences. It is likely that organic matter was preserved by episodic high-energy events which deposited clay-clast-rich and ripple-cross laminated laminae of facies 1 and 2. Entrapment and burial of organic matter within these laminae contributed to protecting the organics from exposure to oxidizing agents, such as bioturbating organisms. Since very little organic matter is contained within the completely bioturbated structurless facies as opposed to less bioturbated facies with abundant event laminae, bioturbation is interpreted to have played a major role in destruction of organic matter in the mudstones of the Tøyen Shale Formation. This interplay of the burial rate and destruction of organic matter by microorganisms is also reflected in the formation-scale variability in TOC values: the highest TOC accumulations were found in sections dominated by siliciclastic sediment input that created mostly high-energy conditions on the sea-floor conditions during deposition thereby not allowing substrate-feeding microorganisms to establish a habitat and rework the sediment.

DISCUSSION

Storm deposition on the Tøyen Shelf

The depositional model of the Tøyen Shale Formation shows three depositional zones, each characterized by a distinct facies association, two of them being comprised of siliciclastic mudstones, and one consisting of mostly fine-grained carbonates with some siliciclastic mudstones. In this model, storm deposition is evident mostly in the most distal of the three facies associations, which at first seems counter-intuitive. In a model that assumes a general decrease of depositional energy down-slope, the influence of storms should decrease the further the water-depth (or paleo-water-depth) increases. This is not the case for the Tøyen Shale Formation, and it requires some additional explanation.

The factor that seems to most heavily influence facies characteristics in the Tøyen Shale Formation is bioturbation. Typically for any depositional model, bioturbation is higher the closer the facies is deposited relative to the shoreline (e. g. Borcovsky et al. 2017). For the Tøyen Shale Formation this means that FA 3 and FA 2 experienced a much higher amount of burrowing than FA 1. Considering the potential preservation of facies 1 (exclusive to FA 1) and therewith the storm-produced laminae in the Tøyen Shale Formation, these distinct tempestite beds were preserved only in this distal depositional zone. Similar expressions of storms in other facies are burrowed through and, therefore, not preserved, so that no storm activity can be detected. This process has two consequences: (1) shales are seen as massive and not reflecting traces of life because the burrowing cannot easily, if at all, be identified in massive siliciclastic mudstones; as a result, deposition in an anoxic setting is assumed based on the lack of obvious burrows, yet the contrary is the case; and (2) storm deposits are only preserved once the burrowing depth decreases allowing storm deposits to be preserved; it is therefore likely that many siliciclastic mudstones were influenced by event deposition, though the massive nature of these rocks, which stems from burrowing, is seen as evidence that no storm has reached these depth. This assumption is most likely equally incorrect.

Storm Wave Base in Open Shelf Systems

On a modern open shelf in the southern US, Peters and Loss (2012) observed storm wave base to reach a maximum depth of around 250 meters. Based on the maximum modern shelf depth, which is around 200 meters (https://www.britannica.com/science/continental-shelf), all of the shelfal areas worldwide could be situated above storm wave base. Even at times of the highest sea-level stands during the Lower to Middle Ordovician (cf. Haq and Schutter 2008), it is possible that most, if not all, shelves were located within the depths of large storm-driven wave agitation. The Tøyen Shale Formation is, therefore, expected to have been deposited within water depths affected by storm waves. This is also reflected in the transition from siliciclastic to carbonate mudstones, a facies change that occurs in the modern Persian Gulf at about 15-50 meters water depth (cf. Purser 1973) which is significantly shallower than the potential depth of the storm wave base. It is, therefore, proposed that the storm wave base as currently used is a hypothetical depth that likely defines the preservation potential of sedimentary structures, rather than an actual depth characterized by a change in depositional processes. According to this study, the storm wave base cannot be recognized in the Tøyen Shale Formation because it may be located further offshore than the studied sections record.

A problem associated with placing the storm wave base in the rock record is the criterion applied to define such a theoretical surface. Based on the theory, storm waves should be reflected in some kind of wave-formed structure in the rock record (e.g. wave ripples, see Macquaker and Bohacs 2007; Wilson and Schieber 2014). Wave-formed structures are rare in siliciclastic mudstones, partly because these rocks are often reworked by thorough bioturbation that destroys all indicative structures. Remnants of structures that point to high-energy processes, nevertheless, occur relatively commonly in these rocks (e.g. Schieber 2003; Macquaker et al. 2010b; Borcovsky et al. 2017), but do not clearly indicate which process led to their formation – it could have been waves or currents, or a combined flow, initiated during coincident river flooding and storm activity (Ogston et al. 2000; Aplin and Macquaker 2011). The causing mechanism behind many sedimentary structures, e.g. clay clasts, therefore remains unclear, and so is the position of the storm wave base.

It can, therefore, be assumed that the largest part of continental shelves throughout Earth history was affected by storm waves. The variability we observe in shelfal siliciclastic mudstone successions today may largely reflect differences in burrowing activity and not necessarily changes in sedimentary processes. The implication is also that wave-enhanced sediment gravity flows (WESGFs), as suggested by Macquaker et al. (2010b), must have been able to transport mud out to any place on the shelf and beyond through most of Earth history. This argumentation is in agreement with our observations that current- and wave-induced deposition is common in many black shale units (e.g. Bakken, Woodford, Alum Shale; Schieber 2009; Borcovsky et al. 2017; Fishman et al. 2013; Egenhoff et al. 2015), and therefore played a major role in the transport and deposition of siliciclastic mudstone facies worldwide and throughout the rock record.

The carbonate-siliciclastic mudstone transition

Within FA 3, a distinct transition from carbonates on the proximal side to siliciclastics on the distal side is evident. This facies transition is present throughout all carbonate systems, and also typical for low-inclined types such as carbonate ramps (e.g. Burchette and Wright 1992). Nevertheless, even though this is such a well-known facies change its origin and the controlling processes behind this transition have not been well understood.

One possibility to approaching this facies transition is by looking into the rocks on both sides of that boundary and trying to see how absolute this transition is. The siliciclastic mudstones of FA 2 still contain a significant amount of carbonate, and equally do the carbonate mudstones of FA 3 contain clay. The transition is therefore not quite as absolute as often sketched: carbonate is still transported further distally than the carbonate-siliciclastic mudstone transition and incorporated into the siliciclastic mudstones there. The facies belt where carbonate mudstones prevail (FA 3) just defines the area where carbonate mud is always deposited by the processes that bring in this type of sediment. The question would be – what processes could that be?

If the carbonates are brought in by suspension clouds, then the carbonate-siliciclastic mudstone transition represents the boundary above which most carbonate particles have been deposited out of the water column and formed part of the surficial sediment on the ocean floor. On the one hand, if carbonate sediment is derived from suspension settling, the carbonate-siliciclastic mudstone transition is likely controlled by base-level fluctuations as well as distance from the carbonate-producing area where the carbonate mud is derived from and the proximity to the source of clastic sediment. On the other hand, if carbonate facies are a product of bed-load transport processes, then the change from carbonates to siliciclastics could be controlled by storm-induced currents on the deep shelf that are influenced by the Coriolis force. It is likely that bed-load transport in distal carbonate environments is to a large degree influenced by high-energy events, such as storms (e.g. Burchette and Wright 1992). Storm-induced currents deflect from perpendicular to near-parallel to the shoreline on their path offshore under the effect of the Coriolis force (Myrow 1992), thereby influencing how far fine-grained carbonate can be transported from the factory to the deep shelf. Nevertheless, the carbonate-siliciclastic transition may be controlled by a combination of these two mechanisms, suspension and along-shore bed-load transport of fine-grained carbonate material, including possible contributions of base-level change and lateral distribution of sediment point-sources.

Sequence stratigraphy

The sequence stratigraphic interpretation of the Tøyen Shale Formation and the regional correlation of sections show distinct stratal hierarchies comprised of likely 5th order cycles reflected in parasequences, and 3rd order regressive and transgressive cycles; 4th order cycles maybe recorded as parasequence sets in the Tøyen Shale Formation yet the signal is not very strongly if at all recorded. The development of parasequences (and maybe parasequence sets) could therefore have been largely controlled by climatic changes and local variability in sediment supply, while lower-order regressive and transgressive cycles could have formed as a response to higher-amplitude sea-level fluctuations. The number and timing of marine transgressions identified within the rocks of the Tøyen Shale Formation corresponds to the global eustatic sea-level changes suggested by Haq and Schutter (2008) (Fig. 12). According to these sea-level curve reconstructions, the Hagastrand member of the Tøyen Shale Formation, which spans roughly 9 million years in duration, consists of three 3rd-order sequences, each of them 2-3 myr in duration; the Galgeberg member, which was deposited in approximately 6 million years, comprises four sequences with 1.2-1.3 myr periodicities each. The sea-level curve of Haq and Schutter (2008) also suggest an average sea-level change of 50-100 meters during each 3rd-order cycle in the Early to Middle Ordovician, which can only be achieved by glacioeustatic controls (Pitman and Golovchenko 1983). The Early to Middle Ordovician, however, is known since decades as a greenhouse time (Crowell and Frakes 1970). This discrepancy between different literature sources resulted in intense discussions on the control mechanisms of the 3rd-order sea-level changes in a greenhouse world.

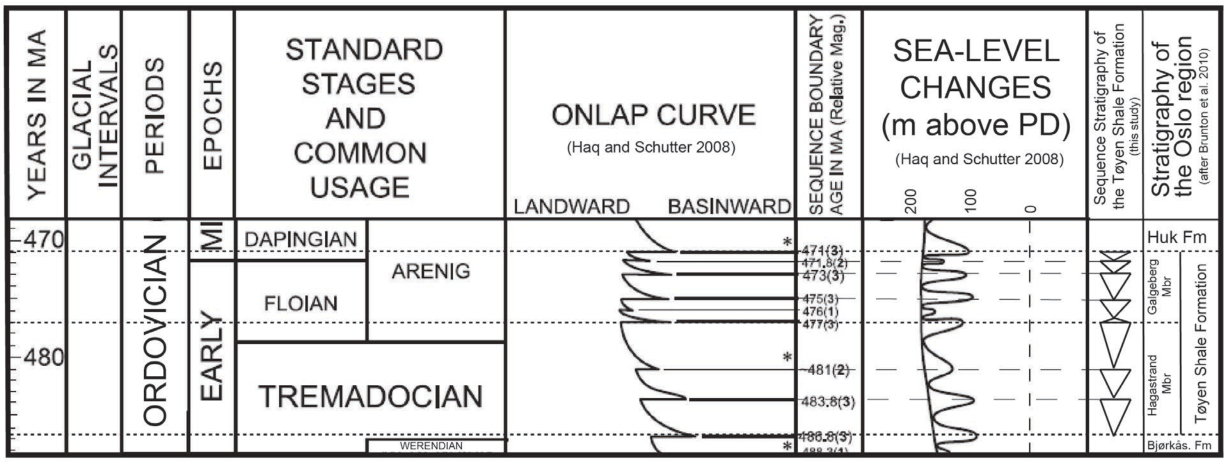

Figure 12: Sea-level and onlap curves suggested by Hag and Schutter (2008) correlated with the 3rd-order cycles identified within the Tøyen Shale Formation in this study. Oslo region stratigraphy modified after Brunton et. al (2010). PD – present day; Mag. – magnitude.

Turner et al. (2011), for instance, suggest the presence of an Early Ordovician polar ice cap and a polar front at latitudes of ~40ºS; in their interpretation, this Early Ordovician glaciation represents an amalgamation of existing small ice sheets. In the Early Ordovician, Baltica was located between latitudes 30ºS and 60ºS (Cocks and Torsvik 2005), and if Turner et al.'s (2011) implications for an Early Ordovician ice cap are valid it is likely that deposition of the Tøyen Shale Formation was influences by glacioeustasy.

Alternatively to glasio-eustasy, storage of lake-water and groundwater on continents is capable of producing sea-level fluctuations of Milankovitch periodicities during interglacial times (Jacobs and Sahagian 1993). Independent of the amount of ice at a time, the continental water storage capacity depends on the amount of precipitation, temporal variations in the sediments pore space volume, and changes in infiltration and discharge rates over time (Hay and Leslie 1990).

Tectono-eustasy has been also suggested to play a role in greenhouse sea-level changes. Cloetingh et al. (1985), for instance, proposed a model based on the interactions between regional changes in inplane stresses and the deflections of the lithosphere caused by sediment loading that accounts for potential sea-level changes of up to 100 meters, formerly attributed to exclusively glacio-eustasy (c.f. Pitman and Golovnichenko 1983). Such stress regime adjustments reflected in cycles of crustal compressions and relaxations have been documented in multiple basins worldwide (e.g. Megard et al. 1984; Wortel and Cloetingh 1981). It is unclear whether the Tøyen Shale Formation was affected by the abovementioned lithospheric stress reorganizations, however it seems more likely to have influenced 3rd-order sea-level fluctuations during the Tøyen Shale Formation, as opposed to glacio-eustasy. Other non-cyclic tectonic events, for example the collision of Baltica with an island arc which resulted in the uplift of the western Baltica margin and development of shallow-marine environment and deposition of the Bjørkåsholmen Formation (Greiling and Garfunkel 2007; Egenhoff et al., 2010), are unlikely to have influenced 3rd-order cyclicity throughout the entire Early to Middle Ordovician.

The number of sea-level changes recorded in the Tøyen Shale Formation corresponds to other well-documented and well-dated examples from elsewhere and, while that is not necessarily an argument (see Miall 1992), it does hint at the fact that whether those sea-level changes were glacially-, aquifer- or tectonically-driven, or else, they recorded consistent sedimentary signatures worldwide.

Implications for paleogeographic reconstructions

The model presented in this paper shows that the northwestern most sections around Slemmestad (Norway) are overall more proximal, and the cores from Sweden (Lerhamn, Fågelsångdalen) both represent a more distal setting containing FA 1. This facies distribution is in general agreement with reconstructions focusing on Baltica paleogeography undertaken by Cocks and Torsvik (2005) which show an island arc on Baltica's western margin. The model proposed in this study is also supported by several other reconstructions, e.g. the one from Greiling and Garfunkel (2007), and the general one by Blakey (2019) used in many geological reconstructions.

Greiling and Garfunkel's (2007) idea of an island arc colliding with Baltica during the upper Early

Ordovician is based mostly on structural data combined with sediment thicknesses of sandy flysch deposits in Norwegian nappes. This island arc would represent the land mass shown more pronounced in Blakey (2019), and less prominent in Cocks and Torsvik (2005). It would explain why paleo water depths decreased in a northwestern direction during Tøyen Shale Formation deposition in the four localities used in this study.

Nevertheless, several questions remain open regarding the facies and composition of the sediments derived from this arc. It seems curious that the carbonate facies should be the shallowest facies recorded in the succession, but the northwesternmost section in the Slemmestad area does not show carbonates in the upper part of the Tøyen Shale Formation succession (Galgeberg Member) even though it is closer to shore according to everybody's reconstructions. A possible explanation could be that the Slemmestad localities are too close to a source of siliciclastic sediment coming off the highlands/arc to the west, and the fine-grained siliciclastic material supplied into the water prevented the formation of thick carbonates such as in time-equivalent strata further to the south. This sediment source, however, must have ceased to exist or avulsed during the Middle Ordovician as the Huk Formation carbonates were deposited directly on top of the Tøyen Shale Formation in Slemmestad.

Thickness variations in the Tøyen Shale Formation are attributed to the position of the depositional area relative to continental land masses. The Tøyen Shale Formation shows well that Avalonia further to the south was shedding large amounts of fine-grained material towards Baltica and was likely not too far away from this microcontinent during the late Early and early Middle Ordovician when the Tøyen Shale Formation was deposited. The amount of siliciclastic detritus also reflects that Avalonia must have been a much larger continental block than the island arc colliding with Baltica in the west. This is reflected in a very much thicker Tøyen Shale Formation succession in the Lerhamn core as the amount of detrital material derived from Avalonia is significantly higher than from the arc west of Baltica.

Preservation of organic matter

This study suggests that the organic matter is preferentially buried and thereby preserved in facies 1. Nevertheless, sedimentary structures found in facies 1 do not support deposition in a low-energy environment. The organic matter in facies 1 was not preserved in an anoxic, quiet-water environment as assumed by older models for other black shales (e.g. Potter et al. 2005), but in event laminae reflecting relatively high-energy conditions.

Several lines of evidence, however, indicate that preservation of organic matter by rapid burial as described among others by Bohacs et al. (2005), is most likely not an unusual process in sedimentology, especially for black shales. It is generally believed that the presence of oxygen destroys organic matter (e.g. Bohacs et al. 2005), which explains models favoring anoxic environments for black shale deposition. One of the main causes for introducing oxygen into the sediment and thereby destroying a potentially oxygen-free setting below the sediment-water interface is bioturbation. As indicated by several studies (e.g. Schieber 2003; Macquaker et al. 2010a; Egenhoff and Fishman 2013) burrowing in black shales is common, and therewith finding traces of bioturbation in these rocks is nothing unusual. Deposition in pulses, e.g. by events, seems to be equally common in black shales throughout the rock record (Schieber 2003; Egenhoff and Fishman 2013; Borcovsky et al. 2017). In the Tøyen Shale Formation it seems reasonable to assume that a syndepositional anoxic environment in the water column cannot play a crucial role in preserving organic matter, considering the amount of burrowing present in these rocks that suggests some amount of oxygen within the sediment near and even slightly below the sediment-water interface. Nevertheless, rapid deposition and translation of organic matter from being oxidized near the surface to burial beyond the reach of burrowing organisms seems to be a viable mechanism to quickly and effectively preserve organic matter. This process is only working well where bioturbation depth is low so that storms are seen as the main mechanism to rapidly bury organic matter. The process that ultimately determines whether the organic matter is preserved or not is therefore bioturbation. Sedimentary rocks that are not completely bioturbated by organisms consuming organic matter or introducing oxygen will preserve significant amounts of TOC; sedimentary rocks that show a large consumption of organic matter by bioturbating organisms or reflect a significant introduction of oxygen through bioturbation will not contain high amounts of TOC.

The organic matter in the Tøyen Shale Formation most likely includes a significant amount of graptolite rhabdosomes based on visual estimation in thin section. However, the Rock-Eval analyses show that in the Slemmestad outcrops the organic matter is inert, meaning that it has been strongly oxidized. Whether this oxidation happened during the formation of the rocks in the Ordovician or is partly a present-day effect from weathering cannot be ultimately determined by the present data set.

The Tøyen Shale Formation as a witness to increasing burrowing depth since the Cambrian.

Droser and Bottjer (1989) were the first to recognize that Early Paleozoic ecospace utilization changed significantly from the Cambrian into the Ordovician: burrowing depth increased worldwide, and hence the make-up of mudstones located in similar positions on a shelf should equally change. The Tøyen Shale Formation is a case in point: during the Middle to Late Cambrian, the Alum Shale was deposited in a position similar to the Tøyen Shale Formation seaward of a carbonate mid-shelf facies belt (see Álvaro et al. 2010). The Alum Shale shows percentages of total organic carbon (TOC) of up to about 15% (Andersson et al. 1985,) yet the Tøyen Shale Formation, even though deposited nearly on top of the Alum Shale in many places with only the Bjørkåsholmen Formation in-between (cf. Egenhoff et al. 2010), has an average TOC content of about an order of magnitude less. Even though *Phycosiphon incertum* fecal strings are present in both units, complete homogenization of siliciclastic mudstones as proposed for the Tøyen Shale Formation has not been described from the Alum Shale (Egenhoff et al. 2015). It is therefore likely that the Tøyen Shale Formation records exactly what Droser and Bottjer (1989) describe from the Great Basin of the US – an increase in homogenization of the fine-grained siliciclastic sediment caused by a progressive increase in burrowing depth of infaunal organisms that, as one consequence, restricted valuable source rocks in the Scandinavian Early Paleozoic succession to just the Cambrian. It is, therefore, expected that all other, younger shale units in the Scandinavian Ordovician succession that have been deposited relatively proximal to shore (Owen et al. 1990), likely in an environment similar to the Tøyen Shale Formation, contain only minor amounts of generative organics, and most likely record an increase in burrowing activity compared to the Tøyen Shale Formation.

CONCLUSIONS

1) The Tøyen Shale Formation comprises 7 sedimentary facies that were grouped into 3 facies associations: organic matter-enriched laminated siliciclastic mudstones (FA 1), quartz and carbonate silt-rich faintly bedded to massive siliciclastic mudstones (FA 2), and mixed carbonate-siliciclastic massive mudstones (FA 3). These facies associations occupy distinct depositional zones on a medial to distal offshore shelf profile, where FA 1 represents the most distal part of the system, FA 2 constitutes the intermediate zone with slightly higher energy and shallower water conditions than FA 1, and FA 3 occupies the most proximal position on the shelf transect and contains the carbonate-siliciclastic mudstone transition zone.

2) The Tøyen Shale Formation mudstones were deposited primarily by current- and potentially wave-induced bed-load processes during intermittent high-energy events. The sedimentary record that unveils the depositional history of the Tøyen Shale Formation suggests that a large number of marine open shelf mudstone successions could have been deposited under the influence of storm waves and, likely, above storm wave base.

3) Two to three orders of cyclicity have been defined in the Tøyen Shale Formation reflected in parasequences (5^{th}-order), poorly defined to unidentified parasequense sets (4^{th}-order) and regressive and transgressive (3^{rd}-order) cycles. The entire succession records 7 sequences comprising regressive and transgressive cycles bounded by 13 maximum regressive and flooding surfaces and a subaerial unconformity marking the transition from the lower Hagastrand member of the Tøyen Shale Formation to the upper Galgeberg member in the Oslo Region. The 3^{rd}-order cycles correspond to the global sea-level changes proposed by Haq and Schutter (2008), and could be controlled by glacially-, aquifer- or tectonically-driven eustasy.

4) As demonstrated with the Tøyen Shale Formation example, the transition between carbonate and siliciclastic sedimentation in mixed fine-grained siliciclastic-carbonate open shelf systems is likely controlled by either suspension settling or bed-load transport, or both, of fine-grained carbonates, water

depth of the shelf, and the Coriolis force. In a succession, it also depends on base-level fluctuations and proximity to the source of siliciclastic sediment.

5) While preservation of organic matter was most likely determined by episodic event-deposition of clay-clast-rich laminae burying the organics so that it is out of reach of bioturbating organisms inhabitating the seafloor, bioturbation is what dictated destruction of organic matter in the mudstones of the Tøyen Shale Formation. Universally for other potential source rock successions worldwide, an increase of burrowing depths and/or insufficient burial of organic better with sediment could lead to significant oxidation and destruction of organic matter.

REFERENCES

Álvaro, J. J., Ahlberg, P., and Axheimer, N., 2010, Skeletal carbonate productivity and phosphogenesis at the lower–middle Cambrian transition of Scania, southern Sweden: Geological Magazine, v. 147, no. 01, p. 59-76. doi:10.1017/S0016756809990021.

Andersson, A., Dahlman, B., Gee, D.G., and Snäll, S., 1985, The Scandinavian Alum Shales: Sveriges Geologiska Undersökning, Avhandlingar och Uppsatser, v. 56, p. 1–50.

Aplin, A. C., and Macquaker, J. H. S., 2011, Mudstone diversity: Origin and implications for source, seal, and reservoir properties in petroleum systems: AAPG Bulletin, v. 95, no. 12, p. 2031–2059. doi:10.1306/03281110162.

Björlykke, K., 1974, Geochemical and mineralogical influence of Ordovician Island Arcs on epicontinental sedimentation. A study of Lower Palaeozoic sedimentation in the Oslo Region, Norway: Sedimentology, v. 21, p. 251-272.

Bohacs, K. M., 1998, Contrasting expressions of depositional sequences in mudrocks from marine to non marine environs, *in* Schieber, J., Zimmerle, W., and Sethi. P., eds., Shales and Mudstones (vol. 1): Basin Studies, Sedimentology and Paleontology: Stuttgart, Schweizerbart'sche Verlagsbuchhandlung, p. 33-78.

Bohacs, K. M., Grabowski, G. J., Carroll, A. R., Mankiewicz, P. J., Miskell-Gerhardt, K. J., Schwalbach, J. R., Wegner, M. B., and Simo, J. A., 2005, Production, Destruction, and Dilution - The Many Paths to Source-Rock Development: Deposition of Organic-Carbon-Rich Sediments: Models, Mechanisms, and Consequences, SEPM Special Publication, v. 82, p. 61-101. doi.org/10.2110/pec.05.82.0061.

Borcovsky, D., Egenhoff, S., Fishman, N., Maletz, J., Boehlke, A., and Lowers, H., 2017, Sedimentology, facies architecture, and sequence stratigraphy of a Mississippian black mudstone succession - The upper member of the Bakken Formation, North Dakota, United States: AAPG Bulletin, v. 101, no. 10, p. 1625 – 1673. doi:10.1306/01111715183.

Blakey, R., 2011, Paleogeography of Europe Series: Colorado Plateau Geosystems Inc. (Accessed May 9). http://deeptimemaps.com/europe-series-thumbnails/.

Bruton, D.L., Gabrielsen, R.H., and Larsen, B.T., 2010, The Caledonides of the Oslo region, Norway – stratigraphy and structural elements: Norwegian Journal of Geology, v. 90, p. 93–121.

Burchette, T.P. and Wright, V.P., 1992, Carbonate Ramp Depositional Systems: Sedimentary Geology, v. 79, p. 3-57.

Calner, M., Ahlberg, P., Lehnert, O., and Erlström, M., 2013, The Lower Palaeozoic of southern Sweden and the Oslo Region, Norway: Field Guide for the 3rd Annual Meeting of the IGCP project 591, Sveriges geologiska undersökning Rapporter och meddelanden 133, 96 pp.

Cardott, B. J., 2012, Thermal maturity of Woodford Shale gas and oil plays, Oklahoma, USA: International Journal of Coal Geology, v. 103, p. 109–119, doi:10.1016/j.coal.2012.06.004.

Catuneanu, O., 2002, Sequence stratigraphy of clastic systems: African Earth Sciences, v. 35, no. 1, p. 1–43.

Church, J.A., Roemmich, D., Domingues, C.M., Willis, J.K., White, N.J., Gilson, J.E., Stammer, D., Köhl, A., Chambers, D.P., Landerer, F.W., Marotzke, J., Gregory, J.M., Suzuki, T., Cazenave, A., and Le Traon, P. Y., 2010, Ocean temperature and salinity contributions to global and regional sea-level change, *in* Church, J.A., Woodworth, P.L., Aarup, T., Wilson, W.S., Eds., Understanding Sea-Level Rise and Variability (1st ed.): Chichester, Wiley-Blackwell, p. 143–176.

Cloetingh, S., McQueen, H., Lambeck, K., 1985, On a tectonic mechanism for regional sea level variations:. Earth Planet. Sci. Lett., v. 75, p. 157–166. http://dx.doi.org/10.1016/0012-821X(85)90098-6.

Cocks, L. R. M., and T. H. Torsvik, 2005, Baltica from the late Precambrian to mid-Palaeozoic times: The gain and loss of a terrane's identity: Earth-Science Reviews, v. 72, no. 1–2, p. 39–66, doi:10.1016/j.earscirev.2005.04.001.

Cocks, L. R. M., and Torsvik, T. H., 2002, Earth geography from 400 to 250 Ma: a palaeomagnetic, faunal and facies review: Journal of the Geological Society, v. 159, p. 631–644, doi:10.1144/0016-764903-098.

Crowell, J. C., and Frakes, L. A., 1970, Phanerozoic glaciation and the causes of ice ages: American Journal of Sciences, v. 268, no. 3, p. 193-224. doi: 10.2475/ajs.268.3.193.

Droser, M. L., and D. J. Bottjer, 1989, Ordovician increase in extent and depth of bioturbation: implications for understanding early Paleozoic ecospace utilization: Geology, v. 17, no. 9, p. 850–852. doi:10.1130/0091-7613(1989)017<0850:OIIEAD>2.3.CO;2.

Droser, M. L., Bottjer, D. J., 1986, A semiquantitative field classification of ichnofabric: Journal of Sedimentary Research, v. 56, no. 4, p. 558–559. doi.org/10.1306/212F89C2-2B24-11D7-8648000102C1865D.

Dworatzek, M., 1987, Sedimentology and petrology of carbonate intercalations in the Upper Cambrian Olenid shale facies of southern Sweden: Sveriges Geologiska Undersökning, Avhandlingar och Upsatser, ser. C, v. 81, no. 5, 73 p.

Egenhoff, S. O., Fishman, N. S., Ahlberg, P., Maletz, J., Jackson, A., Kolte, K., Lowers, H., Mackie, J., Newby, W., and Petrowsky, M., 2015, Sedimentology of SPICE (Steptoean positive carbon isotope excursion): A high-resolution trace fossil and microfabric analysis of the middle to late Cambrian Alum Shale Formation, southern Sweden, *in* Larsen, D., Egenhoff, S.O., and Fishman, N.S., eds., Paying Attention to Mudrocks: Priceless!: The Geological Society of America Special Paper, v. 515, p. 87–102, doi:10.1130/2015.2515(05).

Egenhoff, S. O., Fishman, N. S., Lowers, H. A., and Ahlberg, P., 2019, The complexity of mudstone diagenesis – some insight from the Tøyen Shale, Lower to Middle Ordovician, southern Sweden: GFF, v. 141, no. 1, p. 54–67. doi:10.1080/11035897.2018.1525620.

Egenhoff, S., and Fishman, N., 2013, Traces In the Dark - Sedimentary Processes and Facies Gradients In the Upper Devonian-Lower Mississippian Upper Shale Member of the Bakken Formation, Williston Basin, North Dakota, U.S.A.: Journal of Sedimentary Research, v. 83, no. 9, p. 803–824. DOI:10.2110/jsr.2013.60.

Egenhoff, S., and Maletz, J., 2007, Graptolites as Indicators of Maximum Flooding Surfaces in Monotonous Deep-Water Shelf Successions: Palaios, v. 22, no. 4, p. 373–383.

Egenhoff, S., and Maletz, L., 2012, The sediments of the Floian GSSP: depositional history of the Ordovician succession at Mount Hunneberg, Västergötland, Sweden: GFF, v. 134, no. 4, 237-249.

doi:10.1080/11035897.2012.749943.

Egenhoff, S., Cassle, C., Maletz, J., Frisk, Å. M., Ebbestad, J. O. R., and Stübner, K., 2010, Sedimentology and sequence stratigraphy of a pronounced Early Ordovician sea-level fall on Baltica - The Bjørkåsholmen Formation in Norway and Sweden: Sedimentary Geology, v. 224, p. 1–14, doi:10.1016/j.sedgeo.2009.12.003.

Embry, A. F., 2002, Transgressive-Regressive (T-R) Sequence Stratigraphy, *in* Armentrout, J.M., and Rosen, N.C., eds., Sequence Stratigraphic Models for Exploration and Production: Evolving Methodology, Emerging Models, and Application Histories: Proceedings of the 22nd Annual Gulf Coast Section SEPM Foundation Bob F. Perkins Research Conference, p. 151–172. doi:10.5724/gcs.02.22.0151.

Encyclopedia Britannica, 2012, Continental shelf. (Accessed June 7). https://www.britannica.com/science/continental-shelf

Erdtmann, B.D., 1965, Eine spät-Tremadocische Graptolithenfauna von Töyen in Oslo: Norsk Geologisk Tidsskrift, v. 45, p. 97–112.

Fishman, N. S., Ellis, G. S., Paxton, S. T., Abbott, M. M., and Boehlke, A. R., 2010, Gas storage in the Upper Devonian-Lower Mississippian Woodford Shale, Arbuckle Mountains, Oklahoma—How Much of a Role Do the Cherts Play?, *in* Chatellier, J., and Jarvie, D., eds., Critical assessment of shale resource plays: AAPG Hedberg Conference, #90122, p. 81–108. DOI: 10:1306/13401726H53493.

Greiling, R. O., and Garfunkel, Z., 2007, An Early Ordovician (Finnmarkian?) foreland basin and related lithospheric flexure in the Scandinavian Caledonides: American Journal of Science, v. 307, no. 2, p. 527–553. doi:10.2475/02.2007.07.

Hammes, U., and G. Frébourg, 2012, Haynesville and Bossier mudrocks: A facies and sequence stratigraphic investigation, East Texas and Louisiana, USA: Marine and Petroleum Geology, v. 31, no. 1, p. 8–26, doi:10.1016/j.marpetgeo.2011.10.001.

Hay, W.W., Leslie, M.A., 1990, Could possible changes in global groundwater reservoir cause eustatic sea level fluctuations?, *in* National research Council, Sea Level Change: Studies in Geophysics:

Washington, D. C., National Academy Press, p. 161–170.

Jaanusson, V., 1982, Introduction to the Ordovician of Sweden, *in*: Bruton, A., and Williams, L., (eds.), Fourth International Symposiumon the Ordovician System: University of Oslo, Oslo, Norway, p. 1–9.

Jacobs, D.K., and Sahagian, D.L., 1993, Climate induced fluctuations in sea level during nonglacial times: Nature, v. 361, p. 710–712. http://dx.doi.org/10.1038/361710a0.

Leiter, C., and Altenbach, A. V., 2010, Benthic Foraminifera from the Diatomaceous Mud Belt Off Namibia: Characteristic Species for Severe Anoxia: Palaeontologia Electronica, v. 13, no. 2, p.11-19.

Li, Z., and Schieber, J., 2018, Detailed facies analysis of the Upper Cretaceous Tununk Shale Member, Henry Mountains Region, Utah: Implications for mudstone depositional models in epicontinental seas: Sedimentary Geology, v. 364, p. 141–159. doi:10.1016/j.sedgeo.2017.12.015.

Loucks, R. G., and Ruppel, S. C., 2007, Mississippian Barnett Shale: Lithofacies and depositional setting of a deep-water shale-gas succession in the Fort Worth Basin, Texas: AAPG Bulletin, v. 91, no. 4, p. 579–601, doi:10.1306/11020606059.

Macquaker, J. H. S., and Bohacs, K. M., 2007, On the accumulation of mud: Science, v. 318, no. 5857, p. 1734 – 1735. doi.org/10.1126/science.1151980.

Macquaker, J.H.S., Keller, M.A., And Davies, S.J., 2010a, Algal blooms and ‘‘marine snow’’: mechanisms that enhance preservation of organic carbon in ancient finegrained sediments: Journal of Sedimentary Research, v. 80, p. 934–942.

Macquaker, J. H. S., Bentley, S. J., and Bohacs, K. M., 2010b, Wave-enhanced sediment-gravity flows and mud dispersal across continental shelves: Reappraising sediment transport processes operating in ancient mudstone successions: Geology, v. 38, no. 10, p. 947–950. doi.org/10.1130/G31093.1.

Maletz, J., and Ahlberg, P., 2011, The Lerhamn drill core and its bearing for the graptolite biostratigraphy of the Ordovician Tøyen Shale in Scania, southern Sweden: Lethaia, v. 44, no. 3, p. 350–368, doi:10.1111/j.1502-3931.2010.00246.x.

Maletz, J., and Ahlberg, P., 2018, The Lower Ordovician Tøyen Shale succession in the Fågelsång-3 drill core, Scania, Sweden: Gff, v. 140, no. 4, p. 293–305, doi:10.1080/11035897.2018.1470201.

Maletz, J., Löfgren, A. and Bergström, S.M., 1996, The base of the Tetragraptus approximatus Zone at Mount Hunneberg, S.W. Sweden: a proposed Global Stratotype for the base of the Second Series of the Ordovician System: Newsletters on Stratigraphy, v. 34, p. 129–159. doi:10.1127/nos/34/1996/129.

Megard, F., Noble, D. C., McKee, E.H., and Bellon, H., 1984, Multiple pulses of Neogene compressive deformation in the Ayacucho intermontane basin, Andes of Central Peru: Geol. Soc. Am. Bull., v. 95, p. 1108-1117.

Miall, A. D., 1992, Exxon Global cycle chart: An event for every occasion?: Geology, v. 20, p. 282-790.

Mitchum, R., M., Jr., and Van Wagoner, J., C., 1990, High-frequency sequences and eustatic cycles in the Gulf of Mexico basin: Proceedings of the Gulf Coast Section SEPM 11th Annual Research conference, p. 257–267.

Monsen, A., 1938, Die Graptolithenfauna im unteren Didymogratusschiefer (Phyllograptusschiefer) Norwegens: Norsk Geologisk Tidsskrift, v. 16. P. 57-266.

Myrow, P., 1992, Bypass-zone tempestite facies model and proximality trends for an ancient muddy shoreline and shelf: Journal of Sedimentary Petrology, v. 62, no. 1, p. 99-115.

Nielsen, A. T., and Schovsbo, N. H., 2011, The Lower Cambrian of Scandinavia: Depositional environment, sequence stratigraphy and palaeogeography: Earth-Science Reviews, v. 107, no. 3–4, p. 207–310, doi:10.1016/j.earscirev.2010.12.004.

Ogston, A. S., Cacchione, D. A., Sternberg, R. W., and Kineke, G. C., 2000, Observations of storm and river flood-driven sediment transport on the northern California continental shelf: Continental Shelf Research, v. 20, no. 16, p. 2141–2162. doi:10.1016/S0278-4343(00)00065-0.

Owen, A.W., Bruton, D.L., Bockelie, J.F., and Bockelie, T.G., 1990, The Ordovician successions of the Oslo region, Norway: Norges Geologiske Undersøkelse, Special Publication, v. 4, 54 pp.

Peters, S. E., and Loss, D. P., 2012, Storm and fair-weather wave base: A relevant distinction?: Geology, v. 40, no. 6, p. 511–514. doi:10.1130/G32791.1.

Peters, K. E., Curry, D. J., and Kacewicz, M., 2012, An overview of basin and petroleum system modeling: Definitions and concepts, *in* Peters, K. E., Curry, D. J., and Kacewicz, M., eds., Basin

Modeling: New Horizons in Research and Applications: AAPG Hedberg Series, no. 4, p. 1–16. DOI:10.1306/13311426H4139.

Potter, P. E., Maynard, J. B., and Depetris, P. J., 2005, Mud and mudstones; Introduction and overview: Berlin, Springer-Verlag, 297 p.

Pitman, W. C., and Golovchenko, X., 1983, The effect of sealevel change on the shelfedge and slope of passive margins: SEPM Special Publication 33, p. 41-58.

Purser, B. H., 1973, The Persian Gulf: New York, Springer-Verlag, 471 pp.

Schieber, J., 2003, Simple gifts and buried treasures—Implications of finding bioturbation and erosion surfaces in black shales: Sedimentary Record, v. 1, no. 2, p. 4–8.

Schieber, J., 2009, Discovery of agglutinated benthic foraminifera in Devonian black shales and their relevance for the redox state of ancient seas: Palaeogeography, Palaeoclimatology, Palaeoecology, v. 271, no. 3–4, p. 292–300. doi:10.1016/j.palaeo.2008.10.027.

Schieber, J., 2011, Shifting paradigms in shale sedimentology; the implications of recent flume studies for interpreting shale fabrics and depositional environments: Proceedings of the CSPG CSEG CWLS Conference, 4 pp.

Schieber, J., and Southard, J. B., 2009, Bedload transport of mud by floccule ripples - Direct observation of ripple migration processes and their implications: Geology, v. 37, no. 6, p. 483–486, doi:10.1130/G25319A.1.

Schieber, J., Southard, J. B., and Schimmelmann, A., 2010, Lenticular Shale Fabrics Resulting from Intermittent Erosion of Water-Rich Muds--Interpreting the Rock Record in the Light of Recent Flume Experiments: Journal of Sedimentary Research, v. 80, no. 1, p. 119–128. doi:10.2110/jsr.2010.005.

Schieber, J., Southard, J. B., Kissling, P., Rossman, B., and Ginsburg, R., 2013, Experimental Deposition of Carbonate Mud From Moving Suspensions: Importance of Flocculation and Implications For Modern and Ancient Carbonate Mud Deposition: Journal of Sedimentary Research, v. 83, no. 11, p. 1025–1031. doi:10.2110/jsr.2013.77.

Schieber, J., Southard, J., and Thaisen, K., 2007, Accretion of mudstone beds from migrating floccule ripples: Science, v. 318, no. 5857, p. 1760–1763. doi.org/10.1126/science.1147001.

Spjeldnaes, N., 1953, The Middle Ordovician of the Oslo Region, Norway, 3. Graptolites dating the beds below the Middle Ordovician: Norsk Geologisk Tidsskrift, v. 31, p. 171-185.

Stridsberg, S., 1980, Sedimentology of Upper Ordovician regressive strata in Västergötland: Geologiska Föreningens i Stockholm Förhandlindar, v. 102, no. 3, p. 213-221.

Turner, B. R., Armstrong, H. A., and Holt, P., 2011, Visions of ice sheets in the early Ordovician greenhouse world: Evidence from the Peninsula Formation, Cape Peninsula, South Africa: Sedimentary Geology, v. 236, no. 3–4, p. 226–238. doi:10.1016/j.sedgeo.2011.01.009.

Van Wagoner, J.C., H.W. Posamentier, R.M. Mitchum, P.R. Vail, J.F. Sarg, T.S. Loutit and J. Hardenbol, 1988, An overview of sequence stratigraphy and key definitions, *in* Wilgus, C. K., Hastings, B. S., Posamentier, H., Van Wagoner, J., Ross, C. A., Kendall, C. G. St. C., (eds.), Sea level changes: an integrated approach: Society of Economic Peontologists and Mineralogists special publication, v. 42, p. 39- 45. doi.org/10.2110/pec.88.01.0039.

Wilson, J. L., 1975, Carbonate facies in geologic history, New York, Springer-Verlag, 471 pp.

Wilson, R. D., and Schieber, J., 2014, Muddy Prodeltaic Hyperpycnites in the Lower Genesee Group of Central New York, USA: Implications For Mud Transport In Epicontinental Seas: Journal of Sedimentary Research, v. 84, no. 10, p. 866–874. doi:10.2110/jsr.2014.70.

Wortel, R., and Cloetingh, S., 1981, On the origin of the Cocos Nazca spreading center: Geology, v. 9, p. 425-430.

PART II: FACIES ARCHITECTURE AND CARBONATE-SILICICLASTIC MIXING IN AN INTRACRATONIC BASIN: INSIGHT FROM THE LATE DEVONIAN – EARLY CARBONIFEROUS MIDDLE BAKKEN MEMBER OF THE WILLISTON BASIN, ND, USA.

INTRODUCTION

Mixed carbonate-siliciclastic systems are not as well understood as either pure carbonate or pure siliciclastic systems (e.g. Mount, 1984; Goldhammer, 2003). This holds especially true for the siliciclastic-dominated end member of shallow-marine environments characterized by coeval deposition of carbonates and siliciclastics (Schwarz et al., 2018), in contrast to mixed systems characterized by reciprocal sedimentation (Kidwell, 1988; Southgate et al., 1993; Kerans and Tinker, 1999). Existing studies on siliciclastic-dominated examples focus on relatively limited study areas that are well-suited for correlating parasequences and/or facies associations with sufficient accuracy (Coffey and Sunde, 2014; Schwarz et al., 2018). Current understanding of siliciclastic and carbonate mixing lacks examples that would encompass the evolution of an entire basin, or a major portion of a single basin, that could be used for characterizing a certain basin type, e.g. a passive margin (Coffey and Sunde, 2014), a backarc-basin (Schwartz et al., 2018), or on a wide-spanned but shallow-marine shelf sea (Labaj and Pratt, 2016).

The present study has two primary objectives. First, it will present the middle member of the Upper Devonian-Lower Mississippian Bakken Formation, a complex mixed carbonate-siliciclastic system composed of laminated mud- and siltstones and fine-grained sandstones and limestones, as a prime example for a siliciclastic-dominated mixed system developed in the low-inclined settings of an intracratonic basin, a sedimentary environment heavily under-represented in literature. This unit occurs exclusively in the subsurface, and is described in this study based on 89 cores that are distributed throughout the North Dakota portion of the Williston basin. The study area covers more than half of the US portion of this intracratonic trough (cf. Gerhard et al., 1990) including its northeastern margin, which further extends into Canada, and the southern to south-western margin, continuing into Montana. The distribution of facies is highlighted using these two opposite basin sides; however, the core density allows one to trace individual parasequences through the entire middle Bakken succession, from one margin of the basin in ND to the other. Combining the basin-centric approach to this unit with time-equivalency from correlating parasequences provides a more accurate identifications of parameters controlling facies distribution during middle Bakken times.

Middle Bakken sediments also show a unique mixture of siliciclastic sediments and carbonates: none of the carbonate facies contains exclusively carbonate grains or matrix, and only very few of the siliciclastic facies consists exclusively of siliciclastic particles. This intimate mixing of these two lithologies has not been described from mixed carbonate-siliciclastic systems before. Therefore, the second aim of this contribution is to explore why the middle Bakken shows this close combination of carbonates and siliciclastics, and how such mixing of lithologies could occur.

GEOLOGICAL SETTINGS

The Williston basin is elliptical in shape and represents a classical intracratonic trough located in North Dakota, Montana and South Dakota in the USA, and the Saskatchewan and Manitoba provinces of Canada (Fig. 1). The basin covers an area of approximately 250000 km^2 and has a maximum sediment thickness of 4900 meters (Kent and Christopher, 1994) in the Watford deep, southeast of Williston, North Dakota (Gerhard et al., 1990). It hosts hydrocarbons in many stratigraphic levels; however, one of the most important is the upper Devonian to lower Mississippian Bakken petroleum system that includes the Three Forks, the Bakken itself, and the overlying lower Lodgepole Formations (Nordeng, 2010; LeFever et al., 2011). This petroleum-rich system has been an exploration target since the early nineteen fifties (Laird, 1952), and is currently one of the major US onshore hydrocarbon plays (Anna et al., 2011) containing a total of 7383 MMB of oil and 6726 BCF of gas according to the assessment of Gaswirth et al. (2013).

The subsidence mechanism of the Williston basin remains unclear, however, some of it may be attributed to wrench-fault tectonics (Brown and Brown, 1978) reflected in recurrent movements of the basement blocks along the major northeast-southwest and northwest-southeast trending lineaments. Structural elements that formed as a product of the basin’s structural evolution are the primary target areas for hydrocarbon exploration (Gaswirth et al., 2013) as structural traps and zones of enhanced natural fracturing (Murray, 1968; Freisatz, 1995).

The Bakken Formation is subdivided into four members (Fig. 2): the basal Pronghorn, which is dominated by siliciclastics but also contains carbonates (LeFever et al., 2011); the overlying lower Bakken shale, a prominent black shale unit; the middle Bakken member representing a mixed carbonate-siliciclastic succession; and the top upper Bakken shale, which is another black shale unit. The Bakken Formation as a whole has a maximum thickness of 45 meters in western Mountrail county of North Dakota (Meissner, 1978; Webster, 1984). Its age is constrained biostratigraphically by conodonts to be Late Devonian - Early Mississippian based on data from the lower and upper Bakken shale members.

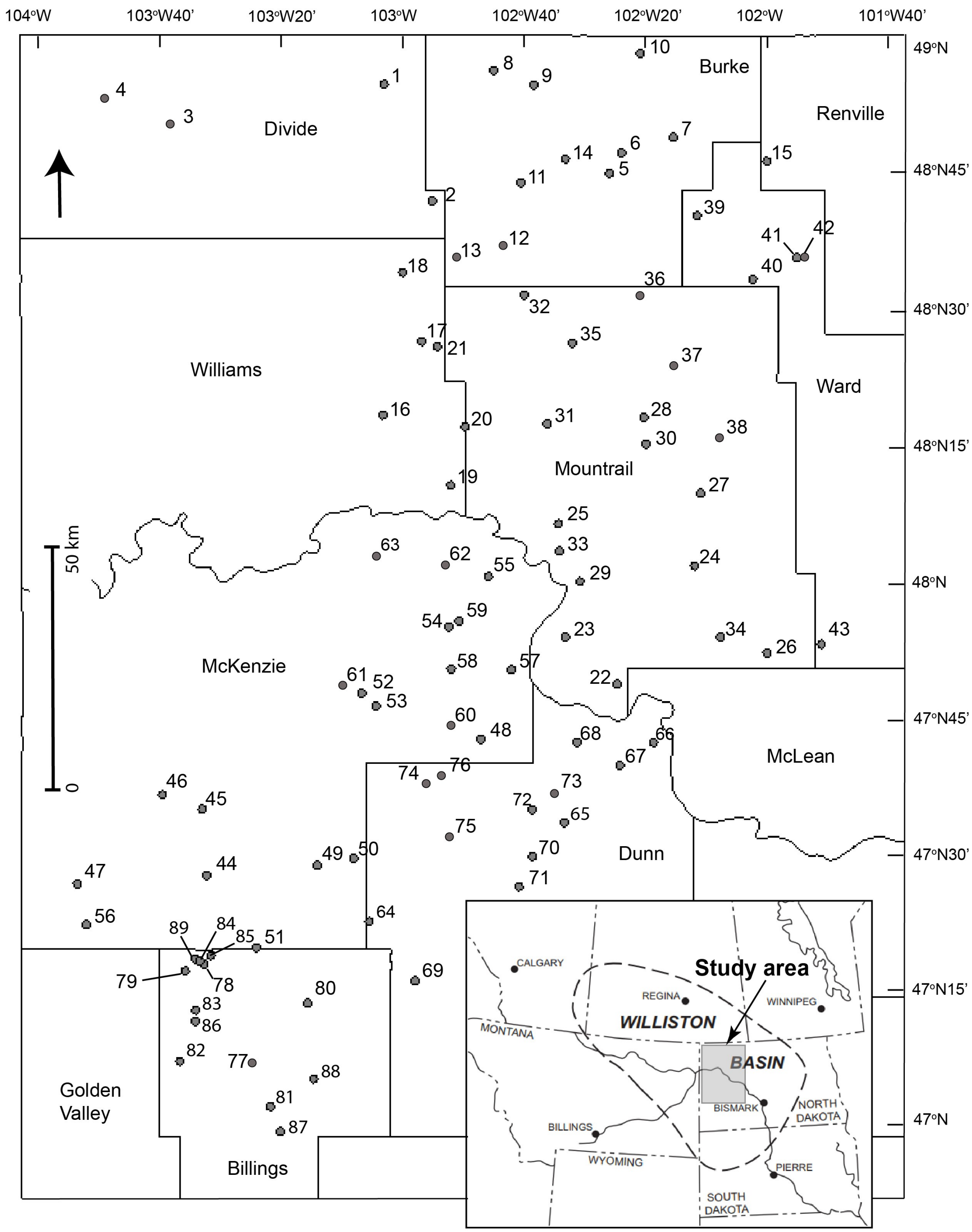

Figure 1: Map depicting the studied portion of the Williston basin (Modified from Novak and Egenhoff, 2019). The inset on the bottom right shows the location of the study area in the USA and Canada (modified from Pitman et al., 2001). Locations of cored wells containing the middle member of the Bakken Formation that used in this study are shown in gray circles: 1 – Ansbro Petroleum Loucks 44-30; 2 – Conoco Waterud "A" #17, 3 – SM Energy Tomlinson 3-1HN; 4 - Murex Petroleum Jennifer Abigail 16-21H; 5 – Clarion Resources 1-24 Slater; 6 – Northern Pump Louis Peterson #1; 7 – Clarion Resources Mertes #1-32; 8 – Clarion Resources Negaard #1; 9 – Clarion Resources Nelson 1-29; 10 – Cornerstone

Natural Resources Jorgensen 4-4H; 11 – Samson Resources OAS 31-161-92H; 12 – Samson Resources Saratoga 12-1-161-92H; 13 – St. Mary Land & Exploration Company Douts 4-7H; 14 – Petro-Hunt Producer`s Corporation 159-94-17C-8-2H; 15 – Clarion Resources Pierce #1-18; 16 – Petro Devel Corp. Violet Olsen 31-29H; 17 – Texacota H. Borstad #1; 18 – Dallea Petroleum Corp. Hamlet U. #2; 19 – Pan American Petroleum Corp. Clifford Marmon #1; 20 – Headington Oil Co. Nesson State 42x-36; 21 – Hess Corp. H. Bakken 12-07H; 22 – Dakota E&P Co. George Evans 11V; 23 – Marathon Oil Co. Mylo Wolding 14-11; 24 – EOG Resources Parshall 2-36H; 25 – American Hunter Exploration Ahel et al Sanish #36-44 H4; 26 – Hess Corp. St-Andes-151-89-2413H-1; 27 – Marathon Oil Co. Jensen #12-44; 28 – Marathon Oil Co. Laredo #26-1; 29 – Whiting Oil and Gas Corp. Bartleson 44-1H; 30 – Brooks Exploration Rogstad #1-11; 31 – Shell Oil Co. L. Texel #21-35; 32 – Amerada Hess Corp. State ND 1-11H; 33 – Whiting Oil and Gas Corp. Mildred Roggenbuck 41-24TFX; 34 – EOG Resources Fertile 1-12H; 35 – Fidelity E&P Co. Farhart 11-11H; 36 – EOG Resources Sidonia 1-06H; 37 – Hess Corp. RS-STATE C-157-90- 3603H-1; 38 – EOG Resources McAlmond 1-05H; 39 – Clarion Resources 1-20 Fleckton; 40 – Clarion Resources 1-33 Pullen; 41 – Golden Eye Resources Steinberger #1-16; 42 – Golden Eye Resources J. Brekhus #2-14; 43 – Marathon Oil Co. Dobrinski #18-44; 44 - Pennzoil Co. 15-22 BN Flat Top Butte; 45 – True Oil Slash Federal 44-33 4-9H; 46 – Pennzoil Co. Spring Creek #27X-31BN; 47 – Shell Oil Co. USA 33-23-154; 48 – Helis O&G Co. Linseth 13-13/12H; 49 – American Hunter Exploration Ahel et al Grassy Butte #12-31 H3; 50 – GMX Resources Pojorlie 21-2-1H; 51 – Cities Services 1 Federal DG; 52 – Lyco Energy Corp. Titan E-Gierke 20-1-H; 53 – Oryx Energy Stenehjem HD 27 #1; 54 – Texaco F. P. Keogh #4; 55 – Amerada Petroleum Corp. Jens Strand #1; 56 – Meridian Oil MOI #44-13; 57 – Petro-Hunt Fort Berthold 150-94-3B-10-2H; 58 – Hess Corp. Lars Rothie 32-29H; 59 – Hess Corp. HA-Nelson-152-95-3328H-9; 60 - Helis Oil & Gas Co. Linseth 4-8H; 61 - Denbury Onshore Ludinin 11-13SEH; 62 - Burlington Resources Oil & Gas Co. Uberwachen 22-34; 63 - Whiting Oil And Gas Corp. Tarpon Federal 44-19TFHU; 64 – Gulf Oil Corp. Martin Weber #1-18-1C; 65 – Shell Oil Co. Burbank #23-8; 66 – Mobil Producing Co. Pegasus DIV Solomon Bird Bear #F-22-22-1; 67 – Shell Oil Co. Young Bear #32-4; 68 – Socony-Vacuum Oil Co. Angus Kennedy #F32-24-P; 69 – Oxy USA Evelyn Kary 2-22-15H-144-97; 70 – Marathon Oil Co. Stohler 21-3H; 71 – Marathon Oil Co. Corrine Olson 34-20; 72 – Petro-Hunt Fort Berthold 147-94-3B-10-3H; 73 – Simray GP Roberts Trust 1-13H; 74 - Headington Oil Co. Jane Federal 11X-20; 75 - Continental Resources Hawkinson 14-22H2; 76 – NEWFIELD PRODUCTION COMPANY JORGENSON 1-15H; 77 - Tenneco Oil 3-17 TOC MEE USA; 78 – Florida Exploration 1-12 Federal; 79 – Tenneco Oil Graham USA #1-15; 80 – Texaco 5-1 Thompson Unit; 81 – Whiting Oil & Gas Corp. Franks Creek State 21-16TFH; 82 – Maxus Exploration Crooked Creek State #31-16; 83 – Meridian Oil MOI Elkhorn #33-11; 84 – Milestone Petroleum Federal #12-12; 85 – Supron Energy Corp. F-6-144-101 #3; 86 – Coastal Oil & Gas Corp. & Al-Aquitaine 23-143-102 BN #1; 87 – Florida Exploration Co. Federal 34-1; 88 – XTO Energy Chruszch 43X-29; 89 – Florida Exploration 11-4 Federal; details for each well are listed in Appendix J.

It is assumed that the Devonian-Mississippian boundary is located in the lower portion of the middle Bakken member (Karma, 1991; Hogancamp and Pocknall, 2018).

During Bakken deposition, the Williston basin occupied a near-equatorial position in the southern hemisphere (Scotese, 1994). After significant exposure following Three Forks deposition, the basin was likely flooded from the NW depositing the Pronghorn sandstones and carbonates. The overlying lower Bakken shale is seen as a first highstand of sea-level (Smith and Bustin, 2000; Angulo and Buatois, 2012). It is unclear whether an erosional surface separates the lower Bakken shale from the overlying middle Bakken member: Smith and Bustin (2000) proposed this erosional contact based on Canadian data, and Egenhoff (2017) described carbonates from the lower-middle Bakken contact that he saw as transgressive deposits, following a regression subsequent to lower Bakken shale deposition. Nevertheless, the middle Bakken member reflects the stepwise lowering of sea-level with parasequences moving towards the basin center, and the overlying transgressive portion is represented by poorly developed parasequences, and ultimately overlain by the upper Bakken shale, representing another sea-level highstand (Egenhoff et al., 2011; Angulo and Buatois, 2012; Borcovsky et al., 2017; Egenhoff, 2017).

Facies distribution through the different stages of Bakken deposition is not well established. However, the lower Bakken seems to contain bioturbated shales closer to shore and black shales with successively finer-grained sediments towards distal areas (Albert, 2013). The middle Bakken member represents deposition on a shallow-marine low-inclined shelf with coarse-grained mostly sandy deposits in proximal, and fine-grained muddy and silty sediments in distal positions (Egenhoff et al., 2011). The Upper Bakken shale was deposited offshore in a low-energy setting with intermittent storm events on the distal portion of a ramp during the initial flooding preserving abundant organic matter and radiolarite deposits (Borcovsky et al., 2017); however, when the initial Lodgepole regression set in, the basin was characterized by mostly carbonate deposition, followed by an episode of marine transgression responsible for the deposition of the siliciclastic False Bakken shale interval (Mackie, 2013).

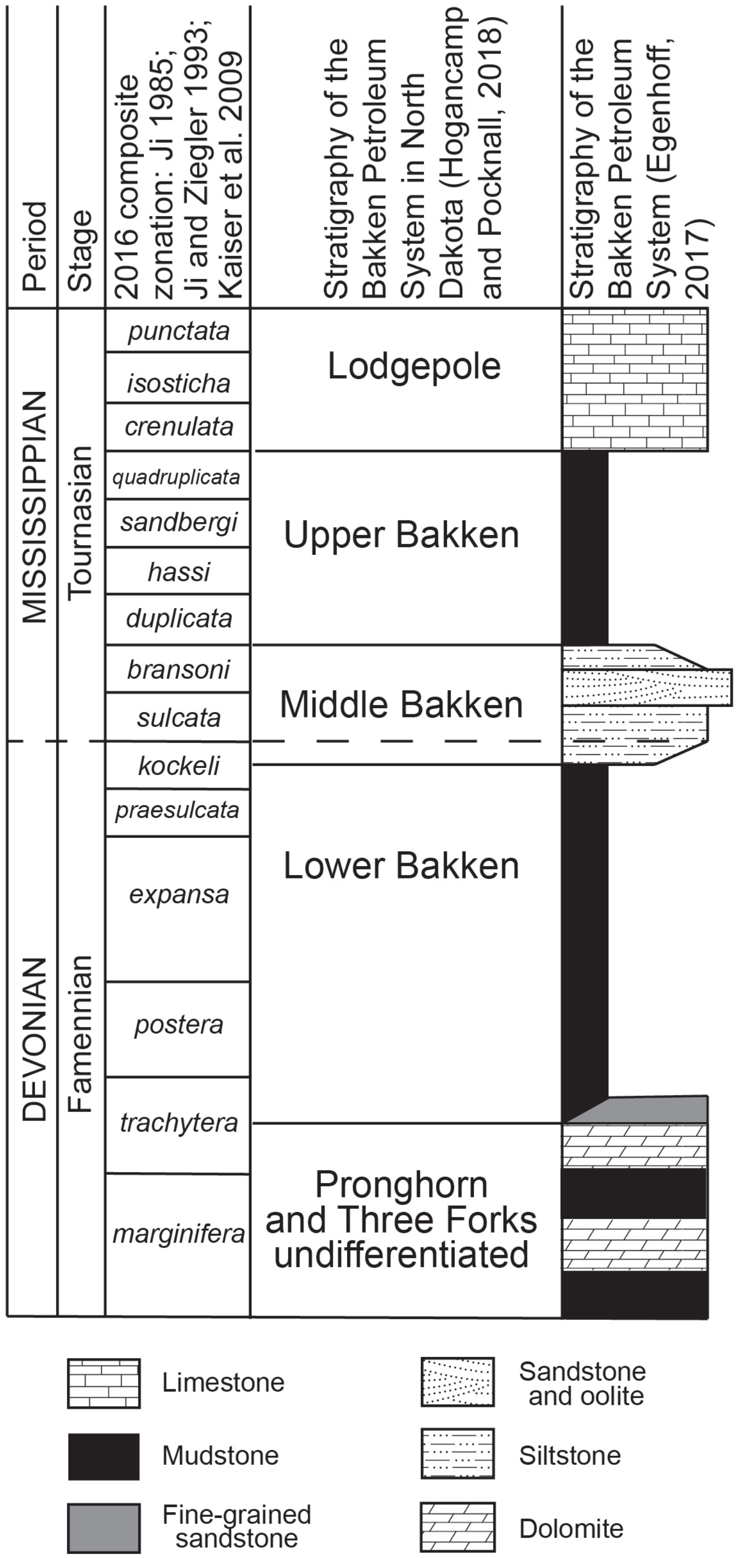

Figure 2: Stratigraphy of the Bakken Petroleum System. Biostratigraphic data is adopted from Karma (1991) and Hogancamp and Pocknall (2018), stratigraphy is modified after Egenhoff (2017).

METHODS

Eighty nine slabbed drill core sections were described in detail in order to characterize the sedimentary system and its stratal architecture. The cores used in this study are stored at the North Dakota Geologic Survey's Wilson M. Laird Core and Sample Library in Grand Forks, North Dakota, and the United States Geological Survey's Core Research Center in Denver, Colorado. Twenty three thin sections were prepared for microscopic analysis of facies. Thin section were cut normal to bedding, 20µm-thick for fine-grained siliciclastic and 30 µm-thick for coarse-grained siliciclastic and carbonate samples, and polished. Sedimentological features, such as grain size, angularity, sorting and mineralogy were determined using transmitted light Nikon Eclipse Ci-L petrographic microscope with a magnification range from 2x to 40x. Sedimentary facies were classified into predominantly carbonate, predominantly siliciclastic and purely siliciclastic based on the visual estimations of the amounts of siliciclastic and carbonate material. Depth measurements of the cores were taken in imperial units as provided by the operator, however, small-scale sedimentological and stratigraphic features are herein given in metric units.

FACIES DESCRIPTION AND INTERPRETATION

Predominantly carbonate facies

Facies 1 – Bioclastic Mud- to Wackestone

Description: The bioclastic mud- to wackestone facies consists of tan to gray massive carbonate mudstone matrix with randomly oriented fragments of shells, crinoids and rare echinoderms and less than 10% of sub-angular silt-size quartz grains (Fig. 3 A). All carbonate bioclasts are angular to sub-rounded and show a marginal micritic rim of sub-millimeter thickness. This facies contains some well-developed *Phycosiphon* burrows (cf. Egenhoff, 2017); however, distinct burrows or fecal strings are generally absent. The matrix, however, has an overall cloudy appearance with different size sub-millimeter carbonate components that are irregularly distributed throughout samples. Facies 1 shows gradational contacts to both over- and underlying facies. Beds of this facies can be as thin as 2 centimeters and, in places, reach up to 1-2 meters in thickness.

Interpretation: The fine-grained nature of the sediment and primarily carbonate mud content advocates for deposition in a low-energy environment away from the siliciclastic sediment source: nevertheless, such sediment can also be deposited by bed-load transport (Schieber et al., 2013). Regardless if this sediment represents high- or low-energy deposition, the presence of silt-sized quartz grains indicates intermittently high energy settings, e. g. storms, which facilitated the input of siliciclastic material from a different, more landward source. The random distribution of the quartz silt grains throughout the carbonate matrix, the presence of variously oriented bioclasts (brachiopods, crinoids and echinoderms) and the absence of any bedding structures suggests intense burrowing of the sediment (cf. Flügel, 2004), most likely within a sediment that was well oxygenated and favorable for benthic life during deposition. The micritic rim observed on all bioclastic particles is characteristic of microborings produced by microorganisms (Golubic et al., 1975). This observation serves as an additional argument to suspect that the bioclasts were not originally encased in the micritic matrix but most likely exposed in open water conditions on the sea floor before being reworked by benthic organisms.

Facies 2 – Bioclastic Pack- to Grainstone

Description: The Bioclastic Pack- to Grainstone facies consists of coquina-like beds or 'lags' composed of grain-supported bioclastic debris with individual particles being millimeter- to centimeter in size (Fig. 3 B). Facies 2 generally shows a carbonate mud matrix but is locally cemented with calcite. The bioclasts (shell, crinoid and echinoderm fragments) are generally arranged parallel to bedding, but are in places randomly oriented. Beds of this facies vary from 1 centimeter to several centimeters in thickness and generally show no distinct grain size trends but can be normally graded in places. The lower contact of this facies is typically sharp and erosional, and the upper contact can be either sharp or gradational.

Interpretation: Each accumulation of coarse-grained bioclastic debris most likely reflects a high-energy event that suspended carbonate mud and concentrated all larger particles, mostly to exclusively shell fragments in this facies, on the sea floor. This high-energy event, most likely a storm, also led to the formation of the sharp erosional bases this facies generally shows. The waning of the storm is not directly reflected in many of the coquinas; however, as some of the pack- to grainstones show normal grading the decrease of energy during the late phase of this high-energy event is shown locally (cf. Aigner, 1985). The origin of the bioclastic debris is largely unclear; they may have been sourced locally, or introduced from a different part of the shelf. Pieces of shells confirm the high energy environment that must have prevailed during deposition that was able to break shells; nevertheless, the fact that many bioclasts are still intact may point to a less violent mode of deposition. However, it is well known that shells can easily survive even storm transport (e.g. Miller et al., 1988). The accumulation of mud in the matrix, where present, represents background sedimentation or deposition when the energy had significantly decreased, most likely during the final waning phase of the storm.

Facies 3 – Bioclastic Packstone with Peloids

Description: The facies is comprised of poorly sorted various skeletal, non-skeletal and detrital grains. The framework consists of 40% bioclasts that are more than a half of a millimeter long (brachiopod shells, ostracod shells, mollusks shells and annelid tubes), 20% sub-millimeter-size peloids, 7-10% quartz grains (coarse silt to fine sand size), and 3-5% of sub-millimeter-size aggregate grains (lumps) containing mainly siliciclastic grains and carbonate mud (Fig. 3 C). Individual leached eccentric ooids around 200μm in diameter were also observed in this facies (Fig. 3 D). The remaining 25-30% of the rock volume is taken up by the carbonate mud matrix. The clasts are recrystallized and show well-developed micritic coatings. No distinct orientation of the grains or distinct bedding structures can be observed in this facies. The facies was found in only one well (Gulf Oil Martin Weber 1-18-10), where it occurs as a 12 centimeter-thick unit with sharp lower and upper contacts.

Interpretation: The presence of particles of several sizes, from sub-millimeter (peloids) to more than half millimeter particles (shells and worm tubes), argues for varying energy conditions during deposition. This is also reflected in the presence of carbonate mud filling all of the pore spaces which generally requires much less energy to deposit than grains of up to centimeter size (Flügel, 2004; but see Schieber et al., 2013 for bed load transport of carbonate mud). Nevertheless, the high quantity of carbonate mud and the fact that the shells are generally intact argue for either gentle bursts of high energy, or just moderate energy that did not break the shells. Similarly, the micritic coatings, likely originating from microborings (Flügel, 2004), argue for dominantly quiet water conditions throughout deposition of this facies. Common in peloidal packstones eccentric ooids indicate deposition in overall low-energy environment characterized by periodically agitated waters and hydrodynamic changes controlling the switching between suspension, saltation and traction processes on the seafloor (Gasiewicz, 1984). Eccentric ooids coatings form during short periods of water agitation, and the micritic envelopes develop during non-turbulent periods. Leaching of ooids implies meteoric influence leading to ooid dissolution and recrystallization (Carozzi, 1963; Milroy and Wright, 2000). The presence of quartz grains reflects an active influx of siliciclastic material during the deposition of this facies itself as well as during the formation of aggregate grains that are here interpreted to represent rip-up clasts brought in from a carbonate environment, likely preceding the one represented by this packstone. Nevertheless, the carbonate factory producing this facies was never completely shut off by the episodic influx of the siliciclastic grains but seemed to have locally prevailed as it is present in only one core.

Facies 4 – Bioclastic Packstone with Aggregate Grains

Description: The facies consists of approximately 35-40% of randomly oriented annelid tubes sub-millimeter to about 0.5 millimeter in size, approximately 25-30% aggregate grains that are roundish to elongate/irregular in shape and sub-millimeter to about one centimeter in size, up to 10% of mostly sub-angular and of coarse silt to very fine sand size quartz grains (Fig. 3 E). The remaining 25-30% are interstices filled up to two thirds of it with strongly recrystallized carbonate mud, and up to about one third with calcite cement. Minor amounts of plagioclase, ostracod shells and bioclasts, as well as peloids are present in places. The aggregate grains and the annelid tubes both contain quartz grains and, to a lesser degree, shell fragments throughout. All grains have a structureless micritized envelope, generally tens of microns thick and irregular in size and shape. Only several millimeter-large aggregate grains are orientated roughly parallel to bedding; most of the other grains, however, seem to have a random orientation.

Interpretation: The bioclastic packstone with aggregate grains facies reflects alternation of low-and high-energy settings during the deposition. Extensive micritization and partial encrustation of grains implies prolonged low-energy conditions, which could have developed in quiet protected areas allowing for biogenic reworking of the surfaces of sediment particles. The lumps represent rip-up clasts that were eroded and transported from the adjacent carbonate environment that was located close to the source of siliciclastic sediment as indicated by the presence of quartz grains in the aggregate grains, as well as throughout this facies. The environment must have been well oxygenated as indicated by the worm tubes, the ostracods, peloids, and likely bacteria-induced micritic rims on carbonate particles with the micritic rims being produced by bacteria, algae, annelids or other organisms (Cros, 1979).

Facies 5 – Stromatolitic Bindstone

Description: This facies consists of light gray laminated cyanobacterial mats and laterally linked and stacked hemisperoid domes. The cyanobacterial mats comprise vertically stacked irregular, mm-scale mudstone laminae; however, they can also show up as millimeter- to centimeter-scale fragments of cyanobacterial mats, generally encased in siltstones of facies 8 (Fig. 4 A). The laminae of the

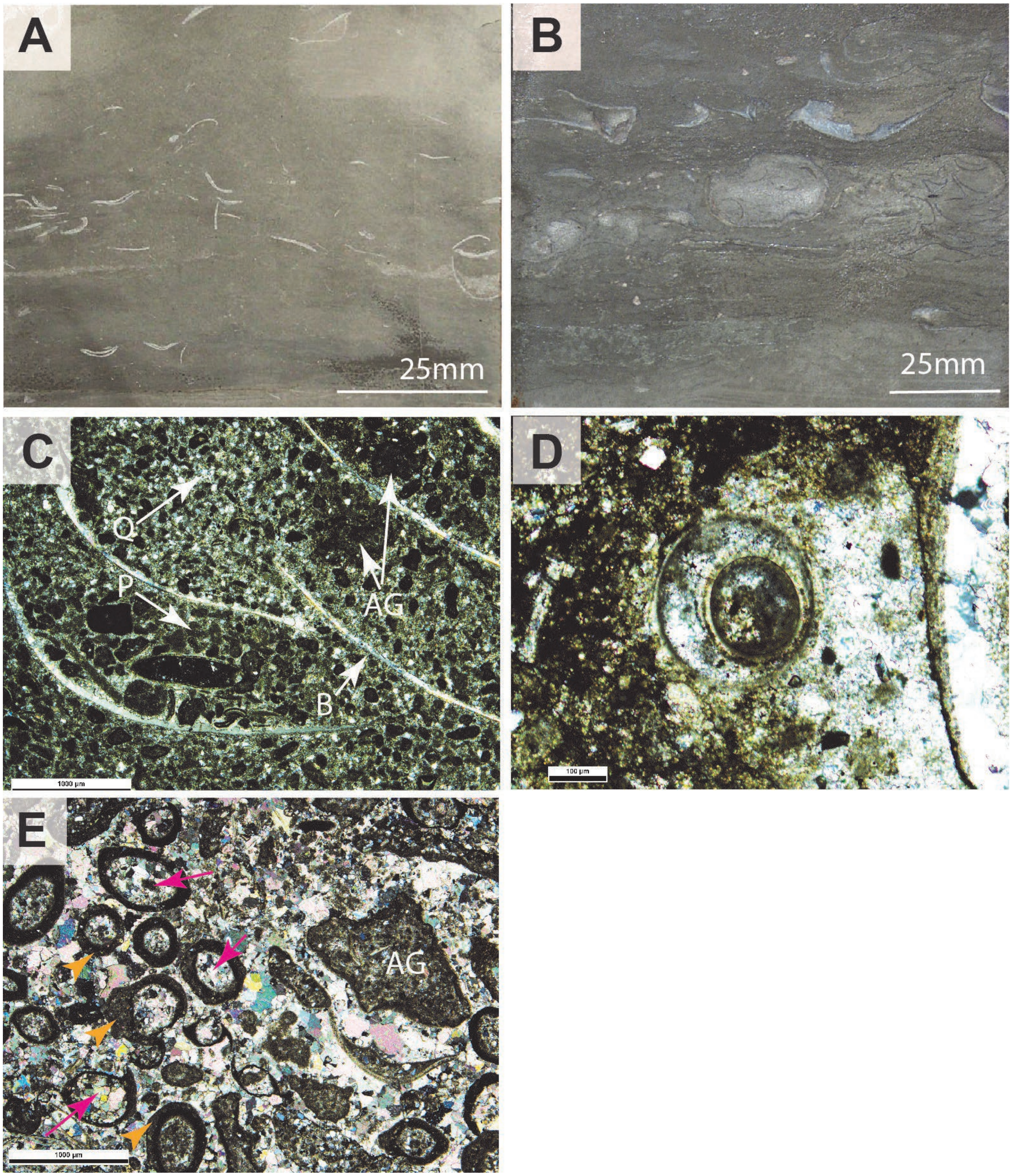

Figure 3: Photos and photomicrographs illustrating sedimentological features of the middle Bakken facies. A) Bioclastic mud- to wackestone facies 1; B) Bioclastic pack- to grainstone facies 2; C) Bioclastic packstone with peloids facies 3, AG – aggregate grain, Q – quartz grain, P – peloidal grain, B – bioclast; D) Individual eccentric ooid in bioclastic packstone with peloids facies 3; E) Bioclastic packstone with aggregate grains facies 4, pink arrows point at annelid tubes, yellow arrows indicate micritic rims and envelopes.

stromatolitic bindstone facies typically contains fine- to medium-grained silt to fine-grained sand particles of both carbonate and siliciclastic lithologies (Fig. 4 B). In places, stromatolitic domes show signs of corrosion and vuggy porosity, filled with carbonate cement. Stromatolitic domes reach the heights of up to 10 centimeters; however, beds of this facies vary between 2 and 40 centimeters.

Interpretation: This facies likely formed in a generally tranquil environment as indicated by the presence of the microbial mats forming the bindstones. Analogous to recent environments of microbial mat growth (e.g. Shark Bay, Australia; Logan et al., 1974), it is likely that the environment where the middle Bakken microbial mats thrived was likely sheltered and somewhat stressed as indicated by the absence of any signs of benthic life (e.g. Stal, 2012). Nevertheless, the presence of silt-sized grains within the mats shows that some high-energy event most likely deposited them there. The environment, therefore, must have been generally tranquil but characterized by some amount of high-energy influence from time to time. It is also likely that the depositional environment was relatively sediment-starved. This is indicated by the fact that these mats could grow undisturbed for a while, and that not a lot of detrital material is integrated into the mats themselves – which shows that during the growth stage of the mat not much detrital sediment was available that could have been incorporated into the bindstone. Nevertheless, the allochthonous pieces of the bindstones and the authochthonous microbial mats are both encased in and buried by the siltstones of facies 8; it therefore seems reasonable to assume that the microbial mats represent temporary sediment starvation in an area that was afterwards again characterized by other siliciclastic and carbonate sedimentation. Corrosion and dissolution features within some stromatolites likely point to subaerial exposure and influence of meteoric water, which resulted in a break of stromatolitic growth, dissolution and visible distortion of the internal structure (Nehza and Woo, 2006).

Sub-facies 6a – Oolitic Pack- to grainstone

Description: This facies consists of radial-fibrous ooids that are spherical to oval/elongate in shape, sub-millimeter in size, and make up 70-90% of the framework grains. Other components include bioclasts (shell debris, echinoderm fragments, gastropods; all of them sub-millimeter to several millimeters in size) that form about 5-10% of the framework (Fig. 5 A). Around 5-15% is taken up by

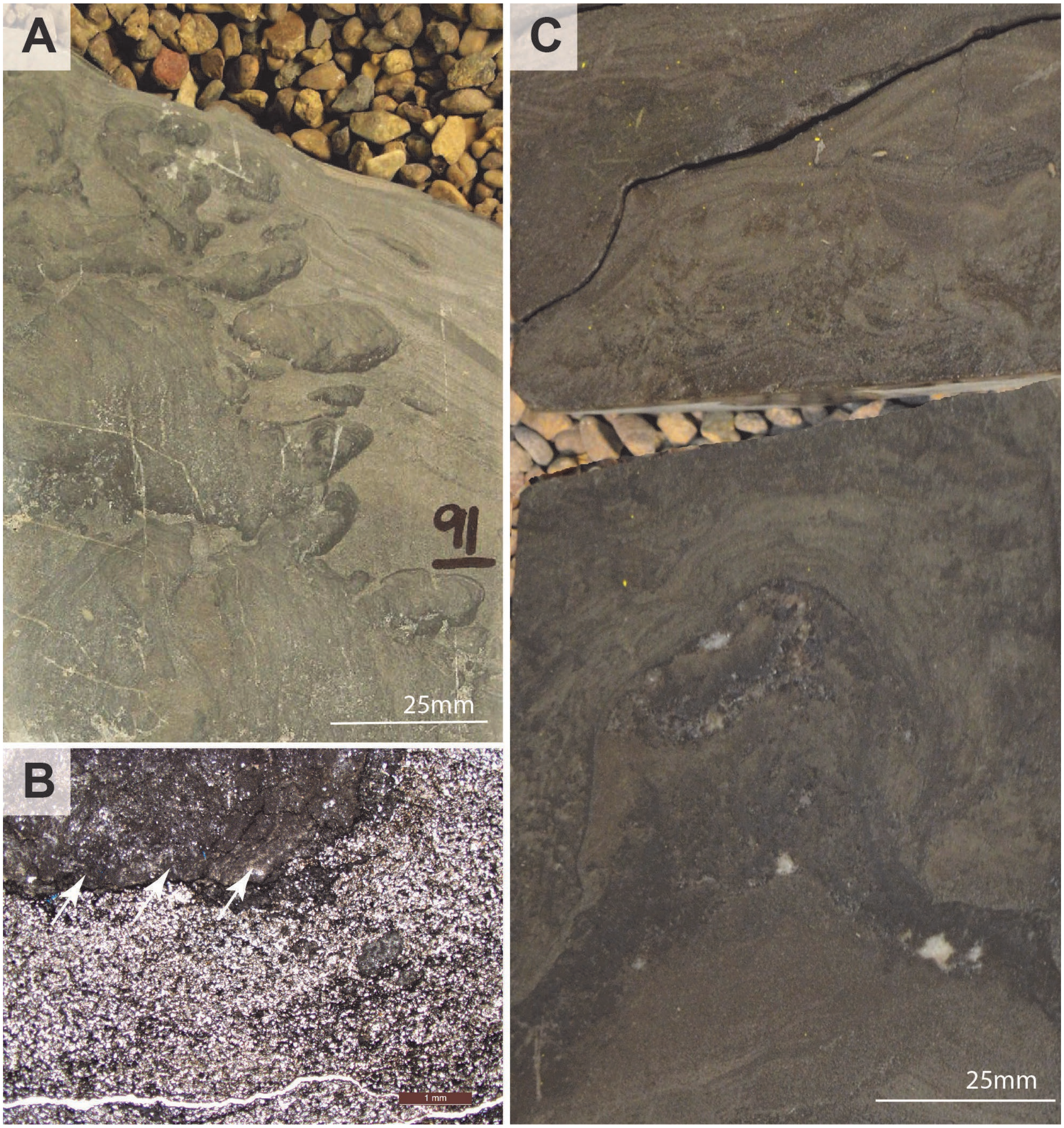

Figure 4: Photos and photomicrographs of stromatolitic bindstone facies 5. A) Distorted stromatolitic lamina and domes pointing slightly sideways; B) A fragment of a stromatolitic dome (white arrows) with entrapped fine-grained quartz and carbonate silt grains encased in the surrounding siliciclastic siltstone; C) Deformed stromatolitic dome with signs of corrosion and vuggy dissolution.

elongate aggregate grains that are up to several millimeters long and consist of fine-grained carbonate matrix with silt-size carbonate and, in places, quartz grains. The remaining 10% consists of medium to coarse silt-size quartz grains. With very few exceptions, all grains are coated on at least one side, mostly all around. Most ooids show several well-developed coatings; however, elongate shell fragments often only have one poorly developed coating and may therefore represent 'superficial ooids' (Carozzi, 1964). All observed ooids are single ooids, this facies does not contain compound ooids. In places, shell fragments form part of the coatings of ooids, preferentially in their outer parts (Fig. 5 A, pink arrow). Rarely, fragments of ooids occur; however, if present they generally show an even outer coating that surrounds the entire ooid fragment. The ooids are overall poorly sorted, however, they are arranged in distinct sub-millimeter to millimeter-thick laminae with the smaller ooids, quartz grains, and bioclasts forming laminae that contains carbonate mud, and the larger ooids and bioclasts forming up to several millimeters-thick laminae with calcite cement and no matrix. Both types of laminae are laterally irregular in thickness, and especially the laminae with small ooids often contain interspersed large ooids. Aggregate grains are generally associated with the large ooids and arranged parallel to bedding. In places, the laminae show a poorly developed inverse grading. Beds consisting exclusively of oolites of facies 5a are between several centimeters and several meters thick.

***Interpretation*:** The intercalation of laminae containing smaller and larger ooids reflects changing energy conditions during deposition: the up to half a millimeter-size ooids indicate higher energy, the small ooids up to hundred microns in diameter lower energy conditions. This interpretation is also supported by the amount of matrix/cement in the particle interstices: while the large ooids have exclusively calcite cement indicating the pore spaces were left open during deposition, typical for grainstones showing high-energy conditions (Dunham, 1962), the small ooids show both micrite and carbonate cement in pore spaces reflecting moderate energy conditions. In this scenario, the carbonate mud may have been introduced during the waning stage of the flow depositing the small ooids, or represents post-depositional infill of the interstices. Intermixing of large ooids with the small ooids and the micrite is most likely due to that the large ooids have not been transported in suspension (as the small ooids likely did; see summary in Flügel,

2004) but may have been brought into their place of deposition by saltation on the sea-floor before the smaller ooids and the mud matrix was deposited between them, or as traction deposits.

While the bioclasts are seen as just the nuclei for ooid formation, judging by at least one coating on every single one of them, the aggregate grains are viewed as rip-up clasts of strong currents or waves scouring the ocean floor. The fact that they generally occur associated with the large ooids shows that, perhaps, the same high-energy event that deposited the large ooids might have been responsible for scouring and transporting the aggregate grains and depositing them with the large ooids. Alternatively, the high energy event may just have been sufficient to transport and deposit the clasts ripped up by other high-energy scouring events. Nevertheless, the aggregate grains indicate that there must have been an environment containing carbonate mud as well as both silt-size carbonate and quartz grains in relative proximity to the site of oolitic pack- to grainstones deposition. The rare ooid fragments in this facies most likely result from ooids breakage. Radial structure, relatively small size and recoating of broken fragments of the ooids comprising this facies indicates that these ooids were most likely aragonitic in composition, suggesting that they were structurally weaker than other types, which resulted in sporadic syndepositional breakage of ooids in the marine realm (Halley, 1977).

Predominantly siliciclastic facies

Sub-facies 6b – Bioclast-rich quartz-oolitic pack- to grainstone

Description: The Bioclast-rich quartz-oolitic pack- to grainstone consists to about 35-40% of coarse silt to fine sand-size quartz grains that are mostly sub-angular; 10-30% of sub-rounded to rounded bioclasts of varying origin, sub-millimeter in size; and 10-20% of ooids that are either round and complete, or are pieces of ooids with some of them comprising the core of these grains (Fig. 5 B); ooids and their fragments are either radial or micritic (Fig. 5 C), in the range of some hundreds of microns in size, and generally show only few laminae and large cores that consist of carbonate particles or quartz. Both single and compound ooids occur. Bioclasts are mostly shell fragments and echinoderm pieces with rare conodonts; phosphate clasts other than conodonts occur but make up less than 1% of the rock; they are roundish to elongate in shape, in places concentric, and in the order of a hundred microns in size. The rock seems to consist majorly of grains; however, in some places a carbonate matrix is visible that is made up of mostly recrystallized carbonate mud. Locally, calcite cement is evident. At the microscope scale, this facies appears largely massive; however, macroscopically, especially the quartz grains seem to be arranged in sub-millimeter- to one millimeter-thick planar or low-angle laminae with several millimeter-thick laminae of carbonate-dominated facies in-between (Fig. 5 D). This texture is further emphasized by elongate particles being roughly aligned parallel to these laminae. This facies forms beds of 1 to 30 centimeters in thickness and is often interbedded with facies 11.

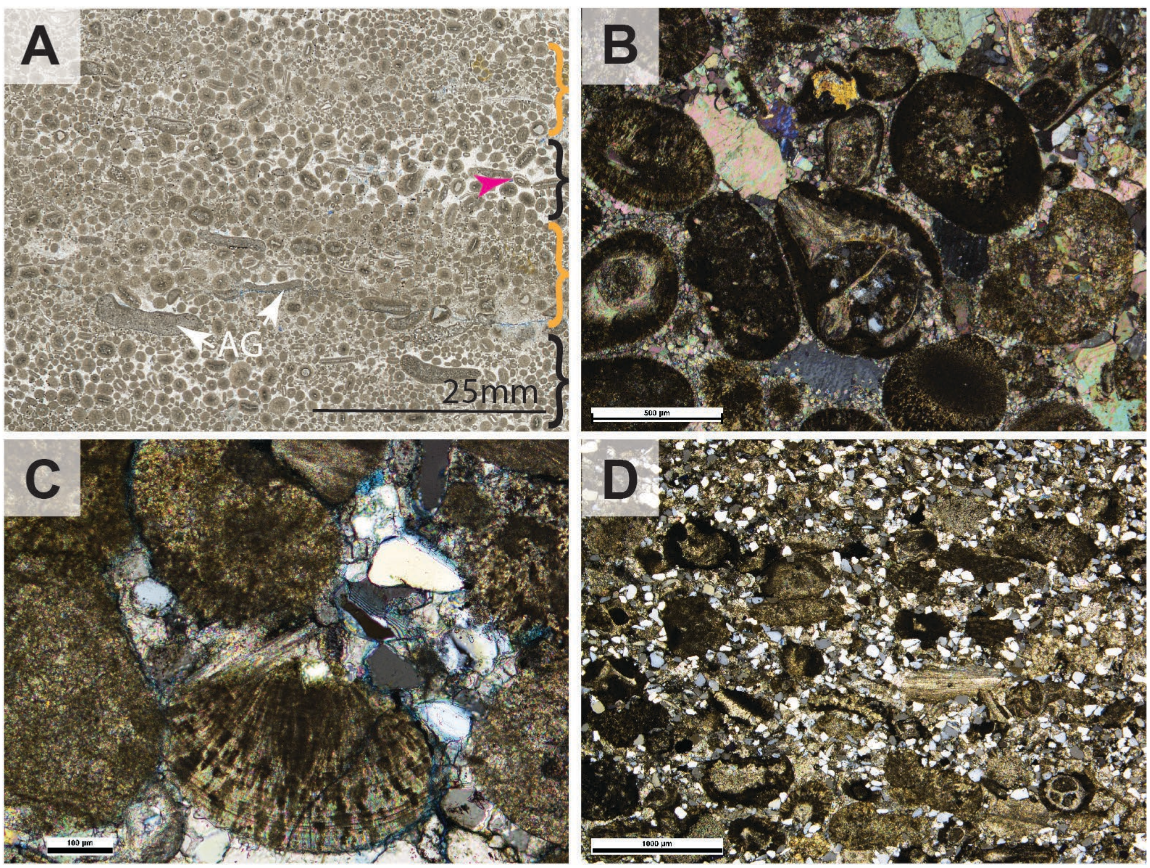

Figure 5: Photomicrographs illustrating sedimentary features of the middle Bakken facies. A) Oolitic pack- to grainstone facies 6a, AG – aggregate grains, pink arrows point at ooid coatings containing a shell fragment, orange brackets outline the lamina comprised of small ooids with some carbonate mud, black brackets highlight the lamina consisting of larger ooids and primarily cement; B) Individual ooids with bioclasts serving as ooid nuclei; C) Fragments of broken ooids in bioclast-rich quartz-oolitic pack- to grainstone facies 6b; D) Faintly planar laminated siliciclastic grains and ooids in in bioclast-rich quartz-oolitic pack- to grainstone facies 6b.

Interpretation: Planar to low-angle crossbedding points to upper flow regime conditions, or deposition in subaqueous dunes. The ooids are envisioned to be brought in to the depositional site during high-energy, likely storm-induced, events from an area within the basin where a carbonate environment was established. Minor amounts of carbonate mud were most likely brought in along with ooids during storms. Oolitic and biogenic grains that were deposited as fragments originally formed in a shallow, warm-water environment. The micritic ooids further indicate that they remained in a subaqueous environment in quiet waters in order to become completely micritized (Flügel, 2004). The broken ooid pieces are interpreted to have formed as a result of breaking of originally complete ooids likely during re-deposition. It is assumed here that many of the components of the facies 5b pack- to grainstones have experienced multiple episodes of reworking. Compound ooids are generally interpreted as reflecting numerous (at least two) times of sedimentation, subsequent erosion and re-deposition. The same is assumed for the phosphate grains which are interpreted as detrital, with their angularity reflecting not a very long distance from their source. The small number of coatings on the superficial ooids and other particles, such as shell fragments, shows that these grains were coated immediately in the marine environment where they have originated, and likely represent an early stage of coating of grains, before being transported away from their primary depositional site.

Facies 7 – Nereites-bearing Siltstone

Description: The *Nereites*-bearing siltstones consist of gray-colored fine- to medium-grained silt grains that are well- to sub-rounded and composed of mainly quartz. Throughout this facies, roundish carbonate grains with a diameter of between 40 and 80 µm occur, and are in places embedded into laminae of carbonate mud that are arranged parallel to bedding (Fig. 6 A, B). Rarely, this facies also contains sub-rounded 50-150 µm diameter glauconite that makes up 10-15 % of framework grains and exclusively occur in well Pan American Petroleum Corp. Clifford Marmon #1 (Fig. 6 C). The matrix is composed of clay minerals, and clay-size grains of other composition as indicated by SEM measurements (quartz, feldspar). This facies contains large amounts of *Nereites missouriensis* burrows (Angulo and Buatois, 2012) that are elongate in shape, millimeters to several centimeters long, sub-millimeters high, and filled with dark gray mud (Fig. 6 D, white arrows). Sub-mm size *Phycosiphon incertum* (Angulo and Buatois, 2012) occur in places but are less common. Overall, this facies is extensively burrowed (BI 4-5); however, distinct beds that are up to several centimeters thick contain high quantities of quartz silt grains and are present in places, separated by beds of gray, clay-rich siltstones, and millimeter-thick carbonates. All of these beds show diffuse upper and lower boundaries. In places, this facies contains up to 10% of randomly oriented brachiopod shell, crinoid and echinoderm fragments. Stratigraphic intervals consisting of this facies are present in nearly every core, and vary from 0.3-10.5 m in thickness. Contacts of this facies to overlying facies can be sharp or gradational; however, the contact to underlying units is typically exclusively gradational.

Interpretation: The presence of predominantly siltstone making up this facies indicates an overall medium- to low-energy environment in order to deposit these relatively fine grains. The clay in this facies (see Pitman et al., 2001), in contrast, suggests low-energy conditions during deposition. This apparent slight difference in interpretation indicates varying energy conditions during deposition: during relatively high-energy events, e.g. storms, mostly silt grains were deposited. The silt grains formed up to several centimeter-thick beds, and these thin beds are still observed in places reflecting event deposition. An event origin of the siltstone beds is also indicated by the relatively poor rounding of a significant population of the quartz grains: this suggests only minor reworking pre-sedimentation without much transport on the shelf. The clay-rich units and carbonate laminae interbedded with these siltstones represent fair-weather deposition. In this study, it is suggested that places with abundant sediment supply did not deposit carbonates, and that locations away from clay deposition seem to have deposited primarily carbonates. These carbonate laminae must have partly been ingested by small benthic organisms that produced the roundish pellets, likely fecal pellets based on their shape and lack of internal structures (cf. Flügel, 2004). It is most likely that the tropical water in the Williston Basin promoted a rapid cementation and therefore early hardening of these fecal pellets: their isolated occurrence throughout this facies suggests that thorough bioturbation, indicated by the near absence of bedding features and an abundance of burrows, destroyed most of the carbonate laminae and mixed the fecal pellets with the surrounding sediment. Burrowing is envisioned to be especially well established during fair weather conditions in times of little sedimentation. This way, fine-grained sediments such as clay-rich beds became thoroughly bioturbated while some storm beds are still fairly

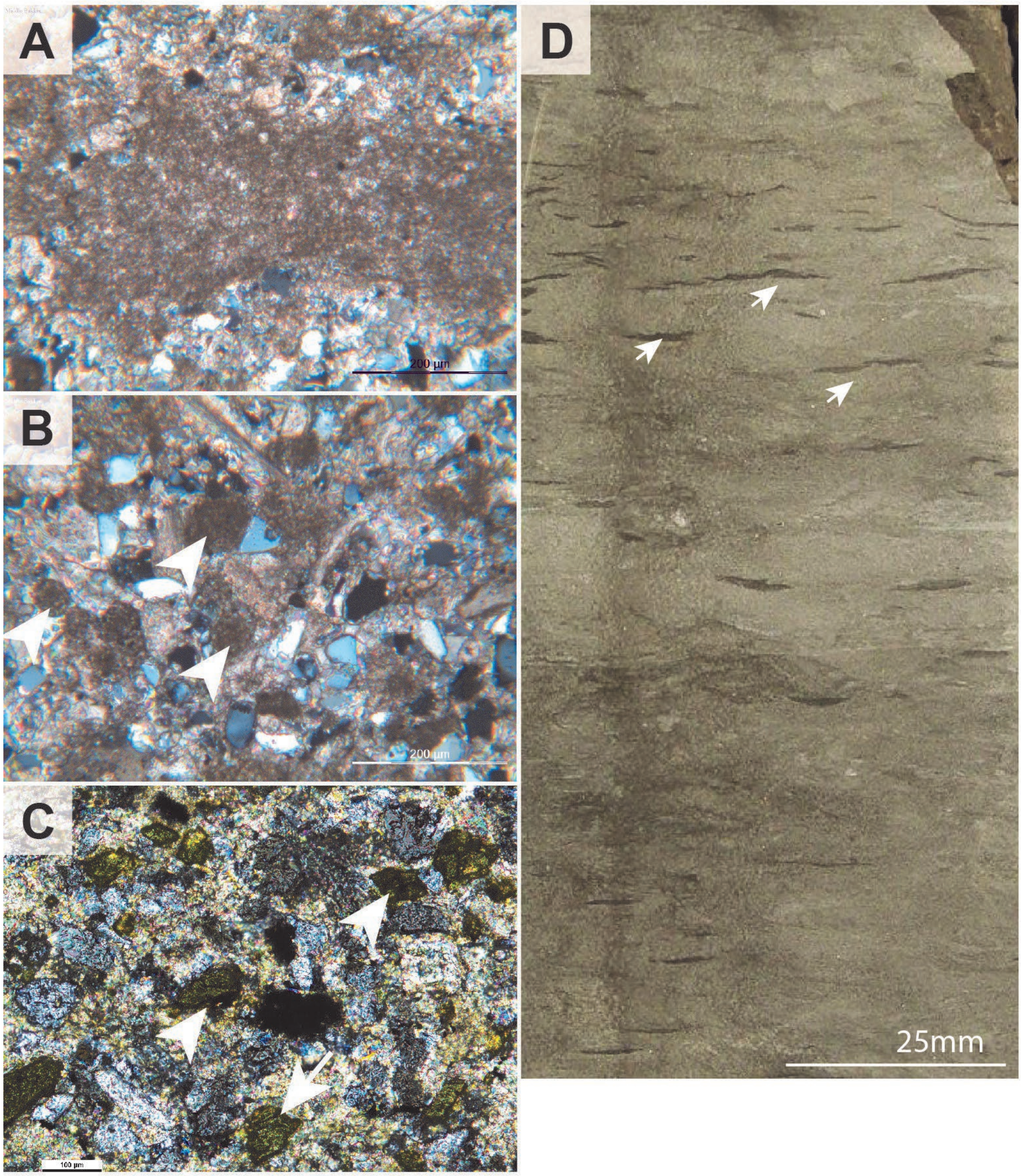

Figure 6: Photomicrographs illustrating sedimentary features of the Nereites-bearing siltstone facies 7. A) A laminae or a lens of carbonate mud in the overall massive siltstone matrix; B) White arrows point at dark gray roundish peloidal grains arranged with no preferred orientation; C) White arrows point at green sub-rounded to rounded glauconite grains distributed in the matrix with no preferred orientation; D) Core photo displaying characteristic for Nereites-bearing siltstone facies 7 *Nereites missouriensis* burrows (white arrows).

intact or at least recognizable in places. Bioturbation may also play a role in the presence of bioclasts close to the boundary with the underlying carbonate mud- to wackestones of facies 1 (Egenhoff, 2017): some of the echinoderms and brachiopod shells may simply reflect reworking of the underlying carbonates by burrowing organisms. The presence of glauconite in the *Nereites*-bearing siltstones, most likely diagenetic in origin (Scholle and Ulmer-Scholle, 2003) indicates low sedimentation rates or sediment starvation (Amorosi, 1995; Hugget and Gale, 1997) in the basin during deposition of facies 7. It is likely that conditions on the sea floor were well oxygenated during deposition, and the marine waters showed normal marine salinity; this is indicated by the abundance and variety of trace fossils (e.g. Angulo and Buatois, 2012).

Purely siliciclastic facies

S*ub-facies 8a: Irregularly Laminated Siltstone*

Description: The irregularly laminated siltstones consist predominantly of light gray medium to coarse grained well- to sub-rounded silt-size grains that are arranged in parallel laminae. The mineralogy is mostly quartz, and in places minor amounts of plagioclase. Individual siltstone laminae are between millimeters to about one centimeter in thickness, and alternate between medium silt and coarse silt which results in the laminated character of this facies. All laminae are roughly equal in thickness laterally; however, lamina boundaries appear slightly irregular and 'fuzzy' (Fig. 7 A). The facies is bioturbated (BI ~2); the predominant ichnospecies in these rocks is *Planolites montanus* (Angulo and Boutois, 2012). Lower and upper contacts of this facies are generally gradational. Overall thickness of units containing this facies range from tens of centimeters to more than a meter.

Interpretation: The planar lamination, even though slightly irregular in nature, argues for this facies to have been deposited in an upper flow regime. This environment was characterized by overall relatively high energy as reflected in the dominant silt grain size of the coarse-grained laminae; however, the grain size variations show slight variations in depositional energy, likely from slightly varying flow conditions. It is most likely that directly after deposition, the laminae had been regularly flat but were modified by burrowing organisms shortly after sedimentation, e.g. the producer of *Planolites montanus*. This process is also reflected in a BI of about 2 for these sediments. The burrowing also resulted in the fuzzy appearance of individual laminae and may have added to irregular lower facies boundaries.

Sub-facies 8b: Thinly Parallel-Laminated Siltstone

Description: This facies consists of light to dark gray, coarse-grained, well- to sub-rounded quartz siltstone that is generally millimeter-scale horizontally laminated. The laminae are often very distinct with sharp upper and lower boundaries (Fig. 7 B). Small current ripples (up to several millimeters in height) occur in places. This facies lacks bioturbation. Units consisting of this facies usually have gradational upper and lower contacts; in places, however, these contacts can be sharp and well-defined. Thickness of beds of facies 8b is generally 90-120 centimeters; however, this facies can occur in intervals as thin as 5-10 centimeters and reach a maximum thickness of up to 4.3 meters in places.

Interpretation: The parallel lamination in the siltstones of facies 8b indicate deposition by a current in the upper flow regime. Nevertheless, the current ripple cross-stratification present in places shows that some lower flow regime deposition happened at times when the flow velocity slowed down. The fact that these ripples are interbedded into planar lamination indicates that deposition likely occurred in pulses alternating between dominantly supercritical and some subcritical flow conditions. The gradational contacts of this facies reflect the gradual advancement of the flows depositing this sediment towards the place of deposition, and the sharp contacts indicatate, alternatively, local scoring into underlying facies. The lack of trace fossils in these strata is thought to reflect the high energy of deposition without the possibility of organisms burrowing through these rocks, and likely at least in part reworking of potentially colonized surface deposits.

Facies 9: Wave-Rippled Siltstone

Description: This facies consists of light to dark gray coarse-grained, well- to sub-rounded quartz siltstones that show well-developed symmetrical wave-ripple cross stratification. Individual ripple marks are between 5 millimeters and about 2 centimeters in thickness and consist of undulating laminae of siltstones that show ripple marks stacked on top of each other (Fig. 7 C). Rarely, they alternate with siliciclastic mudstones. Generally, facies 9 forms up to 30 centimeters thick intervals with gradational contacts to both over- and underlying facies. Bioturbation is absent in this facies.

Interpretation: The excellent sorting of grains in this facies, and the fact that it is only rarely alternating with other lithologies indicates that facies 9 was deposited by fairly constant energy conditions that in general seem not to have varied much throughout sedimentation of these rocks. The exclusivity of wave ripples indicates that only wave action was responsible for the formation of this facies (cf. de Raaf et al., 1977). Nevertheless, few examples of wave-rippled siltstones that show alternation with mudstones reflect overall relatively quiet sedimentary conditions, and probably an alternation between more agitated and tranquil waters.Gradational contacts to over- and underlying facies show that the dominance and ceasing of wave-control versus other processes did not happen suddenly but likely represents a gradual switch. The lack of bioturbation most likely reflects constant reworking of the sand forming the ripples, thereby destroying all signs of biogenic activity in this facies.

Facies 10: Macaronichus-bearing Siltstone

Description: This facies is a light gray medium- to coarse-grained siltstone consisting of sub-angular quartz grains. The siltstones of this facies appear pervasively bioturbated (BI 5), most likely by *Macaronichnus segregatis* (Clifton and Thompson, 1978). These characteristic burrows are 1-3mm in diameter, and have a rounded to slightly elongate shape (Fig. 7 D). *Macaronichnus*-bearing siltstone units are between 2 and 15 cm thick and shows sharp lower and upper contacts.

Interpretation: Altough the environmental interpretation of *Macaronichnus* isp. is somewhat problematic, *Macaronichnus*-bearing siltstones are thought to be deposited in a relatively high energy environment (Clifton and Thompson, 1978; Nummedal and Moleaar, 1995; but see Curran, 1985; Pollard et al., 1993). Given that the organisms producing these burrows can dig up to 80 centimeters deep below the sediment-water interface (Clifton and Thompson, 1978), the *Macaronichnus*-bearing siltstones may only represent a portion of a deep tier, or, alternatively, colonization of sediment shortly after storm deposition when sediment becomes more oxygenated. Furthermore, the complete bioturbation led to obliteration of any of the original sedimentary structures, if any were originally present. As the complete bioturbation is also seen as a sign of potentially low sedimentation rates, giving the *Macaronichnus* *segregatis* producers time to completely burrow through these siltstones, it is likely that this facies represents condensation at a time in basin evolution where sediment input from nearshore areas was low to negligible.

Facies 11: Massive, Planar and Cross-Bedded Sandstone

Description: Facies 11 consists dominantly of fine- to medium-grained, poorly sorted quartz grains that are generally sub-rounded to sub-angular. Upper and lower contacts of this facies are usually sharp. The facies consists of well-defined beds, each between 17 cm and 5 m thick. No burrowing has been observed in these rocks. Interstitial pores are generally filled with calcite and dolomite cements. Facies 11 consists of three sub-facies which are differentiated based on their sedimentary bedding style:

Sub-Facies 11a – Massive Fine-Grained Sandstone: this sub-facies is massive in nature and does not contain any bedding features (Fig. 7 E). Locally, various soft sedimentary deformation structures occur in this sub-facies. Beds of this sub-facies seem to have laterally varying thicknesses.

Sub-Facies 11b – Planar-Bedded Fine-Grained Sandstone: this sub-facies comprises horizontal beds of mostly fine-grained quartz sandstone that is in places interbedded with oolitic grainstones of sub-facies 5b (Fig. 7 F).

Sub-Facies 11c – Cross-Bedded Fine-Grained Sandstone: this sub-facies includes both through- and high-angle planar cross-stratified quartz sandstone that in places is interbedded with oolitic grainstones of sub-facies 5b (Fig. 7 G).

Interpretation: The dominance of quartz sand grains in this facies as well as the absence of fine-grained material filling the pores indicates that facies 11 was deposited in a high-energy environment in constantly agitated water. Frequent re-deposition of grains lead to the destruction of any type of burrows if they had ever been present.

Sub-Facies 11a – Massive Fine-Grained Sandstone: the massive appearance of this sub-facies is here interpreted as a result of liquefaction processes, likely due to movements along tectonic structures (Novak and Egenhoff, 2019), which obliterated all types of depositional bedding by a rearrangement of grains (Obermeier, 1996). Liquefaction as a potential process to form this sub-facies is also indicated by local ball-and-pillow-structures, and the uneven thicknesses of beds in cores.

Sub-Facies 11b – Planar-Bedded Fine-Grained Sandstone: the planar bedding characterizing this sub-facies is interpreted to have formed under constantly high-energy upper-flow regime conditions. It is most likely that the planar bedding is a result of constant moving of grains during fair-weather conditions; a storm origin of the planar lamination does not seem plausible as the succession does not show an alternation of event and low-energy fair-weather sediments.

Sub-Facies 11c – Cross-Bedded Fine-Grained Sandstone: the trough and high-angle planar cross stratification of this sub-facies reflects lower-flow regime conditions (e.g. Clifton et al., 1971). These structures are interpreted as the product of migrating subaqueous dunes.

Facies 12: Bioturbated Sand- to Siltstone

Description: The sand- to siltstones of facies 12 are composed of structureless, highly bioturbated (BI 4-5) sediments, consisting of sub-angular to sub-rounded poorly to moderately sorted fine- to coarse-grained silt- and fine-grained sandstones. In places, “fuzzy” bedding planes are preserved and show abundant burrowing (Fig. 7 H, K). Recognizable ichotaxa include dominant *Planolites montanus*, *Phycosiphon incertum, Palaeophycus tubularis* and subordinate *Nereites missouriensis, Rosselia* and *Teichichnus rectus* (Angulo and Boutois, 2012). Contacts with over- and underlying facies are typically gradational. The thickness of this facies ranges from 30 cm to 3 m.

Interpretation: The grain sizes that make up this facies, fine silt- to fine-grained sand, reflect both low- as well as medium- to relatively high-energy conditions during deposition. It is therefore most likely that facies 12 originally consisted of an intercalation of beds and laminae of different grain sizes that were indicative of varying energy conditions during deposition but got mixed by burrowing post-sedimentation. The large variety of burrows preserved reflects hospitable living conditions during deposition allowing many different benthic organisms to thrive. The remnants of bedding structures still preserved in these rocks indicates that the massive nature of facies 12 deposits is not a depositional feature but a consequence of burrowing. No flow regime can be deducted from just the grain sizes alone.

Facies 13: Micro-Hummocky Cross-Stratified Siltstone

Description: This facies comprises coarse-grained tan siltstones that consist predominantly of moderately- to well-sorted sub-rounded silt-size quartz grains. This facies shows well-developed micro-hummocky cross-stratification (micro-HCS), and the micro-HCS do not exhibit internal irregularities such as downlap or ripple-bedding of laminae (Fig. 7 K). Individual micro-HCS are characterized by a well-developed thickening of laminae into the troughs, and a thinning of laminae towards the thin part of the hummock. Hummocks do not occur as stacks in this facies but are always separated by facies 12 siltstones. Beds of facies 13 show wavelength upwards of 10 cm, are up to 7.5 cm thick, and have sharp and well-defined tops and bases. They are either non-bioturbated, or moderately bioturbated with *Teichichnus rectus* traces (Angulo and Buatois 2012), generally from the top of the structure downwards (BI ~0-1).

Interpretation: The micro-HCS characteristic for this facies suggests deposition in a high-energy environment affected by large storm waves (e.g. Duke, 1985). Hummocky beds most likely developed under prevalent oscillatory conditions as they do not show irregularities (Dott and Bourgeois, 1982). Deposition is envisioned to have occurred at a depth where waves were already pretty weak leading to the formation of micro-HCS rather than fully developed, long-wavelength HCS as in many open shelf successions (Pemberton et al., 2012).

Stacking patterns, facies architecture and distribution

The sedimentary facies architecture of the middle Bakken member succession illustrates the vertical order and lateral facies relationships within the Williston basin. There is a clear distinction between three types of facies stacking patterns: (1) the basal few centimeters to decimeters of the succession; (2) the lower two thirds to three quarters of the middle Bakken excluding the basal part; and (3) the upper one third to one quarter of the succession. The lower and the upper stacking patterns of the middle Bakken are characterized by repeating, generally coarsening-upward and in places fining-upward units which are correlatable over long distances across the study area (Appendix A-H).

The basal few centimeters to decimeters are characterized by a fining-upward trend, and comprises a

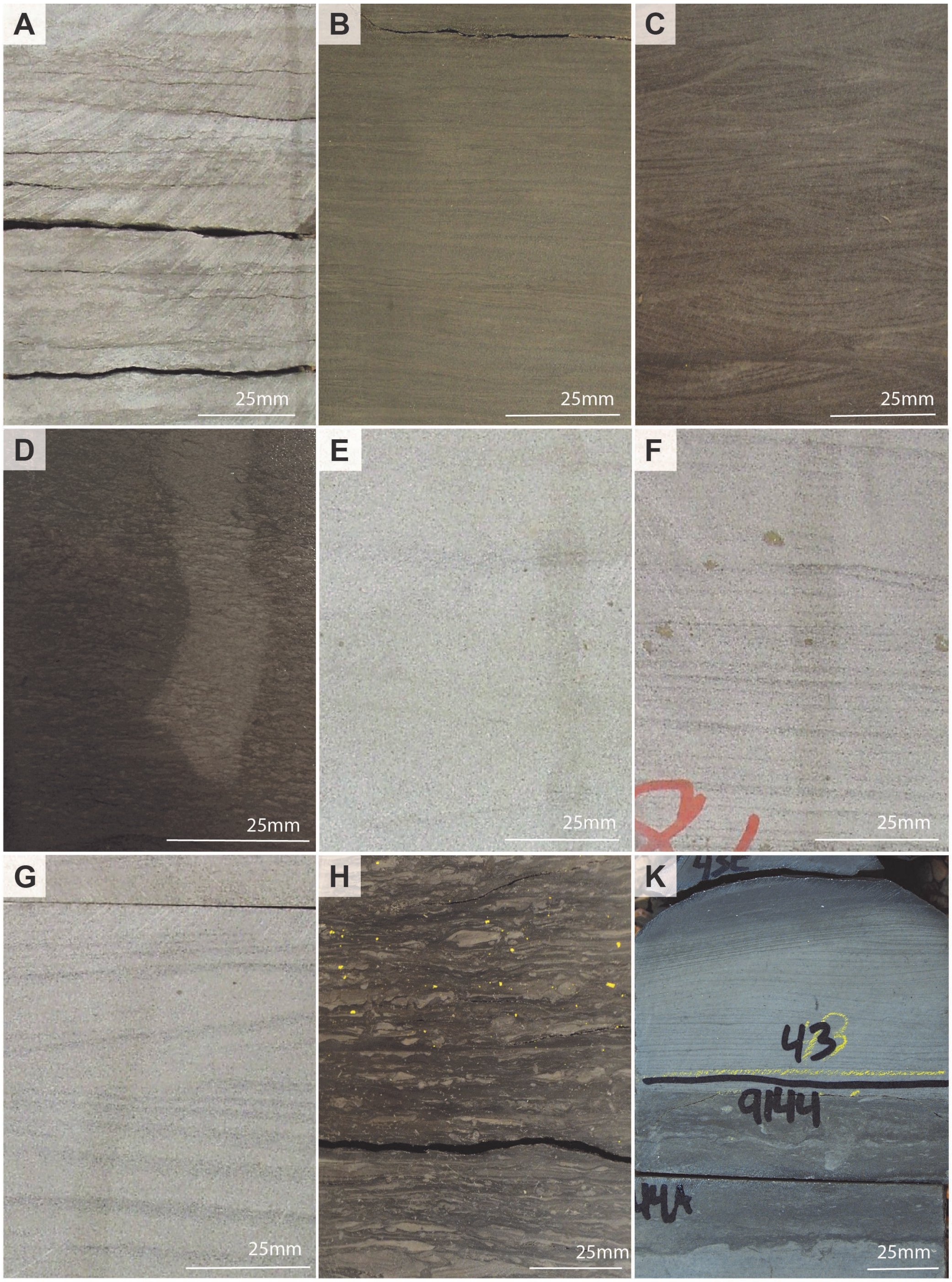

Figure 7: Core photographs demonstrating the purely siliciclastic facies of the middle Bakken member. A) Irregularly laminated siltstone sub-facies 8a; B) Thinly parallel-laminated siltstone sub-facies 8b; C) Wave-rippled siltstone facies 9; D) *Macaronichus*-bearing siltstone facies 10; E) Massive fine-grained sandstone sub-facies 11a; F) Planar-bedded fine-grained sandstone sub-facies 11b; G) Cross-bedded fine-grained sandstone sub-facies 11c; H) Bioturbated sand- to siltstone facies 12; K) Micro-hummocky cross-stratified siltstone facies 13 (top) interbedded with bioturbated sand- to siltstone facies 12 (bottom).

laterally varying in thickness unit that occupies the transition between the lower Bakken shale member and the middle Bakken member. This unit is composed of echinoderm wacke- to packstone with shell fragments, carbonate mud- to wackestone, and glauconitic carbonate-rich siliciclastic mudstone facies, described in detail in Egenhoff (2017).

The lower stacking pattern, excluding the basal several centimeters to decimeters thick part, is characterized by an overall coarsening-upward trend. Internally, it consists of 1 at the margin to 6 in the basin center small-scale internal coarsening-upward stratal packages up to several meters in thickness. The coarsening-upward packages are arranged in a repeating succession of facies from more mud-rich at the base to sand-rich at the top (cf. Egenhoff et al., 2011), however not all facies are present in each of these cycles. An idealized vertical facies succession containing every facies that occurs within the lower portion of the middle Bakken can be constructed to demonstrate the relative position of each of the facies to the under- and overlying strata (Fig. 8 A).

Describing this idealized facies succession (Fig. 8 A), the base is formed by the *Nereites*-bearing siltstones of facies 7. While internally this facies is often massive, it shows differences in spacing between silt-rich beds accompanied by thickness variations of these silt-rich lithologies. The general trend is that silt-rich beds are thinner and more widely spaced in the stratigraphically lower portion of the *Nereites*-bearing facies while becoming thicker and more closely-spaced upsection. In the idealized cycle characterizing the lower stacking pattern, the *Nereites*-bearing siltstone facies grades upwards into the irregularly laminated siltstones of sub-facies 8a, and those into the wave-rippled siltstones of facies 9. The wave-rippled siltstones, in turns, transition abruptly of gradually into the thinly planar-laminated siltstone sub-facies 8b. These siltstones are overlain by the cross-bedded sandstones of sub-facies 11c, which transition into the planar-bedded sandstones of sub-facies 11b above. The massive sandstone sub-facies 11a may occur either sandwiched between sandstone sub-facies 11b and 11c or by itself, and its position relative to other sandstone sub-facies may strongly vary in different wells. The top this idealized cycle lower stacking pattern is marked by bioclast-rich quartz-oolitic pack- to grainstone sub-facies 6b.

The *Nereites*-bearing siltstones and the planar- and the irregularly laminated siltstone sub-facies 8a commonly occur in adjacent wells across the basin (Appendix A-H), the wave-rippled siltstones of facies 9, in contrast, have a limited lateral distribution and are restricted to the western-southwestern parts of the study area (Appendix A-H; Fig. 9).

Four other facies are typical for the top of the lower portion of the middle Bakken. These facies are distributed locally, and appear to be restricted to the southern to southwestern margin of the study area (Fig. 9). While the typical facies make-up of the lower portion of the middle Bakken is predominantly siliciclastic, the only locally occurring four facies at the top of this coarsening-upward succession are predominantly carbonate with minor presence of siliciclastic grains. These facies include bioclastic packstone with peloids (facies 3), oolitic pack- to graistone (facies 6a), bioclastic packstone with aggregate grains (facies 4) and stromatolitic bindstones (facies 5).

The upper part of the succession, generally about one third to one quarter of the middle Bakken, reflects the overall fining-upward trend. This part of the unit contains up to 3 small-scale coarsening- and rarely fining-upwards sediment packages. Similarly to the lower portion of the middle Bakken, an idealized facies succession can be constructed for the upper part.

Macaronichnus-bearing siltstones of facies 10 occupy the base of the upper fining-upward unit (Fig. 8 B). However, this facies occurs only locally, and is present exclusively in the northeastern portion of the study area in Mountrail, Burke and Ward counties (Fig. 9). Where *Macaronichnus*-bearing siltstones are absent, the base of the upper portion of the middle Bakken is marked by the thinly planar-laminated siltstones of sub-facies 8b, overlain by locally-present wave-rippled siltstone facies 9. Irregularly-bedded siltstone sub-faces 8a occupies a position directly on top of the wave-rippled siltstones. Bioturbated sand- to siltstone facies 12 is situated on top of the laminated siltstones in this idealized cycle, and is typically overlain by or interbedded with micro-hummocky cross-stratified siltstone facies 13. The top of the upper fining-upward unit is characterized by the carbonates of the biclastic pack- to grainstone (facies 2) intercalated into the bioclastic mud- to wackestones of facies 1. Coquina beds of facies 2, however, were also found within the upper portion of facies 12.

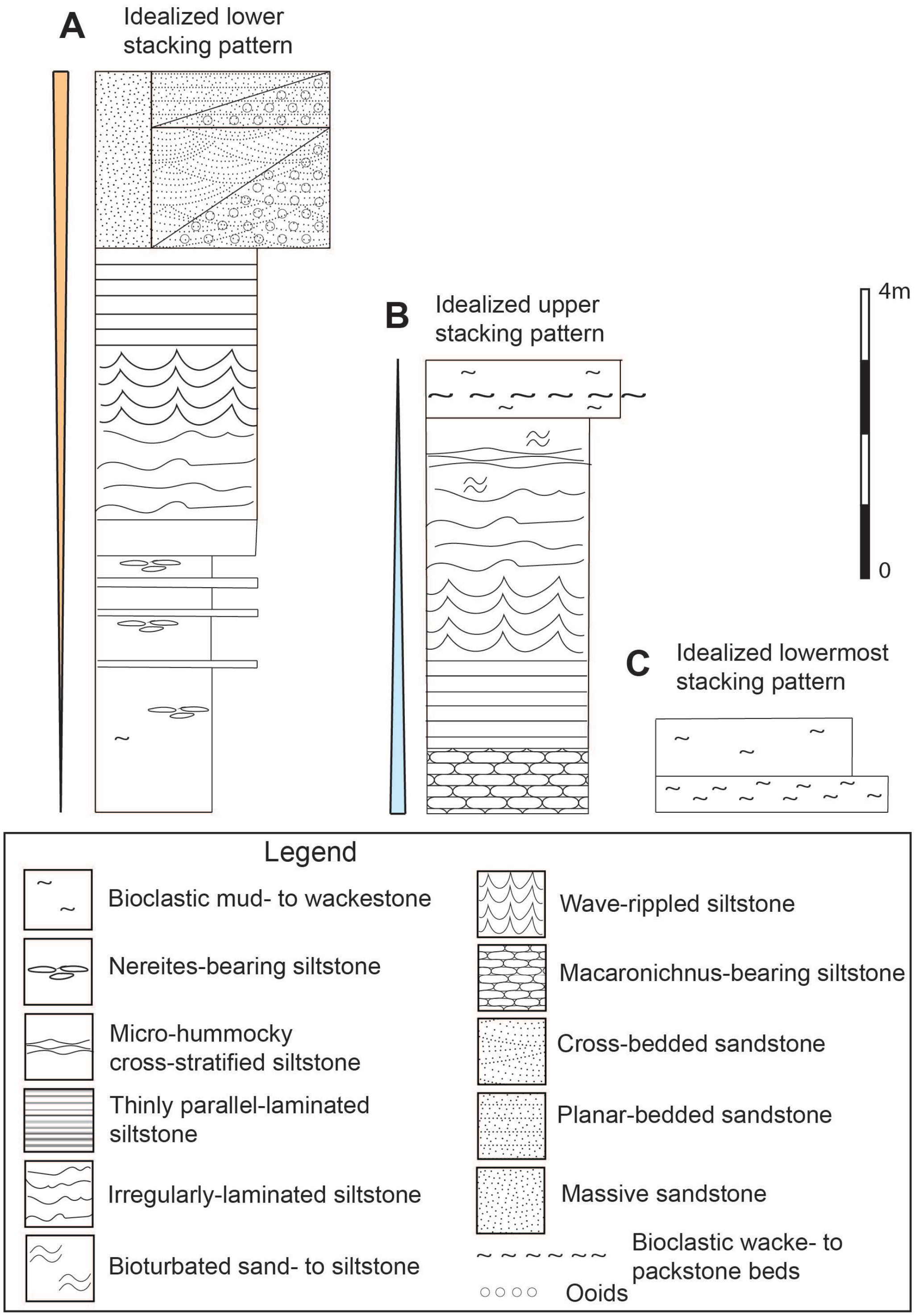

Figure 8: Idealized facies successions characteristic for A) the lower two thirds to three quarters of the middle Bakken succession, excluding the lowermost few centimeters to decimeters; B) the upper third to quarter of the middle Bakken succession; and C) lowermost few centimeters to decimeters of the middle Bakken succession (see Egenhoff, 2017).

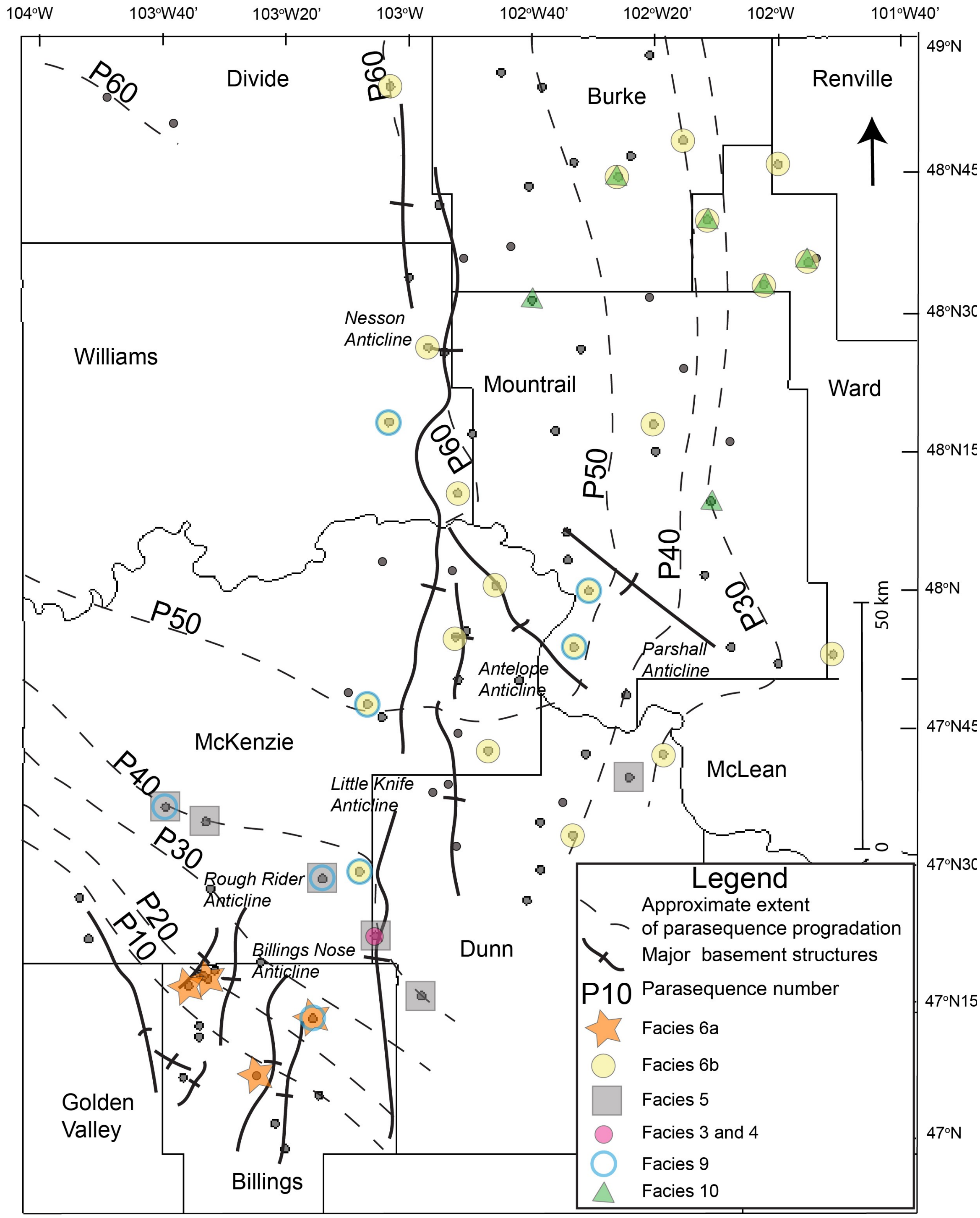

Figure 9: Map depicting the extent of each "regressive" parasequence progradation and distribution of facies that are confined to specific areas within the studied portion of the Williston basin.

INTERPRETATION

Sequence Stratigraphy

The sequence stratigraphic interpretation of the middle Bakken member is based on the correlation of stacking patterns across the study area. The repeating coarsening and in places fining upward stratal packages that build the lower and the upper parts of the succession are herein interpreted as parasequences (Van Wagoner, 1985; Catuneanu, 2006), each of them representing one fluctuation of relative sea-level. Parasequences were identified and correlated using marine flooding surfaces which were recognized by the presence of deeper/low energy facies on top of shallower/high energy facies (Van Wagoner et al., 1988). Generally, parasequences are well defined in the lower portion of the middle Bakken. However, not all flooding surfaces are easy to recognize in this succession. *Nereites*-bearing siltstone of facies 7, especially, often do not show a clear internal architecture organized into distinct parasequences. In this particular case, individual parasequences were defined using the grain size and bioturbation trends: parasequence tops were placed where a trend of upsection thickening and becoming closely-spaced silt-rich beds of the *Nereites*-bearing facies, interpreted as tempestites, resets into upsection thinning- and more widely-spaced siltstone beds, indicating a deepening of the environment. In the upper third to a quarter of the middle Bakken succession, well-defined flooding surfaces are rare to absent as distinct vertical grain size variations are generally lacking. In this part of the succession, parasequences were recognized based on general facies trends determined by the upper stacking pattern, e.g. parasequence tops were placed at the abrupt transitions from relatively shallow to relatively deep facies.

Parasequences bounded by marine flooding surfaces likely represent the highest-frequency cycles of sea-level fluctuations recorded in the middle Bakken strata. They a stacked into parasequence sets that are interpreted as the longer-term lower frequency cycles: regressive systems tract represented by the lower part of the middle Bakken, and transgressive systems tract reflected in the upper part of the middle Bakken member (e.g. Smith and Bustin, 2000; Egenhoff et al., 2011; Angulo and Buatois, 2012).

The carbonates in the basal centimeters to decimeters of the middle Bakken member represent the Falling Stage Systems Tract (FSST) followed by the Lowstand (LST) and the subsequent Transgressive Systems Tracts of the basal middle Bakken succession (Egenhoff et al., 2011). Translating that into the scheme introduced by Embry and Johannessen (1992) and adopted in this study, this part of the succession would be equivalent to the late Regressive (FSST+LST of Egenhoff (2017)) and the overlying Transgressive Systems tracts within one T-R (Transgressive-Regressive) sequence. A condensed section consisting of fine-grained and in places glauconite-rich material marks the maximum flooding interval on top of the transgressive portion of this initial T-R cycle, and thereby the switch from a deepening- and retrogradational to a shallowing-upward and progradational trend.

Overlying this initial middle Bakken cycle is what is here termed the lower part of the middle Bakken succession and is interpreted to represent the Regressive Systems Tract (RST) of Embry (2002). The base of the lower part of the middle Bakken is defined by the gradational switch from carbonate to clastic deposition and a noticeable change from deepening trend to stepwise shallowing and shoreline progradation (see also Egenhoff et al., 2011). The shoreline progradation of shoreface to foreshore deposits is reflected in the presence of sandstones of sub-facies 11 and sub-facies 6b in subsequently younger parasequences moving from the margins of the basin towards the center (Appendix D). The progradation can be observed moving from the nearshore well Mobil Producing Company Pegasus Solomon Bird Bear #F-22-22-1, which contains sandstones in parasequence P30, to a deeper basinward well Dakota-3 George Evans 11V that shows sandstones in parasequence P40, and to an even deeper wells Whiting Oil and Gas Bartleson 44-1H and Pan American Petroleum Clifford Marmon #1, which records sandstone deposits in the youngest of the entire regressive interval parasequence P60.

The top of the regressive systems tract represents the lowest position of the sea-level during middle Bakken time and is interpreted as the maximum regressive surface. This surface marks the surface of subaerial exposure and erosion in marginal areas. The maximum regression is mirrored in the laterally varying number of parasequences within the underlying regressive portion of the succession: the number of parasequences increases from being completely absent in the southwestern margin of the basin in well

Maxus Exploration Crooked Creek State #31-16 (Appendix A) to 6 parasequences in wells Murex Petroleum Jennifer Abigail 16-21H, Ansboro Petroleum Loucks 44-30, and Pan American Petroleum Clifford Marmon #1 located in the basin center (Appendix B). This increase in the number of parasequences from the margin to the basin center reflects receding sea-level during middle Bakken deposition, and that while younger parasequences were being deposited towards the basin center, the margins of the basin were most likely subaerially exposed and subjected to erosion (Egenhoff et al., 2011).

The outbuilding of shoreface-foreshore facies basinward and erosion at the margins indicate progradation during the relative sea-level fall and signifies forced regression (Posamentier and Allen, 1999). Based on the general topography of the Williston basin margins, which most likely had a very low relief, such forced regressions must have been quite common throughout the middle Bakken succession. It is envisioned here that even small drawdowns of sea-level must have had an enormous impact on shrinking of the submerged area within the basin considering its negligible relief (Fig. 9). The upper third to quarter of the succession is here interpreted to reflect a part of a transgression of third order expressed in the agradational to retrogradational stacking of parasequences and an overall fining and deepening upward trend. This portion of the middle Bakken is in agreement with Smith and Bustin (2000), Egenhoff et al. (2011), Angulo and Buatois (2012), and Egenhoff (2017) herein interpreted as the Transgressive Systems Tract in the sense of Embry (2002). The transgressive character of this portion of the middle Bakken is reflected in the progressive deepening of facies as indicated in the idealized transgressive cycle for this part of the succession. Some marginal parasequences in the upper portion of the middle Bakken can be correlated to the basinal upper Bakken parasequences, with the transgressive systems tract culminating in a maximum flooding surface/interval that is located within the overlying upper Bakken member at the top of Interval 1 of Borcovsky et al. (2017).

Depositional model

The middle Bakken depositional environment shows a complex array of facies with a rather unusual distribution throughout the basin. This facies mosaic is not only controlled by the paleo-depth of the area and the relative distance to the coast, but also by the position within the basin and the overall sea-level trend. This chapter introduces two depositional facies profiles of the middle Bakken member, further interpreted as one formed during the regression and another one during the subsequent transgression, characterized by the unique facies belts, and explain why some facies were deposited in specific areas during certain sea-level positions. Additionally, facies that are not included in either of transects but only occur in distinct basin positions are interpreted separately based on their stratigraphic and paleogeographic distribution (Fig. 10).

The depositional transect that characterizes the regressive part of the middle Bakken member encompasses a complex arrangement of facies deposited in offshore to foreshore sedimentary environments (Fig. 10 A). On the most distal end of this depositional transect, furthest away from the shore, *Nereites*-bearing siltstones (facies 7) were deposited in an environment that was relatively tranquil, yet experienced storm reworking at times that is still evident in silt-rich storm beds deposition despite thorough bioturbation. As this facies consistently occurs within the basal parasequences in adjacent wells, it is assumed that the *Nereites*-bearing siltstones formed quite wide facies belts, occupying a significant portion of the Williston basin seafloor during deposition. Closer to shore, the offshore transition zone is characterized by irregularly laminated siltstones (sub-facies 8a) and wave-rippled siltstones (facies 9). After deposition during high-energy events or slightly rough weather, the siltstones were extensively burrowed, likely during fair weather, and were preserved as irregularly laminated siltstones of sub-facies 8a. Wave-rippled siltstones were deposited in mostly wave-dominated areas in the lower shoreface potentially extending to offshore transition and middle shoreface zone. The wave-ripples represent periods of active wave movement, which did not allow for colonization and subsequent bioturbation of sediment by microorganisms.

Shoreface sediments show constant movement of grains, and are characterized by a variety of facies in the middle Bakken succession: ripple-containing thinly planar-laminated siltstones (sub-facies 8b), wave-rippled siltstones (facies 9) and cross-bedded sandstones (sub-facies 11c). Planar-laminated siltstones are thought to be typical for shoreface to foreshore deposition; as waves approach the beach

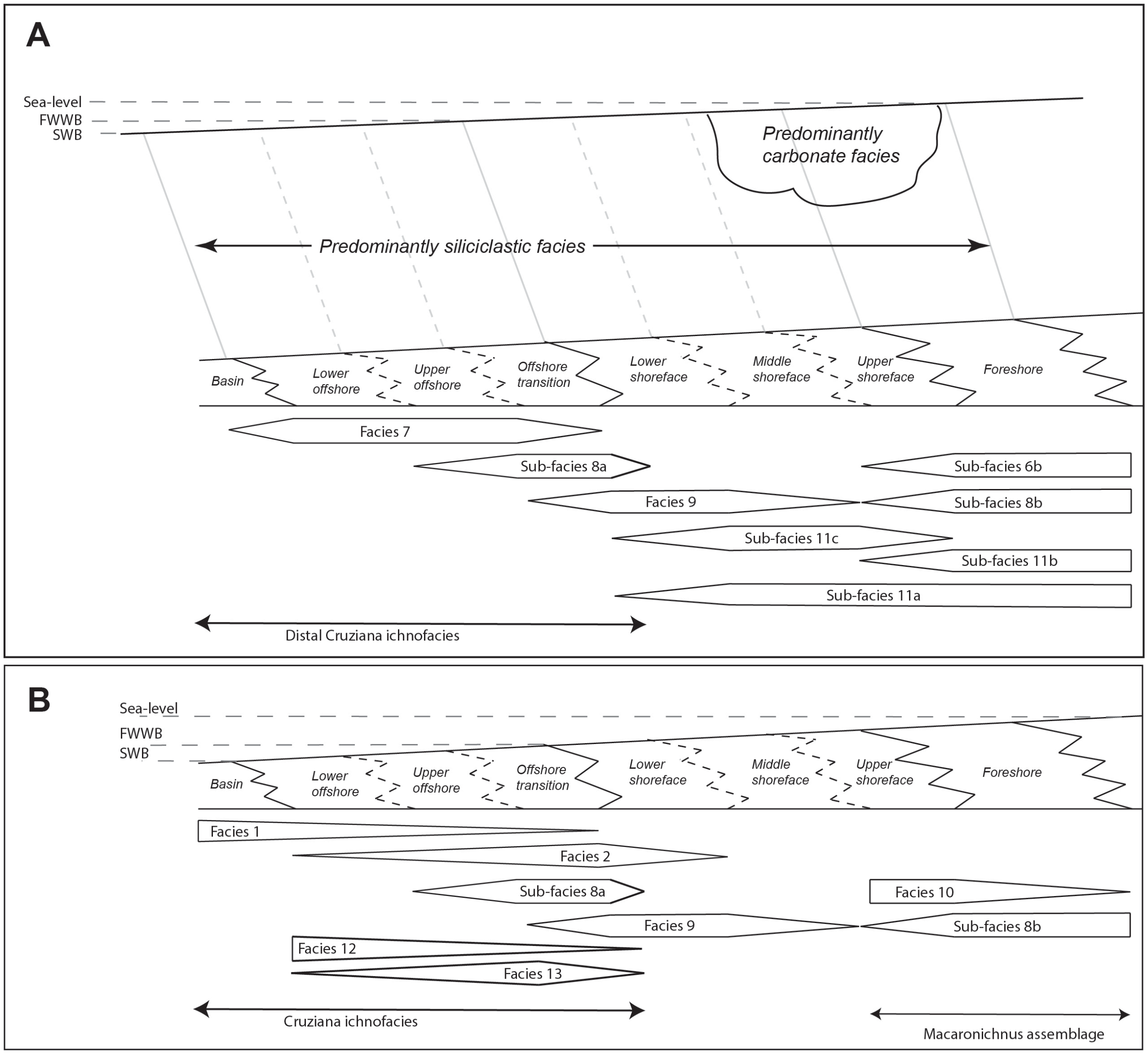

Figure 10: A schematic depositional model showing the relative position of the middle Bakken facies. A) The depositional transect characterizing the facies distributions in the regressive portion of the middle Bakken; B) The depositional transect demonstrating the facies distribution in the transgressive portion of the studied middle Bakken succession. Ichnological references are adopted from Angulo and Buatois, (2012) and Pemberton et al. (2012).

through the shoreface area, sediment affected by the waves experiences an increase in energy that is reflected in a change from ripple to planar lamination in the foreshore area. Cross-bedded sandstones (sub-facies 11c) and intermixed sandstones with ooids sub-facies 6b are interpreted to represent subaqueous dunes or bars in shallow shoreface waters.

The foreshore beach zone is thought to be in part represented by planar-laminated sandstones (sub-facies 11b), siltstones (sub-facies 8b) and sandstones with ooids (sub-facies 6b). It is likely that the lithology of carbonate-bearing and siliciclastic laminae is a reflection of currents redistributing carbonate and clastic material along and down the shelf.

The transgressive part of the succession comprising the upper third to quarter of the succession shows a different array of facies some of which are exclusive to this part of the middle Bakken (Fig. 10 B). The most distal part of this transgressive transect was characterized by generally quiet water depositing the bioclastic mud- to wackestones of facies 1. Storms rarely reached this part of Williston Basin, however, they may have at times accumulated shells and shell debris into local lags which got mixed in with the carbonate mud by later burrowing. Crossing over from the basin into the offshore realm, storms start leaving their mark in the sediment by depositing bioclastic pack- to grainstones (facies 2) and siliciclastic micro-HCS siltstones (facies 13). These classical storm deposits are interbedded with fair-weather sediments, completely homogenized by intense burrowing sand- to siltstones of facies 12. Constant water movement in the shoreface and foreshore areas during the transgression is indicated by thinly parallel-laminated siltstones (sub-facies 8b). Wave-rippled siltstones (facies 9) and irregularly-bedded siltstones (sub-facies 8b) are also present on the transgressive transect, and occupy offshore transition to middle shoreface zone. Short-term sediment starvation is assumed during the formation of the *Macaronichnus*-bearing siltstones (facies 10) as the lack of siliciclastic input is likely responsible for the complete burrowing of the sediment in these siltstone beds being deposited preferentially in upper shoreface positions (Pemberton et al., 2012).

Other middle Bakken facies that are not included in either regressive or transgressive transects are carbonate in composition, appear to be stratigraphically positioned within the regressive cycle, and geographically restricted to southern-southwestern part of the studied portion of the Williston basin (Fig. 9). This group of facies includes stromatolitic bindstone (facies 5), bioclastic packstone with peloids (facies 3), bioclastic packstone with aggregate grains (facies 4) and oolitic pack- to grainstones (sub-facies 6a). Typically, it is assumed that the growth of microbial mats is limited to photic zones with little to no siliciclastic input during deposition. As microbial mats are generally prone to consumption by grazing organisms in normal marine or fresh-water environments (Stal, 2012), it is likely that these shallow areas might have been slightly saline in order to allow the microbial mats to grow. Being located far enough away from siliciclastic input promoted the development of carbonate environment, where oolitic pack- to grainstones of facies 6a occupied a marginal position on the middle Bakken shelf (upper shoreface), experiencing times of high-energy regime when grainstones with relatively large ooids developed, and low energy when packstones with relatively small ooids formed. Similar to oolitic pack- to grainstones (facies 5a), bioclastic packstone with peloids (facies 3) and bioclastic packstone with aggregate grains (facies 4) represent strongly diminished siliciclastic input in comparison to correlative facies and therefore a sheltered area within the basin. Both of these facies are rich in carbonate mud, also arguing for a predominantly low-energy environment during deposition. It remains unclear, though, what the paleo-water depth of these facies was, as any protected lagoonal area is also rich in carbonate mud (see Bahamas, e.g. Purdy, 1963) even though estimated lagoonal depth during most times of Earth history is not more than a few tens of meters (e.g. Vecsei, 2003).

DISCUSSION

Controls on siliciclastic-carbonate mixing and facies architecture

The depositional settings of the regressive and transgressive parts of the middle Bakken generally resemble those of most shallow-marine low-inclined shelfal successions, where facies are typically distributed in wide belts mirroring the orientation of the shoreline. However, the presence of several predominantly carbonate facies localized on the southwestern margin of the study area as well as intermixing of ooids with quartz grains in sandstones and presence of carbonate mud and peloids in the *Nereites*-bearing siltstones facies 7 represent an exception from a classical mixed facies distribution pattern and implies coeval deposition of siliciclastic and carbonate sediments. Although various models have been developed for the mixed of carbonate and siliciclastic deposition (e.g. Chiarella and Longhitano, 2012; Zeller et al., 2015; Schwartz et al., 2018 and examples therein), the true mixing in space and time and lateral along-strike facies variability, in contrast to the reciprocal siliciclastic-carbonate mixing (e.g. Wilson, 1967), is rarely explained in literature (but see Zecchin and Catuneanu, 2015). Moreover, such mixing of siliciclastic and carbonate sediment has never been discussed for the middle Bakken member neither in the American (Canter et al., 2009; Egenhoff et al., 2011; Simenson et al., 2011; Steptoe, 2012) nor in the Canadian (Smith and Bustin, 1996, 2000; Kohlruss and Nickel, 2009; Angulo and Buatois, 2012; Zhang and Buatois, 2014) counterparts of the Williston basin. This study demonstrates three different mechanisms of carbonate-siliciclastic mixing in the middle Bakken member: the reciprocal carbonate sedimentation during marine transgressions, co-deposition of carbonate and siliciclastic sediment in situ during a regression, and lateral variation in carbonate-siliciclastic content.

Reciprocal Sedimentation

Widely distributed across the entire study area carbonates comprised of bioclastic mud- to wackestones of facies 1 and bioclastic wacke- to packstones of facies 2 (Appendix A-H) occur during late stages of transgressive systems tracts twice during middle Bakken deposition. The first basin-wide transgressive carbonate sedimentation occurs at the onset of middle Bakken deposition, and is recorded in the basal few centimeters to decimeters. Subsequent relative sea-level fall resulted in siliciclastic dominated mixed carbonate-siliciclastic sedimentation, see discussion herein, followed by the second transgressive episode recording carbonate facies during the later stage of the marine transgression in the youngest parasequence identified within the middle Bakken member. Both times, relatively high sea-level resulted in flooding of likely the entire basin, thereby hindering the input of siliciclastics into the basin. Therefore, a wide-spread carbonate factory is established as a function of relative a sea-level change and sediment supply (e.g. Van Siclen, 1958; Kerans and Tinker, 1999).

Co-deposition of carbonate and siliciclastic sediment

This study reports both peloids and carbonate mud in siliciclastic siltstones referred to as *Nereites*-bearing facies (facies 7). It is interpreted in this study to reflect coeval deposition of carbonates (the peloids, carbonate mud and some bioclasts; Fig. 6 A, B) and siliciclastics (the bulk of the rock – silt-size grains of quartz, clay minerals, etc.). This coeval deposition of silt-size siliciclastics and carbonates, however, has not been reported for relatively fine-grained material typical of distal mixed ramp deposits so far and requires some additional discussion.

The *Nereites*-bearing facies is typical for a distal, lower to upper offshore, position on the middle Bakken regressive transect (Fig. 10) that was deposited during the initial stages of regression, following a basin-wide carbonate sedimentation during a preceding transgression. During sedimentation of the *Nereites*-bearing facies, the source of the siliciclastic sediment was likely relatively far away from the site of deposition, and, despite the intense bioturbation, it is clear that deposition of the *Nereites*-bearing facies occurred in pulses: storms seemed to have supplied coarser material to the outer ramp, while fine-grained material was deposited during fair weather. During the quiet time between sediment pulses, carbonates seem to have developed on the outer ramp; organisms inhabited and burrowed through the substrate, resulting in the intimate mixing of carbonate and clastic material and leaving peloids and burrows as their trace. This facies is to a large degree siliciclastic yet it contains some primary carbonate and is, therefore, a unique example of a carbonate factory being put on hold during the storm-induced episodes of siliciclastic input. When siliciclastic deposition is halted, carbonate production readily becomes active again. It is, therefore, likely that in the Williston basin during middle Bakken time, the water was supersaturated in calcium carbonate, just like it is today in tropical realms (Broecker and Takahashi, 1966).

Lateral variation in carbonate and siliciclastic content

A fully carbonate system develops on the southwestern margin of the study area. Correlation of parasequences presented in this study and analysis of sedimentary facies suggest that this carbonate depositional system must have already existed during the formation of at least parasequence PS20 (Appendix A). This assumption is supported by the presence of ooids intermixed with shoreface to foreshore sandstones of facies 11, which have been observed as early in the succession as in PS20.

In this study, the ooid-bearing facies are subdivided into two different sub-facies: the oolitic pack- to grainstone sub-facies 6a formed in shallow subaqueous environment during times of alternating high and low energies of deposition, and the bioclast-rich quartz-oolitic pack- to grainstone sub-facies 6b, in which ooids are interpreted to represent reworking of the oolitic pack- to grainstones of sub-facies 6a. Although each of the oolite-bearing sub-facies shows a unique paleogeographic distribution pattern, the origin of ooids intermixed with quartz sand grains in the rocks of facies 6b is not entirely clear. An eolian origin of middle Bakken oolites has been suggested before (Jaffri, 2009) based on stratification patterns and depositional fabrics of these rocks. Wind-lain oolites are also abundant in other carbonates from the Recent and throughout the rock record (Loope and Abbegg 2001, and references therein), however they cannot be reliably differentiated from subaqueously formed dunes based on limited criteria and subsurface exposure (Kocurek and Dott, 1981). Assuming that ooids of facies 6b were transported from their original depositional site by wind and redeposited in an eolian dune environment, a prevalent paleowind direction from southwest to northeast must have existed in this part of the basin during deposition. This assumption, however, has two main shortcomings: (1) the assumed paleowind direction in this part of the continent is most likely from north to south, considering that the Williston basin was located just northwards of the equator and assuming that modern wind directions also hold true for the Latest Devonian and Early Mississippian, trade winds should blow nearly in an opposite direction to the one assumed here to form the observed transport direction of allochthonous ooids; (2) the basin is roundish in shape but also slightly elongated in a northwest-southeast orientation (Gerhard et al., 1990). If the oolites that are still in place are located in the southwestern part of the basin as assumed in this study (Fig. 9), it is difficult to imagine that a wind direction to the NE could have transported these ooids through the parts of the basin that may have been still submerged, and then back out of the subaqueous environment onto the opposite basin's margin to form dunes in a subaerial environment. Seasonal variations of wind directions could have existed in near-equatorial latitudes where the Williston basin was located during the late Devonian –Early Carboniferous (Gerhard et al., 1990) producing monsoonal winds caused by differences in energy absorption of land areas versus the sea during different times of the year, similarly to the present (Prell and Kutzbach, 1987). There are, however, no hydrodynamic studies of sediment transport or paleocurrent measurements that would confirm any prevalent paleowind direction during deposition of the middle Bakken. Based on the abovementioned considerations, it seems unlikely that the ooids of sub-facies 6a were reworked and transported from the southwest toward the northeast by eolian processes.

Moreover, a detailed investigation of the grains comprising sub-facies 6b shows that the quartz grains range from sub-angular to sub-rounded in shape and are poorly to moderately sorted. Eolian sands, on the contrary, are typically well-rounded to rounded and well-sorted (Loope and Abegg, 2001). Additionally, Jaffri (2009) suggested eolian transport and subaerial deposition based on the presence of broken ooids. The ooids in middle Bakken sediments are less than 1 millimeter in diameter, have a radial internal structure, and most likely were originally high-Mg or aragonitic in composition. These characteristics make this type of ooids structurally weaker than comparable tangential and/or low-Mg calcitic variations (Halley, 1977). The breakage of ooids along the radial fractures could have, therefore, easily occurred during high-energy events in a subaqueous environment, e.g. by bedload transport (Heller et al., 1980) or storm/washover events, and is not necessarily an indication of a terrestrial environment, or the presence of deposition in eolian dunes.

Localized paleogeographic distribution of stromatolitic bindstones of facies 5 along the northwest-southeast-oriented transect F-F' (Appendix F) most likely indicates the northernmost extent of the carbonate system (Fig. 9). The development of a pure carbonate environment south of the stromatolitic "front" is most likely due to at least partial isolation of that area from the main source of siliciclastic input. One explanation can be poor circulation within the basin during this time of middle Bakken deposition, resulting in major sediment transport processes not being able to deliver siliciclastic sediment to this part of the basin (e.g. Zeller et al., 2015). That being said, the sediment source for the middle Bakken member was likely located northeast of the study area, potentially extending into Canada. It is also possible that there was not enough siliciclastic sediment delivered into the system due to insignificant elevation of the hinterland and weathering, which is supported by the absence of coarse-grained fraction in the middle Bakken rocks. It is unlikely that the source of siliciclastic sediment was too far away from the study area as, according to Hogancamp and Pocknall (2018), the percentage of terrestrial in origin phytoclasts in the middle Bakken member as well as the angularity of quartz grains imply a nearby terrestrial input.

The position of algal mats, particularly in well American Hunter Exploration Grassy Butte #12-31 H3 and the parasequence progradation pattern (Fig. 9; Appendix F) suggest a potential presence of an intrabasinal structural high corresponding with the southerly extension of the Nesson anticline and/or the Billings Nose anticline. Whether this local high already existed prior to middle Bakken deposition, or formed syndepositionally (Novak and Egenhoff, 2019), or both, it is possible that the topographic expression of basinal structures played a role in sheltering the carbonate environment from an active input of the siliciclastics. This structurally-determined control on carbonate deposition during middle Bakken time is further supported by the pattern of the southernmost extent of siliciclastic sandstones (facies 11) in the regressive portion of the succession. This can be seen in cross-section A-A' (Appendix A) that illustrates successive progradation of sandstones to the south, until they are absent in well American Hunter Exploration Grassy Butte #12-31 H3, where the entire middle Bakken succession is atypically thin and contains algal mats with meteoric dissolution features as a result of subaerial exposure (Nehza and Woo, 2006) at the top of the regressive cycle (Fig. 4 C). Southwest of American Hunter Exploration Grassy

Butte #12-31 H3, the Middle Bakken thickens again but does not contain any sandstones (facies 11), instead, it shows oolitic pack- to grainstone deposits (facies 6a). It is, therefore, suggested that the southern part of the Williston basin is likely situated beyond a structurally-controlled “barrier”, possibly active during deposition (Novak and Egenhoff, 2019), that shelters this area from siliciclastic input from the north.

CONCLUSIONS

1) The middle Bakken member is a siliciclastic-dominated mixed Late Devonian – Early Carboniferous system developed on a gently sloping margin of the Williston basin. Seventeen facies and sub-facies were identified in the middle member of the Bakken formation. Five facies consist of predominantly carbonate material with varying amounts of siliciclastic components, two facies are dominated by the siliciclastic fraction with a high amount of carbonate, and the rest ten facies are purely siliciclastic in composition.

2) These facies developed in diverse depositional environments from the lower offshore to foreshore zones distinguished based on the depositional energy. Facies distribution and architecture is controlled by the hydrodynamic regime of the depositional environment and the relative distance to the coast as well as by the position within the basin and the overall sea-level trend. This study introduces two distinct depositional profiles to explain the distribution of facies in the middle Bakken strata: one characterizing the lower two thirds to three quarters, or the "regressive", portion of the succession, and another one characterizing the upper third to quarter, or the "transgressive", portion.

3) Defined in this study sedimentary facies and sub-facies comprise shallowing- and rarely fining-upward parasequences that build larger scale regressive and transgressive systems tracts. The lowermost few centimeters to decimeters of the succession is defined by typically one parasequence and represents a transgressive systems tract. The lower two thirds to three quarters of the succession comprise from 1 to 6 prograding parasequences and constitute a regressive systems tract. The uppermost third to quarter of the middle Bakken consists of 1 to 4 parasequences that in places are time-equivalent to the lowermost lower Bakken shale strata, and together represent another transgression.

4) Mixing of siliciclastic and carbonate material in the middle Bakken member can be explained with three mechanisms: (1) Reciprocal sedimentation model applies to the transgressive carbonates deposited as facies 1 and facies 2 at the base and at the top of the unit; (2) Coeval deposition of carbonate and siliciclastic material is reflected in the close mixing of carbonate grains (bioclasts and peloids) and

mud with silt-size quartz grains in the *Nereites*-bearing facies 7; (3) Lateral variation in carbonate and siliciclastic content is manifested in the development of a carbonate-dominated environment on the southwestern margin of the study area, and presence of some carbonate grains (oods and bioclasts) in bioclast-rich quartz-oolitic pack- to grainstone facies 6b distributed in the central-northeastern portion of the study area.

5) A combination of sea-level fluctuations, geometric modifications of a basin due to tectonic movements, prevalent sediment transport processes and siliciclastic dilution of carbonate production have influenced mixed clastic and carbonate sedimentation on the middle Bakken shelf. Carbonate-siliciclastic mixing in an intracratonic basin is likely a function of sea-level changes, sediment supply and distribution within a basin, and tectonic evolution of a basin. Reconstructing the sedimentary architecture in such basin would therefore require an integrated basin-centric approach in order to adequately predict important reservoir facies distributions and estimate reservoir geometries.

REFERENCES

Aigner, T., 1985. Storm Depositional Systems. Lecture Notes in Earth Sciences, Springer Verlag, Berlin, 174 pp.

Albert, S., 2014. Sedimentology, Facies Architecture, and Sequence Stratigraphy of the Lower Bakken Shale Member in the Williston Basin, North Dakota, United States of America. Master thesis. Colorado State University, 90 pp.

Allen, J.R.L., 1984. Sedimentary Structures: Their Character and Physical Basis. Elsevier, Amsterdam, 663 pp.

Amorosi, A., 1995. Glaucony and sequence stratigraphy: a conceptual framework of distribution in siliciclastic sequences. Journal of Sedimentary Research, v.65, p. 419-425.

Angulo, A., and Buatois, L.A., 2012. Integrating depositional models, ichnology, and sequence stratigraphy in reservoir characterization: the middle member of the Devonian-Carboniferous Bakken Formation of subsurface southeastern Saskatchewan revisited. American Association of Petroleum Geologists Bulletin, v. 96, p. 1017-1043.

Anna, L. O., Pollastro, R., and Gaswirth, S. B., 2011. Williston Basin Province—Stratigraphic and Structural Framework to a Geologic Assessment of Undiscovered Oil and Gas Resources, Chap. 2 of U.S. Geological Survey Williston Basin Province Assessment Team, Assessment of Undiscovered Oil and Gas Resources of the Williston Basin Province of North Dakota, Montana, and South Dakota, 2010. U.S. Geological Survey Digital Data Series 69–W, 17 pp.

Borcovsky, D., Egenhoff, S., Fishman, N., Maletz, J., Boehlke, A., and Lowers, H., 2017. Sedimentology, facies architecture, and sequence stratigraphy of a Mississippian black mudstone succession - the upper member of the Bakken Formation, North Dakota, United States. American Association of Petroleum Geologists Bulletin, v. 101, no. 10, p. 1625–1673.

Broecker, W. S., and T. Takahashi, 1966. Calcium carbonate precipitation on the Bahama Banks. Journal of Geophysical Research, v. 71, no. 6, p. 1575–1602, doi:10.1029/jz071i006p01575.

Brown, D., and Brown, D., 1987. Wrench-style deformation and paleo structural influence on sedimentation in and around a cratonic basin. RMAG Williston Basin, anatomy of a cratonic oil province, p. 57-70.

Canter, L., Skinner, O., and Sonnenfeld, M. D., 2009. Facies and mechanical stratigraphy of the middle Bakken, Mountrail County, North Dakota: Abstract, SEPM Rocky Mountain Section meeting, Denver, Colorado.

Carozzi, A. V., 1964. Complex ooids from Triassic lake deposits, Virginia. American Journal of Science, v. 262, p. 231-241.

Carozzi, A.V., 1963. Half-moon ooids. Journal of Sedimentary Petrology, v. 33, p. 633-645.

Catuneanu, O., 2006. Principles of sequence stratigraphy. Elsevier, Netherlands, 387 pp.

Chiarella, D., and Longhitano, S. G., 2012. Distinguishing depositional environments in shallow-water mixed, bio-siliciclastic deposits on the basis of the degree of heterolithic segregation (Gelasian, southern Italy). Journal of Sedimentary Research, v. 82, p. 969-990.

Clifton, H. E., and Thompson, J. K., 1978. Macaronichnus segregatis a feeding structure of shallow polychaetes. Journal of Sedimentary Petrology, v. 48, p. 1293-1302.

Clifton, H. E., Hunter, R. E., and Phillips, R. L., 1971. Depositional structures and processes in the non-barred, high-energy nearshore. Journal of Sedimentary Petrology, v. 41, p. 651-670.

Clifton, H.E., 1969. Beach lamination: nature and origin. Marine Geology, v. 7, p. 553–559.

Coffey, B. P., and R. F. Sunde, 2014. Lithology-based sequence-stratigraphic framework of a mixed carbonate-siliciclastic succession, Lower Cretaceous, Atlantic coastal plain. American Association of Petroleum Geologists Bulletin, v. 98, no. 8, p. 1599–1630, doi:10.1306/08211312087.

Cros, P. G., 1979. Genesis of oolites and grapestones, the Bahama Platform (Joulters Cays and the Great Bank). Bulletin des Centres de Recherches Exploration - Production Elf-Aquitaine, v. 3, p. 63-139.

Curran, A. H. 1985. The trace fossil assemblage of a Cretaceous nearshore environment: Englishtown Formation of Delaware, U.S.A., in: A. H. Curran (ed.), Biogenic structures: Their use in interpreting depositional environments. Society of Economic Paleontologists and Mineralogists, Special Publication

35, p. 261–276.

De Raaf, J. F. M., Boersma, J. R., and van Gelder, A., 1977. Wave-generated structures and sequences from a shallow marine deposit, Lower Carboniferous, County Cork, Ireland. Sedimentology, v. 24, p. 451-483.

Dott Jr., R.H., and Bourgeois, J., 1982. Hummocky stratification: significance of its variable bedding sequences. Geological Society of America Bulletin, v. 93, p. 663–680.

Duke, W.L., 1985. Hummocky cross-stratification, tropical hurricanes, and intense winter storms. Sedimentology, v. 32, p. 167–194.

Dunham, R. J., 1962. Classification of Carbonate Rocks According to Depositional Textures, in: W. E. Ham (ed.), AAPG Memoir 1 Classification of carbonate rocks; a symposium, p. 108-121.

Egenhoff, S.O., 2017. The lost Devonian sequence - sequence stratigraphy of the middle Bakken member, and the importance of clastic dykes in the lower Bakken member shale, North Dakota, USA. Marine and Petroleum Geology, v. 81, p. 278–293.

Egenhoff, S.O., van Dolah, A., Jaffri, A., Maletz, J., 2011. Facies architecture and sequence stratigraphy of the middle bakken member, Williston basin, North Dakota, in: Robinson, L., LeFever, J.A., Gaswirth, S. (eds.), Bakken-Three Forks Petroleum System in the Williston Basin. Rocky Mountain Association of Geologists Guidebook, Denver, Colorado. Rocky Mountain Association of Geologists, p. 27–47.

Embry, A. 1992. Transgressive-regressive (T-R) sequence analysis of the Jurassic succession of the Sverdrup Basin, Canadian Arctic Archipelago: Canadian Journal of Earth Science, v.30, p. 301-320.

Embry, A., and E. Johannessen, 1992. T-R sequence stratigraphy, facies analysis and reservoir distribution in the uppermost Triassic-Lower Jurassic succession, western Sverdrup Basin, Arctic Canada, in: T. Vorren (ed.), Arctic Geology and Petroleum Potential: Norwegian Petroleum Society Special Publication 2, p. 121-146.

Flügel, E., 2004. Microfacies of carbonate rocks. Analysis, Interpretation and Application, 2nd edition. Springer, Heidelberg, 984 pp.

Freisatz, W. B., 1995. Fracture-enhanced porosity and permeability trends in the Bakken Formation, Williston Basin, North Dakota. Seventh International Williston Basin Symposium Guidebook, v. 12, p. 389-398.

Gaswirth, S.B., Marra, K.R., Cook, T.A., Charpentier, R.R., Gautier, D.L., Highley, D.K., Klett, T.R., Lewan, M.D., Lillis, P.G., Schenk, C.J., Tennyson, M.E., and Whidden, K.J., 2013. Assessment of undiscovered oil resources in the bakken and three Forks formations, Williston Basin province, Montana, North Dakota, and South Dakota, 2013. U. S. Geological Survey Fact Sheet 2013-3013, 4 pp.

Gerhard, L.C., Anderson, S.B., and Fisher, D.W., 1990. Petroleum geology of the Williston basin, in: Leighton, M.W., Kolata, D.R., Oltz, D.T., Eidel, J.J. (eds.), Interior Cratonic Basins, AAPG Memoir v. 51, p. 507–559.

Goldhammer, R.K., 2003. Cyclic sedimentation, in: G.V. Middleton, M.J. Church, M. Coniglio, L.A. Hardie and F.J. Longstaffe (eds.), Encyclopedia of Sediments and Sedimentary Rocks. Springer, Netherlands, p. 271–293.

Golubic, S., Perkins, R. D., and Lukas, K. J., 1975. Boring microorganisms and microborings in carbonate substrates, in: Frey R.W. (ed.), The Study of Trace Fossils. Springer, Berlin, Heidelberg, 562 pp.

Halley, R.B., 1977. Ooid fabric and fracture in the Great Salt Lake and the geological record. Journal of Sedimentary Petrology, v. 47, p. 1099-1120.

Heller, P.L., Komar, P.D. and Pevear, D.R., 1980. Transport processes in ooid genesis. Journal of Sedimentary Petrology, v. 50, p. 943-952.

Hogancamp, N.J., and Pocknall, D.T., 2018. The biostratigraphy of the Bakken Formation: A review and new data. Stratigraphy, v. 15, no. 3, p. 197–224.

Howard, J. D., 1975. The sedimentological significance of trace fossils, in: R. W. Frey (ed.), The study of trace fossils. Springer-Verlag, New York, p. 131-146.

Huggett, J.M., and Gale, A.S., 1997. Petrology and palaeoenvironmental significance of glaucony in the Eocene succession at Whitecliff Bay, Hampshire Basin, UK. Journal of the Geological Society, v. 154, p. 897– 912.

Jaffri, A. R., 2009. Enhanced recovery from ancient carbonate ramps: lessons and analogs from Paleozoic successions and the Persian Gulf. Dissertation. Colorado State University, 194 pp.

Karma, R., 1991. Conodonts of the Bakken Formation (Devonian-Mississippian) in Saskatchewan, northern Williston basin, in: Christopher, J.E., Haidl, F.M. (eds.), Sixth International Williston Basin Symposium, vol. 11, Saskatchewan Geological Society, Special Publication, p. 70–73.

Kent, D.M., and Christopher, J.E., 1994. Geological history of the Williston basin and the Sweetgrass arch, in: G.D. Mossop, I. Shetson, (eds.), Geological Atlas of Western Canada. Canadian Society of Petroleum Geologists and Alberta Research Council, p. 421–430.

Kerans, C. and Tinker, S., 1999. Extrinsic stratigraphic controls on development of the Capitan reef complex, in: A.H. Saller, P.M. Harris, B.L. Kirkland and S.J. Mazzullo (eds), Geological Framework of the Capitan Reef. SEPM Special Publication 65, p. 15–36.

Kidwell, S. M., 1988. Reciprocal sedimentation and noncorrelative hiatuse in marine-paralic siliciclastics: Miocene outcrop evidence. Geology, v. 16, p. 609–612.

Kocurek, G., and Dott, R. H. Jr., 1981. Distinctions and uses of stratification types in the interpretation of eolian sand. Journal of Sedimentary Petrology, v. 51, no. 2, p. 579-595.

Kohlruss, D. and Nickel, E., 2009. Facies analysis of the Upper Devonian–Lower Mississippian Bakken Formation, southeastern Saskatchewan. Summary of Investigations 2009, Volume 1, Saskatchewan Geological Survey, Saskatchewan Ministry of Energy and Resources, Miscellaneous Report 2009-4.1, Paper A-6, 11 pp.

Łabaj, M. A., and B. R. Pratt, 2016. Depositional dynamics in a mixed carbonate–siliciclastic system: middle–upper Cambrian Abrigo Formation, southeastern Arizona, U.S.A. Journal of Sedimentary Research, v. 86, p. 11-37.

Laird, W., 1952. Geology of the Williston basin in North Dakota. World Petroleum, v. 23, issue 1, part 2, p. 42-47.

LeFever, J.A., LeFever, R.A., Nordeng, S., 2011. Revised nomenclature for Bakken Formation (Mississippian-Devonian), North Dakota, in: L., Robinson, J.A. LeFever, S. Gaswirth (eds.), Bakken-

Three Forks Petroleum System in the Williston Basin. RMAG Guidebook, p. 11–26 (on CD).

Loope D. B., and Abegg, F. E., 2001. Recognition and geologic preservation of ancient carbonate eolianites. SEPM Special Publication 71, p. 3-16.

Logan, B. W., Hoffman, P., and Gebelein, C. D., 1974. Algal Mats, Cryptalgal Fabrics, and Structures, Hamelin Pool, Western Australia, in: B. W. Logan, J. F. Read, G. M. Hagan, P. Hoffman, R. G. Brown, P. J. Woods, and C. D. Gebelein (eds.), Evolution and Diagenesis of Quaternary Carbonate Sequences, Shark Bay, Western Australia. AAPG Memoir 22.

Mackie, J., 2013. Sedimentology and diagenesis of the lower Lodgepole Formation, Williston basin, North Dakota. Master thesis. Colorado State University, 113 pp.

Meissner, F.F., 1978. Petroleum geology of the Bakken Formation, Williston Basin, North Dakota and Montana, in: D. Rehrig (ed.), 1978 Williston Basin Symposium. Montana Geological Society, p. 207–227.

Miller, K. B., Brett, C. E., and Parsons, K. M., 1988. The Paleoecologic significance of storm-generated disturbance within a Middle Devonian muddy epeiric sea. Palaios, v. 3, p. 35-52.

Milroy, P.G., and Wright, V. P., 2000. A highstand oolitic sequence and associated facies from a Late Triassic lake basin, south-west England, Sedimentology, v. 47, p. 187-209.

Mount, J.F., 1984. Mixing of siliciclastic and carbonate sediments in shallow shelf environments. Geology, v. 12, p. 432–435.

Murray, G. H. J., 1968. Quantitative fracture study – Sanish pool, McKenzie County, North Dakota. AAPG Bulletin, v. 52, no. 1, p. 57-65.

Nehza, O., and K. S. Woo, 2006. The effect of subaerial exposure on the morphology and microstructure of stromatolites in the Cretaceous Sinyangdong Formation, Gyeongsang Supergroup, Korea 1. Sedimentology, v. 53, no. 5, p. 1121–1133, doi:10.1111/j.1365-3091.2006.00804.x.

Nordeng, S.H., LeFever, J.A., Anderson, F.J., Bingle-Davis, and Johnson, E.H., 2010. An Examination of the Factors that Impact Oil Production from the Middle Member of the Bakken Formation in Mountrail County, North Dakota. Report of Investigation No. 109. North Dakota Geological Survey, 85 pp.

Novak, A., and Egenhoff, S., 2019. Soft-Sediment Deformation Structures as a Tool to Recognize Synsedimentary Tectonic Activity in the middle member of the Bakken Formation, Williston Basin, North Dakota. Journal of Marine and Petroleum Geology. Marine and Petroleum Geology, v. 105, p. 124-140.

Nummedal, D., and Molenaar, C.M., 1995. Sequence stratigraphy of ramp-setting strand plain successions: the Gallup Sandstone, New Mexico. Sequence stratigraphy of foreland basin deposits, v. 64, p. 277-310.

Obermeier, S.F., 1996. Use of liquefaction-induced features for paleoseismic analysis — an overview of how seismic liquefaction features can be distinguished from other features and how their regional distribution and properties of source sediment can be used to infer the location and strength of Holocene paleo-earthquakes. Engineering Geology, v. 44, p. 1–76.

Payton, C. E., 1977. Seismic stratigraphy – applications to hydrocarbon exploration, AAPG Memoir 26, Tulsa, OK, 516 pp.

Pemberton, G., Maceachern, J. A, Dashtgard, S. E, Kerrie, L. B., Gingras, M., and Zonneveld, J. P., 2012. Shorefaces, in: D. Knaust, R. G. Bromley (eds.), Trace Fossils as Indicators of Sedimentary Environments, v. 64, 960 pp.

Pitman, J.K., Price, L.C., and LeFever, J.A., 2001. Diagenesis and Fracture Development in the Bakken Formation, Williston Basin: Implications for Reservoir Quality in the Middle Member. U. S. Geological Survey Professional Paper 1953, 24 pp.

Plint, A. G., 2010. Wave- and storm-dominated shoreline and shallow-marine systems, in: N. P. James and R. W. Dalrymple (eds.), Facies Models 4, Geological Association of Canada, St. John's, 86 pp.

Pollard, J. E., Goldring, R. and Buck, S. G. 1993. Ichnofabrics containing Ophiomorpha: significance in shallow-water facies interpretation. Journal of the Geological Society of London, v. 150, p. 149–164.

Posamentier, H. W., and Allen, G. P., 1999. Siliciclastic Sequence Stratigraphy—Concepts and Applications, SEPM Concepts in Sedimentology and Paleontology, no. 7.

Prell, W. L., and Kutzbach, J. E., 1987. Monsoon variability over the past 150,000 years. Journal of

Geophysical Research, v. 92, no. D7, p. 8411-8425.

Purdy, E. G., 1963. Recent calcium carbonate facies of the Great Bahama Bank. 2. Sedimentary Facies. The Journal of Geology, v. 71, no. 4, p. 472-497.

Reineck, H. E., and Singh, I. B., 1975. Depositional Sedimentary Environments. Springer-Verlag, Berlin, 439 pp.

Schieber, J., J. B. Southard, P. Kissling, B. Rossman, and R. Ginsburg, 2013, Experimental Deposition of Carbonate Mud From Moving Suspensions: Importance of Flocculation and Implications For Modern and Ancient Carbonate Mud Deposition: Journal of Sedimentary Research, v. 83, no. 11, p. 1025–1031, doi:10.2110/jsr.2013.77.

Scholle, P.A., Ulmer-Scholle, D.S., 2003. A color guide to the petrography of carbonate rocks: grains, textures, porosity, diagenesis. AAPG Memoir 77, 477 pp.

Schwarz, E., G. D. Veiga, G. Álvarez Trentini, M. F. Isla, and L. A. Spalletti, 2018, Expanding the spectrum of shallow-marine, mixed carbonate–siliciclastic systems: Processes, facies distribution and depositional controls of a siliciclastic-dominated example: Sedimentology, v. 65, no. 5, p. 1558–1589, doi:10.1111/sed.12438.

Scotese, C.R., 1994. Carboniferous paleocontinental reconstructions. U. S. Geological Survey Bulletin, v. 2110, p. 3–6.

Simenson, A. L., Sonnenberg, S. A., Cluff, R. M., and Field, P., 2011. Depositional Facies and Petrophysical Analysis of the Bakken Formation , Parshall Field and Surrounding Area , Mountrail County , North Dakota: in: L. Robinson, J.A. LeFever, S. Gaswirth (eds.), Bakken-Three Forks Petroleum System in the Williston Basin. Rocky Mountain Association of Geologists Guidebook, Denver, Colorado. Rocky Mountain Association of Geologists, p. 48–101.

Smith, M.G., and Bustin, R.M., 2000. Late Devonian and Early Mississippian Bakken and Exshaw black shale source rocks, Western Canada sedimentary basin; a sequence stratigraphic interpretation. American Association of Petroleum Geologists Bulletin, v. 84, no. 7, p. 940–960.

Southgate, P. N., Kennard, J. M., Jackson, M. J., O'Brian, P. E., and Sexton, M. J., 1993. Reciprocal

Lowstand Clastic and Highstand Carbonate Sedimentation, Subsurface Devonian Reef Complex, Canning Basin, Western Australia: Chapter 6, in: R. Sarg (ed.), Carbonate Sequence Stratigraphy, AAPG Memoir 57, p. 157-179.

Stal, L. J., 2012. Cyanobacterial Mats and Stromatolites, in: B. A. Whitton (ed.), Ecology of Cyanobacteria ll. Springer, Berlin, 753 pp.

Steptoe, A., 2012. Petrofacies and Depositional Systems of the Bakken Formation in the Williston Basin, North Dakota. Master's thesis. West Virginia University, 165 pp.

Scwartz, E., Veiga, G. D., Trentini, G. A., Isla, M. F., and Spalletti, L. A., 2018. Expanding the spectrum of shallow-marine, mixed carbonate–siliciclastic systems: Processes, facies distribution and depositional controls of a siliciclastic-dominated example. Sedimentology, v. 65, p. 1558-1589.

Van Siclen, D.C., 1958. Depositional topography – examples and theory. American Association of Petroleum Geologists Bulletin, v. 42, p. 1897–1913.

Van Wagoner, J. C., 1985. Reservoir facies distribution as controlled by sea-level change (abs.): Society of Economic Paleontologists and Mineralogists, Annual Midyear Meeting, Abstracts with Programs, v. 2, p. 91-92.

Van Wagoner, J. C., Posamentier, H. W., Mitchum, R. M., Vail, P. R., Sarg, J. F., Loutit, T. S., and Hardenbol, J., 1988. An overview of the fundamentals of sequence stratigraphy and key definitions. SEPM Special Publication 42, p. 39-45.

Vecsei, A., 2003. Systematic yet enigmatic depth distribution of the world's modern warm-water carbonate platforms: the 'depth window'. Terra Nova, v. 15, p. 170-175.

Webster, R.L., 1984. Petroleum source rocks and stratigraphy of the Bakken Formation in North Dakota, in: J. Woodward, F.F. Meissner, J.C. Clayton (eds.), Hydrocarbon Source Rocks of the Greater Rocky Mountain Region. Rocky Mountain Association of Geologists, Denver, p. 57–81.

Wilson, J.L., 1967. Cyclic and reciprocal sedimentation in Virgilian Strata of Southern New Mexico. Geological Society of America Bulletin, v. 78, p. 805–818.

Zecchin, M., and O. Catuneanu, 2017. High-resolution sequence stratigraphy of clastic shelves VI: Mixed siliciclastic-carbonate systems. Marine and Petroleum Geology, v. 88, p. 712–723, doi:10.1016/j.marpetgeo.2017.09.012.

Zeller, M., K. Verwer, G. P. Eberli, J. L. Massaferro, E. Schwarz, and L. Spalletti, 2015. Depositional controls on mixed carbonate-siliciclastic cycles and sequences on gently inclined shelf profiles. Sedimentology, v. 62, no. 7, p. 2009–2037, doi:10.1111/sed.12215.

Zhang, L. and Buatois, L.A., 2014. Sedimentary facies and depositional environments of the Upper Devonian–LowerMississippian Bakken Formation in eastern Saskatchewan. Summary of Investigations 2014, Volume 1, Saskatchewan Geological Survey, Sask. Ministry of the Economy, Miscellaneous Report 2014-4.1, Paper A-3, 18p.

APPENDIX A

CROSS-SECTION A-A’

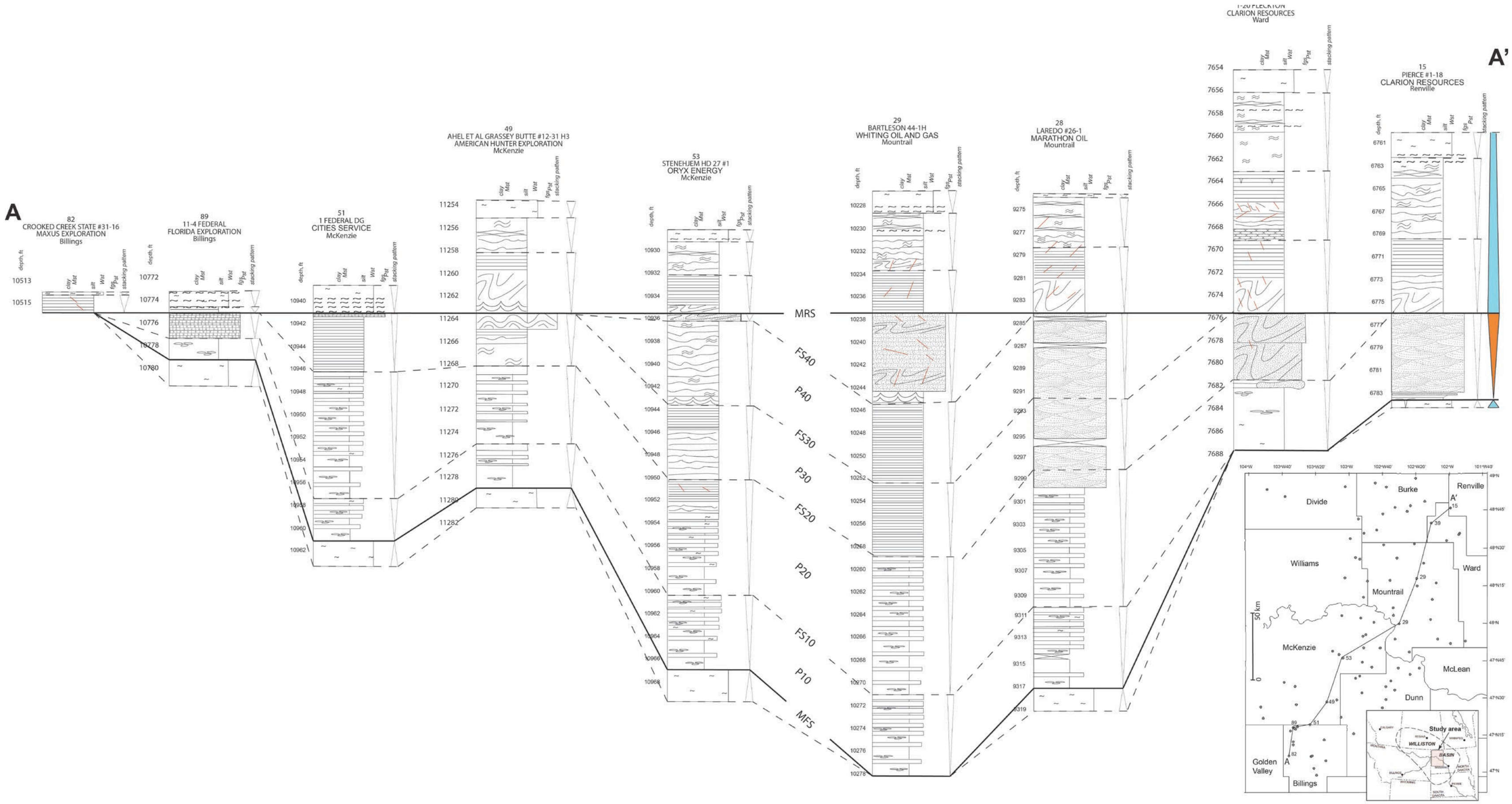
A
A'
82
CROOKED CREEK STATE #31-16
MAXUS EXPLORATION
Billings
89
11-4 FEDERAL
FLORIDA EXPLORATION
Billings
51
1 FEDERAL DG
CITIES SERVICE
McKenzie
49
AHEL ET AL GRASSEY BUTTE #12-31 H3
AMERICAN HUNTER EXPLORATION
McKenzie
53
STENEHJEM HD 27 #1
ORYX ENERGY
McKenzie
29
BARTLESON 44-1H
WHITING OIL AND GAS
Mountrail
28
LAREDO #26-1
MARATHON OIL
Mountrail
CLARION RESOURCES
Ward
15
PIERCE #1-18
CLARION RESOURCES
Renville
depth, ft
clay
Mst
silt
Wst
Pst
stacking pattern
MRS
FS40
P40
FS30
P30
FS20
P20
FS10
P10
MFS
Divide
Burke
Renville
Williams
Mountrail
Ward
McKenzie
McLean
Dunn
Golden Valley
Billings
50 km
0
Study area
WILLISTON
BASIN

APPENDIX B

CROSS-SECTION B-B’


B
4
JENNIFER ABIGAIL 16-21H
MUREX PETROLEUM CORPORATION
Divide
1
LOUCKS 44-30
ANSBRO PETROLEUM COMPANY
Divide
9
NELSON 1-29
CLARION RESOURCES
Burke
7
MERTES #1-32
CLARION RESOURCES
Burke
1-20 FLECKTEN
CLARION RESOURCES
Ward
40
1-33 PULLEN
CLARION RESOURCES
Ward
B'
depth, ft
clay Mst
silt Wst
fgs Pst
stacking pattern
MRS
P60
FS50
P50
FS40
P40
FS30
P30
FS20
P20
FS10
P10
MFS
Divide
Burke
Renville
Williams
Ward
Mountrail
McKenzie
McLean
Dunn
Golden Valley
Billings
50 km
Study area
WILLISTON
BASIN

APPENDIX C

CROSS-SECTIONC-C’

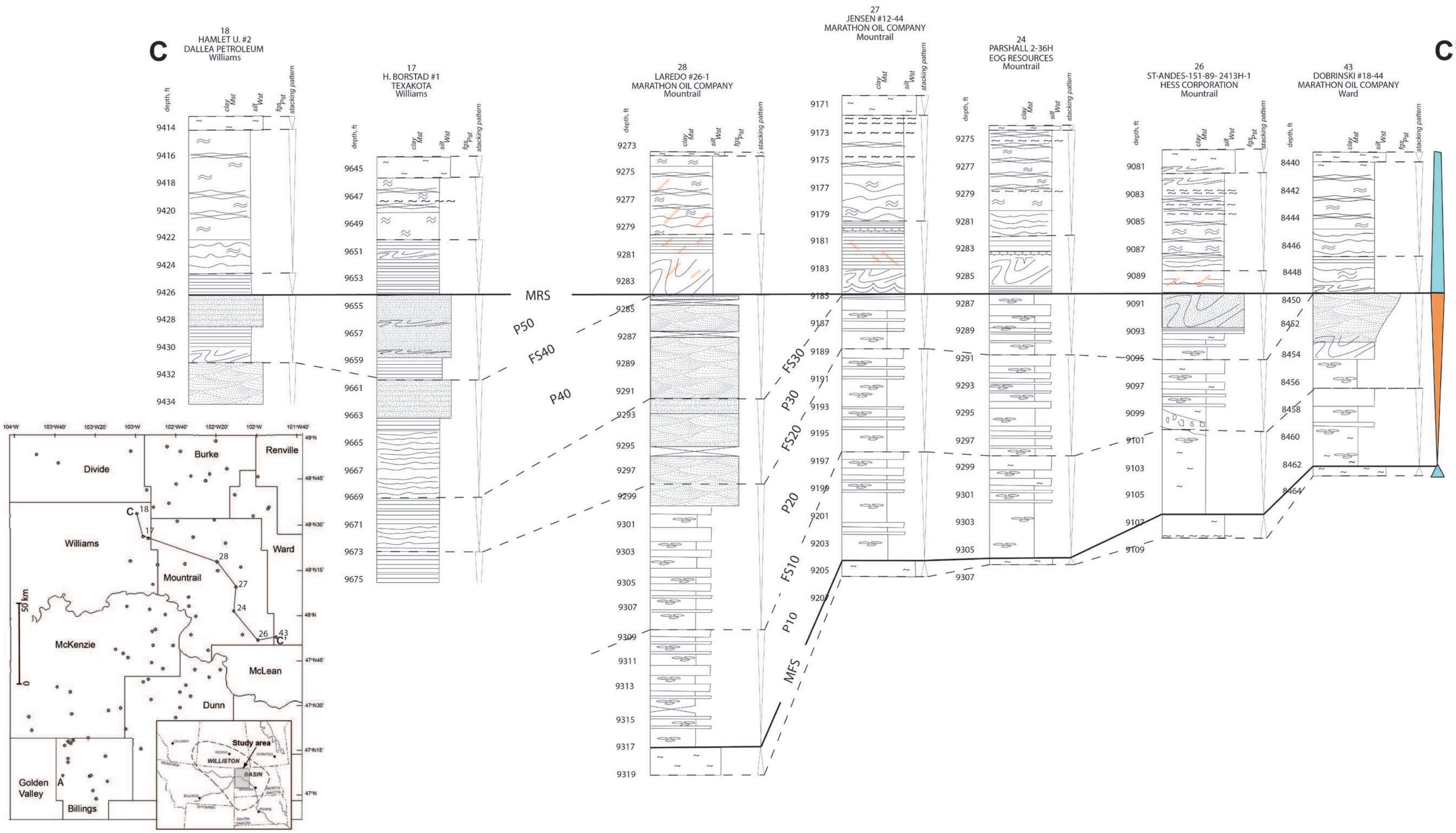
C
18
HAMLET U. #2
DALLEA PETROLEUM
Williams
17
H. BORSTAD #1
TEXAKOTA
Williams
28
LAREDO #26-1
MARATHON OIL COMPANY
Mountrail
27
JENSEN #12-44
MARATHON OIL COMPANY
Mountrail
24
PARSHALL 2-36H
EOG RESOURCES
Mountrail
26
ST-ANDES-151-89- 2413H-1
HESS CORPORATION
Mountrail
43
DOBRINSKI #18-44
MARATHON OIL COMPANY
Ward
C'
MRS
P50
FS40
P40
FS30
P30
FS20
P20
FS10
P10
MFS
Divide
Burke
Renville
Williams
Ward
Mountrail
McKenzie
McLean
Dunn
Golden Valley
Billings
Study area
WILLISTON
BASIN
50 km

APPENDIX D

CROSS-SECTIOND-D’

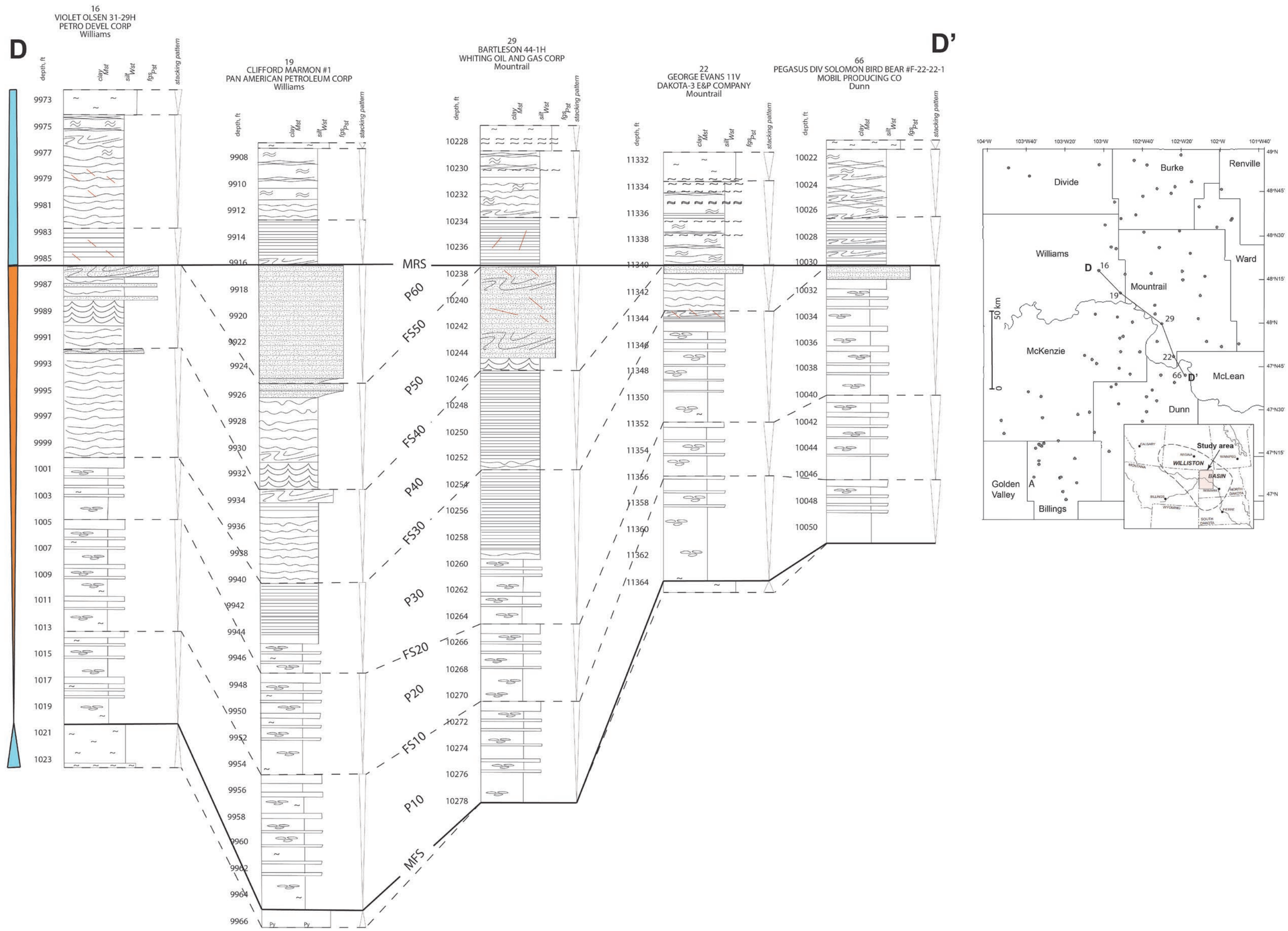
D
D'
16
VIOLET OLSEN 31-29H
PETRO DEVEL CORP
Williams
19
CLIFFORD MARMON #1
PAN AMERICAN PETROLEUM CORP
Williams
29
BARTLESON 44-1H
WHITING OIL AND GAS CORP
Mountrail
22
GEORGE EVANS 11V
DAKOTA-3 E&P COMPANY
Mountrail
66
PEGASUS DIV SOLOMON BIRD BEAR #F-22-22-1
MOBIL PRODUCING CO
Dunn
depth, ft
clay Mst
silt Wst
fgs Pst
stacking pattern
MRS
P60
FS50
P50
FS40
P40
FS30
P30
FS20
P20
FS10
P10
MFS
Divide
Burke
Renville
Williams
Mountrail
Ward
McKenzie
McLean
Dunn
Golden Valley
Billings
50 km
Study area
WILLISTON
BASIN

APPENDIX E

CROSS-SECTION E-E’

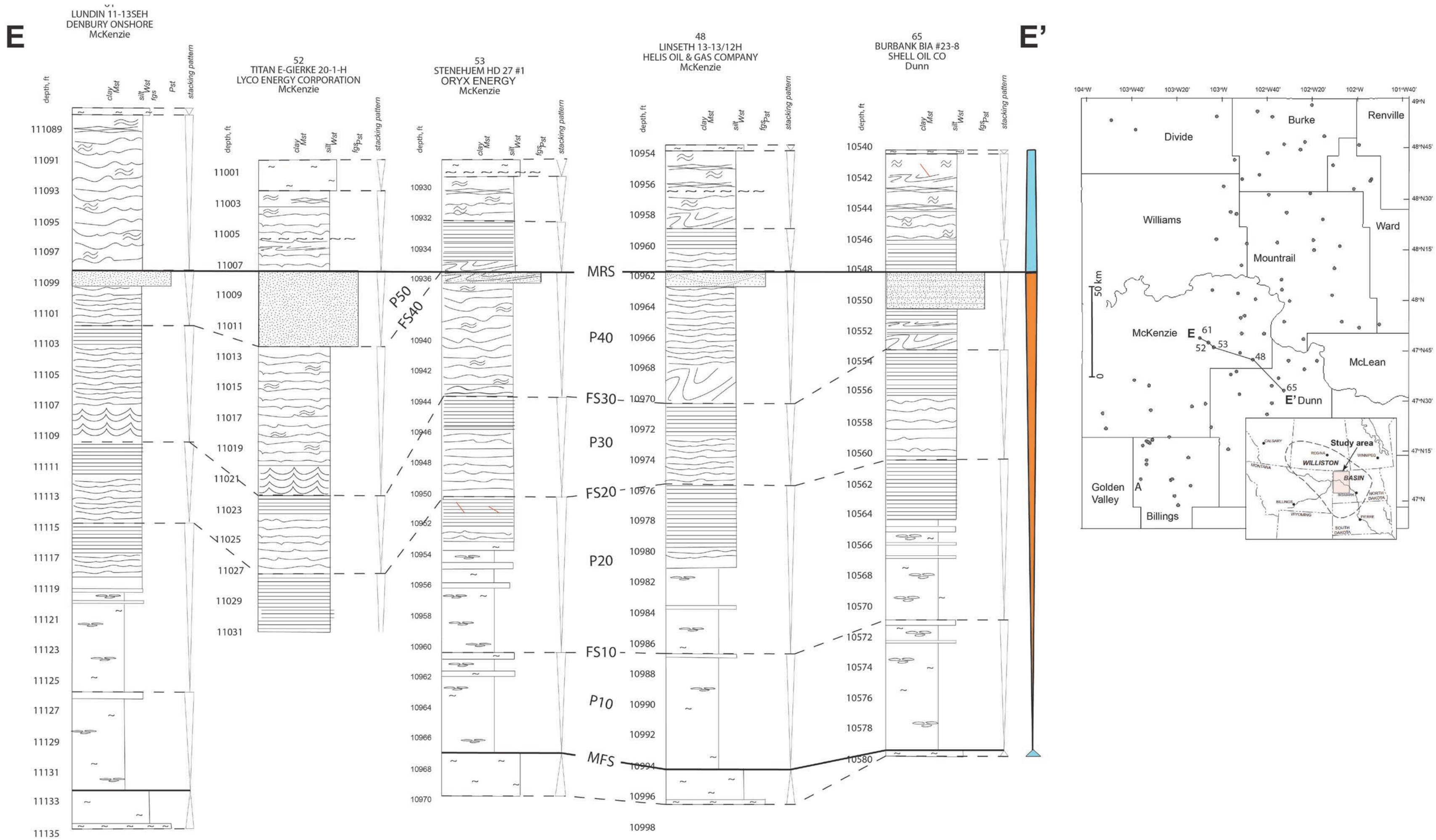
E
E'
LUNDIN 11-13SEH
DENBURY ONSHORE
McKenzie
52
TITAN E-GIERKE 20-1-H
LYCO ENERGY CORPORATION
McKenzie
53
STENEHJEM HD 27 #1
ORYX ENERGY
McKenzie
48
LINSETH 13-13/12H
HELIS OIL & GAS COMPANY
McKenzie
65
BURBANK BIA #23-8
SHELL OIL CO
Dunn
depth, ft
clay Mst
silt Wst
fgs Pst
stacking pattern
MRS
P50
FS40
P40
FS30
P30
FS20
P20
FS10
P10
MFS
Divide
Burke
Renville
Williams
Ward
Mountrail
McKenzie
McLean
Dunn
Golden Valley
Billings
50 km
Study area
WILLISTON
BASIN

APPENDIX F

CROSS-SECTION F-F'

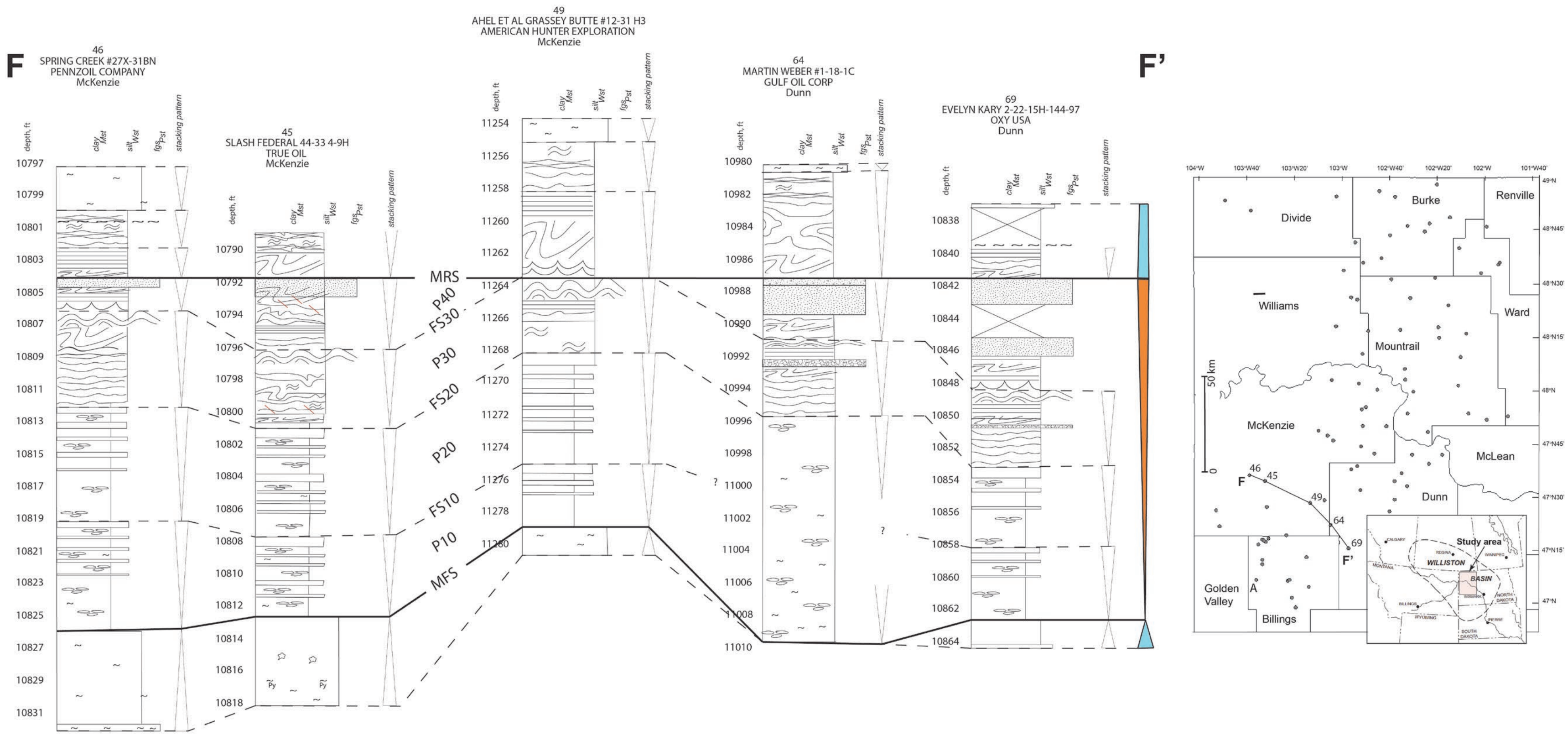

F
F'
46
SPRING CREEK #27X-31BN
PENNZOIL COMPANY
McKenzie
45
SLASH FEDERAL 44-33 4-9H
TRUE OIL
McKenzie
49
AHEL ET AL GRASSEY BUTTE #12-31 H3
AMERICAN HUNTER EXPLORATION
McKenzie
64
MARTIN WEBER #1-18-1C
GULF OIL CORP
Dunn
69
EVELYN KARY 2-22-15H-144-97
OXY USA
Dunn
depth, ft
stacking pattern
MRS
P40
FS30
P30
FS20
P20
FS10
P10
MFS
Divide
Burke
Renville
Williams
Ward
Mountrail
McKenzie
McLean
Dunn
Golden Valley
Billings
50 km
Study area
WILLISTON
BASIN

APPENDIX G

CROSS-SECTION G-G’

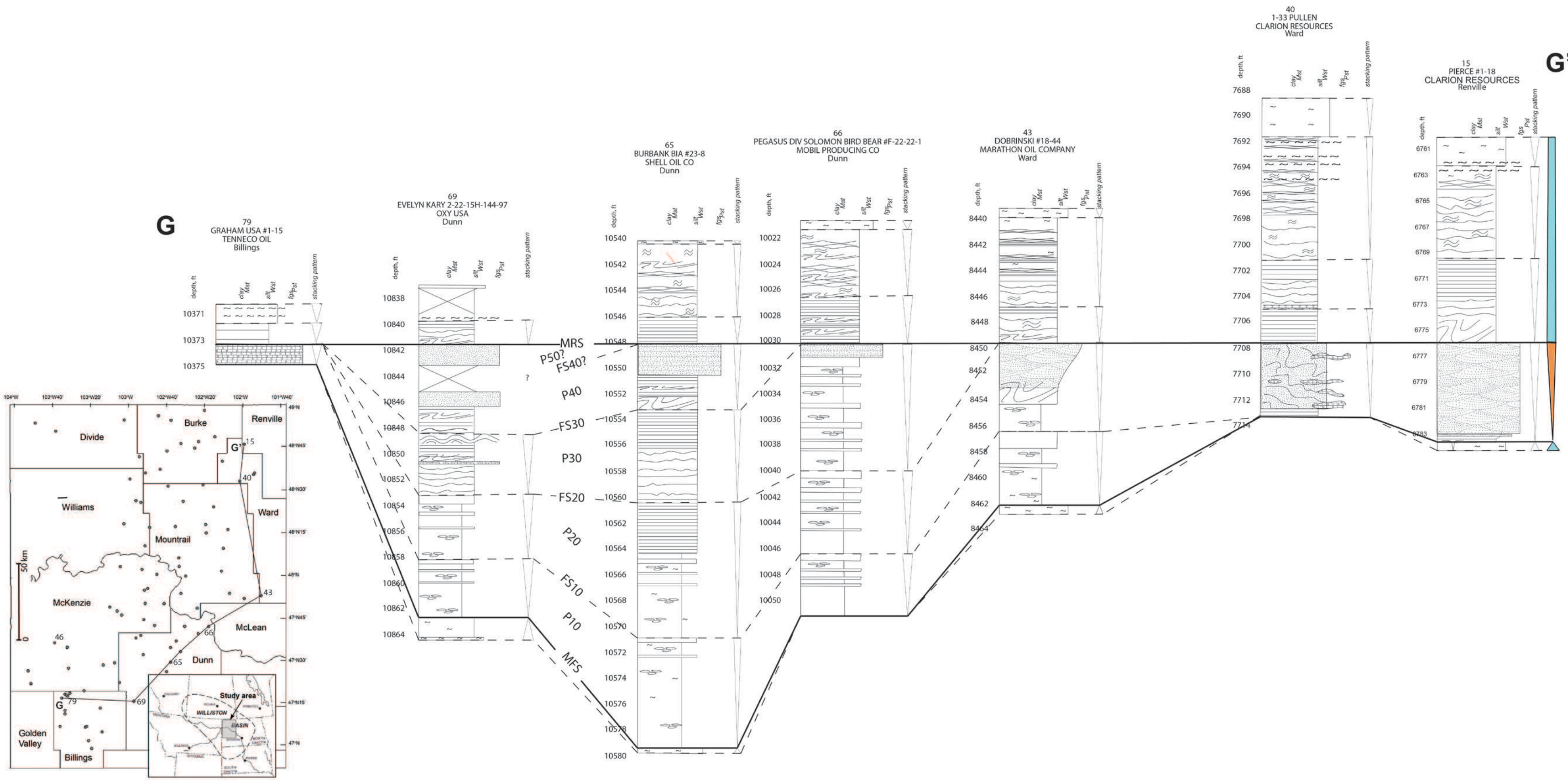
G
G'
79
GRAHAM USA #1-15
TENNECO OIL
Billings
69
EVELYN KARY 2-22-15H-144-97
OXY USA
Dunn
65
BURBANK BIA #23-8
SHELL OIL CO
Dunn
66
PEGASUS DIV SOLOMON BIRD BEAR #F-22-22-1
MOBIL PRODUCING CO
Dunn
43
DOBRINSKI #18-44
MARATHON OIL COMPANY
Ward
40
1-33 PULLEN
CLARION RESOURCES
Ward
15
PIERCE #1-18
CLARION RESOURCES
Renville
MRS
P50?
FS40?
P40
FS30
P30
FS20
P20
FS10
P10
MFS
Divide
Burke
Renville
Williams
Mountrail
Ward
McKenzie
McLean
Dunn
Golden Valley
Billings
Study area
WILLISTON
BASIN
50 km

APPENDIX H

CROSS-SECTION H-H’

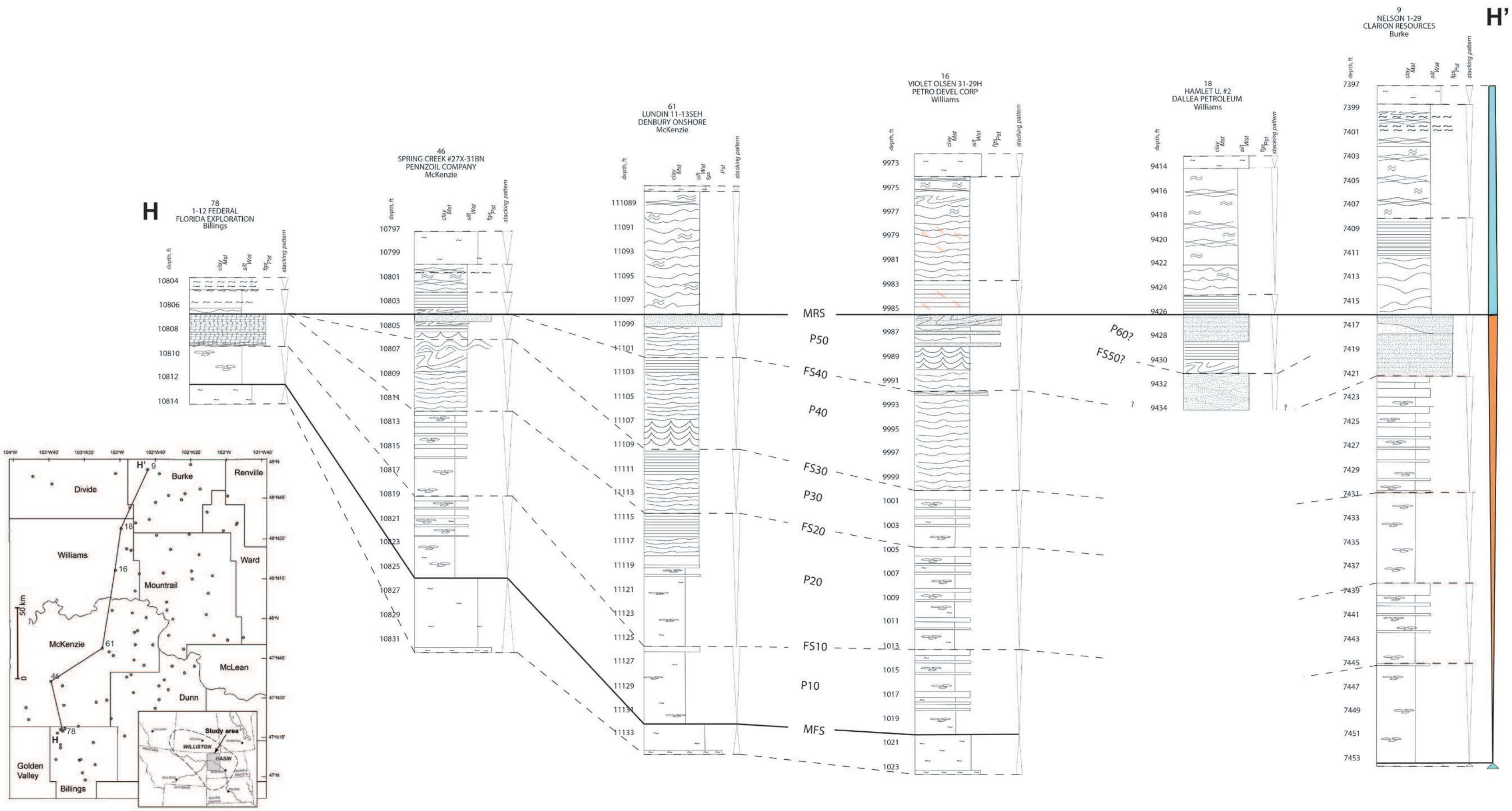
H
H'
78
1-12 FEDERAL
FLORIDA EXPLORATION
Billings
46
SPRING CREEK #27X-31BN
PENNZOIL COMPANY
McKenzie
61
LUNDIN 11-13SEH
DENBURY ONSHORE
McKenzie
16
VIOLET OLSEN 31-29H
PETRO DEVEL CORP
Williams
18
HAMLET U. #2
DALLEA PETROLEUM
Williams
9
NELSON 1-29
CLARION RESOURCES
Burke
MRS
P50
FS40
P40
FS30
P30
FS20
P20
FS10
P10
MFS
P60?
FS50?
Divide
Burke
Renville
Williams
Ward
Mountrail
McKenzie
McLean
Dunn
Golden Valley
Billings
Study area
WILLISTON
BASIN
50 km

APPENDIX I

KEY TO CROSS-SECTIONS A-A’ TO H-H’

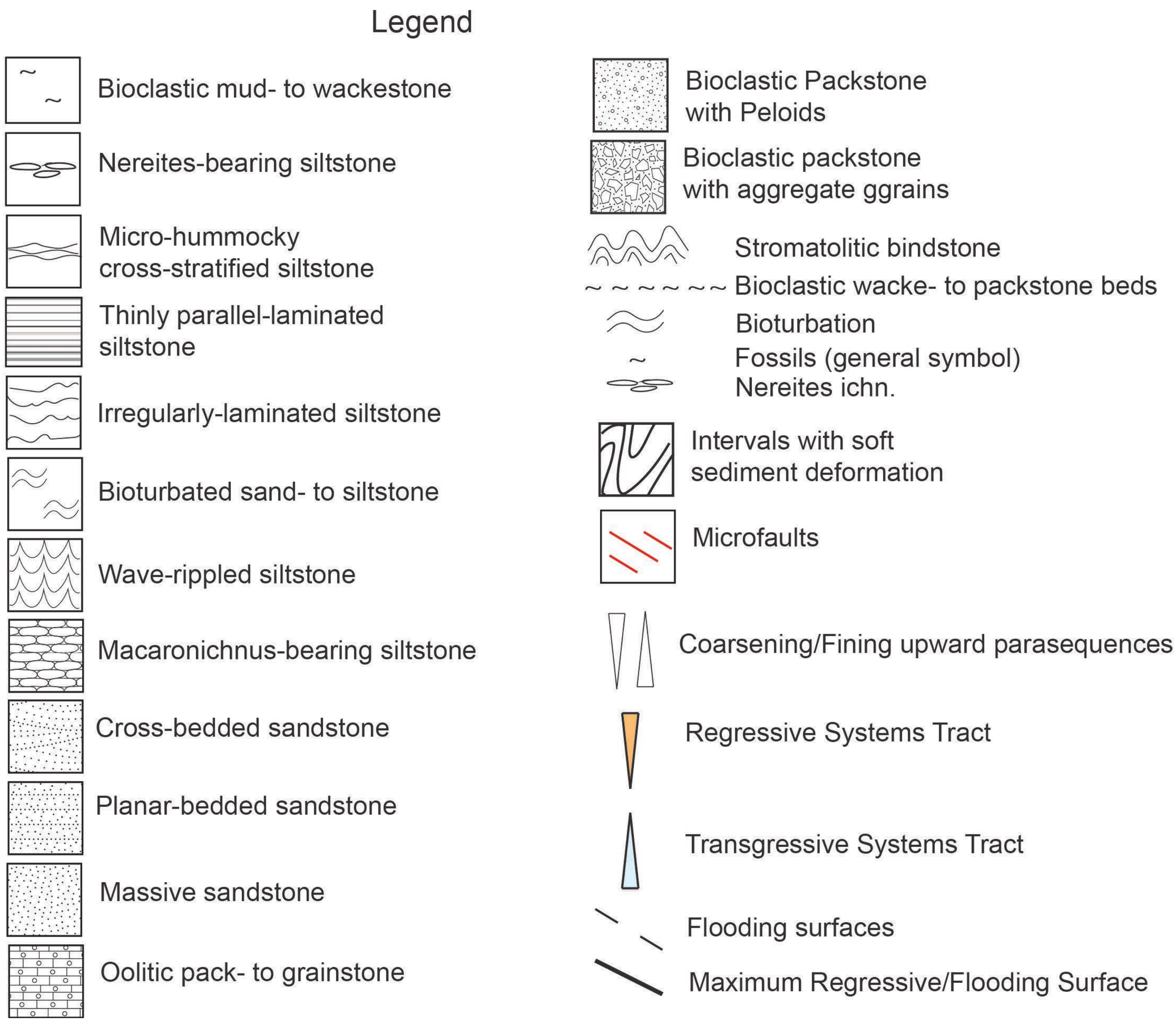
Legend
Bioclastic mud- to wackestone
Nereites-bearing siltstone
Micro-hummocky cross-stratified siltstone
Thinly parallel-laminated siltstone
Irregularly-laminated siltstone
Bioturbated sand- to siltstone
Wave-rippled siltstone
Macaronichnus-bearing siltstone
Cross-bedded sandstone
Planar-bedded sandstone
Massive sandstone
Oolitic pack- to grainstone
Bioclastic Packstone with Peloids
Bioclastic packstone with aggregate ggrains
Stromatolitic bindstone
Bioclastic wacke- to packstone beds
Bioturbation
Fossils (general symbol)
Nereites ichn.
Intervals with soft sediment deformation
Microfaults
Coarsening/Fining upward parasequences
Regressive Systems Tract
Transgressive Systems Tract
Flooding surfaces
Maximum Regressive/Flooding Surface

APPENDIX J

LIST OF WELLS UTILIZED IN THIS STUDY

Map Annotation Number	Original Well Name	Original Operator	API	County	Library File Number
1	LOUCKS 44-30	ANSBRO PETROLEUM COMPANY, LLC	3302300471	Divide	15722
2	WATTERUD "A" #17	CONOCO INC.	3302300412	Divide	13318
3	TOMLINSON 3-1HN	SM ENERGY COMPANY	3302301120	Divide	26745
4	JENNIFER ABIGAIL 16-21H	MUREX PETROLEUM CORPORATION	3302300975	Divide	24642
5	1-24 SLATER	CLARION RESOURCES	3301300853	Burke	B679
6	LOUIS PETERSON #1	NORTHERN PUMP CO.	3301300699	Burke	4508
7	MERTES #1-32	CLARION RESOURCES, INC.	3301300862	Burke	8819
8	NEGAARD #1	CLARION RESOURCES, INC.	3301300877	Burke	9001
9	NELSON 1-29	CLARION RESOURCES, INC.	3301300867	Burke	8850
10	JORGENSEN 4 - 4H	CORNERSTONE NATURAL RESOURCES LLC	3301301491	Burke	18829
11	OAS 31-161-92H	SAMSON RESOURCES COMPANY	3301301383	Burke	16810
12	SARATOGA 12-1-161-92H	SAMSON RESOURCES COMPANY	3301301667	Burke	22572
13	DOUTS 4-7H	ST MARY LAND & EXPLORATION COMPANY	3301301412	BURKE	17265
14	PRODUCER`S CORPORATION 159-94-17C-8-2H	PETRO-HUNT, L.L.C.	3301301530	BURKE	19773
15	PIERCE #1-18	CLARION RESOURCES, INC.	3307500873	Renville	8637
16	VIOLET OLSEN 31-29H	PETRO DEVEL CORP	3310501551	Williams	E968
17	H. BORSTAD #1	TEXAKOTA, INC.	3310500732	Williams	5656
18	HAMLET U. #2	DALLEA PETROLEUM CORP.	3310500606	Williams	3007
19	CLIFFORD MARMON #1	PAN AMERICAN PETROLEUM CORP.	3310500667	Williams	4340
20	NESSON STATE 42X-36	HEADINGTON OIL COMPANY LLC	3310501667	Williams	17015
21	H. BAKKEN 12-07H	HESS CORPORATION	3310501618	Williams	16565
22	GEORGE EVANS 11V	DAKOTA-3 E&P COMPANY, LLC	3306102032	Mountrail	22421
23	MYLO WOLDING 14-11	MARATHON OIL COMPANY	3306101194	Mountrail	18511

24	PARSHALL 2-36H	EOG RESOURCES, INC.	3306100503	Mountrail	16324
25	AHEL ET AL SANISH #36-44 H4	AMERICAN HUNTER EXPLORATION LTD.	3306100398	Mountrail	12807
26	ST-ANDES-151-89- 2413H-1	HESS CORPORATION	3306100653	Mountrail	17043
27	JENSEN #12-44	MARATHON OIL COMPANY	3306100257	Mountrail	8069
28	LAREDO #26-1	MARATHON OIL COMPANY	3306100394	Mountrail	12786
29	BARTLESON 44-1H	WHITING OIL AND GAS CORPORATION	3306100495	Mountrail	16068
30	ROGSTAD #1-11	BROOKS EXPLORATION, INC.	3306100252	Mountrail	7851
31	L. TEXEL #21-35	SHELL OIL CO.	3306100187	Mountrail	5088
32	STATE ND 1-11H	AMERADA HESS CORPORATION	3306100498	Mountrail	16160
33	MILDRED ROGGENBUCK 41-24TFX	WHITING OIL AND GAS CORPORATION	3306102049	Mountrail	22532
34	FERTILE 1-12H	EOG RESOURCES, INC.	3306100557	Mountrail	16743
35	FARHART 11-11H	FIDELITY EXPLORATION & PRODUCTION COMPANY	3306100680	Mountrail	17096
36	SIDONIA 1-06H	EOG RESOURCES, INC.	3306100884	Mountrail	17676
37	RS-STATE C-157-90- 3603H-1	HESS CORPORATION	3306100666	Mountrail	17071
38	MCALMOND 1-05H	EOG RESOURCES, INC.	3306100587	Mountrail	16862
39	1-20 FLECKTON	CLARION RESOURCES	3310100273	Ward	B706
40	1-33 PULLEN	CLARION RESOURCES	3310100272	Ward	B678
41	STEINBERGER #1-16	GOLDEN EYE RESOURCES, LLC	3310100476	Ward	17377
42	J. Brekhus #2-14	GOLDEN EYE RESOURCES, LLC	3310100475	Ward	17347
43	DOBRINSKI #18-44	MARATHON OIL COMPANY	3310100260	Ward	8177
44	15-22 BN Flat Top Butte	PENNZOIL COMPANY	3305301030	McKenzie	D284
45	SLASH FEDERAL 44-33 4-9H	TRUE OIL LLC	3305303925	McKenzie	22180
46	SPRING CREEK #27X-31BN	PENNZOIL COMPANY	3305302340	McKenzie	12983
47	USA 33-23-154	SHELL OIL CO.	3305301391	McKenzie	8902
48	LINSETH 13-13/12H	HELIS OIL & GAS COMPANY, L.L.C.	3305303693	McKenzie	21217
49	AHEL ET AL GRASSEY BUTTE #12-31 H3	AMERICAN HUNTER EXPLORATION LTD.	3305302308	McKenzie	12772
50	POJORLIE 21-2-1H	GMX RESOURCES INC	3305303872	McKenzie	21884

51	1 FEDERAL DG	CITIES SERVICE	3305301536	McKenzie	T418
52	TITAN E-GIERKE 20-1-H	LYCO ENERGY CORPORATION	3305302672	McKenzie	15923
53	STENEHJEM HD 27 #1	ORYX ENERGY CO.	3305302357	McKenzie	13098
54	F. P. KEOGH #4	TEXACO INC.	3305300477	McKenzie	2820
55	JENS STRAND #1	AMERADA PETROLEUM CORP.	3305300144	McKenzie	1202
56	MOI #44-13	MERIDIAN OIL, INC.	3305302188	McKenzie	12160
57	FORT BERTHOLD 150-94-3B-10-2H	PETRO-HUNT, L.L.C.	3305303623	McKenzie	20915
58	LARS ROTHIE 32-29H	HESS CORPORATION	3305302769	McKenzie	16433
59	HA-NELSON- 152-95-3328H-9	HESS CORPORATION	3305305469	McKenzie	26980
60	LINSETH 4-8H	HELIS OIL & GAS COMPANY, L.L.C.	3305302809	McKenzie	16689
61	LUNDIN 11-13SEH	DENBURY ONSHORE, LLC	3305303829	McKenzie	21706
62	UBERWACHEN 22-34	BURLINGTON RESOURCES OIL & GAS COMPANY LP	3305303819	McKenzie	21668
63	TARPON FEDERAL 44-19TFHU	WHITING OIL AND GAS CORPORATION	3305305595	McKenzie	27413
64	MARTIN WEBER #1-18-1C	GULF OIL CORP.	3302500067	Dunn	6082
65	BURBANK BIA #23-8	SHELL OIL CO.	3302500232	Dunn	8709
66	PEGASUS DIV SOLOMON BIRD BEAR #F-22-22-1	MOBIL PRODUCING CO.	3302500005	Dunn	793
67	YOUNG BEAR #32-4	SHELL OIL CO.	3302500347	Dunn	9707
68	ANGUS KENNEDY #F32-24-P	SOCONY-VACUUM OIL COMPANY, INC.	3302500003	Dunn	607
69	EVELYN KARY 2-22-15H-144-97	OXY USA INC.	3302502118	Dunn	25364
70	STOHLER 21-3H	MARATHON OIL COMPANY	3302500597	Dunn	16333
71	CORRINE OLSON 34-20	MARATHON OIL COMPANY	3302501117	Dunn	19118
72	FORT BERTHOLD 147-94-3B-10-3H	PETRO-HUNT, L.L.C.	3302501964	Dunn	24272
73	ROBERTS TRUST 1-13H	SIMRAY GP, LLC	3302500982	Dunn	18355
74	JANE FEDERAL 11X-20	HEADINGTON OIL COMPANY LLC	3302500794	Dunn	17430
75	HAWKINSON 14-22H2	CONTINENTAL RESOURCES, INC.	3302502007	Dunn	24456

76	JORGENSON 1-15H	NEWFIELD PRODUCTION COMPANY	3302500729	Dunn	17086
77	3-17 TOC MEE USA	TENNECO OIL	3300700581	Billings	B659
78	1-12 FEDERAL	FLORIDA EXPLORATION	3300700830	Billings	E383
79	GRAHAM USA #1-15	TENNECO OIL	3300700690	Billings	B658
80	5-1 THOMPSON UNIT	TEXACO INCORPORATED	3300701185	Billings	E349
81	FRANKS CREEK STATE 21-16TFH	WHITING OIL AND GAS CORPORATION	3300701676	Billings	20574
82	CROOKED CREEK STATE #31-16	MAXUS EXPLORATION CO.	3300701162	Billings	12558
83	MOI ELKHORN #33-11	MERIDIAN OIL, INC.	3300701109	Billings	12072
84	FEDERAL #12-12	MILESTONE PETROLEUM, INC.	3300701014	Billings	10989
85	F-6-144-101 #3	SUPRON ENERGY CORP.	3300700820	Billings	9351
86	23-143-102 BN #1	COASTAL OIL & GAS CORP. & AL-AQUITAINE	3300700666	Billings	8363
87	FEDERAL 34-1	FLORIDA EXPLORATION CO.	3300700997	Billings	10803
88	CHRUSZCH 43X-29	XTO ENERGY INC.	3300701632	Billings	17768
89	11-4 FEDERAL	FLORIDA EXPLORATION	3300700914	Billings	E385

PART III: SOFT-SEDIMENT DEFORMATION STRUCTURES AS A TOOL TO RECOGNIZE SYNSEDIMENTARY TECTONIC ACTIVITY IN THE MIDDLE MEMBER OF THE BAKKEN FORMATION, WILLISTON BASIN, NORTH DAKOTA

INTRODUCTION

Seismically induced soft-sediment deformation has been extensively studied worldwide and throughout the geological record in very diverse depositional and structural settings (Gibert et al., 2005; Alsop and Marco, 2011; Berra and Felletti, 2011; Ezquerro et al., 2015; Hilbert-Wolf et al., 2016; Liesa et al., 2016; and others). Despite the wealth of inherent differences highlighted by these studies, the principal mechanism envisioned to cause unconsolidated water-saturated sediment to behave like a fluid is believed to be liquefaction (Owen, 1987) and fluidization, in cases where the water necessary to reduce internal friction clearly originates from below the investigated sediments (Lowe, 1975, 1976; Allen, 1982). Soft-sediment deformation occurs in liquefied to fluidized state as a response to extensional, compressional and shear forces or their combinations and result in brittle to ductile types of deformation features depending on sediment rheology (Pratt, 2019).

Although various processes have been attributed to the cause of soft-sediment deformation, most soft-sediment deformation structures (SSDS) in the rock record seem to have been caused by some kind of shock, often an earthquake (El Taki and Pratt, 2012). Earthquakes are abundant in the Recent (Baskoutas et al., 2007; Dolce and Bucci, 2018; Koper et al., 2018; Ruiz and Madariaga, 2018; earthquakes.usgs.gov) and, according to the sedimentary record, must have been abundant in the geological past as well.

There is a very close relationship of earthquake activity to plate tectonic setting in the Recent (Gibert et al., 2005; Moretti and Sabato, 2007; Gladkov et al., 2016): plate margins are generally seen as places that show high earthquake abundance versus inner plate settings that are regarded as tectonically tranquil

(Klein, 1995; Allen and Allen, 2005). Therefore, intracratonic troughs such as the Williston Basin are not expected to show indicators of synsedimentary tectonics, the envisioned tranquil environment is also reflected in their overall even and non-deformed sediment fill pattern (e.g. Gerhard et al., 1990). However, the arguably most prolific unit in the Williston Basin (Gaswirth et al., 2013), the Bakken Formation, is characterized by a wealth of deformation structures that must have formed during or shortly after deposition. These structures that seem to indicate synsedimentary tectonics during Bakken times are in stark contrast to most current models envisioning an overall tectonically quiet environment for deposition of intracratonic basin successions (Heine et al., 2008; Armitage and Allen, 2010; Vibe et al., 2018; but see e.g. Onasch and Kahle, 1991; El Taki and Pratt, 2012). This study aims at documenting and interpreting soft-sediment deformation structures in the middle Bakken member, and putting them in both a sedimentological and a basin-scale context in order to reconstruct synsedimentary tectonic activity of the Williston basin during middle Bakken time.

GEOLOGICAL SETTING

The Late Devonian to Early Mississippian Bakken Formation is one focal point of the very hydrocarbon-rich succession in the Williston Basin, an elliptic intracratonic trough located primarily in North Dakota and Montana in the USA, but extending into Saskatchewan and Manitoba in Canada; however, some units are traceable southwards into South Dakota, USA. The basin itself is elliptical in shape and covers a surface area of ~250,000 km^2 (cf. Kent and Christopher, 1994). The Cambrian to Tertiary succession is about 5400 m thick (Gerhard et al., 1990) in the depocenter of the basin in northwestern North Dakota (e.g. Borcovsky et al., 2017). Paleogeographic reconstructions show that the Williston Basin was located in proximity to the equator during Bakken deposition, with North Dakota likely being on the southern hemisphere (Scotese, 1994).

The Bakken Formation is very characteristic in both core and well logs: it consists of two prominent black shale units, the lower and upper Bakken members (Albert, 2014; Egenhoff and Fishman, 2013; Borcovsky et al., 2017), with a mixed carbonate-siliciclastic unit in-between, the middle Bakken member (LeFever, 1991; Egenhoff et al., 2011). Locally, the Pronghorn Member (LeFever et al., 2011) forms the base of the succession, a dominantly siliciclastic unit that locally contains carbonates (LeFever et al., 2011). The entire Bakken Formation shows a maximum thickness of about 45 m in western Mountrail County, North Dakota (Meissner, 1978; Webster, 1984), and pinches out along the edges of the basin (e.g. LeFever, 1991; Borcovsky et al., 2017). The age of the Bakken Formation is biostratigraphically constrained by conodonts (Karma, 1991; Hogancamp and Pocknall, 2018) with the Devonian-Mississippian boundary being located in the lower portion of the middle Bakken member.

The middle Bakken member is envisioned to have been deposited on a low-inclined intracratonic shelf with coarse-grained, partly sandy deposits in proximal, and siltstones to mudstones in distal areas (Egenhoff et al., 2011). Novak and Egenhoff (submitted) recognized 16 distinct facies and subfacies, and the deposition of these different lithologies is controlled by the energy gradient of the depositional environment (Fig. 1). In this facies model, the lowest energy facies occupy distal lower to upper offshore positions within the basin, while the highest energy facies are distributed along the margins of the basin on the upper shoreface to foreshore section of the ramp profile (for specific facies names refer to Fig. 1). However, not only the energy of deposition influenced the distribution of the middle Bakken facies

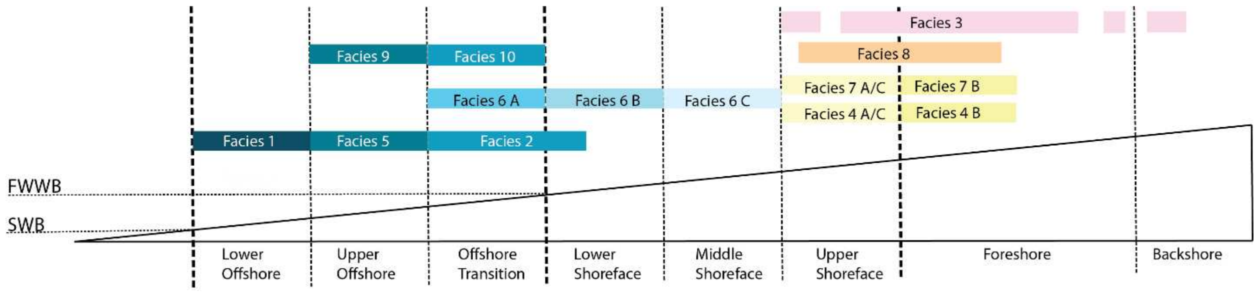

Figure 1: A schematic illustration of the depositional model for the middle Bakken member highlighting the relative bathymetric position occupied by each of the facies on this proximal to distal transect (after Novak and Egenhoff, submitted). The black lines represent the boundaries of depositional zones (e.g. upper shoreface versus foreshore); the horizontal bars indicate the interpreted position of facies on the transect (e.g. 6B would correspond to Lower Shoreface; Facies 1 to Lower Offshore, etc.). The facies names are: Facies 1 - Bioclastic Mud- to Wackestone; Facies 2 - Bioclastic Pack- to Grainstone; Facies 3 - Stromatolitic Bindstone; Facies 4 - Oolitic Grainstone (A - Massive; B - Planar Bedded; C - Cross-bedded); Facies 5 - Nereites Siltstone; Facies 6 - Laminated Siltstone (A - Irregularly Laminated; B - Wave-rippled; C - Thinly Laminated); Facies 7 - Fine-grained Sandstone (A - Massive; B - Planar Bedded; C - Cross-bedded); Facies 8 - Macaronichnus Siltstone; Facies 9 - Bioturbated Siltstone; Facies 10 - Micro-Hummocky Cross-stratified Siltstone; FWWB – Fare Weather Wave Base, SWB – Storm Wave Base.

along the shelf transect, but also the amount of siliciclastic sediment supply and/or the proximity to the clastic sediment sources. Distinct portions of this basin seem to have deposited carbonate, such as carbonate mud-to wackestone, ooids and microbial mats, whereas others show exclusively siliciclastics. The black shales that are believed to be entirely separate units are at times considered as the distal equivalent of the middle member (Egenhoff et al., 2011). For the upper Bakken Shale member, the internal architecture indicates that at least the basal parasequence of the shale in the center of the basin is equivalent to middle Bakken member facies at the margins (Borcovsky et al., 2017). The distinct facies variations throughout the Bakken Formation most likely represent sea-level changes. It remains unclear, however, how many fluctuations of sea-level it records. Smith and Bustin (2000) as well as Angulo and Buatois (2012) envision one, Egenhoff (2017) two, and Egenhoff (2018) three or more sea-level changes during Bakken deposition. Based on the general sediment grain size trend and facies stacking pattern, the middle Bakken member has been subdivided into two systems tracts (Smith and Bustin, 2000; Angulo and Buatois, 2012). The vertical facies architecture shows two distinct stacking patterns: one characteristic of the lower two thirds to three quarters of the succession, and another one of the upper third to quarter portion. The lower two thirds to three quarters of the middle Bakken member are envisioned to represent the Regressive Systems Tract with the Maximum Regressive Surface on top, while the upper third to a quarter portion is interpreted as the Transgressive Systems Tract. Novak and Egenhoff (submitted) suggested that a shift of the depositional center from Mountrail County during the regression towards the northeast (Burke – northwestern Ward counties) happed during the transgression.

METHODS

This study utilizes a comprehensive dataset that includes detailed descriptions of eighty nine measured well core sections (Fig. 2) and forty four porosity and permeability measurements obtained from six wells (Appendix A). The slabbed and polished core samples were visually examined with a hand lens. The cores used in this study are stored at the North Dakota Geologic Survey's Wilson M. Laird Core and Sample Library in Grand Forks, North Dakota, and the United States Geological Survey's Core Research Center in Denver, Colorado. The measurements of the stratigraphic sections and, therefore, mapping of the stratigraphic units is provided in feet according to the imperial measurement system utilized in US drilling operations; nevertheless, small-scale stratigraphic and sedimentological details have been measured in metric units.

Porosity and permeability data were obtained from the well reports accessed at www.dmr.nd.gov using the premium subscription. With the goal to determine the effect of soft-sediment deformation on reservoir quality, we collected porosity and permeability measurements that were taken in both deformed and non-deformed samples of the same 'Laminated Siltstones' facies (Fig. 9; Appendix B). Core samples affected by fracturing were excluded from the dataset. In this study we used porosity values measured at the lowest available net confining stress and Klinkenberg-corrected permeability values at the corresponding pressures due to the low-permeability nature of middle Bakken rocks (Klinkenberg, 1941).

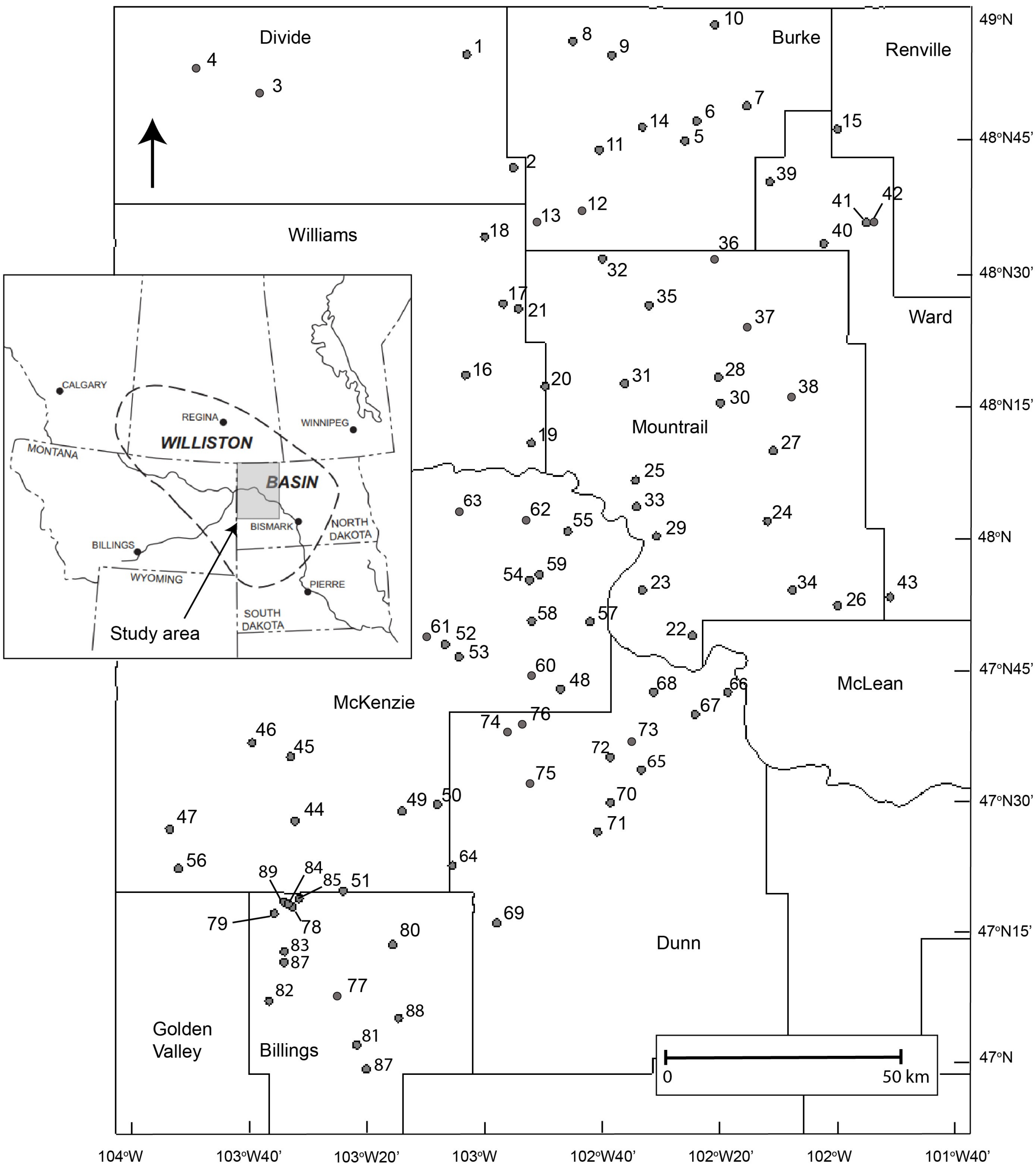

Figure 2: Map of the study area. The inset on the top left illustrates the location of the study area in the USA and Canada (modified from Pitman et al., 2001). Locations of cored wells containing the middle member of the Bakken Formation that used in this study are shown in gray circles: 1 – Ansbro Petroleum Loucks 44-30; 2 – Conoco Waterud "A" #17, 3 – SM Energy Tomlinson 3-1HN; 4 - Murex Petroleum Jennifer Abigail 16-21H; 5 – Clarion Resources 1-24 Slater; 6 – Northern Pump Louis Peterson #1; 7 – Clarion Resources Mertes #1-32; 8 – Clarion Resources Negaard #1; 9 – Clarion Resources Nelson 1-29; 10 – Cornerstone Natural Resources Jorgensen 4-4H; 11 – Samson Resources OAS 31-161-92H; 12 – Samson Resources Saratoga 12-1-161-92H; 13 – St. Mary Land & Exploration Company Douts 4-7H; 14 – Petro-Hunt Producer`s Corporation 159-94-17C-8-2H; 15 – Clarion Resources Pierce #1-18; 16 – Petro

Devel Corp. Violet Olsen 31-29H; 17 – Texacota H. Borstad #1; 18 – Dallea Petroleum Corp. Hamlet U. #2; 19 – Pan American Petroleum Corp. Clifford Marmon #1; 20 – Headington Oil Co. Nesson State 42x-36; 21 – Hess Corp. H. Bakken 12-07H; 22 – Dakota E&P Co. George Evans 11V; 23 – Marathon Oil Co. Mylo Wolding 14-11; 24 – EOG Resources Parshall 2-36H; 25 – American Hunter Exploration Ahel et al Sanish #36-44 H4; 26 – Hess Corp. St-Andes-151-89-2413H-1; 27 – Marathon Oil Co. Jensen #12-44; 28 – Marathon Oil Co. Laredo #26-1; 29 – Whiting Oil and Gas Corp. Bartleson 44-1H; 30 – Brooks Exploration Rogstad #1-11; 31 – Shell Oil Co. L. Texel #21-35; 32 – Amerada Hess Corp. State ND 1-11H; 33 – Whiting Oil and Gas Corp. Mildred Roggenbuck 41-24TFX; 34 – EOG Resources Fertile 1-12H; 35 – Fidelity E&P Co. Farhart 11-11H; 36 – EOG Resources Sidonia 1-06H; 37 – Hess Corp. RS-STATE C-157-90- 3603H-1; 38 – EOG Resources McAlmond 1-05H; 39 – Clarion Resources 1-20 Fleckton; 40 – Clarion Resources 1-33 Pullen; 41 – Golden Eye Resources Steinberger #1-16; 42 – Golden Eye Resources J. Brekhus #2-14; 43 – Marathon Oil Co. Dobrinski #18-44; 44 - Pennzoil Co. 15-22 BN Flat Top Butte; 45 – True Oil Slash Federal 44-33 4-9H; 46 – Pennzoil Co. Spring Creek #27X-31BN; 47 – Shell Oil Co. USA 33-23-154; 48 – Helis O&G Co. Linseth 13-13/12H; 49 – American Hunter Exploration Ahel et al Grassy Butte #12-31 H3; 50 – GMX Resources Pojorlie 21-2-1H; 51 – Cities Services 1 Federal DG; 52 – Lyco Energy Corp. Titan E-Gierke 20-1-H; 53 – Oryx Energy Stenehjem HD 27 #1; 54 – Texaco F. P. Keogh #4; 55 – Amerada Petroleum Corp. Jens Strand #1; 56 – Meridian Oil MOI #44-13; 57 – Petro-Hunt Fort Berthold 150-94-3B-10-2H; 58 – Hess Corp. Lars Rothie 32-29H; 59 – Hess Corp. HA-Nelson-152-95-3328H-9; 60 - Helis Oil & Gas Co. Linseth 4-8H; 61 - Denbury Onshore Ludinin 11-13SEH; 62 - Burlington Resources Oil & Gas Co. Uberwachen 22-34; 63 - Whiting Oil And Gas Corp. Tarpon Federal 44-19TFHU; 64 – Gulf Oil Corp. Martin Weber #1-18-1C; 65 – Shell Oil Co. Burbank #23-8; 66 – Mobil Producing Co. Pegasus DIV Solomon Bird Bear #F-22-22-1; 67 – Shell Oil Co. Young Bear #32-4; 68 – Socony-Vacuum Oil Co. Angus Kennedy #F32-24-P; 69 – Oxy USA Evelyn Kary 2-22-15H-144-97; 70 – Marathon Oil Co. Stohler 21-3H; 71 – Marathon Oil Co. Corrine Olson 34-20; 72 – Petro-Hunt Fort Berthold 147-94-3B-10-3H; 73 – Simray GP Roberts Trust 1-13H; 74 - Headington Oil Co. Jane Federal 11X-20; 75 - Continental Resources Hawkinson 14-22H2; 76 – NEWFIELD PRODUCTION COMPANY JORGENSON 1-15H; 77 - Tenneco Oil 3-17 TOC MEE USA; 78 – Florida Exploration 1-12 Federal; 79 – Tenneco Oil Graham USA #1-15; 80 – Texaco 5-1 Thompson Unit; 81 – Whiting Oil & Gas Corp. Franks Creek State 21-16TFH; 82 – Maxus Exploration Crooked Creek State #31-16; 83 – Meridian Oil MOI Elkhorn #33-11; 84 – Milestone Petroleum Federal #12-12; 85 – Supron Energy Corp. F-6-144-101 #3; 86 – Coastal Oil & Gas Corp. & Al-Aquitaine 23-143-102 BN #1; 87 – Florida Exploration Co. Federal 34-1; 88 – XTO Energy Chruszch 43X-29; 89 – Florida Exploration 11-4 Federal; details for each well are listed in Appendix A.

DESCRIPTION

Soft-Sediment Deformation Structures

This study presents nine distinct types of SSDS that have been identified in middle Bakken cores. The structures vary in size from several millimeters to tens of centimeters and include slump folds, massive silt and sand sheets, ptygmatically-folded clastic dikes, diapiric structures, water-escape structures, lithoclastic breccia, load structures, boudinage-like structures, and microfaults. Soft-sediment deformation in the Bakken Formation has never been described in detail; individual slump folds and microfaults are mentioned in Egenhoff et al. (2011), Simenson et al. (2011) and Zhang and Buatois (2014), however they have never been given proper attention.

Folds and Convolute Beds

Convolute bedding and folding structures are common throughout the middle Bakken member. The folds occur as upright, overturned, recumbent and thrust folds. Both anti- and synforms in the observed slumps are characterized by unequal wavelengths and asymmetrical limbs, and their axes show various orientations. Fold wavelengths vary from as little as a couple of millimeters to several centimeters, while individual slumped beds can reach up to decimeters in thickness (Fig. 3). Nevertheless, it is possible to underestimate the size of folds due to the limited width of core samples. Folded rocks consist of interbedded siltstones and mudstones and fine-grained sandstones. Commonly folding appears chaotic and disconnected and only vaguely resembles depositional bedding (Fig. 4 A, B).

Boudinage Structures

Sedimentary boudinage structures occur in highly heterolithic facies of the middle Bakken member. Boudinage structures are recognized by irregular laminations of light gray siltstone and dark gray mudstone on a several millimeter to centimeter scale in many well cores. The boudins have the shape of segmented, partially disconnected, or continuously lenticular silty lenses (Fig. 4 C). Laterally and vertically, silty boudinaged segments and beds are draped with mudstone. Boudins typically are 0.3 to 8 millimeters long and 2-15 millimeters thick. It is unclear how continuous these beds are due to limited exposure in core samples.

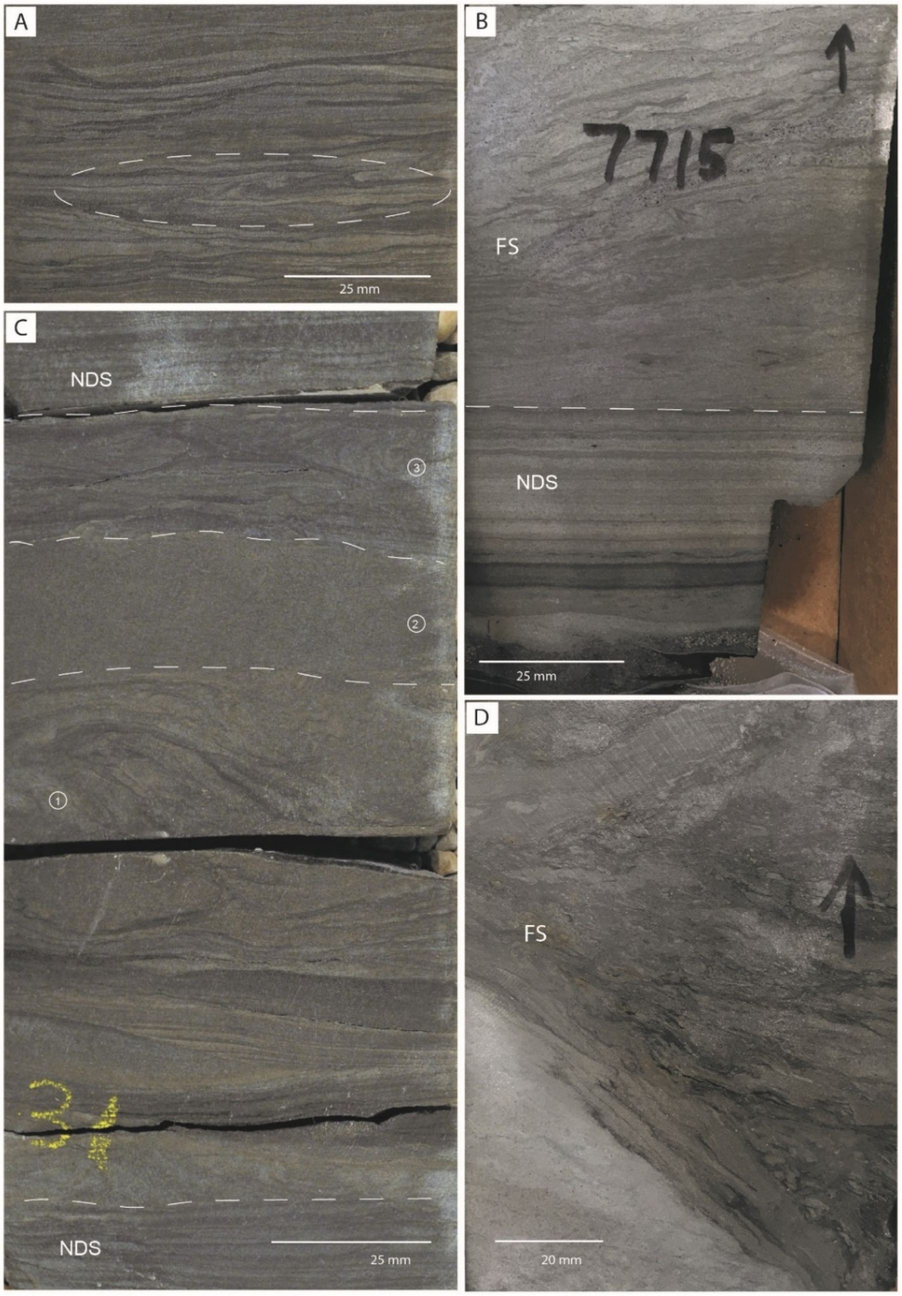

Figure 3. Photos of folds in slabbed vertically-oriented core samples: A) small-scale asymmetrical fold in well Producer's Corporation 159-94-17C-8-2H at 9132ft outlined in dashed, B) a section of a fold on top of non-deformed planar bedded strata in well Clarion Resources Pullen #1-33 at 7715ft; FS – folded section; NDS – non-deformed strata; C) recumbent/assymetrical fold (1) overlain by massive silt sheet (2) and convoluted bedding (3) in well Producer's Corporation 159-94-17C-8-2H at 9131ft; D) Folded strata in well Clarion Resources Fleckton #1-20 at 7675ft.

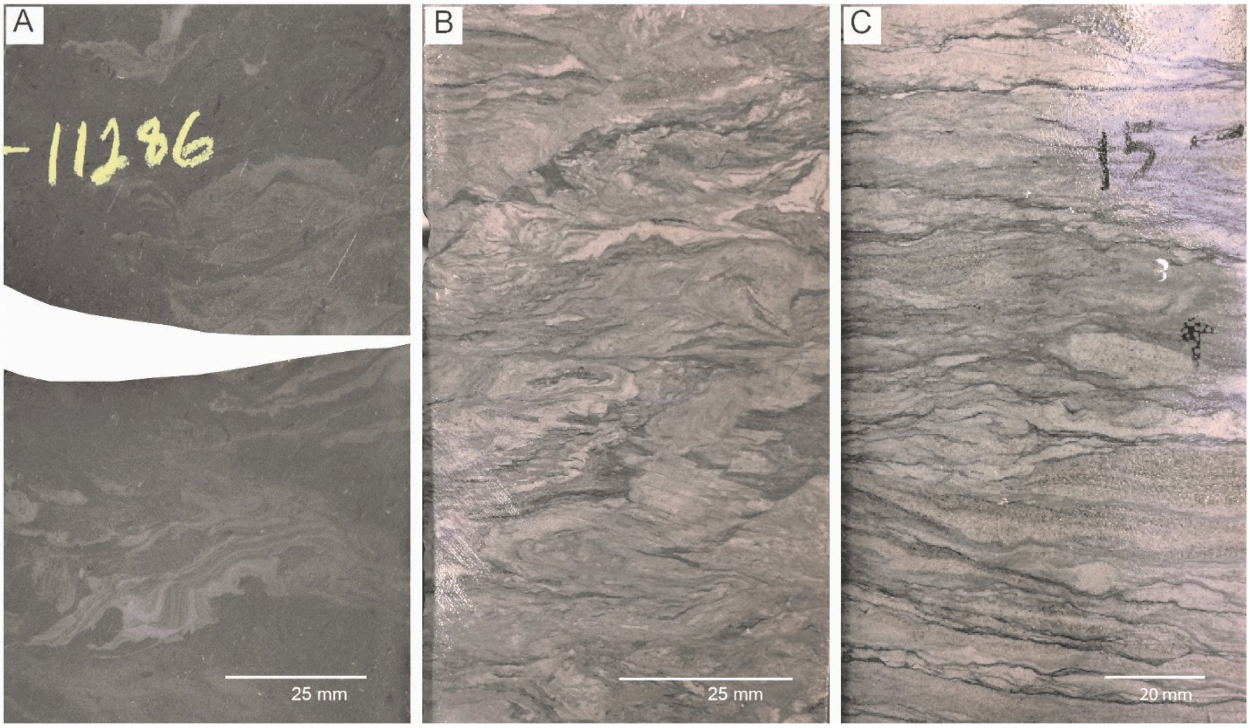

Figure 4. Slabbed vertically-oriented core samples with the examples of SSDS: A) Chaotic folding with remnants of depositional bedding in well GMX Resources Pojorlie 21-2-1H at 11285ft, B) Asymmetrical folding suggesting shearing but preserving remnants of depositional bedding in well Marathon Oil Dobrinski #18-44 at 8449ft, C) Boudinage structures in well Clarion Resources Nelson 1-29 at 7415ft.

Structureless Silt and Sand Sheets

Structureless silt and sand sheets represent sub-horizontal to horizontal units of structureless silt- to fine-grained sandstone sandwiched between bedded sediment (Fig. 5). The contacts between the massive sheets and bedded units are typically gradational. The thickness of massive sand sheets vary from as little as a couple of millimeters to several centimeters.

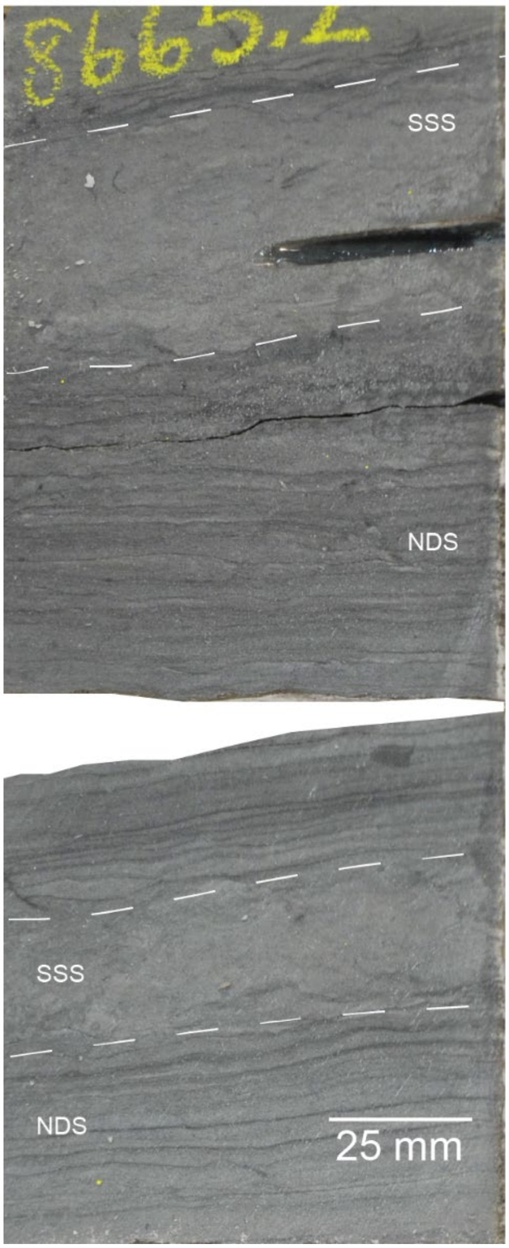

Figure 5. Slabbed vertically-oriented core sample with two structureless silt sheets (SSS) separated by non-deformed planar parallel-bedded units (NDS) in well SM Energy Tomlinson 3-1HN at 8665.2ft. Dashed lines indicate the contacts of the deformed and non-deformed units.

Ptygmaticaly-Folded Clastic Dikes

Ptygmatically-folded clastic dikes are irregularly shaped sub-vertical bodies of sediment that cut across undisturbed beds (Fig. 6 A, B). The silty fill of dikes contains either massive sediment or partially preserved bedding; host material is usually a mudstone. Observed dikes pinch out downward and typically have one shaft that doesn't exceed 1-2 millimeters in width and 2-3 centimeters in height. The dikes are highly irregularly folded and commonly have bulbous convex-up tops.

Load Structures

Load structures are observed at the interface between lithologies with contrasting density, typically coarse silt- or sandstone on top of muddy siltstone or mudstone. Load structures have flat tops and irregular-shaped concave up bottoms. Internal organization of load structures exhibits concave up lamination that follows the shape of the base of the structure (Fig. 6 C, D). Load structures in the middle Bakken member found in Micro-hummocky Cross-stratified Siltstone facies can be as small as several millimeter in diameter, and reach up to several centimeter in diameter in the Laminated Siltstone facies (Fig. 6 D). Individual load structures commonly show largely continuous laminae; however, the bulbous nature of most example exhibits some discontinuous layers that terminate against overlying millimeter-scale sandstone laminae (arrow 1 in Fig. 6 D), and equivalent sandstone layers that pinch out laterally pointing downward into the load structure (arrow 2 in Fig. 6 D). Other irregularities in the geometry of load structures, e.g. internal folding (arrows 3 in Fig. 6 D), faulting, and liquefaction is common. Lateral to the load structures, preferentially towards their bases, sandstone laminae (arrow 4 in Fig. 6 D) are often observed that thicken into irregular, massive sandstone bodies (arrow 5 in Fig. 6 D).

Water-Escape Structures

Small-scale water-escape structures occur relatively rarely in the middle Bakken member. Their size typically doesn't exceed one centimeter in height and width. The structures have a 'volcano' shape, which tapers upward into non-deformed strata, and a visible vertical center shaft that cuts across several beds (Fig. 6 F, G). The water-escape structures typically occur in interbedded silt- and mudstone facies with the shafts made up of and stemming from the silt fraction, protruding through the mudstones.

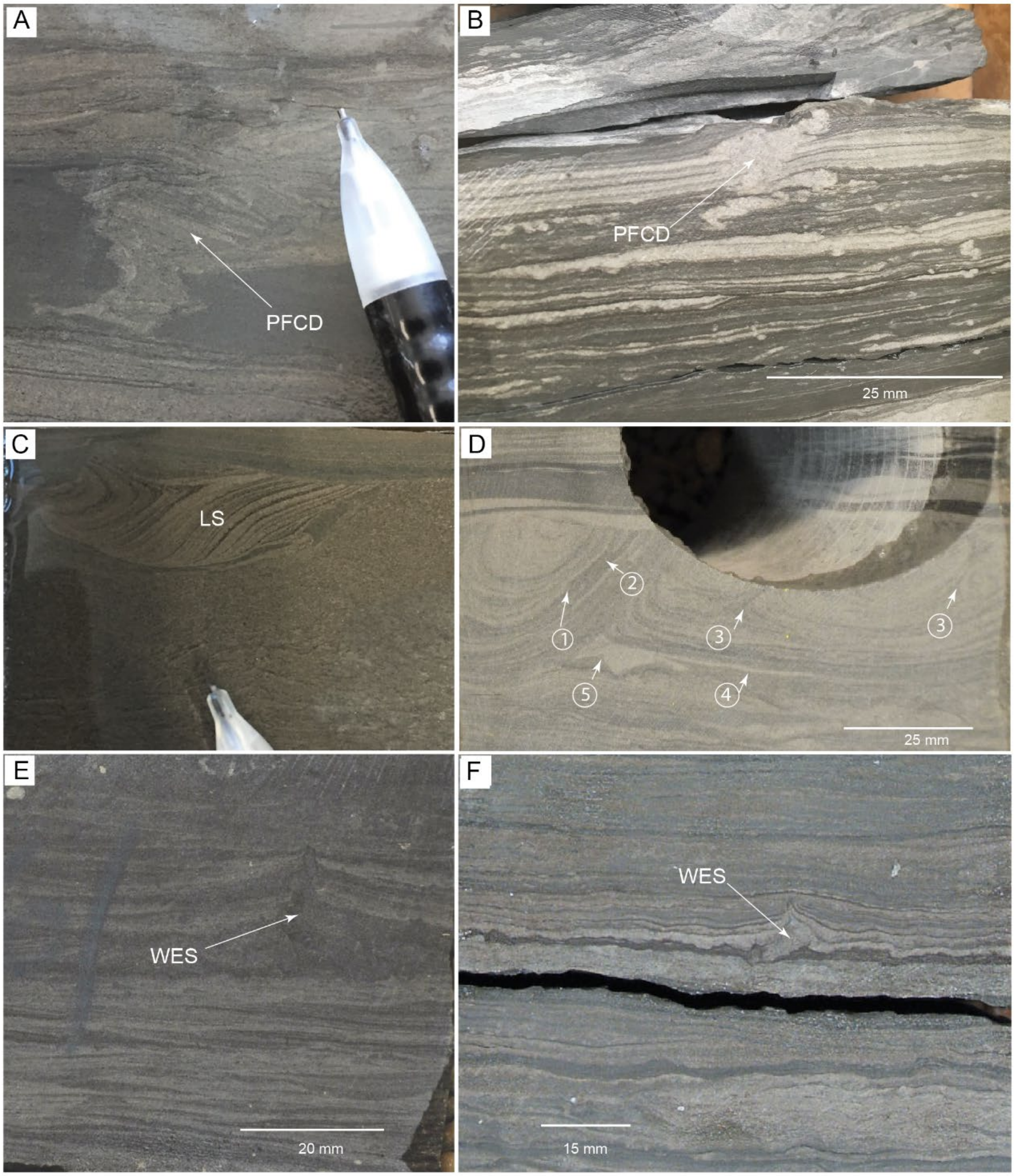

Figure 6. Photos of slabbed vertically-oriented core samples displaying various SSDS: A) ptygmatically-folded clastic dike (PFCD), likely downward-directed, infilled with semi-solidified siltstone clasts from the overlying unit in well EOG Parshall 2-36H at 9283.6ft, B) ptygmatically-folded clastic dike infilled with silty material in well Clarion Resources Fleckton #1-20 at 7663ft, C) load structure (LS) in well Marathon Oil Mylo Wolding 14-11 at 10596ft, D) multiple load structures in well Murex Petroleum Jennifer Abigail 16-21H at 8225ft; 1 - discontinuous layer terminates against overlying millimeter-scale sandstone laminae, 2 - equivalent to lamina (1) sandstone layer pinches out laterally pointing downward into the load structure, 3 - internal folding, 4 – regular sandstone lamina folded and thicken into irregular, massive sandstone body (5); E) water-escape structure (WES) in well Supron Energy F-6-144-101 #3 at 10462ft, F) water-escape structure in well ST Mary Land & Exploration Douts 4-7H at 9966.5ft.

Diapiric Structures

Diapiric structures occur sub-vertically to obliquely to the planar laminated siltstone host sediment (Fig. 7 A), which appears partially contorted around the intrusion. The shape of the diapirs is extremely irregular and has a finger-like shape. The diapirs consist of fine-grained siliciclastic silt- to mudstones. Diapiric structures lack internal organization and exhibit contorted to massive bedding. The size of clastic diapirs observed in middle Bakken cores is somewhere between several centimeters to a decimeter in height.

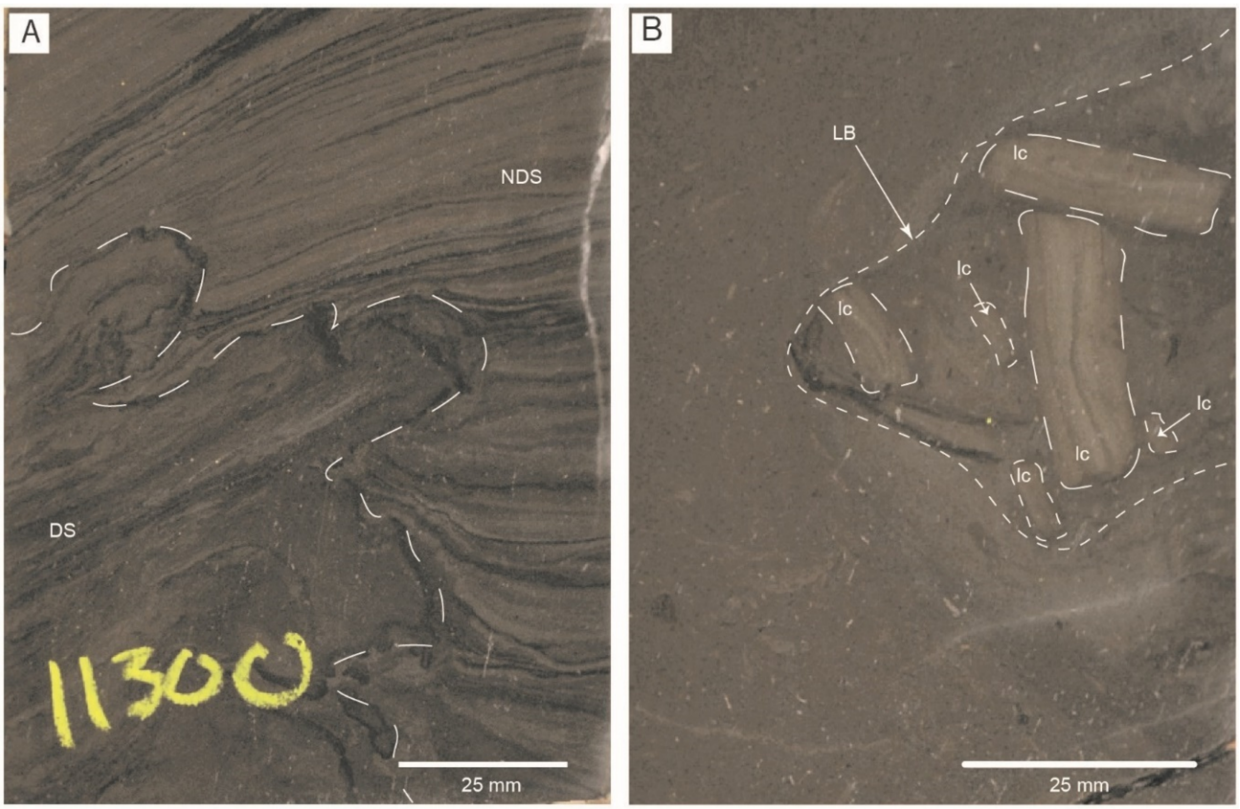

Figure 7. Photos of slabbed vertically-oriented core samples showing: A) diapiric structure (DS) outlined in dashed in well GMX Resources Pojorlie 21-2-1H at 11300ft B) a pocket of lithoclastic breccia (LB) outlined in dashed in homogenized muddy siltstone in well GMX Resources Pojorlie 21-2-1H at 11289ft: lc – lithoclasts, outlined in dashed.

Lithoclastic Breccia

The lithoclastic breccia is comprised of light gray siltstone clasts in massive dark gray silty mudstone matrix. The clasts are subangular rectangle-shaped and have no preferred orientation (Fig. 7 B). The length of the clasts is 2-3 centimeters or less. Large clasts contain slightly contorted remnants of original planar bedding. Fragments of the lithoclastic breccia were found in only one core (GMX Resources Pojorlie 21-2-1H).

Microfaults

Microfaults in the middle Bakken member exhibit a variety of types. Most common fault types are high angle normal and reverse faults (Fig. 8 A, B) as well as some low angle normal faults. Fault throws vary from as little as ~ 1 millimeter to several centimeters, however, the actual displacement might be underestimated due to the limited size of the core samples. Reverse faults are generally subparallel to one another and spaced from one to several centimeters apart. Locally, isolated normal and reverse faults occur. Normal fault complexes arranged in parallel to sub-parallel *en echelon* fashion with a rotational motion toward the direction of slip are common in places (Fig. 8 C). These microfaults are spaced several millimeters to one centimeter apart.

Stratigraphic Distribution of SSDS

Soft sediment deformation structures are observed primarily in the upper third to quarter portion of the middle Bakken succession (Fig. 9). Deformation structures are common in Irregularly Laminated Siltstone, Thinly Parallel-laminated Siltstone and Planar and Cross-Bedded Sandstone facies, and rare in Wave-rippled Siltstone sub-facies and Micro-hummocky Cross-stratified Siltstone facies. No SSDS were observed in Bioturbated Silt- to Sandstone facies, carbonate Bioclastic Pack- to Grainstone, and Bioclastic Mud- to Wackestone facies. Deformation structures found in the lower three quarters to two thirds of the succession (Fig. 8) are associated mainly with Fine-grained Massive, Planar and Cross-bedded Sandstone and Oolitic Grainstone facies. A single occurrence of soft-sediment deformation was reported from the Nereites-bearing Siltstone facies in well Hess Corp. H Bakken 12-07H. Thickness of individual deformed units vary from less than 1 centimeter to several tens of centimeters, while maximum cumulative thickness of a deformed succession in a single well reaches up to 3.4 meters (e.g. in well True Oil 44-33 4-9H Slash Fed).

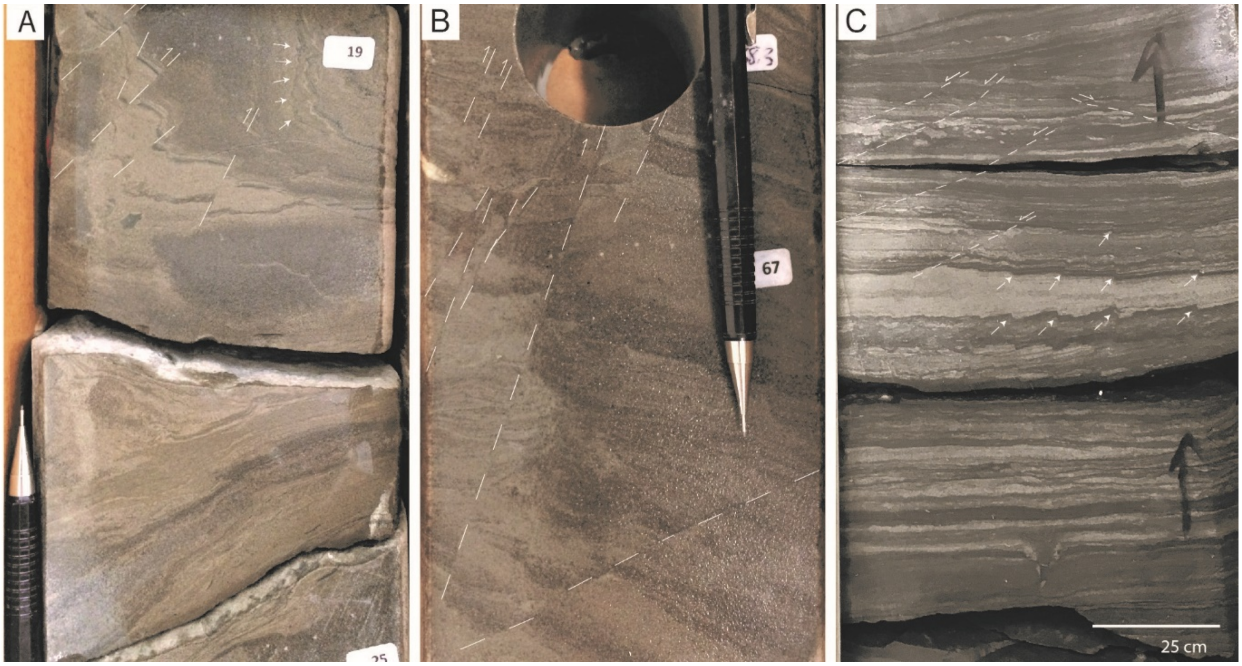

Figure 8: Examples of microfaults in slabbed vertically-oriented Middle Bakken core samples; select fault planes highlighted by dashed lines and arrows: A) high-angle reverse faults in a slumped unit in well Whiting Bartleson 44-1H at 10243ft, B) low- and high-angle normal and reverse faults in well Whiting Bartleson 44-1H at 10241ft, C) *en echelon* normal fault series with a rotational motion in well Clarion Resources Fleckton #1-20 at 7672ft.

Spatial Distribution of SSDS

Soft-sediment deformation structures are present in 63 out of 90 wells measured across North Dakota's portion of the middle Bakken member. They seem to show two distinct distribution patterns, one in the northeastern part of the study area in central to eastern Burke, northwestern Ward, and northern Mountrail Counties, and the other in northwestern Dunn and southern to southeastern Mountrail Counties. However, two isolated maxima occur in southeastern Mountrail County at the border to McLean County and in south-central McKenzie County (Fig. 10).

The distinction of the two SSDS distribution trends is based not only on their maxima but also on the surrounding cores in which the deformation was absent. Burke and Ward Counties show a clear northwest-southeast-oriented distribution trend, and so do the maxima in northeastern Mountrail County. A similar trend can be assumed for the two distinct occurrences of deformed intervals in western to central Divide County, although these observations are based on only two wells. Likewise, deformed

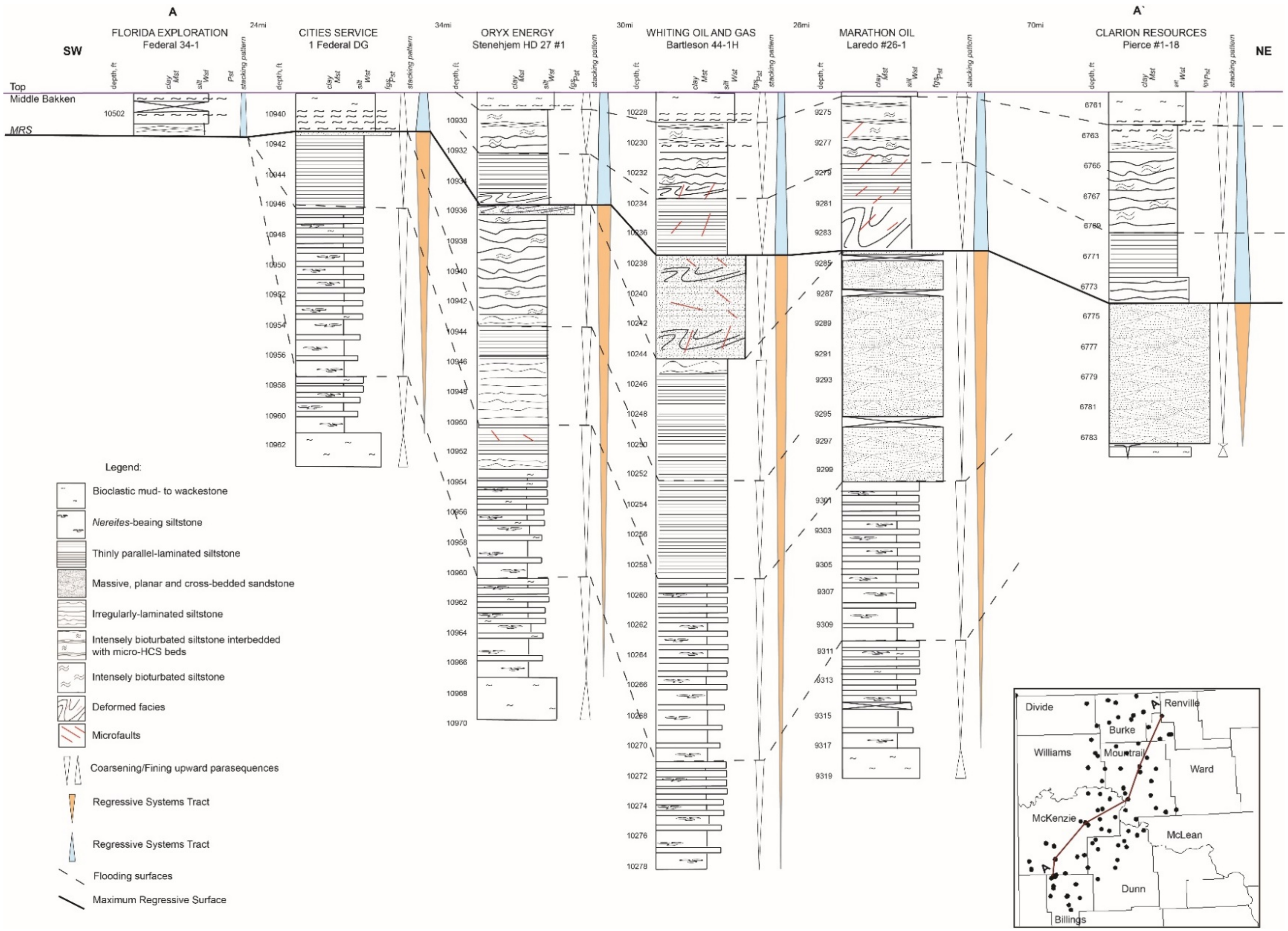

Figure 9: SW-NE cross-section through the middle Bakken member with sequence stratigraphic subdivision showing the distribution of SSDS predominantly in the upper third to quarter portion of the succession (Transgressive Systems Tract). MRS – Maximum Regressive Surface. The insert on the bottom right illustrates the location of the shown transect.

units of around 2 m in thickness oriented northwest-southeast are present in eastern McKenzie County along the Little Knife and southern Antelope Anticlines; these are not quite as obvious as the ones to the northeast. The second trend becomes clear when stepping back and looking at the distribution along the anticlines from Dunn County in the south to Divide County in the north: deformed units are thicker and more pronounced in the south yet do not extend into Billings County, and become successively thinner and less common further north. In the Nesson Anticline area in northern Williams and Divide Counties, only few deformed intervals have been documented, and some cores did not show any deformed units at all.

INTERPRETATION

Soft-Sediment Deformation Structures

Folds and Convolute Beds

Folds and convolute lamination are interpreted to form due to seismic shaking-induced motion that invokes compressional and shear stresses within the liquefied or hydroplastic lamina (Dzulynski and Smith, 1963; Lowe, 1975). The intensity and final appearance of folded and convolute lamina in the middle Bakken member, whether it is intact folds or disconnected and chaotic remnants of lamina, depends on the thickness of the affected sedimentary units (Hildebrandt and Egenhoff, 2007), sediment grain and lithologic composition (Obermeier, 1996; Moretti and Sabato, 2007; El Taki and Pratt, 2012), lithification state (Lowe, 1976; Moretti and Sabato, 2007) and the intensity of an earthquake (Allen, 1986). Given the minor to absent inclination of the depositional slope in the middle Bakken system and the appearance of folds and convolute laminae observed in the succession, it is most likely that the deformation occurred largely *in situ* with minor to no sediment transport.

Boudinage structures

Once the unconsolidated heterolithic facies were subjected to seismic shaking, the silty and sandy components readily became liquefied. As the fluids were trying to escape from the liquefied silty and sandy beds, mudstone laminae acted as fluid barriers preventing the expulsion of the pore-water from silty and sandy packages. This and the subsequent stretching of more rigid silty and sandy sediment under extensional and shear stresses (Allen, 1982) resulted in pulling apart and rearrangement of silty and sandy beds into the irregular-shaped elongate boudins.

Structureless Silt and Sand Sheets

Structureless silt and sand sheets are interpreted to have formed as a result of earthquake-induced liquefaction possibly accompanied by shear stress. Seismically triggered liquefaction caused pore-water pressure to significantly built-up and overcome the shear strength of sediment. Loss of cohesion eventually took place, which lead to severe disruption of the depositional structures. The liquefied sheets of sediment were likely preserved in situ due to relatively flat basin floor topography. Each liquefied unit can be interpreted as a reflection of a single seismic event (Seilacher, 1984) based on the presence of non-deformed under- and overlying strata.

Ptygmatically-Folded Clastic Dikes

In addition to the upward directed clastic dikes that form as intrusions of seismically-fluidized and overpressured coarse silt to sand material into horizontal to sub-horizontal less pressurized beds (Lowe, 1975; Montenat, 1991; Collinson, 1994; Obermeier, 1996), a downward intrusion of sediment also played a role in formation of clastic dikes observed in the middle Bakken (Pratt, 1998). The formation of downward directed dikes is interpreted to occur in extensional stress settings, where overlying sediment intrudes into opening seismic shock-related fissures in the underlying host material (Montenat, 1991; Martel and Gibling, 1992; Collinson, 1994; Moretti and Sabato, 2007). The irregular ptygmatic shape of the dikes was acquired during subsequent dewatering and greater compaction of surrounding mud than infilling silt (Kuenen, 1967; Truswell, 1972; Pratt, 1998), thereby creating the 'folded' geometry of the dikes.

Load Structures

The formation of load structures is caused by seismically-induced liquefaction that triggers gravitational instability at the base of coarse sediment overlying fine-grained laminae and beds due to the high density contrast (Allen, 1970; Obermeier, 1996). In the middle Bakken, triggered by a seismic shock, relatively heavy silty and sandy sediment started to sink down into soft muddy material, forming concave-up coarse-grained lumps encased in fine-grained substrate. The top portion of load structures is, in places, eroded away, leaving load structures with flat tops, which became subsequently covered with new sediment atop of a sharp erosional contact.

Evidence for this mostly vertical transport downwards comes from small-scale features that are associated with the load structures (Fig. 6 D): the crescent moon-shaped structure with layers terminating against overlying sand laminae (arrow 1 in Fig. 6 D) reflects an initial downward movement of the crescent-shaped structure which must have led to the rupture of the laminae, most likely when the

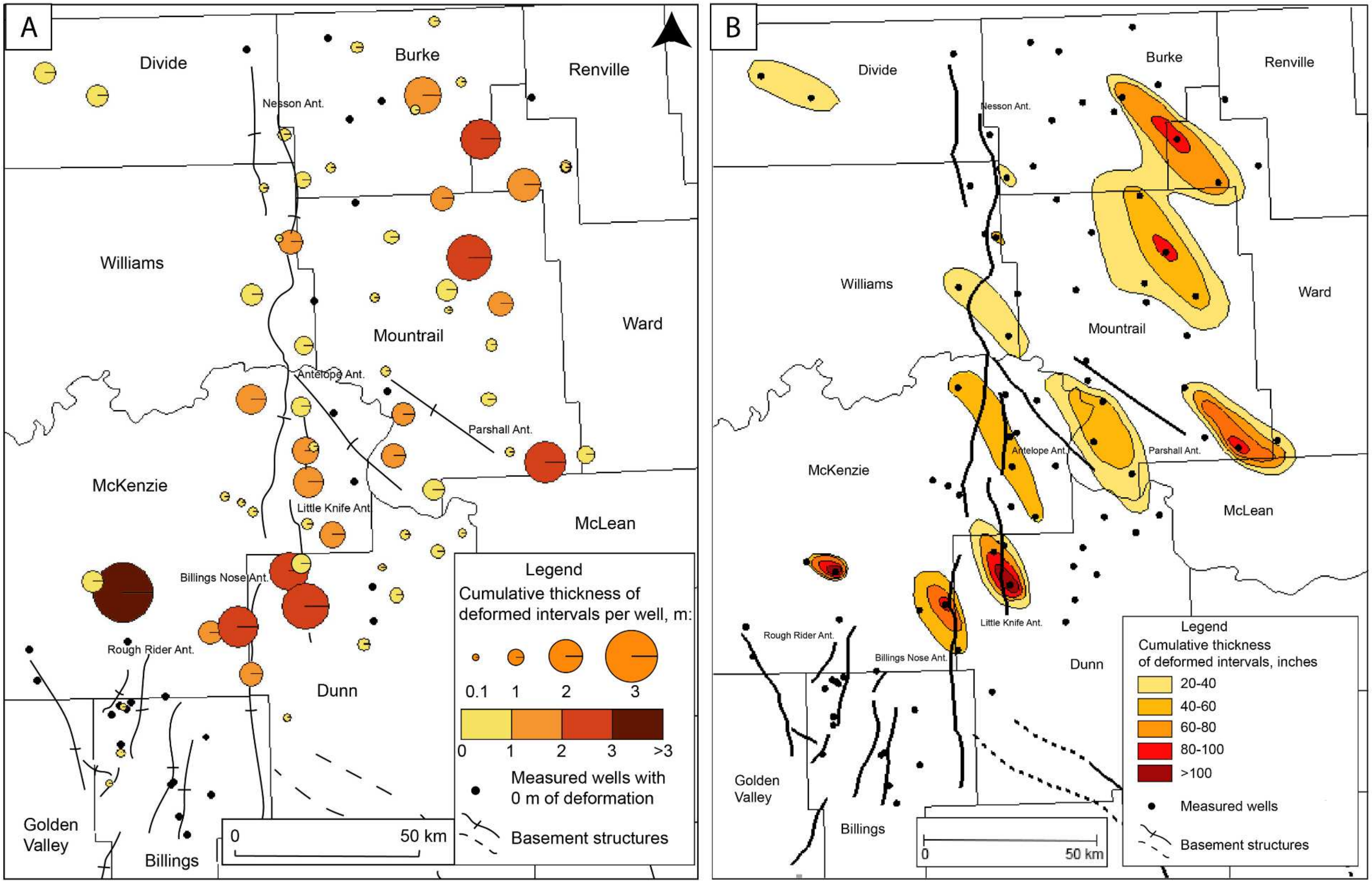

Figure 10. A - Map depicting the cumulative thickness of deformed strata in each studied well. B – Interpretation of SSDS distribution trends based on cumulative thickness of deformed intervals per well. For names of individual wells refer to Fig. 2. Locations of major structural element provided by Timothy O. Nesheim based on Crashell (1991), Chimney (1992) and Nordeng et al. (2010).

overlying bulbous sandstone package began sinking downward at a later moment. This sinking downward in stages corresponds to the formation of load-casted ripples envisioned by Dzulynski and Kotlarczyk (1962) where successive migrating ripples continuously add to the load on top of a mudstone bed at a distinct point and keep being piled on top of each other. The ruptured lamina (arrow 2 in Fig. 6 D) also reflects the vertical downward motion of the structure. Internal folding as indicated by arrows 3 (Fig. 6 D) shows space problems of formerly horizontally arranged laminae when they are folded; furthermore, it may also reflect some vertical (and minor lateral) movement of the laminae post deposition. Lateral thickening of sandstone laminae as observed laterally to load structures (arrow 4 in Fig. 6 D) most likely results from liquefaction as these sandstones are structureless; nevertheless, it may also be the product of thinning of sandstone laminae laterally making the thickest portion of the laminae the only remnant of its original thickness. This thinning probably reflects the vertical movement downwards during which individual laminae are squeezed out and thinned resulting in the observed geometry. Nevertheless, liquefaction may have locally been the most important process as it is envisioned in this study to account for the formation of irregular sandstone bodies (arrow 5 in Fig. 6 D) with liquefaction explaining their massive nature.

Water-escape Structures

The water-escape structures in the middle Bakken member are thought to have formed by the upward intrusion of pore-water, and represent restricted escape routes of fluid trapped in the liquefied silty beds over- and underlain by low-permeability mudstone beds (Lowe, 1975). As a result of seismically-induced liquefaction and fluidization, an elutriated mix of pore-water with fluidized particles has been pushed upward, cutting and deforming overlying beds.

Diapiric Structures

Diapiric structures are interpreted to have formed as a result of seismically-induced liquefaction and fluidization of sediment. Formation of diapiric structures occurred in fluidized sediment when pore-fluid drag exceeded the weight of granular material (Obermeier, 1996). Fluidized flow is typically turbulent (Lowe, 1975), which explains poorly preserved to homogenized internal organization of the diapirs observed in the middle Bakken member (Fig. 6 A). Diapirs moved upward with high energy and followed an irregular 3D pathway (He et al., 2014), deforming and dragging the surrounding sediment along the way. The terminal area of a diapir and the surrounding strata comprise the most deformed sediment – as an intrusion cuts through the host strata, it pushes surrounding lamina into a concave shape. As our well core observations are constricted in 3D, the total length of a sedimentary column deformed by diapirism might be underestimated. For example, if only a terminal part of a diapir is present in the core sample, it is unclear how far away this diapir originated from.

Lithoclastic Breccia

Lithoclasts found in well GMX Resources Pojorlie 21-2-1H are believed to have originated from an over- or underlying bed that was more consolidated than the water-saturated host sediment. This water-saturated bed became liquefied due to a sudden seismic shock and, as it intruded into the indurated layer, caused it to break into clasts (Montenat, 2007).

Microfaults

Microfaults in the middle Bakken member represent brittle deformation when the sediment was somewhat solidified and had sufficient overburden to cause compaction. When the increase in pore pressure exceeded the compressional stress and tensional strength of the sediment (Grimm and Orange, 1997), small-scale faults started to propagate through semi- to fully consolidated sediment. Microfaulting in the middle Bakken sediment reflects various stress settings and a variety of deformation styles. For example, reverse faults originated in compressional settings, while normal faults occurred in areas that underwent extension. Subsequent rotation of beds in the hanging walls of *en echelon* normal fault series could have potentially resulted from a change in the stress regime from extensional to compressional. Shear stress could have caused the formation of transform micro-faults or contribute to more complex deformation styles, such as wrench, transpressional and transtensional faulting.

Stratigraphic Distribution SSDS

Based on a wealth of most likely tectonically-formed SSDS, this study suggests that the Williston Basin, despite being an intracratonic trough, was likely tectonically active during deposition of the middle

Bakken member. The stratigraphic distribution of SSDS in the middle Bakken does not provide clues to what type of structures were active; nevertheless, the increased abundance of synsedimentary deformation structures in the upper quarter to third of the succession, interpreted as transgressive by Novak and Egenhoff (submitted), suggests that tectonic movements were not uniformly distributed throughout middle Bakken deposition. It seems that the tectonic activity reached a peak during the transgression, yet did not strongly affect the preceding regressive portion of the sediment pile that makes up the lower two thirds to three quarters of the succession. Therefore, SSDS can be used as an indicator of varying tectonic activity, even during a most likely relatively short time-span that is represented by the sedimentation of the middle Bakken.

Spatial Distribution of SSDS

The two maxima of SSDS occurrence and the associated trends are interpreted to reflect active structural elements in the Williston Basin during times of middle Bakken deposition that have been known to be oriented northwest-southeast and north-south (e.g. Anna et al., 2011). The northwest-southeast distribution of SSDS is present in the northeast of the study area and further south in the Little Knife and central portion of the Antelope Anticlines indicating that these occurrences of SSDS were also most likely caused by the movement of underlying northwest-southeast-trending basement structures. However, the north-south trend with a decrease in SSDS unit thickness between Dunn and Divide counties seems to indicate that north-south running structures such as the Billings Nose, the Little Knife, and the Nesson Anticline were active during deposition of the middle Bakken member, too.

Furthermore, the focal point of these structural movements must have been in northwestern Dunn County with successively decreasing fault activity towards the north. Billings County, on the contrary, is interpreted to have been tectonically relatively quiet during middle Bakken member deposition as nearly no SSDS have been reported from there despite that it has the highest density of measured wells in the entire study area.

Porosity and Permeability Data

The focus of this study was not only to reveal the potential use of SSDS as a tool to recognize tectonic activity but also to answer the question whether SSDS have an effect on the petrophysical properties of the deformed in comparison to undisturbed rock packages of the same facies. In order to determine the effect of soft-sediment deformation on the quality of the middle Bakken reservoir, we gathered porosity and permeability values from both undisturbed and deformed units. Porosity values from deformed rocks were contrasted with porosity values from the same lithology, but from un-deformed facies.

The results (Fig. 11) show a large similarity in both porosity and permeability values of all facies whether deformed or not; however, despite this similarity, deformed facies generally exhibit slightly increased permeability with respect to non-deformed rocks, and also their porosity overall slightly increases. This means that the liquefaction processes that originally formed SSDS created elevated porosities and permeabilities in these rocks that are still noticeable today. From a reservoir standpoint, despite heavy cementation (e.g. Pitman et al., 2001), some of this original permeability and porosity

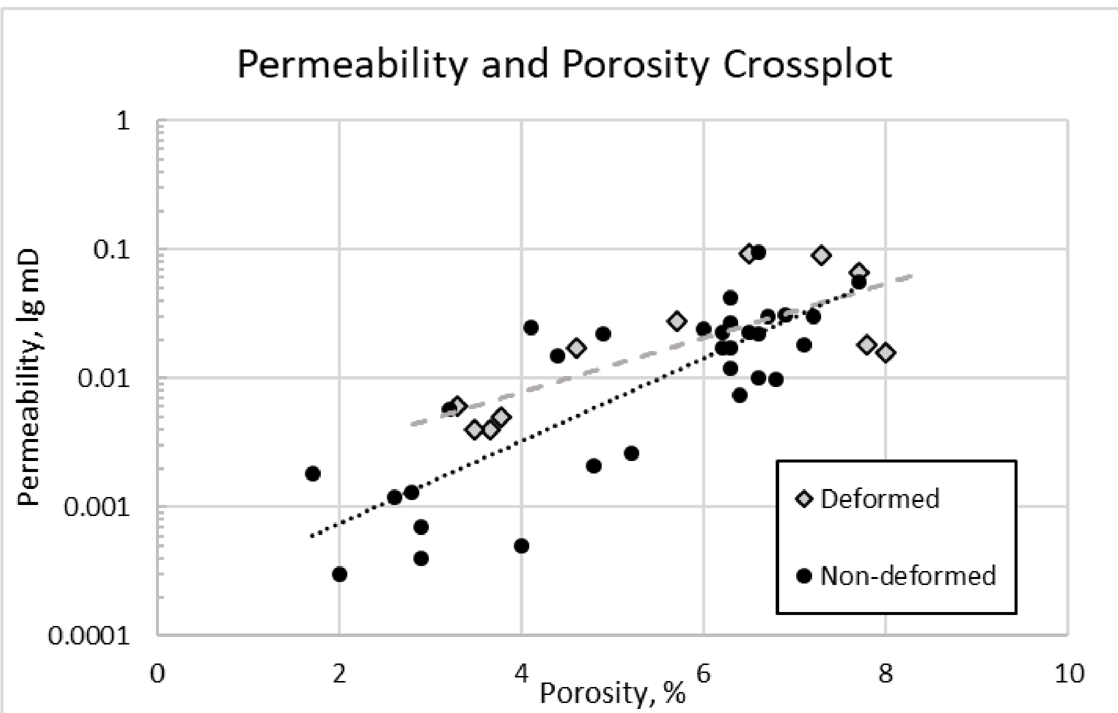

Figure 11: Graph showing the relationship between porosity (x-axis) and permeability (y-axis) in deformed and non-deformed facies; all porosities show a maximum of 8% and below. Permeabilities, however, vary by about 2.5 orders of magnitude.

increase seemed to have survived any diagenetic overprint. This indicates that facies in the upper third to quarter of the Bakken succession, the “transgressive” portion, should be slightly better reservoirs where SSDS occur in the succession in contrast to the facies that are entirely undisturbed.

DISCUSSION

Trigger of SSDS

In this contribution the SSDS are interpreted as having been caused by seismic shaking. However, several other processes are known to produce SSDS similar to those observed and documented in the middle Bakken member (Owen and Moretti, 2011; Owen et al., 2011). One of the processes previously suggested as a trigger for SSDS, wave-induced cyclic loading (Madsen, 1978; Sassa and Sekiguchi, 2001; Chen and Lee, 2013), cannot be solely responsible for the formation of the entire suite of the observed SSDS in all stratigraphic intervals as the majority of SSDS occur in environments that were most likely not strongly influenced by wave action. It would be hard to argue for the SSDS being produced by mechanisms related to tidal flux (Bjerrum, 1973; Greb and Archer, 2007) as the middle Bakken member does not contain any tidally-produced sedimentary structures. Equally, deformation due to freezing and thawing (French, 1986; Vandenberghe, 1992) seems implausible for middle Bakken member sediments as the Williston basin was located in near-equatorial latitudes at sea-level (Scotese, 1994; Blakey, 2013), and, therefore, wasn't subject to the development of permafrost. The middle Bakken member is a relatively thin unit with thicknesses of up to 45 m (Meissner, 1978) and overall slow sedimentation rates (see biostratigraphy of Hogancamp and Pocknall, 2018). Rapid sedimentation as a process to produce SSDS is therefore relatively unlikely, and thick massive sandstones or other evidence of rapid sedimentation are entirely lacking in the middle Bakken member; it therefore seems improbable that this process was a major process responsible for SSDS formation in the middle Bakken member. Tsunami waves are generally thought of as large cyclic storm waves, and typically produce a unique stacking pattern of bedforms: individual or stacked successions of alternating high-energy sediment sheets and mud drapes, structures produced by repeated reversal of current directions, and an upward fining and decreasing in the thickness packages of sediment (Fujiwara, 2008). None of these features have been observed in the middle Bakken member. Apart of the fact that the Williston Basin represented an enclosed inland sea, an environment anyway unlikely to produce or transmit deep-reaching ocean waves, the lack of tsunami-induced sedimentary structures makes it improbable that tsunamis could have caused SSDS formation in the middle Bakken member. Gravity-induced slope collapse can lead to SSDS-like features but seems an unlikely process as all paleogeographic reconstructions of the Williston Basin show it having an extremely low-inclined depositional profile (e.g. Borkovsky et al., 2017, and references therein). There is no record of a meteorite impact during the Late Devonian – Early Mississippian that would cause syndepositional deformation of unconsolidated sediment, e.g. shatter cones (Alvarez et al., 1998); this process is therefore excluded. Salt-dissolution in underlying units, in this case the Devonian Prairie salt, has happened In the Williston Basin, also most likely during Bakken times (LeFever and LeFever, 2005). However, this type of tectonics is most likely not responsible for the formation of SSDS because the magnitude of shaking produced by slipping along salt-dissolution faults is significantly less than of tectonic faults (Guerrero et al., 2014). It seems unlikely that such a process would cause earthquakes that could lead to wide-spread soft-sediment deformation as, e.g., observed in the middle member of the Bakken Formation (cf. Huntoon, 1999; McCalpin, 2009).

It is, therefore, most likely, that the SSDS in the middle Bakken reflect the influence of synsedimentary seismic shocks on the succession. This is based on the following reasoning: 1. The stratigraphic distribution of SSDS is not confined to a particular depositional environment; on the contrary, deformation structures occur in various facies, and are, therefore, most likely largely unaffected by exogenic processes. 2. Sedimentary units of similar petrographic and petrophysical properties occur as both deformed and non-deformed in the same stratigraphic levels; this indicates that deformation only affected selected areas that were proximal to active structures at the time of deposition. 3. Deformed units are intercalated with non-deformed sediment, which indicates the recurrent nature of the trigger process – most likely the reactivation of basin structures that interrupted the otherwise calm sedimentation. 4. The spatial distribution of deformed units reflects the general orientation of some important basin structures. The areas where SSDS are present are elongated in shape and oriented northwest-southeast, similar to the orientation of the Parshall, Antelope and Little Knife anticlines. 4. Soft-sediment deformation structures observed in the middle Bakken member are similar to those obtained experimentally under earthquake-like shaking (Kuenen, 1958; Nichols et al., 1994; Owen, 1996; Moretti et al., 1999). 5. Similar SSDS have been reported in many seismically-active areas characterized by very low to flat basin-floor topography worldwide (Hildebrandt and Egenhoff, 2007; Spalluto et al., 2007; Berra and Felletti, 2011; El Taki and Pratt, 2012; Chen and Lee, 2013; He et al., 2014; Chiarella et al., 2016 and others).

Distribution of Soft-Sediment Deformation Structures

The stratigraphic distribution of SSDS in the middle Bakken member is interpreted in this study as reflecting a variation in synsedimentary tectonic activity in the Williston basin during middle Bakken member deposition. The presence of very few to no SSDS in the lower, regressive part of the middle Bakken succession is seen as reflecting a tectonically relatively quiet time in the basin's history, while the concentration of SSDS in the upper, transgressive portion represents a tectonically active phase. Yet, the absence of SSDS in select sedimentary facies of the transgressive portion, such as bioturbated carbonate mud- to wackestones, could also be due to unfavorable conditions for SSDS preservation, e.g. due to early diagenesis, or subsequent obliteration of SSDS by bioturbation (El Taki and Pratt, 2012).

The areal distribution of SSDS in 90 measured sections shows that the SSDS are concentrated along distinct elongate zones which are interpreted to reflect the activity of the underlying basement structures: the Nesson, Antelope, Parshall, Billings Nose and Little Knife Anticlines. It is suggested that tectonic movements along the basement faults triggered earthquakes of at least magnitude 5 (Ezquerro et al., 2015) capable of deforming unconsolidated sediment. The distribution patterns of cumulative thickness of deformed intervals per well (Fig. 10) suggest a possible relation of the thickness to the magnitude of faulting and/or proximity to an active structure. Based on that, it seems likely that the southern part of the Nesson-Antelope-Little Knife-Billings Nose Anticline structure was tectonically more active than the northern part. Most of the Nesson Anticline, a fault zone in Divide and Williams Counties of North Dakota is thought to have repeatedly reactivated during Paleozoic and Mesozoic times (LeFever et al., 1987; Gerhard and Anderson, 1988; Gerhard et al., 1991; Anna et al., 2013), and was likely largely dormant during middle Bakken deposition as no SSDS have been observed along known fault systems belonging to this structure.

Based on the absence of SSDS in the vicinity of the Rough Rider anticline, we suggest that synsedimentary seismicity in this area was either minor or absent. However, it is possible that either slumping or subsequent erosion may have removed the sediment in the areas which constitute the margins of the Williston basin. Nevertheless, most SSDS record deformation in place, and don't indicate distinct transport of slumped units over long distances. In addition, if large masses of sediment were removed from directly above the fault zone by slumping, the slumped units would have been transported downslope and would be expected to appear in at least some adjacent wells. Therefore, significant removal of sediment on the margins of the Williston basin by slumping seems unlikely. Erosion of the margins during the lowstand that is suggested for the central to upper central part of the middle Bakken member (LeFever, 1991; Egenhoff et al., 2011; Borcovsky et al., 2017) might have also affected the southern realms of the Billings Nose anticline and the Rough Rider anticline area, and is likely to have exposed and removed some of sediment. However, most of the SSDS occur stratigraphically above that lowstand, in the transgressive part of the sedimentary system. So, even if erosion removed some parts of the succession in the Billings Nose anticline area and elsewhere in the basin close to the middle Bakken margins, it will likely not have influenced the outcome of this study, as most SSDS are in situ and located in the younger, stratigraphically higher portion of the succession not affected by erosion.

Most structures underlying the SSDS were previously known. However, the presence of SSDS in Burke and northwestern Ward Counties does not correspond to any basement structure reported to date. Based on SSDS in many other places in the basin, it is probable that the SSDS in this particular area also reflect synsedimentary seismic activity and likely an underlying fault that had been hitherto unknown. It is most probable that this structural element also represents a basement fault as it shares the same northwest-southeast orientation with other known major basement lineaments. Nevertheless, it remains unclear why this structure had not been detected before. This oversight may have been due to a lack of data, or potentially limitations in data processing techniques (e.g. methods of fault detection in Jahan et al., 2017). Indicators of shear stress observed in various SSDS would suggest the presence of a large-scale wrench-style structure that did not stop at the current Canadian-US boundary. The Cedoux-Midale and

Montmartre-Weir Hill structural element in Saskatchewan, Canada (Kreis and Kent, 2000) is a direct northwestward extension of the Ward and Burke-County structural element inferred from this study. Also the two SSDS maxima in central to western Divide County show a northwest extension in Canada (Potter and St Onge, 1991). It is therefore likely that the SSDS described in this study reflect the extension of previously described tectonically active basement structures as their thickness distribution fits well with known structural elements described from north of the border.

The deformed succession found in the True Oil 44-33 4-9H Slash Fed well in the Red Wing Creek field of McKenzie county has the highest net thickness of deformed units among all studied cores; nevertheless, and it lies outside of the general NW-SE trend of any of the hitherto detected faults. In attempt to explain this phenomenon, we considered a meteor impact reported from the Red Wing Creek field (Brenan et al., 1975; Sawatzky, 1977; Koeberl and Reimold, 1995; Herber, 2010). The effect of the impact on the sedimentary fabric has not been studied since the discovery of the feature; however, a seismic interpretation study of Herber (2010) shows that the Bakken formation was affected by the impact. There are several reasons why soft-sediment deformation observed in the middle Bakken member in well True Oil 44-33 4-9H Slash Fed was not produced by this meteorite impact. First, the interval contains SSDS in multiple stratigraphic levels separated by undisturbed sediment evidencing occurrence of multiple events that are unlikely to have been caused by a single-impact meteorite collision; rather, they reflect recurrent faulting-related seismic activity. Second, the Red Wing Creek meteorite is believed to have fallen approximately one to two hundred million years after the middle Bakken was deposited (Brenan et al., 1975; Sawatzky, 1977; Koeberl and Reimold, 1995; Herber, 2010). Although it is possible that a shockwave from the impact propagated as deep as Upper Devonian rocks, it is most likely that the middle Bakken sediment was already completely solidified by the time the meteorite hit. A meteorite impact would only have caused brittle deformation and therefore cannot be responsible for any SSDS observed in the Red Wing Creek field in North Dakota.

Implications for the tectonic history of the Williston Basin

Seismically-induced SSDS or ‘seismites’ (Seilacher 1969) can serve as proxies for paleotectonic reconstructions (Ettensohn et al., 2002; Hildebrandt and Egenhoff 2007; El Taki and Pratt, 2012; Wallace and Eyles, 2015; Myrow et al., 2015, and others). The sedimentary record of seismites allows to recognize synsedimentary fault activity and, in some cases, calculate earthquake recurrence intervals (Sims, 1975; Ezquerro et al., 2015; Jiang et al., 2016; Törő and Pratt, 2016). However, not all seismic events get recorded in the sedimentary column; it has been shown that the magnitude of an earthquake ≥5 (Ezquerro et al., 2015) or >5.5 according to Rodrígez-Pascua et al. (2001) is necessary to deform unconsolidated sediment shortly after deposition. This suggests that faulting-related paleoseismicity in the Upper Devonian – Lower Carboniferous Williston basin was at times strong enough to produce distinct soft-sedimentary deformation structures. Predominant distribution of SSDS in the transgressive systems tract of the middle Bakken member indicates a change from a relative tectonic stillstand during the regression and suggests a connection between relative sea-level rise and tectonism: the middle Bakken marine transgression is linked to a change in basin dynamics, likely including extensional movements, reflected in subsidence and accommodation space modifications in the upper third to upper quarter of the formation. This can be clearly observed in the thickness distribution of the transgressive upper third to upper quarter of the succession versus the regressive lower part of the middle Bakken (Novak and Egenhoff, submitted): the depocenter, which is the part of the basin showing the thickest accumulation of sediments, was located in Mountrail county during deposition of the lower two thirds to three quarters of the middle Bakken succession. However, in the upper, transgressive third to quarter part of the succession, this depocenter shifted to the northeast and was located in Burke and Ward Counties. This change in overall basin geometry is also reflected in the presence of SSDS in the vicinity of all active faults, and may further be linked to establishing a better connection towards the Elk Point Basin in Canada (Gerhard and Anderson, 1988).

Implications for Hydrocarbon Exploration

It remains unclear if and how SSDS influence reservoir performance, or if deforming rocks in a soft state has any significant impact on rock characteristics relevant to reservoir quality at all. It is known, though, that sand injections, for example, serve as conduits for both lateral and vertical fluid flows (Purvis et al., 2002; Hurst and Cartwright, 2007; He et al., 2014). Oil staining was observed in some of the deformed units, which indicates that these deformation structures served as passages for fluid migration and, potentially, as hydrocarbon storage (Hurst et al., 2003). Seismically-triggered synsedimentary fracturing has been suggested to contribute to the enhancement of hydrocarbon migration pathways and reservoir storage capacity (El Taki and Pratt, 2012; He et al., 2014). Zheng et al. (2015) demonstrated better reservoir performance in reservoir units containing seismically-triggered soft-sediment deformation structures when comparing them to un-deformed units in the same succession.

Addressing a similar issue for the middle Bakken member which is the prime reservoir in the Bakken petroleum system (Anna et al., 2011), we plotted porosity and permeability values for rocks showing synsedimentary deformation, and from the same facies ('Laminated Siltstones', Novak and Egenhoff (submitted), which is the main reservoir facies in the basin) without synsedimentary deformation into one graph (Fig. 11). Our porosity-permeability data show that soft-sediment deformation positively affects the reservoir quality in the middle Bakken member by overall increasing its permeability. This result is by itself not surprising because the increase in permeability can be explained by the loss of sediment cohesion and rearrangement of original grain packing after liquefaction, produced by e.g. a seismic shock. This process, particularly in the heterolithic sediment such as the 'Laminated Siltstones' facies, leads to homogenization of sediment and an increase in vertical and lateral permeability. Injection structures, such as ptygmatic clastic dikes and diapiric structures, as well as microfaults, observed in the middle Bakken are also envisioned to increase permeability in this unit. They are generally regarded as conduits for vertical hydrocarbon migration by connecting silty and sandy reservoir intervals by cutting through over- and underlying low-permeability mudstone drapes.

CONCLUSIONS

1) Based on the detailed assessment of 90 cores, nine types of seismically-induced SSDS were identified in the middle member of the Bakken Formation which include: slump structures, boudinage-like structures, massive silt and sand sheets, ptygmatically-folded clastic dikes, load structures, water-escape structures, diapiric structures, lithoclastic breccia, and microfaults. SSDS found in the middle Bakken member are concentrated in the "transgressive" upper third to quarter portion of the succession, and their spatial distribution pattern follows either a northwest-southeastern trend similar to the orientation of the basins major faults systems or a north-south trend parallel to the Nesson-Antelope-Little Knife-Billings Nose anticlines.

2) Previously largely overlooked SSDS in the middle Bakken member record the synsedimentary tectonic history of the Williston basin during Late Devonian – Early Carboniferous times and imply that intracratonic basins are not as tectonically passive as thought. The geographic proximity of SSDS to known structural lineaments of the basin and the variations in the net thickness of deformed units indicate that the Williston basin was characterized by frequent seismic events with magnitudes of at least 5 on the Richter scale which likely resulted from the reactivation of basement-rooted fault zones. The predominant occurrence of SSDS in the "transgressive" upper and their sparse occurence in the "regressive" lower portions of the succession indicates that basin dynamics had likely shifted from a relative stillstand to a tectonically active phase during middle Bakken deposition, which is supported by the north-easterly shift of the depocenter and a rise of relative sea-level.

3) Occurrence of SSDS formed by seismically-produced liquefaction and fluidization processes might have a positive impact on reservoir porosity and permeability which most likely results from the loss in cohesion and further rearrangement of sediment grains. Injection structures, such as clastic dikes and diapirs, and microfaults can potentially serve as conduits for fluid flow and storage.

4) This study demonstrates not only the presence of SSDS in the middle Bakken member and their use in locating active ancient fault zones in the Williston basin, but also serves as an example of how

seismites can be used to recognize paleotectonic activity within other intracratonic troughs worldwide. The direct influence of SSDS on reservoir performance is yet to be fully understood, nonetheless, the modifications of rock properties caused by soft-sediment deformation should be considered in exploration of low-permeability petroleum reservoirs.

REFERENCES

Albert, S., 2014. Sedimentology, Facies Architecture, and Sequence Stratigraphy of the Lower Bakken Shale Member in the Williston Basin, North Dakota, United States of America. Master thesis. Colorado State University, 90 pp.

Allen, J. R. L., 1970. Physical Processes of Sedimentation, American Elsevier, New York, 248 pp.

Allen, J.R.L., 1982. Sedimentary Structures: Their Character and Physical Basis, v. 1-2. Elsevier, Amsterdam, 664 pp.

Allen, P. A., and Allen, J. R., 2005. Basin Analysis: Principles and Applications, second ed. Blackwell Publishing, Oxford, 562 pp.

Alsop, G. I., and Marco, S., 2011. Soft-sediment deformation within seismogenic slumps of the Dead Sea Basin. Journal of Structural Geology. 33, 433-457.

Alvarez, W., Staley, E., O'Connor, D., and Chan, M.A., 1998. Synsedimentary deformation in the Jurassic of southeastern Utah – a case of impact shaking? Geology. 26, 579–582.

Angulo, A., and Buatois, L.A., 2012. Integrating depositional models, ichnology, and sequence stratigraphy in reservoir characterization: the middle member of the Devonian-Carboniferous Bakken Formation of subsurface southeastern Saskatchewan revisited. Am. Assoc. Petroleum Geol. Bull. 96, 1017-1043.

Anna, L.O., Pollastro, Richard, and Gaswirth, S.B., 2011. Williston Basin Province—Stratigraphic and structural framework to a geologic assessment of undiscovered oil and gas resources, chap. 2 of U.S. Geological Survey Williston Basin Province Assessment Team, Assessment of undiscovered oil and gas resources of the Williston Basin Province of North Dakota, Montana, and South Dakota, 2010: U.S. Geological Survey Digital Data Series 69–W, 17 pp.

Armitage, J. J., and Allen, P. A., 2010. Cratonic basins and the long-term subsidence history of continental interiors. Journal of the Geological Society, London. 167, 61-70.

Baskoutas, I., Papadopoulos, G., Karakostas, V., and Papadimitriou, E., 2007. Recent 2005-2006 strong seismic activity in Greece under the aspect of seismicity parameters temporal variation analysis. Bulletin of the Geological Society of Greece. 40(3), 1055-1062. doi:http://dx.doi.org/10.12681/bgsg.16824.

Berra, F., and Felletti, F., 2011. Syndepositional tectonics recorded by soft-sediment deformation and liquefaction structures (continental Lower Permian sediments, Southern Alps, Northern Italy): Stratigraphic significance. Sedimentary Geology. 235, 249-263.

Bjerum, L., 1973. Geotechnical problems involved in foundations of structures in the North Sea. Géotechnique, 23 (3), 319-358.

Blakey, R., 2013. Early Mississippian paleogeography, Colorado Plateau geosystems, North America 345 Ma Mississippian (early to middle) http://deeptimemaps.com/wp-content/uploads /2016/05/NAM_key-345Ma_EMiss.png (accessed 6 November 2018).

Borkovsky, D., Egenhoff, S., Fishman, N., Maletz, J., Boehlke, A., and Lowers, H., 2017. Sedimentology, facies architecture, and sequence stratigraphy of a Mississippian black mudstone succession - The upper member of the Bakken Formation, North Dakota, United States. American Association of Petroleum Geologists Bulletin. 101(10), 1625–1673.

Brenan, R. L., Peterson, B. L., and Smith, H. J., 1975. The origin of the Red Wing structure. The Wyoming Geological Association Earth Science Bulletin. 8(3), 1-41.

Chen, J., and Lee, H. S., 2013. Soft-sediment deformation structures in Cambrian siliciclastic and carbonate storm deposits (Shandong Province, China): Differential liquefaction and fluidization triggered by storm-wave loading. Sedimentary Geology. 288, 81-94.

Chiarella, D., Moretti, M., Longhitano, S. G., and Muto, F., 2016. Deformed cross-stratified deposits in the Early Pleistocene tidally-dominated Catanzaro strait-fill succession, Calabrian Arc (Southern Italy): Triggering mechanisms and environmental significance. Sedimentary Geology. 344, 277-289.

Chimney, P.J., Treska, C.E., and Wolosin, C.A., 1992. Richardton/Taylor Fields – U.S.A. American Association of Petroleum Geologists Treatise of Petroleum Geology, Stratigraphic Traps III, pp. 421-445.

Collinson, J., 1994. Sedimentary deformation structures, in: A. Maltman (ed.): The geological deformation of sediments, Chapman & Hall, London, 94-126.

Crashell, J.J., 1991. Tectonic History of Billings and Southern McKenzie Counties, Southwestern North Dakota. University of North Dakota. Masters of Science Thesis, pp. 265.

Dolce, M., and Bucci, D. D., 2018. The 2016–2017 Central Apennines Seismic Sequence: Analogies and Differences with Recent Italian Earthquakes, in: Pitilakis, K. (Ed.), Recent Advances in Earthquake Engineering in Europe. Geotechnical, Geological and Earthquake Engineering. 46, 603-638.

Dzulynski, S. and Kotlarczyk, J., 1962. On load-casted ripples. Ann. Soc. Geol. Pologne, 32, 148-159.

Dzulynsksi, S. and Smith, A. J., 1963. Convolute lamination, its origin, preservation, and directional significance. Journal of Sedimentary Petrology. 33, 616-627.

Egenhoff, S. O., 2017. The lost Devonian sequence - Sequence stratigraphy of the middle Bakken member, and the importance of clastic dykes in the lower Bakken member shale, North Dakota, USA. Marine and Petroleum Geology. 81, 278-293.

Egenhoff, S. O., van Dolah, A., Jaffri, A., and Maletz, J., 2011. Facies architecture and sequence stratigraphy of the Middle Bakken Member, Williston Basin, North Dakota, in: Robinson, L., LeFever, J. A., and Gaswirth, S. (Eds.), Bakken-Three Forks petroleum system in the Williston Basin. Rocky Mountain Association of Geologists guidebook, Denver, Colorado, Rocky Mountain Association of Geologists, 27–47.

Egenhoff, S., 2018. Proximal Bakken facies – flooding the Williston Basin in the Late Devonian – Early Mississippian, North Dakota, USA. GSA abstracts and program, contribution 221-2.

Egenhoff, S.O., and Fishman, N.S., 2013. Sedimentology of the upper Bakken shale member, North Dakota, USA. J. Sediment. Res. 83, 803-824.

El Taki, H.E., and Pratt, B.R., 2012. Syndepositional tectonic activity in an epicontinental basin revealed by deformation of subaqueous carbonate laminites and evaporites: seismites in Red River strata (Upper Ordovician) of southern Saskatchewan, Canada. Bulletin of Canadian Petroleum Geology, 60, 37–58.

Ezquerro, L., Moretti, M., Liesa, C. L., Luzón, A., and Simón, J. L., 2015. Seismites from a well core of palustrine deposits as a tool for reconstructing the palaeoseismic history of a fault. Tectonophysics. 655, 191-205.

French, H. M., 1986. Periglacial Involutions and Mass Displacement Structures, Banks Island, Canada. Geografiska Annaler, 68 (A), 167-174.

Fujiwara, O., 2008. Bedforms and Sedimentary Structures Characterizing Tsunami Deposits. Tsunamiites - Features and Implications, 51-62. DOI: 10.1016/B978-0-444-51552-0.00004-7.

Gaswirth, S.B., Marra, K.R., Cook, T.A., Charpentier, R.R., Gautier, D.L., Highley, D.K., Klett, T.R., Lewan, M.D., Lillis, P.G., Schenk, C.J., Tennyson, M.E., and Whidden, K.J., 2013. Assessment of undiscovered oil resources in the Bakken and three Forks Formations, Williston basin province, Montana, North Dakota, and South Dakota, 2013. U. S. Geol. Surv. Fact. Sheet 2013-3013 4.

Gerhard, L. C., and Anderson, S. B., 1988. Geology of the Williston Basin (United States portion). Sedimentary Cover – North American Craton: U.S. D-2, 221-241.

Gerhard, L. C., S. B. Anderson, and D. W. Fisher, 1990. Petroleum geology of the Williston Basin, in: Leighton, M. W., Kolata, D. R., Oltz, D. T., and Eidel, J. J. (Eds.), Interior Cratonic Basins. AAPG Memoir 51, 507-559.

Gibert, L., Sanz de Galdeano, C., Alfaro, P., Scott, G., and López Garrido, A. C., 2005. Seismic-induced slump in Early Pleistocene deltaic deposits of the Baza Basin (SE Spain). Sedimentary Geology. 179, 279-294.

Gladkov, A. S., Lobova E. U., Deev, E. V., Korzhenkov, A. M., Mazeika, J. V., Abdieva, S. V., Rogozhinc, E. A., Rodkin, M. V., Fortuna, A. B., Charimov, T. A., and Yudakhind, A. S., 2016. Earthquake-induced soft-sediment deformation structures in Late Pleistocene lacustrine deposits of Issyk-Kul Lake (Kyrgyzstan). Sedimentary Geology. 344, 112-122.

Greb, S.F., and Archer, A.W., 2007. Soft-sediment deformation produced by tides in a mezoseismic area, Turnagain Arm, Alaska. Geology, 35, 435–438.

Grimm, K. A., and Orange, D. L., 1997. Synsedimentary fracturing, fluid migration, and subaqueous mass wasting: intrastratal microfractured zones in laminated diatomaceous sediments, Miocene Monterey Formation, California, U.S.A. Journal of Sedimentary Geology. 67(3), 601-613.

Guerrero, J., Bruhn, R. L., McCalpin, J. P., Gutierrez, F., Willis, G., and Mozafari, M., 2014. Salt-dissolution faults versus tectonic faults from the case study of salt collapse in Spanish Valley, SE Utah (USA). Lithosphere, 7 (1), 46-58.

He, B., Qiao, X., Jiao, C., Xu, Z., Cai Z., Guo, X., and Zhang, Y., 2014. Palaeo-earthquake events during the late Early Palaeozoic in the central Tarim Basin (NW China): evidence from deep drilling cores. Geologos. 20(2), 105-123.

Heine, C., Müller, R. D., Steinberger, B., and Torsvik, T. H., 2008. Subsidence in intracontinental basins due to dynamic topography. Physics of the Earth and Planetary Interiors. 171, 252-264.

Herber, B. D., 2010. 3D Seismic Interpretation of a Meteorite Impact, Red Wing Creek Field, Williston Basin, Western North Dakota. Master's Thesis. University of Colorado, Boulder, 188 p..

Hilbert-Wolf, H. L., Roberts, E. M., and Simpson, E. L., 2016. New sedimentary structures in seismites from SW Tanzania: Evaluating gas- vs. water-escape mechanisms of soft-sediment deformation. Sedimentary Geology, 344, 253-262.

Hildebrandt, C., and Egenhoff, S. 2007. Shallow-marine massive sandstone sheets as indicators of palaeoseismic liquefaction - an example from the Ordovician shelf of Central Bolivia. Sedimentary Geology, 202, 581–595.

Hogancamp, N. J., and Pocknall, D. T., 2018. The biostratigraphy of the Bakken Formation: A review and new data. Stratigraphy, 15(3), 197-224.

Huntoon, P.W., 1999. Field-based identification of salt-related structures and their differentiation from tectonic structures, in Hanson, K.L., Kelson, K.I., Angell, M.A., and Lettis, W.R., eds., Techniques for Identifying Faults and Determining their Origins: Washington, D.C., U.S. Nuclear Regulatory Commission, contract report NUREG/CR-5503, 186 p. plus appendices.

Hurst, A., Cartwright, J., and Duranti, D., 2003. Fluidization structures produced by upward injection of sand through a sealing lithology. Geological Society of London Special Publication, 216, 123-138.

Hurst, A., and Cartwright, J., 2007. Sand injectites: implications for hydrocarbon exploration. AAPG Memoir, 87, 288.

Jahan, I., Castagna, J., Murphy, M., and Kayali, A., 2017. Fault detection using principal component analysis of seismic attributes in the Bakken Formation, Williston Basin, North Dakota, USA. Interpretation, 5(3), T361-T372. https://doi.org/10.1190/INT-2016-0209.1

Jiang, H., Zhong, N., Li, Y., Xu, H., Yang, H., and Peng, X., 2016. Soft sediment deformation structures in the Lixian lacustrine sediments, eastern Tibetan Plateau and implications for postglacial seismic activity. Sedimentary Geology, 344, 123-134.

Karma, R., 1991. Conodonts of the Bakken Formation (Devonian-Mississippian) in Saskatchewan, northern Williston basin, in: Christopher, J.E., Haidl, F.M. (Eds.), Sixth International Williston Basin Symposium, vol. 11. Saskatchewan Geological Society, Special Publication, pp. 70-73.

Kent, D.M., and Christopher, J.E., 1994. Geological history of the Williston basin and the Sweetgrass arch, in: Mossop, G.D., Shetson, I. (Eds.), Geological atlas of Western Canada. Canadian Society of Petroleum Geologists and Alberta Research Council, pp. 421-430.

Klein, G. D., 1995. Intracratonic Basins. Blackwell Science, Cambridge.

Klinkenberg, L. J. 1941. The Permeability of Porous Media to Liquids and Gases. Drilling and Production Practices. American Petroleum Institute, New York.

Koeberl, C., and Reimold, W. U., 1995. The Newporte impact structure, North Dakota, USA. Geochimica Cosmochimica Acta, 59(22), 4747-4767.

Koper, K. D., Pankow, K. L., Pechmann, J. C., Hale, J. M., Burlacu, R., Yeck, W. L., Benz, H. M., Herrmann, R. B., Trugman, D. T., and Shearer, P. M., 2018. Afterslip enhanced aftershock activity during the 2017 earthquake sequence near Sulphur Peak, Idaho. Geophysical Research Letters, 45, 5352–5361.

Kreis, L.K. and Kent, D.M., 2000. Basement controls on Red River sedimentation and hydrocarbon production in southeast Saskatchewan, in: Summary of Investigations 2000. Saskatchewan Geological Survey, Saskatchewan Energy and Mines, Miscellaneous Report 2000-4.1, 21−42.

Kuenen, Ph. H., 1958. I.—Experiments in Geology. Transactions of the Geological Society of Glasgow, 23, 1-28.

Kuenen, P. H., 1967. Origin of ptygmatic features. Tectonophysics, 6(2), 143-158.

Lefever, J.A., Lefever, R.D. and Anderson, S.D. 1987. Structural evolution of the central and southern portions of the Nesson anticline, North Dakota, in: Carlson C.G. and Christopher J.E. (Eds.), Fifth Williston Basin Symposium. Saskatchewan Geological Society, Special Publication 9, pp. 147−156.

LeFever, J.A., 1991. History of oil production from the Bakken Formation, North Dakota, in: Hansen, W.B. (Ed.), 1991 Guidebook to Geology and Horizontal Drilling of the Bakken Formation. Montana Geological Society, Billings, Montana, pp. 3-17.

LeFever, J. A. and LeFever, R. D., 2005. Salts in the Williston Basin, North Dakota. North Dakota Geological Survey Report of Investigation No. 103, 45 pp..

LeFever, J.A., LeFever, R.A., and Nordeng, S., 2011. Revised nomenclature for Bakken Formation (Mississippian-Devonian), North Dakota, in: Robinson, L., LeFever, J.A., Gaswirth, S. (Eds.), Bakken-Three Forks Petroleum System in the Williston Basin. RMAG Guidebook, pp. 11-26 (on CD).

Liesa, C. L., Rodríguez-López, J. P., Ezquerro, L., Alfaro, P., Rodríguez-Pascua, M. A., Lafuente, P., Arlegui, L., and Simón, J. L., 2016. Facies control on seismites in an alluvial–aeolian system: The Pliocene dune field of the Teruel half-graben basin (eastern Spain). Sedimentary Geology, 344, 237-252.

Lowe, D. R., 1975. Water-escape structures in coarse-grained sediments. Sedimentology, 22, 157–204.

Lowe, D. R., 1976. Subaqueous liquefied and fluidized sediment flows and their deposits. Sedimentology, 23, 285–308.

Madsen, O. S., 1978. Wave-induced pore pressures and effective stresses in porous bed. Géotechnique, 28, 377–393.

Martel, A. T., and Gibling, M. R., 1992. Clastic dykes of the Devono-Carboniferous Horton Bluff Formation, Nova Scotia: storm-related structures in shallow lakes. Sedimentary Geology, 87, 103-119.

McCalpin, J.P., 2009. Paleoseismology in extensional tectonic environments, in: McCalpin, J.P., (ed.), Paleoseismology (2nd ed.), San Diego, California, Academic Press, p. 171–277.

Meissner, F. F., 1978. Petroleum geology of the Bakken Formation, Williston Basin, North Dakota and Montana, in: Rehrig D., (Ed.), 1978 Williston Basin Symposium. Montana Geological Society, pp. 207-227.

Montenat, C., Barrier, P., and Ott d`Estevou, P., 1991. Some aspects of the recent tectonics in the Strait of

Messina, Italy. Tectonophysics, 194, 203-215.

Montenat, C., Barrier, P., Ott d`Estevou, P., and Hibsch, C., 2007. Seismites: An attempt at critical analysis and classification. Sedimentary Geology, 196, 5-30.

Moretti, M., Alfaro, P., Caselles, O., and Canas, J. A., 1999. Modelling seismites with a digital shaking table. Tectonophysics, 304, 369-383.

Moretti, M., and Sabato, L., 2007. Recognition of trigger mechanisms for soft-sediment deformation in the Pleistocene lacustrine deposits of the Sant'Arcangelo Basin (southern Italy): seismic shock vs. overloading. Sedimentary Geology, 196, 31–45.

Myrow, P. M., and Chen, J., 2015. Estimates of large magnitude Late Cambrian earthquakes from seismogenic soft-sediment deformation structures: Central Rocky Mountains. Sedimentology, 62, 621-644.

Nichols, R. J., Sparks, R. S., and Wilson, C. J. N., 1994. Experimental studies of the fluidization of layered sediments and the formation of fluid escape structures. Sedimentology, 41, 233-253.

Nordeng, S. H., LeFever, J. A., Anderson, F. J., Bingle-Davis, and Johnson, E.H., 2010. An examination of the factors that impact oil production from the middle member of the Bakken Formation in Mountrail County, North Dakota. Report of Investigation No. 109, North Dakota Geological Survey, 85 p.

Novak, A., and Egenhoff, S. O., 2019. Facies distribution in an intracratonic basin, and its relation to changes in sea-level and basin configuration – middle Bakken member, Williston Basin, ND, USA. Sedimentology. Manuscript submitted for publication.

Obermeier, S.F., 1996. Use of liquefaction-induced features for paleoseismic analysis — an overview of how seismic liquefaction features can be distinguished from other features and how their regional distribution and properties of source sediment can be used to infer the location and strength of Holocene paleo-earthquakes. Engineering Geology, 44, 1–76.

Onasch, C. M., and Kahle, C. F., 1991. Recurrent tectonics in a cratonic setting: An example from northwestern Ohio. GSA Bulletin, 103 (10), 1259-1269.

Owen, G., 1987. Deformation processes in unconsolidated sands, in: M. E. Jones, and R. M. F. Preston, (Eds.), Deformation of Sediments and Sedimentary Rocks. Geological Society, London, Special Publication, 29, pp. 11–24.

Owen, G., 1996. Experimental soft-sediment deformation: structures formed by the liquefaction of unconsolidated sands and some ancient examples. Sedimentology, 43, 279-293.

Owen, G., and Moretti, M., 2011. Identifying triggers for liquefaction-induced soft-sediment deformation in sands. Sedimentary Geology, 235, 141–147.

Owen, G., Moretti, M., and Alfaro, P., 2011. Recognizing triggers for soft-sediment deformation: Current understanding and future directions. Sedimentary Geology, 235, 133-140.

Pitman, J. K., Price, L. C., and LeFever, J. A., 2001. Diagenesis and Fracture Development in the Bakken Formation, Williston Basin: Implications for Reservoir Quality in the Middle Member. U. S. Geological Survey Professional Paper 1953, 24 p.

Potter, D. and St. Onge, A. 1991. Minton Pool, south-central Saskatchewan: a model for the basement induced structural and stratigraphic relationships, in: Sixth Williston Basin Symposium. J.E. Christopher and F.M. Haidl (eds.), Saskatchewan Geological Society, Special Publication 11, 21−33.

Pratt, B. R., 1998. Syneresis cracks: subaqueous shrinkage in argillaceous sediments caused by earthquake-induced dewatering. Sedimentary Geology, 117, 1-10.

Pratt, b. R., 2019. Discussion of ‘Depositional setting of the 2.1 Ga Francevillian macrobiota (Gabon): Rapid mud settling in a shallow basin swept by high-density sand flows’ by Reynaud et al. (2018) Sedimentology, 65, 670–701. Sedimentology, 66, 774-776.

Purvis, K., Kao, J., Flanagan, K., Henderson, J., and Duranti, D., 2002. Complex reservoir geometries in a deep water clastic sequence, Gryphon Field, UKCS: injection structures, geological modeling and reservoir simulation. Marine and Petroleum Geology, 19, 161-179.

Rodríguez-Pasca, M. A., Vicente, G, D., and Calvo, J. P., 2001. Paleoseismological analysis of Late Miocene lacustrine successions in the Prebetic Zone, SE Spain. Acta Geologica Hispanica, 36, 213-232.

Ruiz, S., and Madariaga, R., 2018. Historical and recent large megathrust earthquakes in Chile. Tectonophysics, 733, 37-56.

Sassa, S., and Seikiguchi, H., 2001. Analysis of wave-induced liquefaction of sand beds. Geotechnique, 51(2), 115-126.

Sawatzky, H. B., 1977. Buried impact craters in the Williston basin and adjacent area, in: Roddy D. J., Pepin R. O. and Merrill R. B. (Eds.), Impact and Explosion Cratering. Pergamon Press, New York, pp. 461-480.

Scotese, C.R., 1994. Carboniferous paleocontinental reconstructions. U. S. Geol. Surv. Bull. 2110, 3-6.

Seilacher, A., 1969. Fault-graded beds interpreted as seismites. Sedimentology, 13, 155-159.

Seilacher, A., 1984. Sedimentary structures tentatively attributed to seismic events. Marine Geology, 55, 1-12.

Simenson, A. L., Sonnenberg, S. A., and Cluff, R. M., 2011. Depositional Facies and Petrophysical Analysis of the Bakken Formation, Parshall Field and Surrounding Area, Mountrail county, North Dakota, in: Robinson, L., LeFever, J. A., and Gaswirth, S. (Eds.), Bakken-Three Forks petroleum system in the Williston Basin. Rocky Mountain Association of Geologists guidebook, Denver, Colorado, Rocky Mountain Association of Geologists, 48-101.

Sims, J. D., 1975. Determining earthquake recurrence intervals from deformational structures in young lacustrine sediments. Tectonophysics, 29, 141-152.

Smith, M.G., and Bustin, R.M., 2000. Late Devonian and Early Mississippian Bakken and Exshaw black shale source rocks, Western Canada sedimentary basin; a sequence stratigraphic interpretation. AAPG Bulletin, 84 (7), 940-960. http://dx.doi.org/10.1306/A9673B76-1738-11D7-8645000102C1865D.

Spalluto, L., Moretti, M., Festa, V. and Tropeano, M., 2007. Seismically-induced slumps in Lower-Maastrichtian peritidal carbonates of the Apulian Platform (southern Italy). Sedimentary Geology, 196, 81–98.

Törő, B., and Pratt, B. R., 2016. Sedimentary record of seismic events in the Eocene Green River Formation and its implications for regional tectonics on lake evolution (Bridger Basin, Wyoming). Sedimentary Geology, 344, 175-204.

Truswell, J. F., 1972. Sandstone sheets and related intrusions from Coffee Bay, Transkei, South Africa.

Journal of Sedimentary Petrology, 42, 578-583.

U. S. Geological Survey, 2018. Latest Earthquakes. https://earthquake.usgs.gov/ (accessed January 9).

Vandenberghe, J., 1992. Cryoturbations: A sediment structural analysis. Permafrost and Periglacial processes, 3, 343-352.

Vibe, Y., Bunge, H. P., and Clark, S. R., 2018. Anomalous subsidence history of the West Siberian Basin as an indicator for episodes of mantle induced dynamic topography. Gondwana Research, 53, 99-109.

Wallace, K., and Eyles, N., 2015. Seismites within Ordovician–Silurian carbonates and clastics of Southern Ontario, Canada and implications for intraplate seismicity. Sedimentary Geology, 316, 80-95.

Webster, R.L., 1984. Petroleum source rocks and stratigraphy of the Bakken Formation in North Dakota, in: Woodward, J., Meissner, F.F., and Clayton, J.C. (Eds.), Hydrocarbon source rocks of the greater Rocky Mountain region. Denver, Rocky Mountain Association of Geologists, pp. 57-81.

Zhang, L., and Buatois, L. A., 2014. Sedimentary facies and depositional environments of the Upper Devonian–Lower Mississippian Bakken Formation in eastern Saskatchewan. Summary of Investigations 2014, Volume 1, Saskatchewan Geological Survey, Sask. Ministry of the Economy, Misc. Rep. 2014-4.1, Paper A-3, 18 pp.

Zheng, L., Jiang, Z., Liu, H., Kong, X., Li, H., and Jiang, X., 2015. Core evidence of paleoseismic events in Paleogene deposits of the Shulu Sag in the Bohai Bay Basin, east China, and their petroleum geologic significance. Sedimentary Geology, 328, 33-54.

APPENDIX A

LIST OF WELLS UTILIZED IN THIS STUDY

Map Annotation Number	Original Well Name	Original Operator	API	County	Library File Number
1	LOUCKS 44-30	ANSBRO PETROLEUM COMPANY, LLC	3302300471	Divide	15722
2	WATTERUD "A" #17	CONOCO INC.	3302300412	Divide	13318
3	TOMLINSON 3-1HN	SM ENERGY COMPANY	3302301120	Divide	26745
4	JENNIFER ABIGAIL 16-21H	MUREX PETROLEUM CORPORATION	3302300975	Divide	24642
5	1-24 SLATER	CLARION RESOURCES	3301300853	Burke	B679
6	LOUIS PETERSON #1	NORTHERN PUMP CO.	3301300699	Burke	4508
7	MERTES #1-32	CLARION RESOURCES, INC.	3301300862	Burke	8819
8	NEGAARD #1	CLARION RESOURCES, INC.	3301300877	Burke	9001
9	NELSON 1-29	CLARION RESOURCES, INC.	3301300867	Burke	8850
10	JORGENSEN 4 - 4H	CORNERSTONE NATURAL RESOURCES LLC	3301301491	Burke	18829
11	OAS 31-161-92H	SAMSON RESOURCES COMPANY	3301301383	Burke	16810
12	SARATOGA 12-1-161-92H	SAMSON RESOURCES COMPANY	3301301667	Burke	22572
13	DOUTS 4-7H	ST MARY LAND & EXPLORATION COMPANY	3301301412	BURKE	17265
14	PRODUCER`S CORPORATION 159-94-17C-8-2H	PETRO-HUNT, L.L.C.	3301301530	BURKE	19773
15	PIERCE #1-18	CLARION RESOURCES, INC.	3307500873	Renville	8637
16	VIOLET OLSEN 31-29H	PETRO DEVEL CORP	3310501551	Williams	E968
17	H. BORSTAD #1	TEXAKOTA, INC.	3310500732	Williams	5656
18	HAMLET U. #2	DALLEA PETROLEUM CORP.	3310500606	Williams	3007
19	CLIFFORD MARMON #1	PAN AMERICAN PETROLEUM CORP.	3310500667	Williams	4340
20	NESSON STATE 42X-36	HEADINGTON OIL COMPANY LLC	3310501667	Williams	17015
21	H. BAKKEN 12-07H	HESS CORPORATION	3310501618	Williams	16565
22	GEORGE EVANS 11V	DAKOTA-3 E&P COMPANY, LLC	3306102032	Mountrail	22421
23	MYLO WOLDING 14-11	MARATHON OIL COMPANY	3306101194	Mountrail	18511

24	PARSHALL 2-36H	EOG RESOURCES, INC.	3306100503	Mountrail	16324
25	AHEL ET AL SANISH #36-44 H4	AMERICAN HUNTER EXPLORATION LTD.	3306100398	Mountrail	12807
26	ST-ANDES-151-89- 2413H-1	HESS CORPORATION	3306100653	Mountrail	17043
27	JENSEN #12-44	MARATHON OIL COMPANY	3306100257	Mountrail	8069
28	LAREDO #26-1	MARATHON OIL COMPANY	3306100394	Mountrail	12786
29	BARTLESON 44-1H	WHITING OIL AND GAS CORPORATION	3306100495	Mountrail	16068
30	ROGSTAD #1-11	BROOKS EXPLORATION, INC.	3306100252	Mountrail	7851
31	L. TEXEL #21-35	SHELL OIL CO.	3306100187	Mountrail	5088
32	STATE ND 1-11H	AMERADA HESS CORPORATION	3306100498	Mountrail	16160
33	MILDRED ROGGENBUCK 41-24TFX	WHITING OIL AND GAS CORPORATION	3306102049	Mountrail	22532
34	FERTILE 1-12H	EOG RESOURCES, INC.	3306100557	Mountrail	16743
35	FARHART 11-11H	FIDELITY EXPLORATION & PRODUCTION COMPANY	3306100680	Mountrail	17096
36	SIDONIA 1-06H	EOG RESOURCES, INC.	3306100884	Mountrail	17676
37	RS-STATE C-157-90- 3603H-1	HESS CORPORATION	3306100666	Mountrail	17071
38	MCALMOND 1-05H	EOG RESOURCES, INC.	3306100587	Mountrail	16862
39	1-20 FLECKTON	CLARION RESOURCES	3310100273	Ward	B706
40	1-33 PULLEN	CLARION RESOURCES	3310100272	Ward	B678
41	STEINBERGER #1-16	GOLDEN EYE RESOURCES, LLC	3310100476	Ward	17377
42	J. Brekhus #2-14	GOLDEN EYE RESOURCES, LLC	3310100475	Ward	17347
43	DOBRINSKI #18-44	MARATHON OIL COMPANY	3310100260	Ward	8177
44	15-22 BN Flat Top Butte	PENNZOIL COMPANY	3305301030	McKenzie	D284
45	SLASH FEDERAL 44-33 4-9H	TRUE OIL LLC	3305303925	McKenzie	22180
46	SPRING CREEK #27X-31BN	PENNZOIL COMPANY	3305302340	McKenzie	12983
47	USA 33-23-154	SHELL OIL CO.	3305301391	McKenzie	8902
48	LINSETH 13-13/12H	HELIS OIL & GAS COMPANY, L.L.C.	3305303693	McKenzie	21217
49	AHEL ET AL GRASSEY BUTTE #12-31 H3	AMERICAN HUNTER EXPLORATION LTD.	3305302308	McKenzie	12772
50	POJORLIE 21-2-1H	GMX RESOURCES INC	3305303872	McKenzie	21884

51	1 FEDERAL DG	CITIES SERVICE	3305301536	McKenzie	T418
52	TITAN E-GIERKE 20-1-H	LYCO ENERGY CORPORATION	3305302672	McKenzie	15923
53	STENEHJEM HD 27 #1	ORYX ENERGY CO.	3305302357	McKenzie	13098
54	F. P. KEOGH #4	TEXACO INC.	3305300477	McKenzie	2820
55	JENS STRAND #1	AMERADA PETROLEUM CORP.	3305300144	McKenzie	1202
56	MOI #44-13	MERIDIAN OIL, INC.	3305302188	McKenzie	12160
57	FORT BERTHOLD 150-94-3B-10-2H	PETRO-HUNT, L.L.C.	3305303623	McKenzie	20915
58	LARS ROTHIE 32-29H	HESS CORPORATION	3305302769	McKenzie	16433
59	HA-NELSON- 152-95-3328H-9	HESS CORPORATION	3305305469	McKenzie	26980
60	LINSETH 4-8H	HELIS OIL & GAS COMPANY, L.L.C.	3305302809	McKenzie	16689
61	LUNDIN 11-13SEH	DENBURY ONSHORE, LLC	3305303829	McKenzie	21706
62	UBERWACHEN 22-34	BURLINGTON RESOURCES OIL & GAS COMPANY LP	3305303819	McKenzie	21668
63	TARPON FEDERAL 44-19TFHU	WHITING OIL AND GAS CORPORATION	3305305595	McKenzie	27413
64	MARTIN WEBER #1-18-1C	GULF OIL CORP.	3302500067	Dunn	6082
65	BURBANK BIA #23-8	SHELL OIL CO.	3302500232	Dunn	8709
66	PEGASUS DIV SOLOMON BIRD BEAR #F-22-22-1	MOBIL PRODUCING CO.	3302500005	Dunn	793
67	YOUNG BEAR #32-4	SHELL OIL CO.	3302500347	Dunn	9707
68	ANGUS KENNEDY #F32-24-P	SOCONY-VACUUM OIL COMPANY, INC.	3302500003	Dunn	607
69	EVELYN KARY 2-22-15H-144-97	OXY USA INC.	3302502118	Dunn	25364
70	STOHLER 21-3H	MARATHON OIL COMPANY	3302500597	Dunn	16333
71	CORRINE OLSON 34-20	MARATHON OIL COMPANY	3302501117	Dunn	19118
72	FORT BERTHOLD 147-94-3B-10-3H	PETRO-HUNT, L.L.C.	3302501964	Dunn	24272
73	ROBERTS TRUST 1-13H	SIMRAY GP, LLC	3302500982	Dunn	18355
74	JANE FEDERAL 11X-20	HEADINGTON OIL COMPANY LLC	3302500794	Dunn	17430
75	HAWKINSON 14-22H2	CONTINENTAL RESOURCES, INC.	3302502007	Dunn	24456

76	JORGENSON 1-15H	NEWFIELD PRODUCTION COMPANY	3302500729	Dunn	17086
77	3-17 TOC MEE USA	TENNECO OIL	3300700581	Billings	B659
78	1-12 FEDERAL	FLORIDA EXPLORATION	3300700830	Billings	E383
79	GRAHAM USA #1-15	TENNECO OIL	3300700690	Billings	B658
80	5-1 THOMPSON UNIT	TEXACO INCORPORATED	3300701185	Billings	E349
81	FRANKS CREEK STATE 21-16TFH	WHITING OIL AND GAS CORPORATION	3300701676	Billings	20574
82	CROOKED CREEK STATE #31-16	MAXUS EXPLORATION CO.	3300701162	Billings	12558
83	MOI ELKHORN #33-11	MERIDIAN OIL, INC.	3300701109	Billings	12072
84	FEDERAL #12-12	MILESTONE PETROLEUM, INC.	3300701014	Billings	10989
85	F-6-144-101 #3	SUPRON ENERGY CORP.	3300700820	Billings	9351
86	23-143-102 BN #1	COASTAL OIL & GAS CORP. & AL-AQUITAINE	3300700666	Billings	8363
87	FEDERAL 34-1	FLORIDA EXPLORATION CO.	3300700997	Billings	10803
88	CHRUSZCH 43X-29	XTO ENERGY INC.	3300701632	Billings	17768
89	11-4 FEDERAL	FLORIDA EXPLORATION	3300700914	Billings	E385

APPENDIX B

POROSITY AND PERMEABILITY DATA

Well	Depth, ft	Deformation	Porosity, %	Permeability, mD
GMX RESOURCES INC POJORLIE 21-2-1H	11288	Deformed	5.7	0.028
	11290	Deformed	6.5	0.092
	11294.6	Non-deformed	2.9	0.0007
	11296	Deformed	7.3	0.089
	11298	Non-deformed	2.9	0.0004
	11300	Deformed	4.6	0.017
TEXACO INCORPORATED 5-1 THOMPSON UNIT	11057.3	Non-deformed	5.2	0.0026
TRUE OIL LLC SLASH FEDERAL 44-33 4-9H	10796.6	Non-deformed	4.8	0.0021
HESS CORPORATION ST-ANDES-151-89- 2413H-1	9089.5	Deformed	6.1	0.0003
	9091.5	Deformed	8.3	0.0015
WHITING OIL AND GAS CORPORATION BARTLESON 44-1H	10234.4	Non-deformed	6.2	0.023
	10235.4	Non-deformed	6.6	0.096
	10237.3	Deformed	7.7	0.066
	10244.7	Non-deformed	6.3	0.027
	10245.2	Non-deformed	6	0.024
	10246.3	Non-deformed	6.7	0.03
	10247.3	Non-deformed	2	0.0003
	10248.7	Non-deformed	6.3	0.042
	10249.5	Non-deformed	4.9	0.022
	10250.2	Non-deformed	6.3	0.017
	10251.2	Non-deformed	6.6	0.01
MARATHON OIL COMPANY MYLO WOLDING 14-11	10585.5	Non-deformed	4	0.0005
	10586.55	Non-deformed	6.4	0.0075
	10587.55	Deformed	7.8	0.018
	10588.4	Deformed	8	0.016
	10593.6	Non-deformed	1.7	0.0018
	10594.55	Non-deformed	7.7	0.056
	10595.5	Non-deformed	6.3	0.012
	10596.55	Non-deformed	7.1	0.018
	10597.6	Non-deformed	2.8	0.0013
	10598.5	Non-deformed	6.5	0.023
	10599.5	Non-deformed	7.2	0.03
	10600.5	Non-deformed	4.4	0.015
	10601.55	Non-deformed	6.2	0.017

	10602.45	Non-deformed	6.6	0.022
	10603.45	Non-deformed	3.2	0.0057
	10604.6	Non-deformed	4.1	0.025
	10605.55	Non-deformed	6.9	0.031
	10606.5	Non-deformed	6.8	0.0097
	10607.4	Non-deformed	2.6	0.0012
J. BREKHUS #2-14	7094.5	Deformed	3.77	0.005
	7096.5	Deformed	3.65	0.004
	7098.65	Deformed	3.3	0.006
	7100.6	Deformed	3.49	0.004